

DETECTION OF STRIPPING IN HOT MIX ASPHALT

Final Report

March 11, 2005



Michael I. Hammons, Ph.D., P.E.
Harold Von Quintus, P.E.
Applied Research Associates, Inc.

Kenneth Maser, Ph.D.
Infrasense, Inc.

Soheil Nazarian, Ph.D., P.E.
Consultant



Prepared for:

**Office of Materials and Research
Georgia Department of Transportation
Forest Park, GA 30297-2599**



Applied Research Associates, Inc.
5000 NW 27th Court, Suite E
Gainesville, FL 32606
Phone: (352) 336-5366
Facsimile: (352) 381-0022

ARA Project Number 16355

TABLE OF CONTENTS

Table of Contents	i
List of Figures	iii
List of Tables	v
1 Introduction	1-1
1.1 Background	1-1
1.2 Objective.....	1-1
1.3 Scope.....	1-2
2 Test Methods And Equipment	2-1
2.1 Introduction	2-1
2.2 Cores	2-1
2.3 Detailed Surface Condition Survey.....	2-1
2.3.1 Hypothesis	2-1
2.3.2 Equipment.....	2-1
2.3.3 Method	2-4
2.4 IR.....	2-5
2.4.1 Hypothesis	2-5
2.4.2 Equipment.....	2-5
2.4.3 Method	2-6
2.5 Seismic.....	2-7
2.5.1 Hypothesis	2-7
2.5.2 Equipment.....	2-11
2.5.3 Method	2-13
2.6 FWD.....	2-13
2.6.1 Hypothesis	2-13
2.6.2 Equipment.....	2-13
2.6.3 Method	2-13
2.7 GPR.....	2-16
2.7.1 Hypothesis	2-16
2.7.2 Equipment.....	2-17
2.7.3 Method	2-17
3 Phase I: I-20 Pilot Project	3-1
3.1 Pilot Project Hypotheses.....	3-1
3.2 Pilot Project Description.....	3-1
3.2.1 Location	3-1
3.2.2 Construction History	3-2
3.2.3 Test Conditions	3-3
3.3 Test Results	3-4
3.3.1 Cores.....	3-4
3.3.2 Surface Distress	3-7
3.3.3 Infrared Thermography.....	3-12
3.3.4 Seismic	3-12
3.3.5 Falling Weight Deflectometer.....	3-22
3.3.6 Ground Penetrating Radar	3-27
3.4 Analysis of Results.....	3-37

3.4.1	Baseline HMA Layer Modulus – No Moisture Damage	3-37
3.4.2	Modulus Values Estimated from NDT Technologies	3-40
3.4.3	Stripping Predictions from GPR	3-42
3.4.4	Comparisons to Field Cores	3-44
3.4.5	Laboratory Tests on Field Cores	3-44
3.4.6	Discussion	3-48
3.5	Alternative to Stripping Index	3-50
3.6	Rehabilitation Recommendation for I-20	3-52
3.7	Additional Observation	3-54
3.8	Findings	3-54
4	Phase II: I-75 Pilot Project	4-1
4.1	Pilot Project Hypotheses	4-1
4.2	Pilot Project Description	4-1
4.2.1	Location	4-1
4.2.2	Construction History	4-1
4.2.3	Test Conditions	4-3
4.3	Test Results	4-4
4.3.1	Cores	4-4
4.3.2	Surface Distress	4-7
4.3.3	Seismic	4-11
4.3.4	GPR	4-16
4.4	Analysis of Results	4-19
4.4.1	Baseline HMA Layer Modulus – No Moisture Damage	4-19
4.4.2	GPR Results	4-21
4.4.3	Seismic Tests	4-21
4.4.4	Laboratory Tests	4-23
4.4.5	Summary	4-25
5	Recommended Procedure to Identify Areas with Moisture Damage	5-1
5.1	Procedure to Identify Areas with Moisture Damage	5-1
6	Conclusions and Recommendations	6-1
6.1	Conclusions	6-1
6.1.1	General	6-1
6.1.2	Moisture Damage	6-1
6.1.3	Non-Destructive Techniques	6-1
6.1.4	Pilot Projects	6-2
6.2	Recommendations	6-2
6.2.1	Survey Strategy	6-2
6.2.2	Safety Considerations	6-3
6.2.3	Rehabilitation Strategy for I-20 Pilot Project	6-3
6.2.4	Rehabilitation Strategy for I-75 Pilot Project	6-3
7	References	7-1
	Appendix A: Photographs of Cores from I-20 Eastbound	A-1
	Appendix B: Stress-Strain Curves from IDT Tests on I-20 Cores	B-1
	Appendix C: Photographs of Cores from I-75 Northbound	C-1
	Appendix D: Stress-Strain Curves from IDT Tests on I-75 Cores	D-1
	Appendix E: Dispersion Curves for I-75 Cores Using Short PSPA Spacing	E-1
	Appendix F: I-75 GPR Uniformity Index Charts	F-1

LIST OF FIGURES

Figure 2-1. Rear view of digital survey vehicle	2-2
Figure 2-2. Front view of digital survey vehicle	2-3
Figure 2-3. Typical digital image workstation	2-5
Figure 2-4. IR survey vehicle	2-6
Figure 2-5. Schematic of USW method	2-9
Figure 2-6. Typical time records from an HMA site	2-9
Figure 2-7. Phase spectra obtained from time records in Figure 2-6	2-10
Figure 2-8. Typical dispersion curve	2-10
Figure 2-9. Schematic of impact echo method.....	2-11
Figure 2-10. Portable Seismic Properties Analyzer (PSPA).....	2-12
Figure 2-11. Sensor configuration for FWD testing	2-14
Figure 2-12. GPR survey vehicle	2-17
Figure 3-1. Approximate extent of I-20 pilot project.....	3-1
Figure 3-2. Photograph of I-20 eastbound lanes looking west.....	3-2
Figure 3-3. Longitudinal profile of I-20 HMA thickness as determined from cores	3-6
Figure 3-4. I-20 Lane 3 cracking summary plot.....	3-9
Figure 3-5. I-20 Lane 3 rutting summary plot	3-10
Figure 3-6. I-20 Lane 3 roughness summary plot	3-11
Figure 3-7. Visual and infrared camera images (potential stripping area highlighted in red).	3-12
Figure 3-8. Typical dispersion curves from intact and deteriorated I-20 sections.....	3-14
Figure 3-9. Variation in modulus of with depth for intact I-20 core.....	3-15
Figure 3-10. Experimental and theoretical dispersion curves from intact I-20 core	3-15
Figure 3-11. Variation in modulus of with depth for deteriorated I-20 core.....	3-17
Figure 3-12. Experimental and theoretical dispersion curves from deteriorated I-20 core.....	3-17
Figure 3-13. Variation in average modulus obtained with USW method along I-20 pilot project	3-18
Figure 3-14. Impact echo amplitude spectra from intact and deteriorated locations	3-18
Figure 3-15. Impact echo amplitude spectra converted to thickness	3-19
Figure 3-16. Variation in modulus and impact-echo amplitude from Day 1 of I-20 field tests.....	3-20
Figure 3-17. Variation in modulus and impact-echo amplitude from Day 2 of I-20 field tests.....	3-21
Figure 3-18. I-20 FWD results summary	3-23
Figure 3-19. I-20 bound layer stiffness values from FWD	3-26
Figure 3-20. Comparison of I-20 normalized modulus values from seismic tests and FWD.....	3-26
Figure 3-21. Sample GPR section data from I-20 Lane 3, centerline	3-27
Figure 3-22. I-20 cores showing stripping from 4 to 6 inches from the surface.....	3-27
Figure 3-23. GPR stripping analysis, I-20 Lane 3, STA 820 to 970	3-30
Figure 3-24. GPR stripping analysis, I-20 Lane 3, STA 970 to 1120	3-31
Figure 3-25. GPR stripping analysis, I-20 Lane 2, STA 820 to 970	3-32
Figure 3-26. GPR stripping analysis, I-20 Lane 2, STA 970 to 1120	3-33
Figure 3-27. GPR stripping analysis, I-20 Lane 1, STA 820 to 970	3-34
Figure 3-28. GPR stripping analysis, I-20 Lane 1, STA 970 to 1120	3-35
Figure 3-29. GPR stripping analysis, I-20 Lane 1, STA 1120 to 1270	3-36
Figure 3-30. Dynamic modulus of an intact, good quality HMA binder mixture about 6 inches below the surface.....	3-38
Figure 3-31. Dynamic modulus of an intact, good quality HMA base mixture about 10 inches below the surface.....	3-38
Figure 3-32. Expected high and low total resilient modulus values measured from indirect tensile repeated load testing of HMA mixtures sampled from around the U.S.	3-39
Figure 3-33. Adjusted I-20 HMA seismic modulus as compared to the range of expected modulus values	3-40

Figure 3-34. I-20 HMA elastic modulus calculated from FWD data as compared to the range of expected modulus values	3-41
Figure 3-35. Comparison of the HMA modulus values estimated from the FWD and seismic testing.....	3-42
Figure 3-36. Comparison of GPR SI with adjusted seismic modulus for I-20 Lane 3	3-43
Figure 3-37. Comparison of GPR SI with FWD elastic modulus for I-20 Lane 3.....	3-43
Figure 3-38. Comparison of the IDT dynamic modulus values from I-20 cores with expected values from non-aged cores	3-45
Figure 3-39. Comparison of the average IDT dynamic modulus and tensile strain at failure for the different layer conditions tested	3-47
Figure 3-40. Comparison of the IDT dynamic modulus strain at failure to the typical values expected for a mix without moisture damage.....	3-47
Figure 3-41. Comparison of the IDT dynamic modulus and strain at failure for test specimens prepared from the binder layer with various levels of the GPR SI	3-48
Figure 3-42. Comparison of the average estimated modulus values within ranges of GPR SI	3-50
Figure 3-43. Comparison of seismic modulus to GPR UI for I-20 pilot section, approximate depth range: 3 to 11 inches	3-51
Figure 3-44. Maximum vertical compressive strain in the HMA layer for different milling depths	3-53
Figure 3-45. Distortion strain ratio for different milling depths.....	3-53
Figure 4-1. Approximate extent of I-75 pilot project.....	4-2
Figure 4-2. Photo of I-75 northbound lanes near MP 270.5	4-2
Figure 4-3. Pavement structure and approximate construction dates, I-75.....	4-3
Figure 4-4. Fatigue cracking summary plot, I-75 Lane 3	4-8
Figure 4-5. I-75 Lane 3 rutting summary plot	4-9
Figure 4-6. I-75 Lane 3 roughness summary plot	4-10
Figure 4-7. Typical dispersion curves from intact and deteriorated sections of I-75	4-12
Figure 4-8. Typical dispersion curve from deteriorated section of I-75 using 12-inch PSPA sensor spacing	4-13
Figure 4-9. Variation in average modulus obtained with USW Method along the length of the I-75 pilot project.....	4-14
Figure 4-10. Variation in modulus and impact-echo amplitude from Day 1 of I-75 field tests.....	4-15
Figure 4-11. Variation in modulus and impact-echo amplitude from Day 2 of I-75 field tests.....	4-15
Figure 4-12. Sample GPR section data from centerline of Lane 3, I-75	4-17
Figure 4-13. Comparison of seismic modulus to GPR UI for I-75 pilot section, approximate depth range: 3 to 11 inches	4-18
Figure 4-14. Expected high and low total resilient modulus values	4-20
Figure 4-15. Longitudinal profile of the adjusted seismic modulus along I-75 compared to the expected range without moisture damage.....	4-22
Figure 4-16. Comparison of measured IDT dynamic modulus from I-75 cores to expected values from non-aged mix	4-24
Figure 4-17. Relationship between IDT strength and dynamic modulus for each layer tested along I-75	4-25
Figure 4-18. Comparison of the IDT dynamic modulus and strain at failure to typical values expected for a mix without moisture damage.....	4-26
Figure 5-1. Rehabilitation flow chart, part 1.....	5-3
Figure 5-2. Rehabilitation flow chart, part 2.....	5-4

LIST OF TABLES

Table 2-1. Digital survey vehicle systems.....	2-3
Table 2-2. FWD loading sequence	2-14
Table 3-1. Weather conditions at ATL, April 2004.....	3-4
Table 3-2. I-20 Core results.....	3-5
Table 3-3. Summary of laboratory test results on selected cores recovered from I-20	3-7
Table 3-4. Forward calculated stiffness near I-20 core locations	3-25
Table 3-5. Correlation of SI with I-20 cores.....	3-29
Table 3-6. Summary of expected modulus values for intact HMA without moisture damage.....	3-39
Table 3-7. Summary of GPR SI, average FWD and seismic modulus values, and I-20 core condition data	3-44
Table 3-8. Average IDT mix properties for each of the mixture conditions tested	3-46
Table 3-9. Average HMA modulus values for the areas with different GPR stripping indices	3-49
Table 3-10. Summary of computations with EVERSTRS to determine an appropriate milling depth to minimize potential for distortion.....	3-52
Table 4-1. Weather conditions at ATL, September 2004.....	4-3
Table 4-2. I-75 core descriptions.....	4-5
Table 4-3. Dynamic modulus values measured at different frequencies for each test specimen.....	4-6
Table 4-4. Summary of the laboratory test results on selected cores recovered from I-75	4-6
Table 4-5. Average IDT mix properties for each of the mixture conditions tested	4-7
Table 4-6. UI values at I-75 core locations.....	4-19
Table 4-7. Summary of the expected modulus values for HMA without moisture damage	4-21
Table 4-8. Core condition compared with adjusted seismic modulus.....	4-23

1 INTRODUCTION

1.1 Background

Stripping in hot mix asphalt (HMA) refers to the loss of adhesion between the asphalt cement and the aggregate surface primarily caused by the action of moisture and moisture vapor (Kandhal and Rickards 2001). Moisture damage begins with a reduction of cohesion in the asphalt binder or a reduction of adhesion between the asphalt binder and aggregate surface. Moisture damage often occurs in HMA without actual stripping. When advanced stripping is present, cores recovered from the roadway will often disintegrate during the coring operation.

Stripping within pavement sections is causing problems for the Georgia Department of Transportation (GDOT). In Georgia, routine mill and overlay rehabilitation projects typically consist of milling 2¾ inches followed by an HMA inlay of equal or near equal thickness. When stripped material is encountered below the planned milling depth, it must be removed and replaced causing significant and unexpected cost overruns and time delays.

The stripped layers are described to be generally about 2 to 4 inches thick and are typically about 4 inches below the surface. To assure that the stripped material is removed, planned milling depths could be increased. However, increasing the depth from 2¾ inches to 8 inches could add over \$100,000 of construction costs per lane mile. User delays could also be affected significantly. It is conceivable that a 2¾-inch mill and overlay could be done during a night operation and opened to traffic by morning rush hour. An 8-inch mill and overlay depth is much more difficult to complete in an overnight operation requiring the work be shifted to weekends in high traffic areas or forcing daytime lane closures. Ultimately, the entire construction program is affected, because overruns consume resources that would have otherwise been used on other projects.

The goal of the GDOT is to develop a rapid, comprehensive, and reliable procedure to survey potential mill and overlay projects for the presence of stripping. In current GDOT practice, coring and visual examination is the preferred method for detecting the presence of stripped asphalt. A number of cores are extracted and visually examined and/or tested in the laboratory to identify the presence of stripping. Coring is time-consuming and is a point sampling method thus limiting the area and extent of pavement that can be investigated. AASHTO T283 (Resistance of Compacted Bituminous Mixture to Moisture Induced Damage) is the laboratory method commonly used to determine moisture damage in HMA mixtures. However, many agencies do not have a high level of confidence in this test method for identifying mixes susceptible to stripping. Most agencies use hydrated lime or some anti-stripping additive in those HMA mixtures that are known to be susceptible to moisture damage, simply because the reliability of AASHTO T283 and other test procedures are considered low at best.

1.2 Objective

The objective of this project was to develop an asphalt pavement survey protocol using nondestructive techniques to efficiently detect asphalt stripping in in-place pavement sections. The ultimate goal is to then use the evaluation protocol throughout the State to quantify the extent (area and depth) and severity of stripping that has occurred in asphalt pavements that are mill and overlay candidates.

1.3 Scope

The project scope consisted of two phases. In Phase I, an initial pilot investigation was performed on the eastbound lanes of Interstate 20 (I-20) in Cobb, Fulton, and Douglas Counties. Specifically, a 4½ mile stretch of Lane 3 between Mileposts (MP) MP 43.5 to 48 (Stations 820+00 and 1057+00) was thoroughly investigated and tested. The following NDT methods were evaluated to determine how successful they were individually and in conjunction with each other to identify stripping:

- Continuous survey methods
 - Ground Penetrating Radar
 - Infrared Thermography
 - Surface Condition
 - Surface Cracking
 - Rutting (transverse profile)
 - Longitudinal Profile in the wheel paths
- Point measurement methods
 - Falling Weight Deflection
 - Seismic Measurements

The results of these survey and measurements methods were analyzed to determine their respective capability to locate areas of moisture damage and stripping, either by themselves, or in various combinations. Coring was used to calibrate the methods to detect stripping developed in this project. Visual inspections of the cores and laboratory tests on selected cores were used to validate the results from Phase I.

In Phase II, the most promising technologies were applied on another pilot section of the northbound lanes of Interstate 75 (I-75) in Cobb, Cherokee, and Bartow Counties in northwest Georgia. Only surface condition, rutting, roughness, ground penetrating radar, and seismic testing were performed on the pavement section in the Phase II pilot.

2 TEST METHODS AND EQUIPMENT

2.1 Introduction

This research project included six elements of investigation that were expected to provide information that can be used to define areas where stripping might exist. The specific areas for investigation include:

- Cores with both visual examination and laboratory testing
- Detailed surface condition survey
- Infrared (IR) thermography
- Seismic
- Falling weight deflectometer (FWD)
- Ground penetrating radar (GPR)

Each of these methods and equipment are described in this chapter.

2.2 Cores

Existing cores from the pilot project area (obtained by GDOT) were used as “ground truth” data for comparison with nondestructive test methods. Eight HMA cores were selected from those recovered along I-20 and tested using various forms of the indirect tensile test. The cores were selected to cover the range of moisture damage in the binder or intermediate layer as defined by visual observations. Two test specimens were cut from each core, one test specimen from the HMA base layer and the other from the binder or intermediate layer. The type of indirect tensile tests performed on these test specimens included the dynamic modulus and strength test.

2.3 Detailed Surface Condition Survey

2.3.1 Hypothesis

HMA that is prone to stripping would be categorized as having poor durability. Mixes with poor durability often show other symptoms, such as localized areas of increased surface distress, including severe fatigue cracking, potholing, raveling or a greater frequency of transverse and block cracking. Kandhal and Rickards (2001) observed that stripping in overlays also resulted in “flushing” of stripped asphalt binder to the surface and white staining of the surface where fines in the asphalt concrete have been pumped to the surface. The presence of stripping can also result in more variability that might increase the potential for rutting and/or localized longitudinal profile distortions and/or increases in rutting in localized areas. Shoving is possible when stripping begins to occur in layers near the surface, but not in the wearing surface.

2.3.2 Equipment

The automated video distress survey was conducted using a state-of-the-art vehicle containing the following synchronized survey systems:

- Digital Pavement Imaging System
- Pavement Illumination System
- Road Profiler System (IRI & Rut Data)

- Applanix POS-LV System (GPS, Inertial Navigation and Geometric Data)
- Asset Management Imaging System (ROW and Sign Images)

This equipment simultaneously records the surface condition, rutting, and roughness of the pavement surface. It also records digital images of the roadway ahead and right-of-way. The van-mounted camera and profiler system was manufactured by International Cybernetics Corporation (ICC). The digital survey vehicle is shown in Figures 2-1 and 2-2 with the various survey systems labeled. The survey system characteristics are summarized in Table 2-1.



Figure 2-1. Rear view of digital survey vehicle



Figure 2-2. Front view of digital survey vehicle

Table 2-1. Digital survey vehicle systems

Survey System	Manufacturer	Camera or Sensor Type	No. of Sensors	Resolution or Accuracy	Survey Speed, Max
Digital Pavement Imaging System	International Cybernetics Corporation	Bassler Line-Scan Monochrome	1	2,000 pixels per scan line	50 MPH @ 20-ft image Intervals
Road Profiler	International Cybernetics Corporation	Selcom, 16 kHz, Laser	9	0.002 inches	60 + MPH
GPS Receiver	Trimble	AG 320	1	Sub-meter	60 + MPH
Differential GPS	Applanix	DGPS	2	Sub-meter	60 + MPH
POS LV – X,Y Position	Applanix	N/A	1	0.20 m	15 sec signal outage
POS LV – Z Vert. Position	Applanix	N/A	1	0.20 m	15 sec signal outage
Roll & Pitch	Applanix	N/A	1	0.07 degrees	15 sec signal outage
True Heading	Applanix	N/A	1	0.07 degrees	15 sec signal outage
Asset Management – Windshield & Shoulder Images	International Cybernetics Corporation	Color, Digital Video Camera	2	1300 by 1024 pixels, each	60 + MPH @ 25-ft intervals
Distance Measuring Instrument	International Cybernetics Corporation	N/A	1	1-ft per mile	60 + MPH

The digital pavement imaging system consisted of a Bassler 2000-pixel line-scanning digital video camera. The imaging system was mounted on the rear of the vehicle and recorded continuous images with a width of survey of 14.5 ft. The line scans are accumulated to form an image representing a 20-ft length of pavement. The images are of sufficient resolution that 1-mm defects are readily visible. The pavement beneath the digital line-scanning camera was illuminated by ten 150 W metal halide stage lights mounted on a custom framework on the rear of the vehicle. These lights have special lenses that allow their light to be focused into a narrow band of intense illumination directly under the digital line scan camera.

The Applanix POS-LV system is a differential geographic positioning system (GPS), inertial navigation, and geometric system for land vehicles. It provides the system with GPS coordinates for locations such as survey start, survey stop, section event, and image location. These coordinates have sub-meter accuracy.

Two 1300 by 1024 pixel color digital cameras were used to collect right-of-way (ROW) images. One camera was oriented straight ahead for identifying number of lanes, overhead signs, etc. The side camera was oriented to the right side of the road for identifying traffic signs, mile markers and other roadway assets.

An ICC-manufactured ASTM E950 Class I South Dakota-type Road Profiler was used for road roughness data collection. Profile data were collected in each wheel path using three 16-kHz Selcom lasers in combination with accelerometers and a distance measuring instrument (DMI). The profiler is capable of collecting profile data points at intervals of 1 inch or less and storing average profile measurements at intervals of approximately 3 inches at speeds up to 60 mph. The laser sensors have a height resolution of 0.002 inches or better. The system uses the continuous 16-kHz output of the lasers to determine the height points eliminating narrow cracks and openings from roughness calculations. During the surveying operation, the data are stored in the onboard computer's memory until the end of the portion of roadway is reached. At that point, the data are saved to a computer file on the profiler's hard drive. The system uses industry standard analysis software to convert the sensor and accelerometer readings into longitudinal profiles and International Roughness Index (IRI) in accordance with ASTM E1926-98. Quarter-car simulation (QCS) and half-car simulation (HRI) are used to produce IRI values for the left and right wheel paths and the average IRI value, respectively.

The profiler was validated at validation sites maintained by the Pennsylvania Department of Transportation (PennDOT) near Harrisburg, PA. The sites were selected by PennDOT to cover the range of roughness applicable to most highway systems. Each site is 528 feet long with a 1,056-ft. lead-in to the test section. The Face Technologies Dipstick or AARB Profiling Unit is used to measure the profile of each wheel path between the reference bumps. Both units are ASTM E950 Class I profiling devices. Standard software, as described in World Bank Technical Paper No. 46, is used to generate the reference IRI from the profile data. This data is produced and maintained by PennDOT.

For rutting data collection, South Dakota-type Road Profiler was operated in the 5-sensor configuration. This configuration used two 32-kHz Selcom lasers, combined with accelerometers, four additional acoustic sensors, and a DMI allowing a 9-ft wide, 5-point, transverse profile to be measured.

2.3.3 Method

A detailed pavement distress survey was conducted using a digital image workstation (Figure 2-3). The downward digital photographs of the pavement surface were organized into sample units 20 ft long by one lane wide. The photographs were analyzed and the distress types, severity and extent were observed and recorded. The distresses observed included weathering and raveling, alligator cracking,

longitudinal and transverse cracking, and patching. Using the workstation, the distress data were linked with the corresponding images and the associated pavement management sample unit.



Figure 2-3. Typical digital image workstation.

The surface distresses were identified in accordance with the *Distress Identification Manual for the Long-Term Pavement Performance Program* (FHWA 2003). An exception to the LTPP protocol was made for weathering and raveling. The severity of weathering and raveling was set at the maximum level observed within the sample unit, and that value was assigned to the entire area of the sample unit. All longitudinal cracking in the wheel path was identified as alligator (fatigue) cracking and assigned an appropriate areal extent for purposes of this research.

2.4 IR

2.4.1 Hypothesis

A sensitive IR camera was used to detect localized areas with small surface temperature differences. Infrared thermography has been used to some extent for identifying areas of stripping and debonding of layers on bridge decks. For IR to be successful, the IR scans require conditions with a high rate of warming or cooling and rely on the premise that the stripped areas will have higher moisture contents and corresponding higher specific heat values or will be a poorer conductor of heat (insulation effect) than surrounding intact areas. Higher specific heat means that more energy is required to raise the temperature of the material during a warming cycle, or it will have more energy to give up during a cooling cycle. Less heat conduction (insulation) will have the opposite effect, allowing the surface to get warmer during the daytime or cooler during the nighttime.

2.4.2 Equipment

The infrared system and survey vehicle used on this project is shown in Figure 2-4. The system consists of a FLIR Systems Model SC-1000 infrared camera operating in the 3.4 to 5.0 micron region of the electromagnetic spectrum. The detector is a 256 X 256 platinum silicide focal plane array, which yields a spatial resolution with the wide angle lens (32 angular degrees) of 2.4 milliradians (equivalent

to 0.5 inches on the pavement) The camera has a maximum detection temperature range of from minus 10°C to 1500°C. Camera video output is standard NTSC 30 Hz video. In the video produced by the infrared camera, the “brightness” of each pixel is proportional to the received infrared radiation. The NTSC format produces 30 frames of IR video data per second, with 520 lines of video data per frame. The camera operator is able to set a temperature range, which can be as wide as 100°F and as small as 10°F. For this survey, the temperature range used was between 10°F and 15°F, or 6°C to 10°C. At the 10°C range the 8 bit pixel resolution of the camera yields a temperature resolution of 10/256, or 0.04°C.

During infrared data collection, the distance was recorded using the same wheel-mounted DMI used with the GPR vehicle. The DMI pulses were counted using an electronic counter, and, using the calibrated scale factor, the distance in feet was computed and recorded directly on the infrared and visual videotaped data.



Figure 2-4. IR survey vehicle

2.4.3 Method

Infrared thermography is a diagnostic NDE method which relates changes in surface temperature of a material to subsurface or internal flaws. The surface temperature is measured using an infrared camera mounted to a survey vehicle traveling at approximately 5 mph. Infrared Thermography has been used for over 15 years as a method for evaluation of delaminations in bridge decks. Infrared thermography

for bridge decks is based on thermal differentials generated between delaminated and sound areas of the deck by solar radiation (Maser and Roddis, 1990). The solar radiation heats the deck, and the areas above the delamination are essentially insulated from the remainder of the deck. These delaminated areas heat up faster, and can develop surface temperatures from 1-3 °C higher than the surrounding areas. These differentials are observed with an IR camera. The data from the IR camera is then converted to surface maps that show the location and quantity of delaminated areas. The equipment, data analysis software, and methodology for operation are all well developed.

Detection of stripping in asphalt would follow the same principles as detection of delamination in bridge decks. The low density subsurface layer in the asphalt should impede the flow of heat and thus cause higher surface temperatures. Alternatively, if the stripped area were wet, the wet areas would act as heat sinks and the surface temperatures would appear cooler. In either case, a thermal anomaly, detectable with the infrared camera, would be observed on the pavement surface.

The infrared camera was used in conjunction with a standard color video camera, so that infrared and visual images could be reviewed side by side. This infrared/visual comparison is necessary in order to discriminate infrared anomalies associated with visible surface conditions from those associated with the subsurface (i.e., with stripping). Both cameras were mounted on a mast at approximately 13 feet above the pavement surface. The height and angle of the cameras provided a field of view which was 19 feet wide at the top of the image, 9 feet wide at the bottom, and 13 feet wide at the center of the image. The center point of the infrared image was approximately 17.5 feet forward of the front axle of the survey vehicle. The infrared camera was operated by remote control via an RS-232 link to laptop computer using software provided by the camera manufacturer.

Analysis of the infrared data involves playback of the infrared and video data, and observation and identification of thermal anomalies. The simultaneous playback of infrared and video data is carried out with two VCR's attached to a video monitor with selectable input selections. Locations where thermal anomalies occur are logged in, and images of these locations can be grabbed on a computer using one of many types of frame grabbing devices.

2.5 Seismic

2.5.1 Hypothesis

Moisture damage and/or actual stripping typically will result in a significant decrease in the modulus of the HMA mixture. Seismic methods generate a stress wave at one point on the pavement surface and measure the time required for the waves to propagate to other points on the pavement surface. A shear modulus profile is obtained by measuring the dispersion of the shear waves using Fourier-transformed time records and spectral analysis to obtain phase information.

This study utilized the Portable Seismic Properties Analyzer (PSPA) for assessing the impact of stripping on the variation of HMA modulus with depth. The PSPA uses two methodologies to evaluate the bound layer properties:

- Ultrasonic Surface Waves (USW) - measures the stiffness of the bound layer
- Impact Echo – measures the thickness of the bound layer or identifies delaminated areas.

When the surface of a material, such as HMA, is impacted with a point source, body and surface waves propagate in the material. The focus of this study is primarily on the use of the surface waves. Surface waves contain about two-thirds of the seismic energy generated within a layer, thus the analysis is more

robust. Because surface waves propagate along a cylindrical front, the depth of inspection can be readily controlled.

The goal with seismic methods is to measure the propagation velocity of waves within a medium. The propagation velocity is theoretically related to the linear elastic modulus of a material. The relationship between velocity (V), travel time (Δt), and receiver spacing (ΔX) can be written in the following form:

$$V = \frac{\Delta X}{\Delta t} \quad \text{Equation 1}$$

In this equation, V can be the propagation velocity of any of seismic waves, i.e., compression wave (V_p), shear wave (V_s), or surface (Rayleigh) wave, (V_R). Knowing any one wave velocity, the modulus can be determined using appropriate transformations. V_s can be used to determine shear modulus, G , using

$$G = \rho V_s^2 \quad \text{Equation 2}$$

where ρ is mass density. Young's modulus, E , which is the primary parameter of interest to pavement engineers, can be determined from shear modulus, through the Poisson's ratio, ν , using

$$E = 2(1 + \nu)G \quad \text{Equation 3}$$

To obtain the modulus from V_R , it must first be converted to shear wave velocity using

$$V_s = V_R(1.13 - 0.16\nu) \quad \text{Equation 4}$$

Young's modulus is then determined by using Equations 2 and 3.

USW Method. The USW method, an offshoot of the Spectral Analysis of Surface Waves (SASW) method (Nazarian et al., 1997) is used to obtain the modulus of the HMA. As sketched in Figure 2-5, at wavelengths less than or equal to the thickness of the uppermost layer, the velocity of propagation is independent of wavelength. Therefore, if one simply generates high-frequency (short-wavelength) waves, and if one assumes that the properties of the uppermost layer are uniform, the shear wave velocity of the upper layer can be determined from

$$V_s = (1.13 - 0.16\nu)V_{ph} \quad \text{Equation 5}$$

where V_{ph} is the phase velocity of surface waves. The modulus of the top layer, E_{field} , can be determined from

$$E_{field} = 2\rho V_s^2(1 + \nu) \quad \text{Equation 6}$$

The wavelength at which the velocity of individual frequency component (phase velocity) is no longer constant is closely related to the thickness of the top layer (NCHRP, 1996).

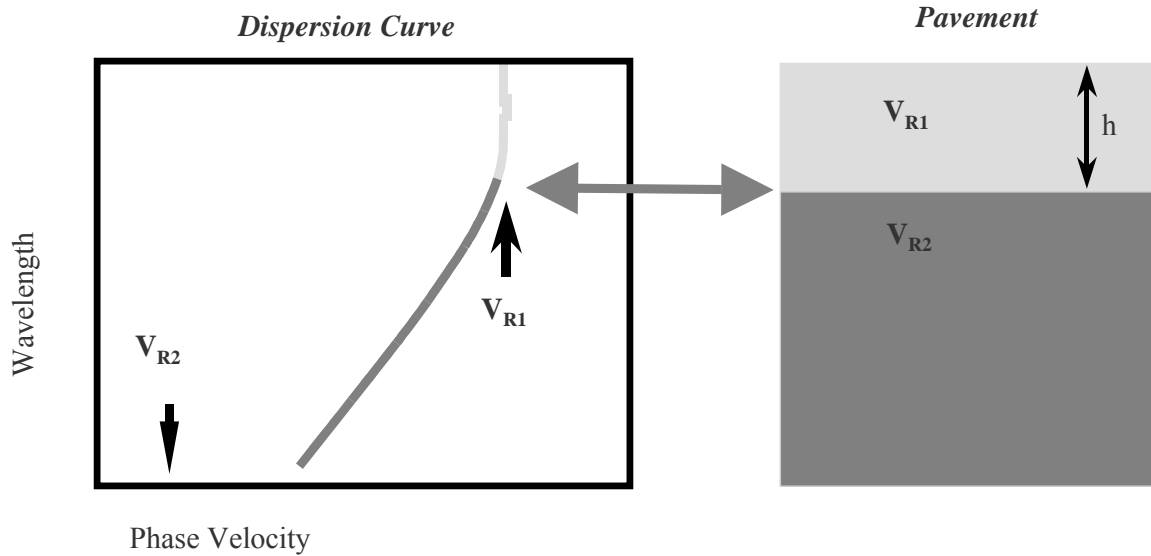


Figure 2-5. Schematic of USW method

Figure 2-6 shows typical time-history records from an HMA site. From these records, phase spectra, shown in Figure 2-7, are calculated by conducting Fourier transform and spectral analysis on the time records from the two sensors. Two phase spectra are shown: one measured from the time records and the other that represents the best estimation of the phase when the effects of the body waves are removed. The second one is used to compute the dispersion curves shown in Figure 2-8 (Nazarian and Desai, 1993). The actual dispersion curve (variation in velocity with wavelength) is presented in Figure 2-8a. As approximated by the solid line, the phase velocity is reasonably constant for the first 3 inches, below which the phase velocity tends towards lower values with depth. One can conclude that the average phase velocity is about 4200 fps and the approximate thickness is about 3 inches. The second dispersion curve (Figure 2-8b) shows the calculated modulus obtained from the phase velocity using Equations 5 and 6.

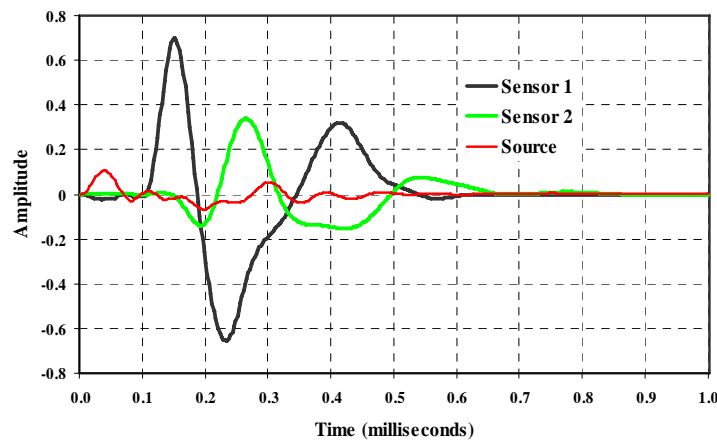


Figure 2-6. Typical time records from an HMA site

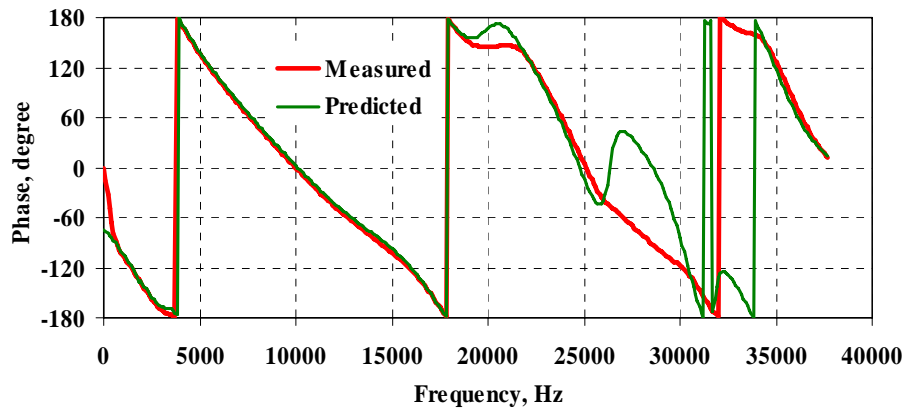


Figure 2-7. Phase spectra obtained from time records in Figure 2-6

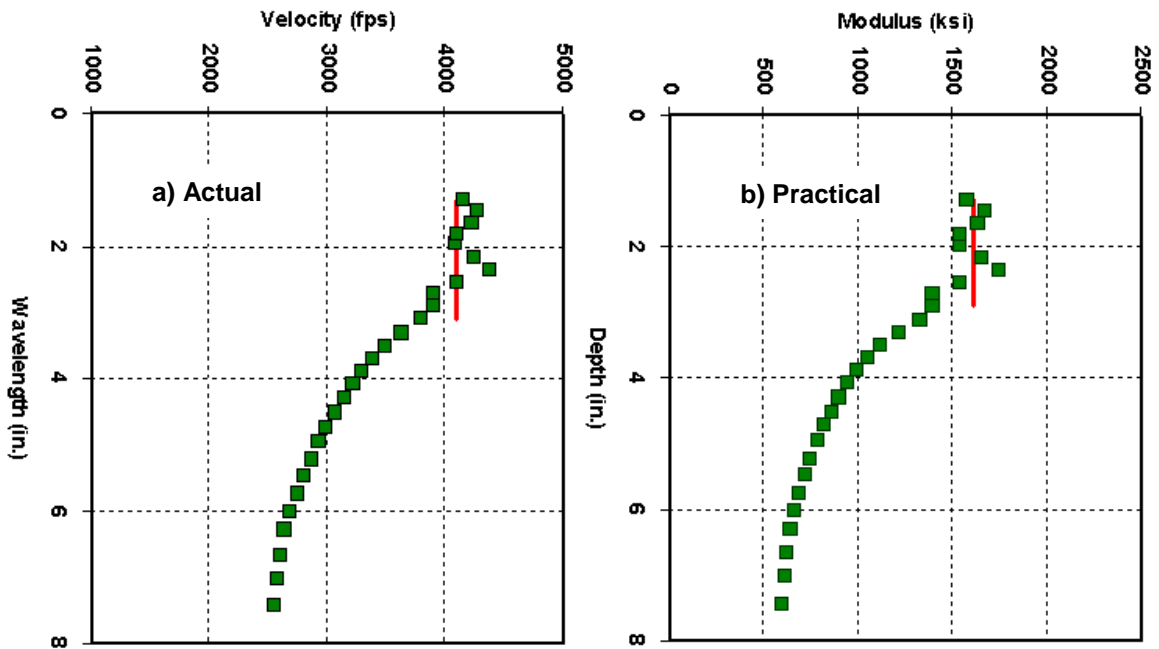


Figure 2-8. Typical dispersion curve

Impact Echo Method. The Impact Echo method primarily provides information about the thickness of a layer. Sansalone and Carino (1986) have also used the method to locate defects, voids, cracks, and zones of deterioration within concrete. As detailed in Nazarian et al. (1997), the method is not applicable to relatively thin layers and layers where the difference in moduli of adjacent layers is small.

The method, as sketched in Figure 2-9, is based on detecting the frequency of the standing wave reflecting from the bottom and the top of the top pavement layer. Upon impact, some of the source energy is reflected from the bottom of the layer, and some is transmitted into the base and subgrade. Since the top of the layer is in contact with air, almost all of the energy is reflected from that interface. The receiver senses the reflected energy at periodic time intervals. The period depends on the thickness and compression wave velocity of the layer. To conveniently determine the frequency associated with the periodic arrival of the signal, one can utilize a fast Fourier transform algorithm. The frequency

associated with the reflected wave appears as a peak in the amplitude spectrum. Using the compression wave velocity of the layer (V_p) the depth-to-reflector, h , can be determined from

$$h = \frac{V_p}{2f} \tag{Equation 7}$$

where f is the resonant frequency obtained by transforming the time record into the frequency domain. The compression wave velocity can be determined if the surface wave velocity is known as follows:

$$V_p = \frac{V_R \sqrt{\frac{1-\nu}{1/2-\nu}}}{0.13-0.16\nu} \tag{Equation 8}$$

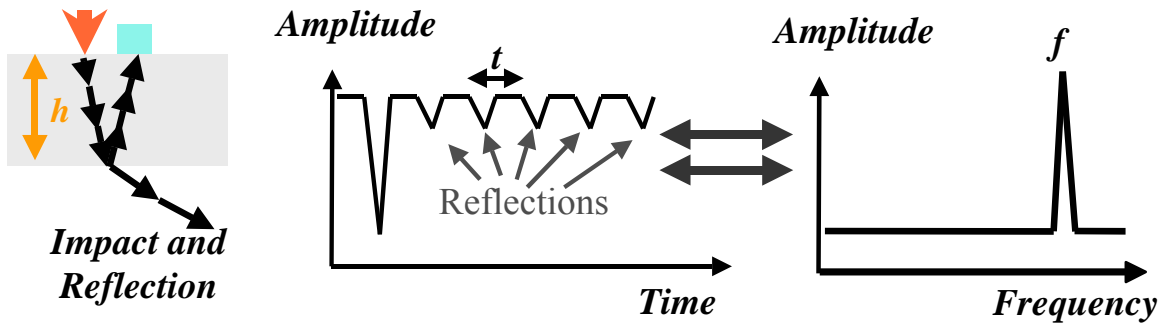


Figure 2-9. Schematic of impact echo method

2.5.2 Equipment

The PSPA was used in this study to implement the methodologies described above. With the PSPA, the average modulus of the exposed surface layers can be estimated within a few seconds in the field. In addition, the variation in modulus with depth can be qualitatively investigated. The PSPA, shown in Figure 2-10, consists of two transducers (accelerometers in this case) and a source packaged into a hand-portable system. The source package is also equipped with a transducer for consistency in triggering and for some advanced analysis of the signals. The device is operable from a computer connected to the hand-carried transducer unit by a cable that carries operational commands to the PSPA and returns the measured signals to the computer.

The operating principle of the PSPA is based on generating and detecting stress waves in a medium. The USW interpretation method, which is implemented in the Spa Manager software in the PSPA computer, is used to determine the modulus of the material.

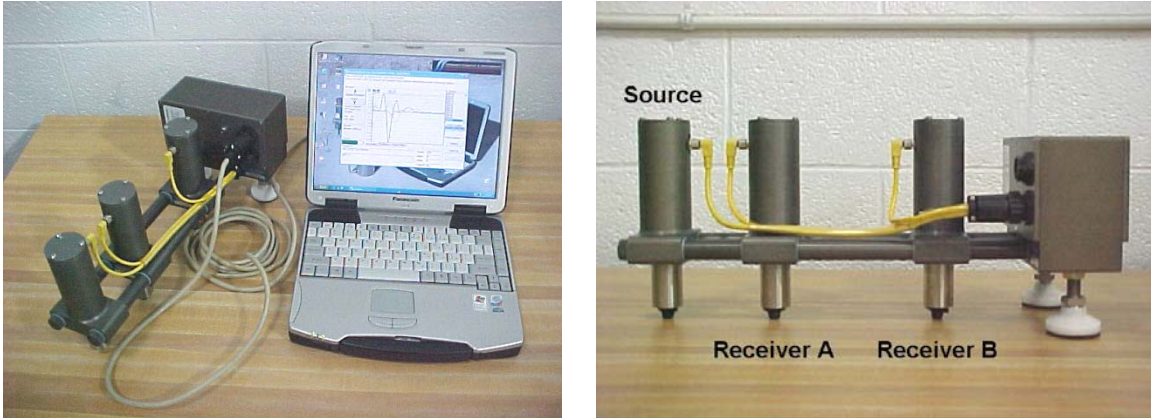


Figure 2-10. Portable Seismic Properties Analyzer (PSPA)

Moduli obtained with seismic measurements are low-magnitude, high-strain-rate values. Vehicular traffic causes relatively high magnitude deformation at low strain rates. Because of the difference, there has been concern in the pavement community regarding how to implement seismic moduli in the design. This concern has been resolved by implementing a master curve concept, which tracks modulus over wide frequency range.

The most desirable way of calculating the design modulus is to develop the master curve based on the recommendations of Witczak et al. (1999). The response of a viscoelastic material, such as HMA, is dependent on the loading frequency and temperature. The general practice has been to perform the testing at various temperatures with similar loading frequencies. A master curve is generated at a reference temperature by using time-temperature shift factors. The following sigmoid function proposed by Ferry (1970) can be used to generate a master curve

$$\log(E^*) = \delta + \frac{\alpha}{1 + e^{\beta + \gamma \times \log t_r}} \quad \text{Equation 9}$$

where E^* is dynamic modulus, t_r is the loading period, δ is the minimum value of dynamic modulus, $\delta + \alpha$ is the maximum value of dynamic modulus, and β and γ are sigmoid function shape parameters. Once the master curve is established, the design modulus can be readily determined from the design vehicular speed and the design temperature. Parameters α , β , γ and δ should preferably be obtained from complex modulus tests. However, in the absence of laboratory testing, Mirza and Witczak (1995) have proposed relationships for obtaining values of α , β , γ and δ from volumetric information about a mixture. Tandon et al. (2004) have shown that the seismic modulus and the master curve from complex modulus correlate well.

Since laboratory testing was not in the scope of this study, the approximate procedure by Aouad et al. (1993), Li and Nazarian (1994) was used to obtain the design modulus. The relationship suggested by Li and Nazarian (1994) for adjusting the modulus of AC to a reference temperature of 77° F (25° C) is used here. That relationship is in the form of

$$E_{77} = \frac{E_t}{1.35 - 0.0078(t - 32)} \quad \text{Equation 10}$$

where E_{77} and E_t are the moduli at 77° F and temperature t (in Fahrenheit). Aouad et al. (1993) have developed an empirical relationship between seismic modulus and design modulus. For a temperature of 77° F (25° C), the design modulus is obtained by dividing the seismic modulus by a factor of 3.2.

2.5.3 Method

To collect data with the PSPA, the technician initiates the testing sequence through the computer. All other data acquisition tasks are handled automatically by the computer. The high-frequency source is activated four to six times. Pre-recording impacts of the source are used to adjust the gains of the amplifiers in a manner that optimizes the dynamic range of the electronics. The outputs of the three transducers from the final three impacts are saved and averaged.

2.6 FWD

2.6.1 Hypothesis

Recent work by Lukanen and Stubstad has shown that “near plate” deflection basin shape factors are sensitive to the bound layer stiffness properties and are reasonably independent of the stiffness of the underlying layers. The selection of this test method was based on the premise that moisture-damaged HMA will have lower stiffness than sound HMA. The intent for using the FWD was to identify whether it can be used as a verification or ground-truth testing method to supplement the visual, IR, and GPR data.

2.6.2 Equipment

The FWD is a rapid, nondestructive means of determining a deflection basin response to a measured dynamic load with amplitudes similar to those imposed by trucks. The FWD consists of a mass mounted on a vertical shaft and housed in a trailer that can be towed by automobile or light truck. The FWD generates an impulse load by dropping a mass from different heights. By varying the drop height and mass, a force of 1,500 to 24,000 lb can be applied to highway pavements. The drop weight falls directly onto the rubber buffers that control the load pulse time. The resulting impulsive load on the pavement approximates a half sine wave. The loading plate is equipped with a strain-gage type load cell to measure applied force. The pavement surface deflection is measured by electronic integration of the signals from seven velocity transducers (geophones). Typically, one geophone is located at the center of the load plate while the remaining six are located along an array emanating from the center of the loading plate.

2.6.3 Method

The sensor spacing used in this research, shown in Figure 2-11, was the same as that used by the Federal Highway Administration (2000) for the Long-Term Pavement Performance (LTPP) study. The LTPP FWDs utilize nine deflection sensors placed at radial offsets from the center of the load as shown in Figure 2-11.

Four drop heights are used in a manner similar to the LTPP flexible pavement studies as indicated in Table 2-2.

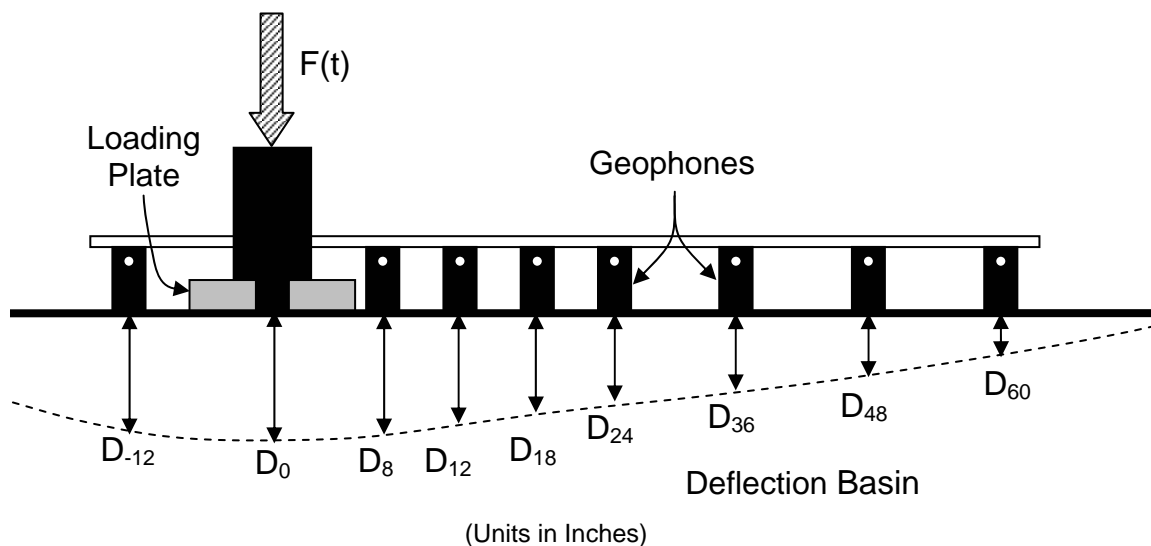


Figure 2-11. Sensor configuration for FWD testing

Table 2-2. FWD loading sequence

Drop Sequence Number	Target Load, kips	Comment
1	6.0	Seating Load (not recorded)
2	6.0	Seating Load (not recorded)
3	6.0	Production Load
4	6.0	Production Load
5	9.0	Production Load
6	9.0	Production Load
7	12.0	Production Load
8	12.0	Production Load
9	16.0	Production Load
10	16.0	Production Load

A forward calculation technique was utilized to calculate the bound layer stiffness from the FWD deflection basin using closed-form solutions. This technique assumes that the bound layer modulus is primarily a function of the near-load deflections as described by the radius of curvature of the deflection basin. Because the resulting surface course stiffness is independent of the moduli of other layers within the pavement system, a unique solution is obtained. However, because the surface course stiffness is calculated independently of the other layers in the pavement structure, in combination the values obtained may or may not be reasonable with respect to the total center deflection.

The forward calculation method chosen was first introduced by Stubstad (2002). This approach is based on the “AREA” concept (a deflection basin curvature index) and the overall composite modulus of the entire pavement structure, E_0 , as defined by Equation 11.

$$E_0 = 1.5 \frac{as_0}{d_0} \quad \text{Equation 11}$$

where:

- E_0 = composite modulus of the entire pavement system beneath the load plate
- a = radius of FWD load plate
- s_0 = (peak) pressure of FWD impact load under the load plate
- d_0 = (peak) center FWD deflection reading

Equation 11 has been extensively used over the past three to four decades (Ullidtz 1987). It assumes a uniform FWD load and a Poisson's ratio of 0.5. Generally, Poisson's ratio will be less than 0.5, while the distribution of the load under the FWD plate will not be truly uniform. These two offsetting factors have resulted in the widely used and straight-forward "1.5 times" composite modulus formula in Equation 11.

For HMA surface layers the AREA term is based on the deflection of the FWD sensors placed at 0-, 8-, and 12-inch offsets as follows:

$$AREA_{AC} = 2 \left(2 + 3 \frac{D_8}{D_0} + \frac{D_{12}}{D_0} \right) \quad \text{Equation 12}$$

where

- $AREA_{AC}$ = “area” beneath the first 12 inches of the deflection basin
- D_0 = FWD deflection measured at the center of the FWD load plate
- D_8 = FWD deflection measured 8 inches from the center of the plate
- D_{12} = FWD deflection measured 12 inches from the center of the plate.

Recent work by Stubstad and Lukanen has shown that the AREA method may be improved by introducing a correction factor derived from elastic layer theory calculations. The correction factor is given by

$$AF_{AC} = \left(\frac{0.752}{1.752 - \frac{AREA_{AC}}{6.85}} \right)^{1.35} \quad \text{Equation 13}$$

where AF_{AC} is an AREA factor, i.e., the "improvement" in $AREA_{AC}$.

Equation (3) can be thought of as a "radius of curvature" stiffness index, based on the stiffness of the bound upper layer(s) compared to the composite stiffness of the underlying unbound layers.

Finally, combining Equations 11 and 13 such that the boundary conditions are correct using the logic of the AREA concept, the stiffness of the bound HMA layer can be given by

$$E_{AC} = \frac{E_0 \cdot AF_{AC} \cdot k_3^{1/AF_{AC}}}{k_3^2} \quad \text{Equation 14}$$

where

E_{AC} = stiffness or modulus of the upper AC (bound) layer(s);

k_3 = thickness ratio of upper layer thickness / load plate diameter = $h_1 / (2a)$.

Equation 14 has been calibrated using a large number of trial elastic layer theory calculations, and it works well for typical materials and modular ratios. Nevertheless, this approach is not totally rigorous or scientific, but rather is empirical in nature. The approach can therefore be used effectively to approximate the relative stiffness of the uppermost bound layer(s) in a pavement cross section for comparative purposes.

2.7 GPR

2.7.1 Hypothesis

GPR operates by transmitting short pulses of electromagnetic energy into the pavement using an antenna attached to a survey vehicle traveling at normal driving speed. These pulses are reflected back to the antenna with an arrival time and amplitude that is related to the location and nature of discontinuities in the material (air/asphalt or asphalt/concrete, reinforcing steel, etc). The reflected energy is received in the form a series of pulses that are referred to as the radar waveform. The waveform contains a record of the properties and thickness of the layers within the deck.

GPR measures changes in the dielectric properties of pavement layers and the velocity of wave propagation within those layers. In a study on Texas highways, Scullion and Rmeili (1997) found that GPR technology was effective at detecting stripping in HMA layers where the deterioration was at a moderate or advanced stage. HMA that has stripped has higher moisture contents or higher air voids, or both. The dielectric constant of the material is affected by both moisture content and air voids, as is the velocity of wave propagation.

In the GPR data analysis, stripping can be identified as a layer within the asphalt structure that displays a reduced dielectric permittivity. Previous studies have shown (Scullion and Rmeili, 1997) that the occurrence of stripping results in increased void content, which leads to an anomalous change in the dielectric constant of the stripped layer. This reduction is identified from the amplitude of the GPR reflections from the layer boundaries that surround the stripped layer. Using this algorithm, a threshold reflection level is established so that the areas identified as stripped matched the results from available cores. The results of this analysis can be quantified and plotted on a linear or plan area plot. The key to establishment of this algorithm is to identify the appropriate thresholds for each of the observed asphalt

layers. The algorithm thus depends on the layer structure for the particular pavement, and is site dependent.

2.7.2 Equipment

The GPR surveys were carried out using a vehicle-mounted GSSI model 4108 air-coupled 1 GHz horn antenna controlled by a SIR-20 data acquisition and control unit. A photo of the survey vehicle and equipment is shown in Figure 2-12. The vehicle was set up with a movable antenna mounting so that the antenna could be positioned over the left wheel path, right wheel path, or centerline of the vehicle. This permitted the vehicle to collect data for all of the passes without having to straddle lanes.

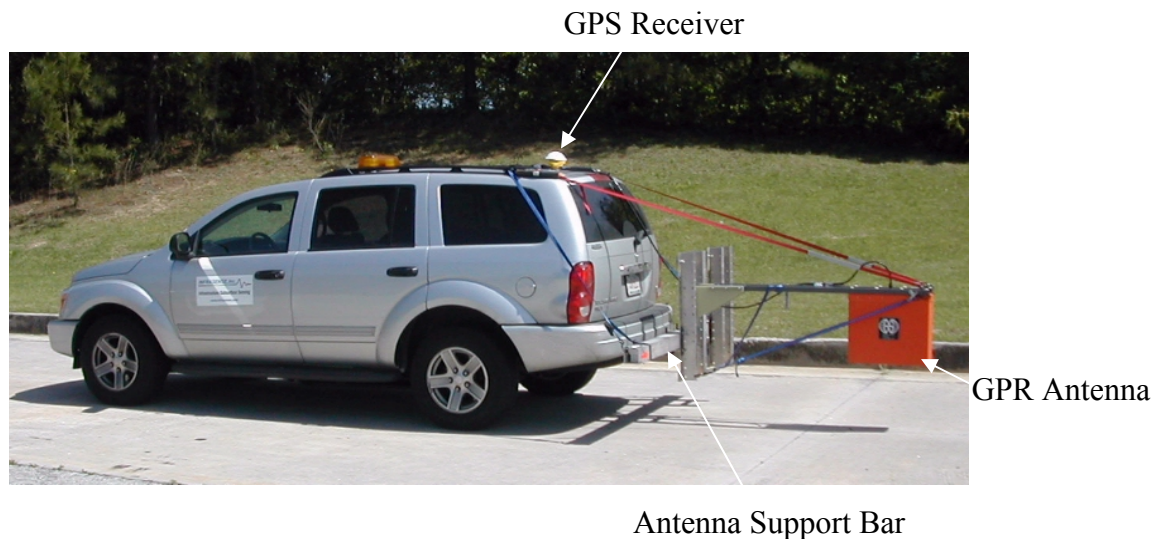


Figure 2-12. GPR survey vehicle

2.7.3 Method

GPR survey lines were collected in the wheel paths, centerline, and lane boundaries of each of the three lanes.

The GPR data was continuously digitized and stored at a controlled rate of 2 scans per foot. The acquisition rate was controlled by a wheel-mounted DMI, which was calibrated prior to the survey. The DMI produces 1000 pulses per vehicle wheel revolution. Using the calibration factor, the GPR system is triggered to record a scan every N pulses, where N is determined from the calibration factor and the scan rate setting. In addition to recording the GPR data, the SIR-20 also records the GPS station data and associated GPR scan numbers every second. The GPS station data were provided by a Trimble Ag114 differential GPS system with sub-meter accuracy.

During the survey, manual markers were placed in the data at mileposts and other reference locations for ground control of the radar distance measurements.

3 PHASE I: I-20 PILOT PROJECT

3.1 Pilot Project Hypotheses

The hypotheses for the Phase I pilot project are as follows:

1. The modulus of HMA is significantly affected by the level of moisture damage; i.e., the modulus of a mixture with moisture damage is significantly less than the modulus measured for the same mixture without any moisture damage. In addition, the HMA modulus will continue to decrease with increasing levels of moisture damage.
2. GPR technology can be used to identify areas with stripping in HMA.
3. Deflection basin data and seismic test results can be used to measure the modulus of HMA. These modulus values will be significantly affected by the level of moisture damage in the mixture.
4. The modulus values from the deflection basin and seismic data will result in similar values when adjustments for temperature and loading frequency are properly taken into account.

3.2 Pilot Project Description

3.2.1 Location

The I-20 pilot project was located on the west side of the Atlanta metropolitan area in Cobb, Fulton, and Douglas Counties. The approximate extent of the project is indicated by the box on the map in Figure 3-1. The project was limited to the eastbound lanes from the Sweetwater Creek Bridge (approximately MP 43.5) to the H.E. Holmes Drive exit (approximately MP 52). The GDOT had previously extracted approximately 40 cores from this section of the roadway.



Figure 3-1. Approximate extent of I-20 pilot project

Figure 3-2 shows a photograph of a typical section of the roadway. The eastbound roadway consists of three mainline travel lanes with an additional fourth outside lane in certain areas. In this study, the travel lanes are numbered sequentially with the inside lane being Lane 1. A variable-width (8 to 15 feet) asphalt concrete shoulder is to the right of the travel lanes with a grassy area to the outside of the paved shoulder. A paved asphalt concrete median of variable width (4 to 12 feet) with a Portland cement concrete barrier separates the eastbound from the westbound traffic lanes.



Figure 3-2. Photograph of I-20 eastbound lanes looking west

Although a total of 24 lane-miles made up the pilot project, only 4½ lane-miles of roadway were subjected to the full suite of tests because of constraints on traffic control in this high-volume traffic area. This section of highway consisted of Lane 3 (outside mainline travel lane) from the east end of Sweetwater Creek Bridge (approximately Station 820+00) to MP 48 (approximately Station 1057+00). This section at the western end of the pilot project was thought by GDOT to have the worst deterioration, and Lane 3 (heavily trafficked by trucks) was thought to be in the worst condition.

The topography of the roadway between Sweetwater Creek and MP 48 consists of two valleys separated by a ridge. Moving from west to east, the section starts in a region of lower elevation in the vicinity of Sweetwater Creek followed by an uphill grade beginning near the State Route 5 (Thornton Road) interchange. This uphill grade continues for approximately one mile, after which a gradual descent follows to the Chattahoochee River crossing just before Mile Post 48.

3.2.2 Construction History

Construction on the roadway was begun in late 1960 and completed in late 1964. The roadway originally consisted of two 12-ft wide travel lanes in each direction with a 4-ft wide inside shoulder and a 10-ft wide outside shoulder. The original traffic lanes were separated by a 64-ft-wide grassy median.

The original pavement structure consisted of 12 inches of compacted select borrow, 8 inches of pervious graded aggregate base (GAB), 10 inches of compacted cement-stabilized GAB, and 4½ inches of asphalt concrete. Perforated pipe underdrains (6 inches in diameter) were placed at selected locations as directed by the Engineer. The locations for the underdrains were selected in the field at the discretion of the Engineer depending upon the ground water conditions encountered during construction.

The original 4½ inches of asphalt concrete and the 10 inches of compacted cement-stabilized GAB were removed in 1974. The cement-stabilized based was replaced by 10 inches of asphalt concrete base. An asphalt concrete leveling course was placed on the surface of the asphalt concrete base, and a new 4½ inches of asphalt concrete were placed over the leveling course. This structure forms the basis for Lanes 2 and 3 of the pilot section.

The roadway was widened in the early 1980s. Additional travel lanes were constructed in the median and the concrete median barrier was added. The structure of these lanes (Lane 1 of the pilot section) includes 8 inches of graded aggregate base, 8 to 9 inches of asphalt concrete base, 4 inches of dense graded asphalt concrete, and a friction course placed at a spread rate of 60 lb/yd².

All traffic lanes were milled and inlaid in 1994. The milling depth varied from 2 inches near the roadway crown to 2¾ inches near the outside shoulder. The roadway was inlaid with a dense-graded asphalt concrete to restore the original profile. An open-graded friction course was placed on the surface at a spread rate of 75 lb/yd². The shoulders were overlaid with a dense-graded asphalt concrete at a thickness tapering from 2¼ inches at the shoulder point to 1½ inches at the shoulder's edge. All of the 1994 inlay and overlay mixes incorporated hydrated lime per the specifications.

3.2.3 Test Conditions

Field testing was conducted on the eastbound lanes of I-20 on April 26, 27, and 28, 2004. GDOT maintenance crews performed daytime lane closures on eastbound Lane 3 between MP 43.5 (Station 820) and MP 48 (Station 1058) on April 26th and 27th between the hours of approximately 9:00 AM to 2:30 PM. All seismic, FWD, and infrared thermography tests were performed during these lane closures. Because of the difficulties in performing lane closures on this heavily-trafficked urban interstate highway, the FWD, seismic, and infrared data were limited to the extent of the lane closure. GPR testing was performed in the flow of traffic at highway speeds on the evenings of April 26th and 27th. The surface distress data (including cracking, roughness, and rutting) were obtained during the daylight hours of April 28th in the flow of traffic at highway speeds. Because the surface distress and GPR data collection did not require traffic control, data were acquired on eastbound Lanes 1, 2, and 3 between Sweetwater Creek and H.E. Holmes Drive.

The weather conditions during the data collection were partly cloudy with mild temperatures. Table 3-1 presents the weather data from Atlanta's Hartsfield-Jackson International Airport (ATL) for the period of April 21 through April 28, 2004. The rainfall reported on April 26th occurred during the early morning hours and had moved out of the area by daylight.

Table 3-1. Weather conditions at ATL, April 2004

Date	High Temperature, °F	Low Temperature, °F	Mean Temperature, °F	Rainfall, inches
April 28, 2004	73	45	59	0.00
April 27, 2004	70	49	60	0.00
April 26, 2004	68	55	62	0.41
April 25, 2004	83	63	73	0.00
April 24, 2004	85	62	74	0.00
April 23, 2004	82	62	72	0.00
April 22, 2004	79	57	68	0.00
April 21, 2004	76	58	67	0.00

3.3 Test Results

3.3.1 Cores

3.3.1.1 Core Locations

Table 3-2 summarizes the information obtained from all cores extracted from I-20 the eastbound lanes by GDOT. All condition information data in the table was observed by GDOT technicians in the Research Office laboratories. The cores listed as having a deteriorated layer were those that had delaminated, while those listed in “Good Condition” were intact. The station numbers of the cores were identified from the digital photographs taken by the digital survey vehicle during the distress survey. The database of photographs of Lanes 1, 2, and 3 were sequentially searched and the locations of the cores were obtained within ± 3 feet of their actual locations. None of the cores in Lane 4 were found, because digital photographs of that Lane (primarily acceleration/deceleration lanes in the vicinity of exit ramps) were not obtained. A few of the cores in Lanes 1, 2, and 3 could not be reliably located in the photographs.

3.3.1.2 Observations from Cores

Appendix A contains photographs of all I-20 cores provided to the research team by GDOT. All forms or levels of moisture damage are present along the I-20 segment that was tested using various NDT technologies. Some cores are believed to have moisture damage but have not progressed to advanced stripping, while other cores began to disintegrate during the wet coring process (at least at specific layers beneath the surface.) Thus, the level of reduction in the modulus of the HMA layer from the baseline value should be expected to vary along the project. The baseline or target modulus value is defined as the average modulus for an intact, good quality HMA mixture without any moisture damage.

More importantly, not all layers show signs of moisture damage. The wearing surface and base (or lowest) layer are not believed to be susceptible to stripping, based on visual observations of the cores recovered along I-20. The layers showing signs of moisture damage are about 4 to 8 inches below the pavement surface. These different mixtures were placed at different times. This complicates the identification of moisture damage, because the baseline modulus value will vary with HMA depth. The same baseline value indicating a good quality HMA mix will be different for the different mixtures that exist along I-20. Thus, the expected baseline HMA modulus must be first estimated for the condition without any moisture damage. The baseline or target value will vary by temperature and loading frequency for each mix.

Table 3-2. I-20 Core results

Core No.	County	Lane	Base Material	Thickness of HMA, inches	Core Date	Station	Core Dia., inches	Core Condition (observed by GDOT)
1	Douglas	1	GAB	14.5	4/6/2003	822+34	4	Good Condition
2	Douglas	2	GAB	15.875	4/6/2003	821+06	4	Good Condition
3	Douglas	2	Soil Agg.	16.25	4/4/2003	841+36	4	Deteriorated layer at 4 inches
4	Douglas	3	Soil Agg.	16.25	4/1/2003	Not Found	6	Deteriorated layer at 5 inches
5	Douglas	3	Soil Agg.	17.375	4/4/2003	841+37	4	Deteriorated layer at 5 inches
6	Douglas	2	Soil Agg.	16.375	4/4/2003	851+60	4	Deteriorated layer at 5 inches
7	Douglas	3	Soil Agg.	16.75	4/4/2003	851+47	4	Deteriorated layer at 4 inches
8	Cobb	3	Soil Agg.	15.5	4/4/2003	876+92	4	Deteriorated layer at 4 inches
9	Cobb	4	Soil	15.25	4/4/2003	Not Found	4	Fair Condition
10	Cobb	1	GAB	16.375	4/6/2003	897+66	4	Good Condition
11	Cobb	3	Soil Agg.	16.75	4/4/2003	912+50	4	Deteriorated layer at 4 inches
12	Cobb	4	Soil	16.75	4/4/2003	Not Found	4	Deteriorated layer at 4 inches
13	Cobb	3	Soil	17.75	4/4/2003	921+67	4	Deteriorated layer at 4 inches
14	Cobb	4	Soil	17	4/4/2003	Not Found	4	Deteriorated layer at 4 inches
15	Cobb	2	Soil Agg.	18.75	4/4/2003	924+86	4	Fair Condition
16	Cobb	3	Soil Agg.	18.75	4/4/2003	923+49	4	Good Condition
17	Cobb	1	GAB	17	4/6/2003	950+37	4	Good Condition
18	Cobb	2	Soil	15.375	4/4/2003	970+86	4	Good Condition
19	Cobb	3	Soil	14.75	4/4/2003	949+10	4	Good Condition
20	Cobb	3	Soil	14.5	4/1/2003	981+22	4	Good Condition
21	Cobb	2	Soil	16.25	4/4/2003	990+93	4	Good Condition
22	Cobb	3	Soil	16.25	4/4/2003	1017+06	4	Good Condition
23	Cobb	1	GAB	15.875	4/6/2003	1003+49	4	Good Condition
24	Cobb	2	Soil	16.5	4/6/2003	1004+51	4	Good Condition
25	Fulton	1	GAB	16.875	4/6/2003	1057+47	4	Good Condition
26	Fulton	2	GAB	16.625	4/4/2003	1075+90	4	Good Condition
27	Fulton	3	Soil Agg.	12.625	4/4/2003	Not Found	4	Good Condition
28	Fulton	1	GAB	15	4/6/2003	1093+74	4	Good Condition
29	Fulton	3	Soil	17.75	4/1/2003	1095+48	4	Poor Condition
30	Fulton	2	GAB	18.75	4/4/2003	1098+82	4	Good Condition
31	Fulton	3	Soil	18	4/4/2003	1098+75	4	Poor Condition
32	Fulton	2	GAB	16.75	4/4/2003	1105+88	4	Good Condition
33	Fulton	3	Soil	17.25	4/4/2003	1105+78	4	Good Condition
34	Fulton	3	Soil Agg.	15.75	3/27/2003	1125+68	6	Good Condition
35	Fulton	4	Soil Agg.	15	3/27/2003	Not Found	6	Good Condition
36	Fulton	3	PCC	8	3/31/2003	1201+36	6	Good Condition
37	Fulton	4	PCC	7.5	3/31/2003	Not Found	6	Good Condition
38	Fulton	1	GAB	18.75	4/6/2003	1204+37	4	Good Condition
39	Fulton	2	PCC	8	4/4/2003	1206+25	4	Deteriorated layer at 3.75 inches
40	Fulton	3	PCC	7.75	4/4/2003	1205+98	4	Stripped at 4 inches
41	Fulton	2	PCC	7.5	3/27/2003	1221+20	6	Poor Condition
42	Fulton	3	PCC	8.75	3/27/2003	1220+63	6	Stripped at 4.5 inches
43	Fulton	1	GAB	19.125	4/6/2003	1237+71	4	Good Condition
44	Fulton	2	GAB	8.125	4/6/2003	1237+70	4	Deteriorated layer at 4 inches
45	Fulton	3	PCC	7.5	3/31/2003	1244+44	6	Good Condition
46	Fulton	4	PCC	7.25	3/31/2003	Not Found	6	Good Condition
47	Fulton	3	PCC	7	3/31/2003	1259+69	6	Good Condition
48	Fulton	4	PCC	7	3/31/2003	Not Found	6	Deteriorated layer at 2.5 inches
49	Fulton	1	GAB	16.75	4/6/2003	Not Found	4	Deteriorated layer at 3.25 inches
50	Fulton	2	PCC	6.875	4/6/2003	1260+84	4	Good Condition

Figure 3-3 shows the thickness profile along I-20 for each lane tested. As shown, Lane 3 does not have an abrupt change in layer thickness, while lanes 1 and 2 have a thinner HMA surface towards the end of the project (between stations 1100 and 1200).

The variation of HMA thickness encountered along I-20 will have a significant effect on the HMA layer modulus values calculated from the FWD deflection basins. This variation is not considered excessive for long projects where different construction activities have occurred within the project over time. However, the amount of variation in thickness that exists along I-20 will cause additional error in the calculated values when using average thickness values. This additional variation creates more noise in the data, making it more difficult to detect areas with moisture damage at different depths in the pavement structure.

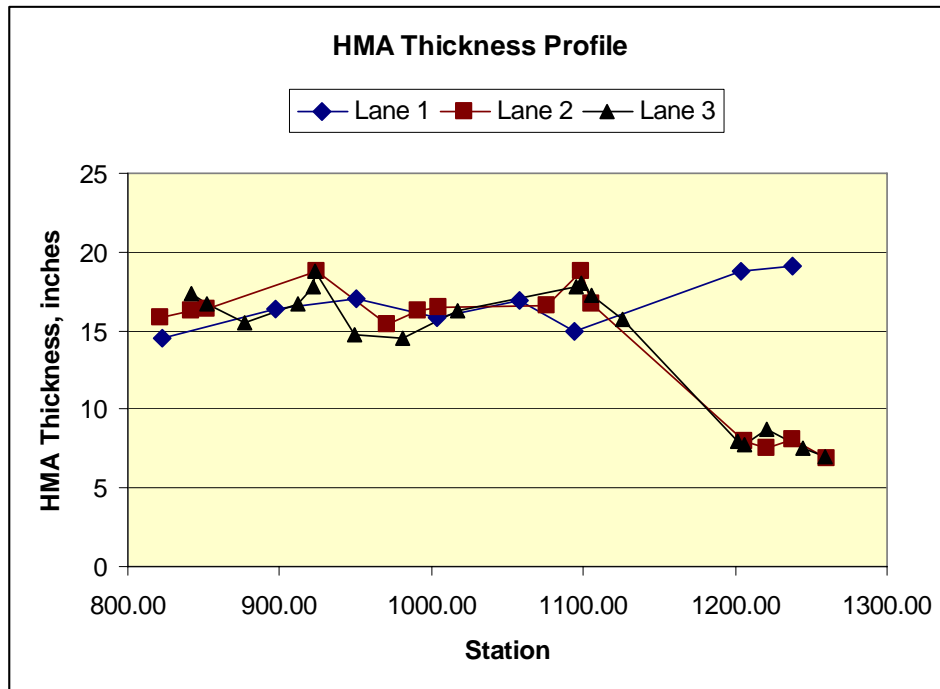


Figure 3-3. Longitudinal profile of I-20 HMA thickness as determined from cores

3.3.1.3 Laboratory Tests on Cores

Eight cores were selected from those recovered along I-20 and tested using various forms of the indirect tensile test (IDT). The cores were selected to cover the range of moisture damage in the binder or intermediate layer as defined by visual observations of the cores. Two test specimens were cut from each core, one test specimen from the HMA base layer and the other from the binder or intermediate layer. The type of indirect tensile tests performed on these test specimens included the dynamic modulus and strength test.

Appendix B presents stress-strain curves from the IDT. Table 3-3 summarizes the results from the laboratory tests including the dynamic modulus and phase angle at a frequency of 10 Hz and a temperature of 77°F, the indirect tensile strain at failure, the tensile strength, and Poisson's ratio. As summarized in Table 3-3, there is a significant difference in the dynamic modulus, tensile strength, Poisson's ratio, and phase angle for those test specimens that show signs of moisture damage and those that do not.

Table 3-3. Summary of laboratory test results on selected cores recovered from I-20

Core	HMA Layer & Condition	IDT Dynamic Modulus	Tensile Strain At Failure, mils/in.	Tensile Strength, psi	Poisson Ratio	Phase Angle
1	Base Mix; No Stripping; Intact	983.6	3.559	242	0.19	30.0
5	Base Mix; No Stripping; Intact	634.9	5.499	188	0.26	26.7
8	Base Mix; No Stripping; Intact	908.2	5.258	257	0.20	31.9
13	Base Mix; No Stripping; Intact	821.3	4.711	237	0.21	29.1
15	Base Mix; No Stripping; Intact	938.1	4.706	223	0.19	25.5
23	Base Mix; No Stripping; Intact	571.8	6.936	181	0.28	38.7
31	Base Mix; No Stripping; Intact	808.7	5.414	213	0.21	30.9
33	Base Mix; No Stripping; Intact	848.4	4.267	220	0.21	33.5
1	Intermediate Layer; Minor Stripping; Intact	1304.4	3.007	280	0.16	27.4
23	Intermediate Layer; No Stripping; Intact	733.2	6.073	210	0.23	27.6
5	Intermediate Layer; Heavy Stripping; Intact	320.1	5.339	91.7	0.36	36.5
8	Intermediate Layer; Heavy Stripping; Broke	299.2	8.796	93.9	0.37	35.1
13	Intermediate Layer; Heavy Stripping; Broke	436.7	5.858	111	0.32	35.6
15	Intermediate Layer; Minor Stripping; Broke	187.9	6.336	72.7	0.40	36.9
31	Intermediate Layer; Heavy Stripping; Broke	230.9	5.601	85.6	0.39	31.9
33	Intermediate Layer; Minor Stripping; Broke	213.1	6.491	90.6	0.39	35.2

3.3.2 Surface Distress

Although surface distress photographs and profile measurements were made of the Lanes 1, 2, and 3 between Sweetwater Creek Bridge and the H.E. Holmes Drive exit, only the data in Lane 3 between MP 43.5 and MP 48 were reduced for purposes of this report.

Virtually the entire surface of the roadway was observed to have moderate weathering and raveling of the friction course. For some of the sample units, the weathering and raveling achieved the severe level. There was no indication of flushing of stripped asphalt cement or pumping of stripped fines to the surface.

Figure 3-4 summarizes the cracking observed in the pilot section. The data points in the uppermost plot represent the total areal extent of alligator cracking severity levels in each 20-ft-long sample unit. To simplify the plot, all severity levels (low, medium and high) were summed to obtain the total areal extent of cracking. The smoothed curve in the plot is a moving average with a sampling window of approximately 1000 ft. By far, the area exhibiting the most alligator cracking was the first mile of the pilot section. An additional area of some significant alligator cracking was located in the 1½ miles of the section. These areas appear to correspond to areas of lower relative elevation.

The middle plot shows the total linear extent of longitudinal and transverse cracking. Here the data points represent the total length of longitudinal and transverse cracking of all severity levels in each 20-ft-long sample unit. The longitudinal construction joint to the right of Lane 3 was open to varying extents, resulting in a nearly continuous low to high severity longitudinal crack throughout the entire 4½ miles of the pilot project. The longitudinal joint between Lanes 2 and 3 was not included in the analysis. Again, the smoothed curve is a moving average with a sampling window of approximately 1000 ft. Other than the longitudinal crack along the construction joint, longitudinal and transverse cracking was most prevalent in the first mile and final 1½ miles of the pilot section.

The lower plot shows the elevation readings obtained from the digital survey vehicle. Also shown in the lower plot are the locations of the cores color-coded to indicate condition. An orange color indicates that the core was delaminated, while a green color indicates the core was intact. Comparing this plot with the plot of alligator cracking shows a correlation between the extent of fatigue cracking and elevation, confirming a qualitative observation made by the research team walking the pavement during the distress survey. While not universally true, it also appears that the longitudinal and transverse cracking is somewhat more extensive at lower relative elevations than at higher.

Transverse profile measurements were used to calculate the average rut depths in the left wheel path (LWP) and right wheel path (RWP) within each 20-ft-long sample unit. The average of the LWP and RWP rut depth was calculated, as well. The data points in Figure 3-5 shows the rut depths for the LWP, RWP, and the average rut depth. The smoothed curves are moving averages with a sampling window of approximately 1000 ft. It appears that the depth of rutting is greater at lower elevations than at the higher elevations.

The longitudinal profile measurements were used to calculate the IRI for 0.1-mi roadway segments in the LWP, RWP, and average of the LWP and RWP. These data are plotted in Figure 3-6. No discernable pattern emerges from these graphs with the possible exception of increased roughness near the end of the pilot sections. This may be due to the presence of several bridges in the last half-mile of the test section.

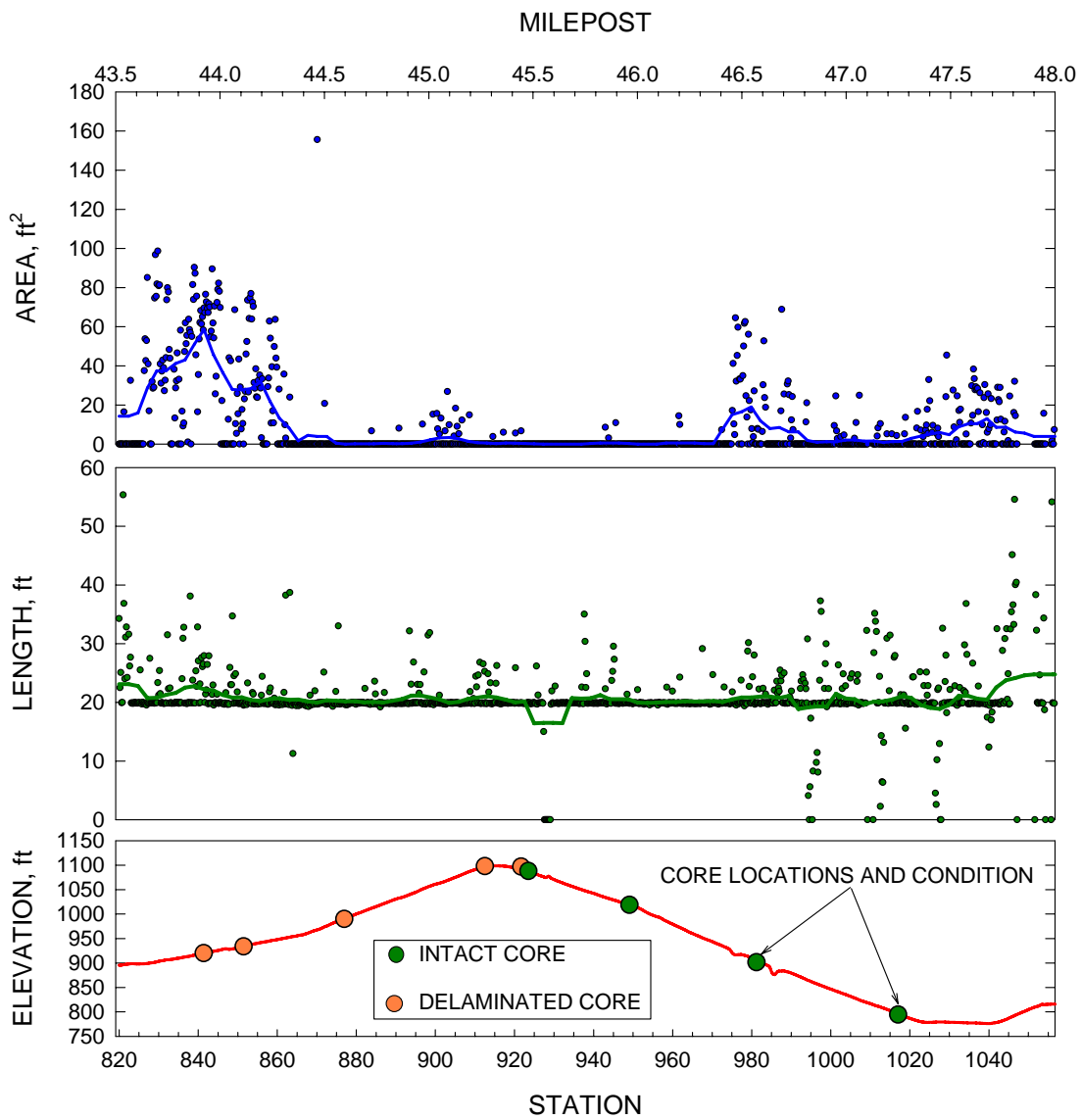


Figure 3-4. I-20 Lane 3 cracking summary plot

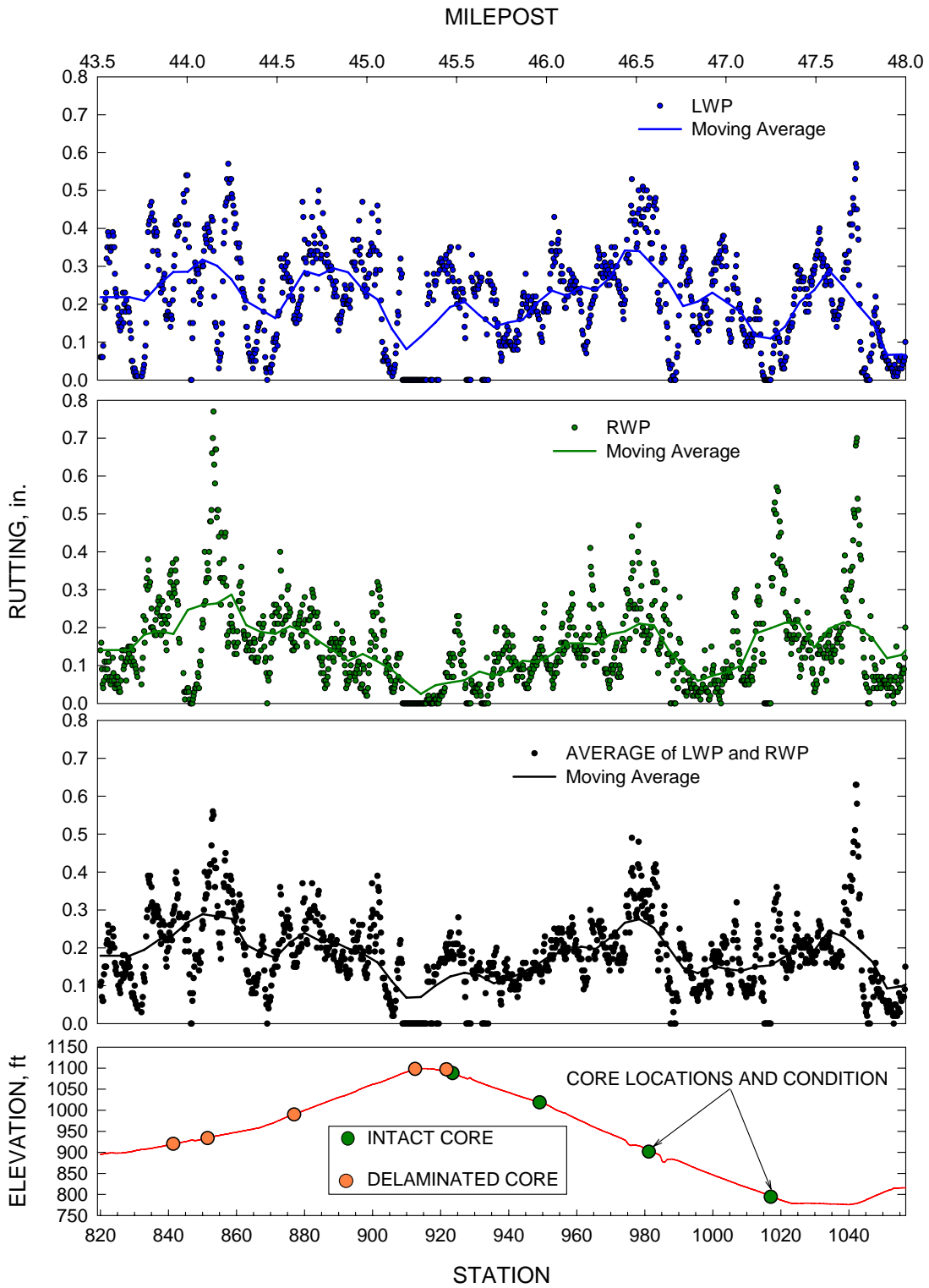


Figure 3-5. I-20 Lane 3 rutting summary plot

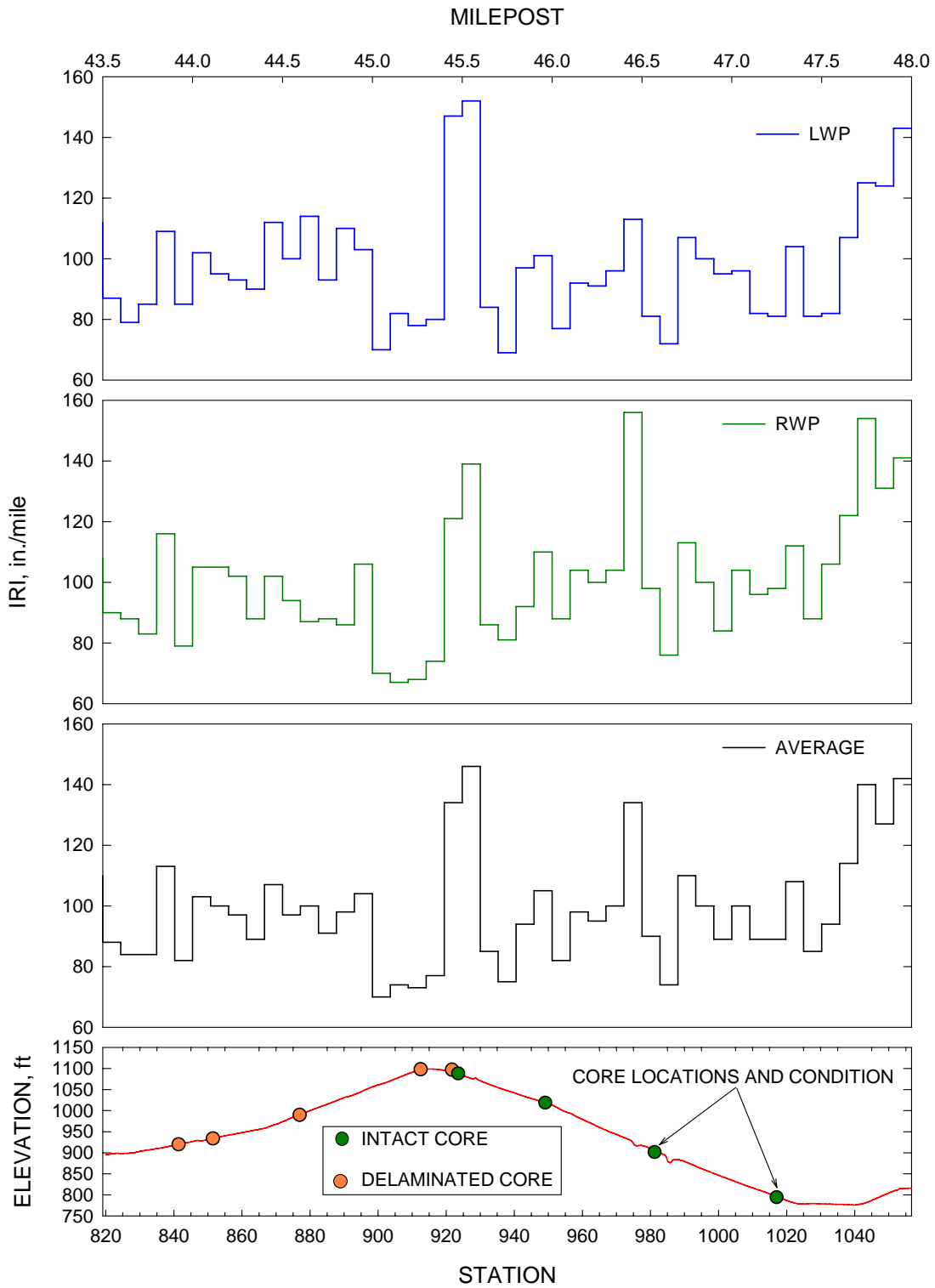


Figure 3-6. I-20 Lane 3 roughness summary plot

3.3.3 Infrared Thermography

Figure 3-7 shows a pair of images collected at 1191 feet from MP 46. The visual image is on the left, and the infrared image at the same location is on the right. The IR image includes a data bar on the left, which shows the temperature range setting of the camera (103.1°F to 114.2 °F), and the data, the time, and the assumed surface emissivity. Note that there is a cool spot on the IR image which does not correspond to any observable surface feature in the video image. This observation indicates that the cool spot is related to subsurface moisture or some other effect that would lower the surface temperature. The IR anomalies were generally localized, and were not as widespread as expected. None of the locations coincided with core locations, and therefore no correlation between these anomalies and the evidence of moisture damage was found.

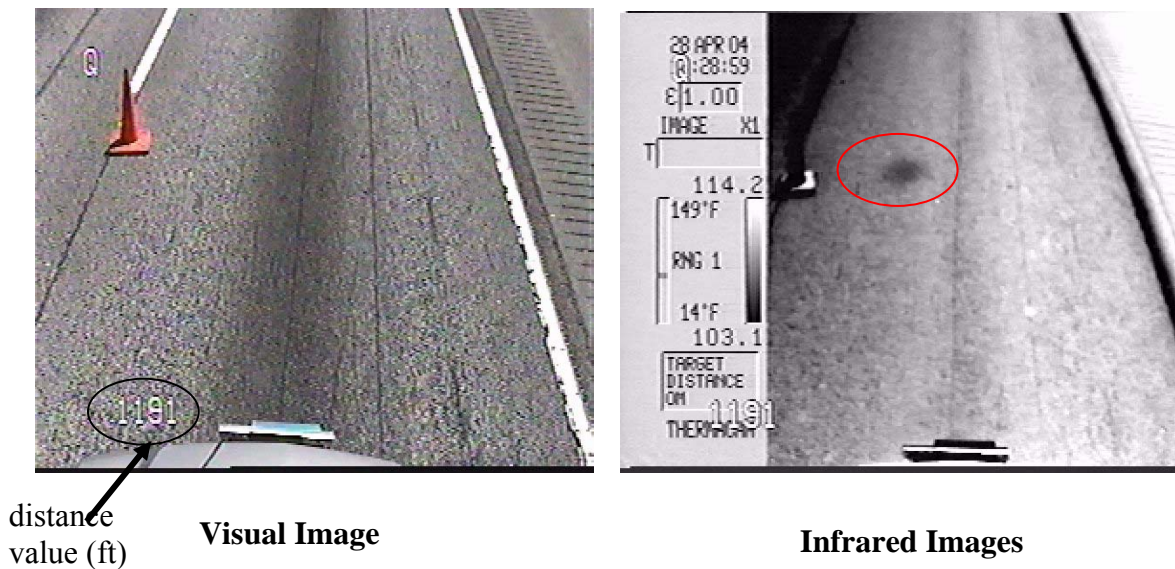


Figure 3-7. Visual and infrared camera images (potential stripping area highlighted in red).

3.3.4 Seismic

Seismic tests were carried out on eastbound Lane 3 of I-20 between MP 43.5 and 48 (Stations 820 through 1058) in two days. The tests were carried out at 200 ft intervals. A section of the road between Stations 908 and 934 was not tested on the first day because of an equipment malfunction. All seismic tests were carried out in the center of the travel lane to avoid areas with alligator cracking and rutting in the wheel paths.

A typical dispersion curve obtained with the USW analysis from the location of an intact core is shown in Figure 3-8a. The variation in modulus from a depth (wavelength) of 2 inches down to 12 inches is demonstrated. The maximum and minimum depths are controlled by the PSPA sensor spacing.

A straightforward but approximate manner of obtaining a representative modulus for the HMA layer at this location is to average the moduli presented in the figure. The solid line in the figure corresponds to this average value. To utilize this average value in the analysis, it was adjusted to a temperature of 77°F, and then it was converted to a design modulus using Aouad et al (1993) procedure described in Chapter 3.

For a comprehensive analysis of the results, the shape of the dispersion curve is also of importance. As reflected in the picture of the core in Figure 3-8a, the top 12 inches of the material consists of at least four different lifts. Had the materials from different lifts exhibited nearly uniform modulus, the dispersion curve would have exhibited a constant modulus with depth. From the measured dispersion curve, the top layer is reasonably stiff. Between wavelengths of 4 inches to 6 inches, the layer is of lower quality. Below 6 inches the quality of the material increases. The intermediate, low-quality material is evident in the core. It should be emphasized that the actual moduli from the second through fourth lift can only be obtained through a sophisticated backcalculation process. However, for the purpose of this study, this step is not necessary, because the trends in the data reveal the condition of the material.

Similarly, a typical dispersion curve from a deteriorated core location is shown in Figure 3-8b. Once again, the top layer is stiff. At the debonding depth the modulus drops significantly, which gradually increases in the lower intact material. Once again, there is rational correspondence between the shape of the dispersion curve and the locations of the deteriorated materials.

To further quantify the differences, the intact core was saw cut into distinct layers, and the seismic modulus of each layer was determined. The core pieces and their corresponding moduli are shown in Figure 3-9. A comparison of the original core (as shown in Figure 3-8a) with the saw cut one (in Figure 3-9) demonstrates that some of the slightly damaged materials between some layers had to be removed. Using the moduli in Figure 3-9, the simulated (theoretical) dispersion curve that would have been measured at this point was developed. The simulated and measured dispersion curves are compared in Figure 3-10. Considering experimental errors and approximation in the modeling process, reasonable agreement between the measured and simulated dispersion curves are observed. This exercise builds confidence in the results from the PSPA.

As shown in Figures 3-11 and 3-12, the same exercise was carried out with the deteriorated core. In this case the simulated dispersion curve is similar to the measured one for shorter wavelengths, but the two curves deviate significantly at longer wavelengths. This pattern demonstrates that the damage due to stripping is causing a significant drop in the modulus of the intermediate layers.

The variation in average modulus along the site is shown in Figure 3-13. The data are categorized into three groups: good, marginal and poor. Since the site was located on an interstate highway, we assigned a value of 600 ksi and above for a good-quality HMA layer. Very few points place in this category. The marginal category was considered as a material with an average modulus between 475 ksi and 600 ksi. As reflected in the figure, most points fall in this category. Finally a poor material is any material with a modulus less than 475 ksi. Several areas tested fall into this category.

The impact echo amplitude spectra obtained from the intact and deteriorated points are shown in Figure 3-14. The two spectra have similar peak frequencies. This is a unique situation at this site which infrequently occurs. For the intact core, the thickness is about 16 inches. For such a thickness, the return frequency is about 3 kHz. For the deteriorated condition, where the flexural mode of vibration is prevalent, the frequency is about 3.5 kHz. As such, the peak frequency of the impact echo is not a suitable parameter for locating severely deteriorated areas at this site. As shown in Figure 3-15, these spectra can be converted to thickness. In the case of the intact location, as shown in Figure 3-15a, the measured thickness is close to the thickness of the composite HMA layer. The differences lie in the method with which the velocity of the core was estimated. However, for the deteriorated area, the thickness is neither related to the thickness of the HMA layer nor the location of deterioration. Even though the peak frequencies are similar, the shapes of the amplitude spectra are rather different.

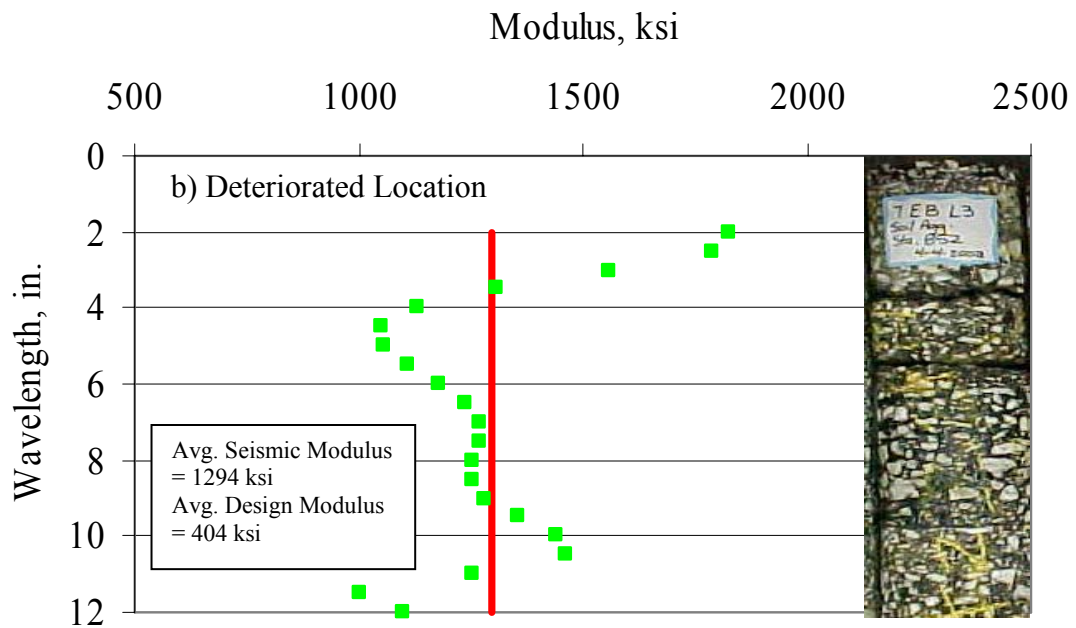
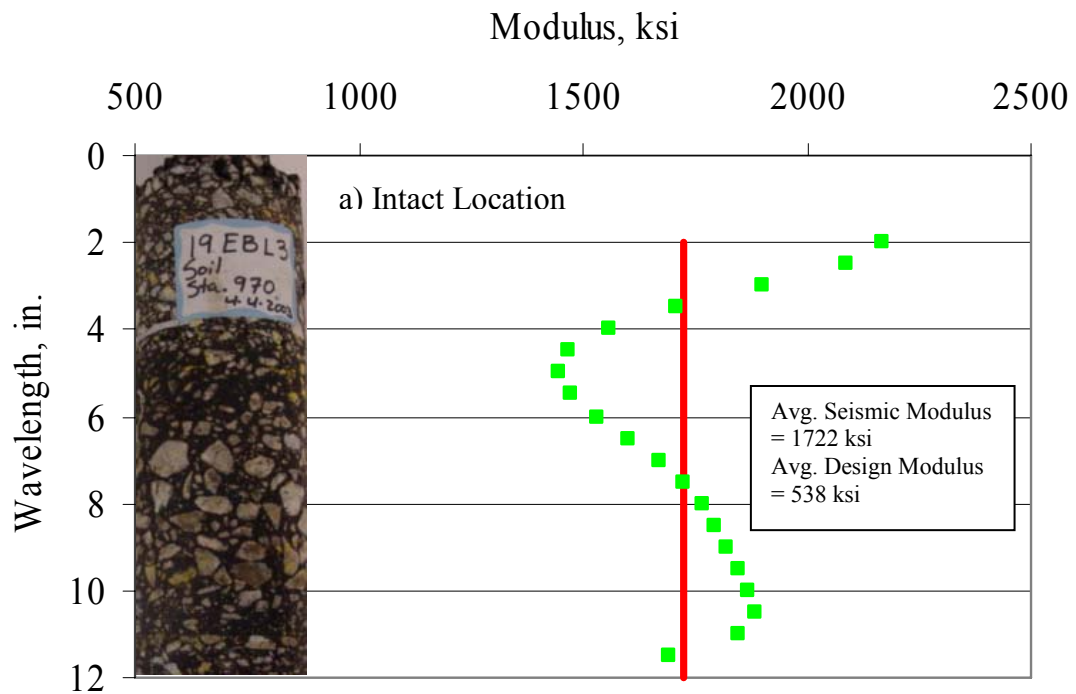


Figure 3-8. Typical dispersion curves from intact and deteriorated I-20 sections

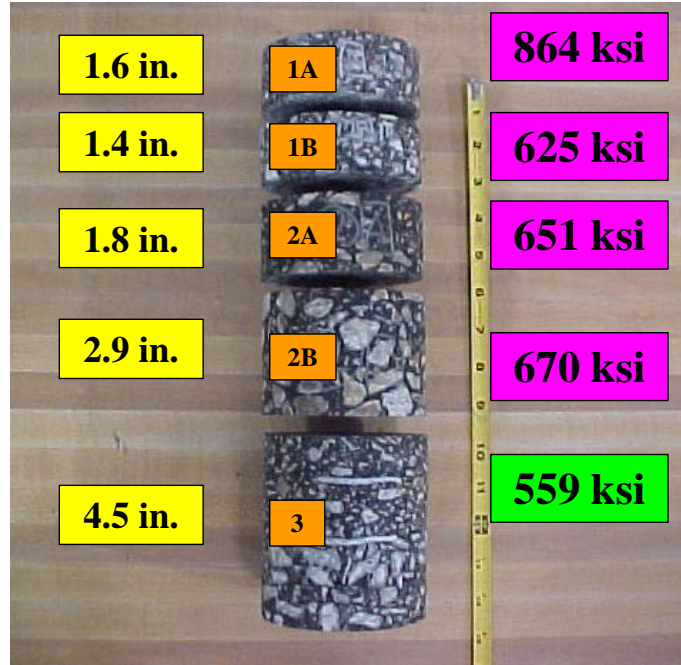


Figure 3-9. Variation in modulus of with depth for intact I-20 core

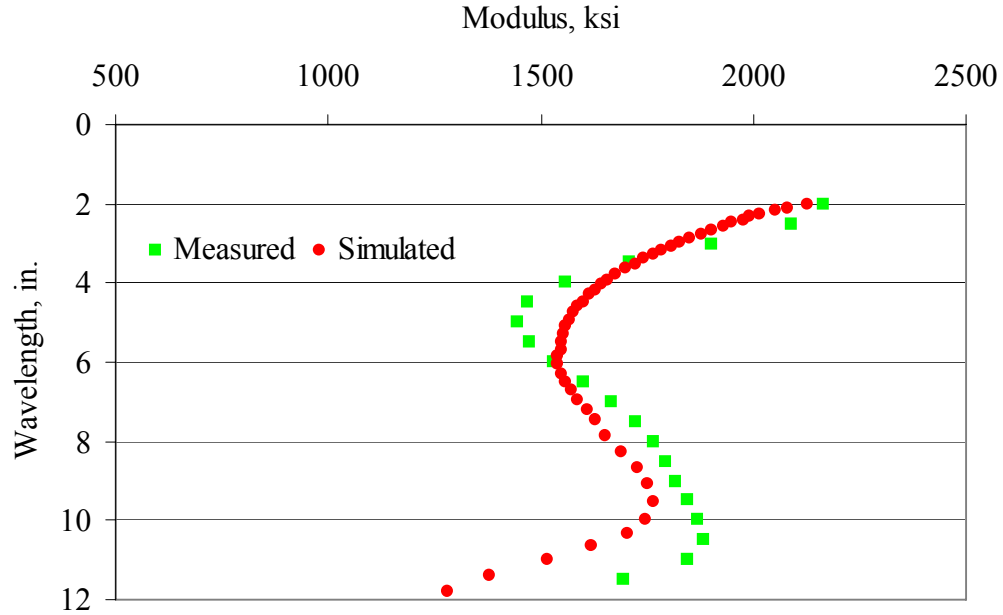


Figure 3-10. Experimental and theoretical dispersion curves from intact I-20 core

The modulus contour and the impact-echo contour maps along the site are shown in Figures 3-16 and 3-17 for the work performed on the first and second day, respectively. In the figures, the x-axes correspond to the milepost.

Figures 3-16a and 3-17a are three-dimensional representations of the dispersion curves obtained with the USW method. As such, the y-axes of these figures are wavelengths that are approximated as thickness. The color-coding used to represent the modulus is as follows:

- Dark Blue: High quality ACP (modulus of 650 ksi and above)
- Light Blue: Reasonable quality ACP (modulus range of 525 ksi to 650 ksi)
- Yellow: Below average quality ACP (modulus range of 400 ksi to 525 ksi)
- Red: Poor quality ACP (modulus of less than 400 ksi).

It should be emphasized that the red and yellow contours may occur for several reasons. The most obvious reason is low quality materials that were placed poorly or have experienced stripping. The second reason can be the debonding of the lower ACP layers from the upper one.

Figures 3-16b and 3-17b are the three-dimensional representations of the impact-echo amplitude. As such, the y-axes of these figures are frequency. The color coding, which used to represent the normalized amplitude is as follows:

- Dark Blue: Normalized amplitude less than 0.7
- Light Blue: Normalized amplitude between 0.7 and 0.8
- Yellow: Normalized amplitude between 0.8 and 0.9
- Red: Normalized amplitude between 0.9 and 1.0.

For tests conducted during the first day, as reflected in Figure 3-16a, the first 4 inches of the HMA layer is typically of good quality. The quality of the material below a depth of 4 inches varies. The underlying moduli are reasonable until MP 44.050, with some small exceptions. However, the impact echo demonstrates signs of deterioration in most of this area. Between MP 44.050 and 44.500, again with some small exceptions, the underlying materials are of lower quality. In this range, the most severe condition occurs around MP 44.400. Between MPs 44.500 and 44.700 the underlying materials are again of higher quality, with one exception at MP 44.590. The lower layers between MP 44.700 and 45.200 are again of lower quality, with materials around MP 44.800, 44.900, and 45+145 being severely deteriorated.

The results from Day 2 of field work are shown in Figure 3-17. Once again, the top 3 to 4 inches of the material is in good condition, while the materials between depths of 4 to 6 inches are of lower quality throughout. Several areas are of more concern. These include the material around MP 45.700, 46.300, and the region between MP 47.750 and 48.000. The area between MPs 47.150 and 47.750 are not severely deteriorated, but they are marginal.

In general, either deterioration due to stripping has occurred or the quality of the material below a depth of 4 to 6 inches is lower than the desirable values anticipated at the site.

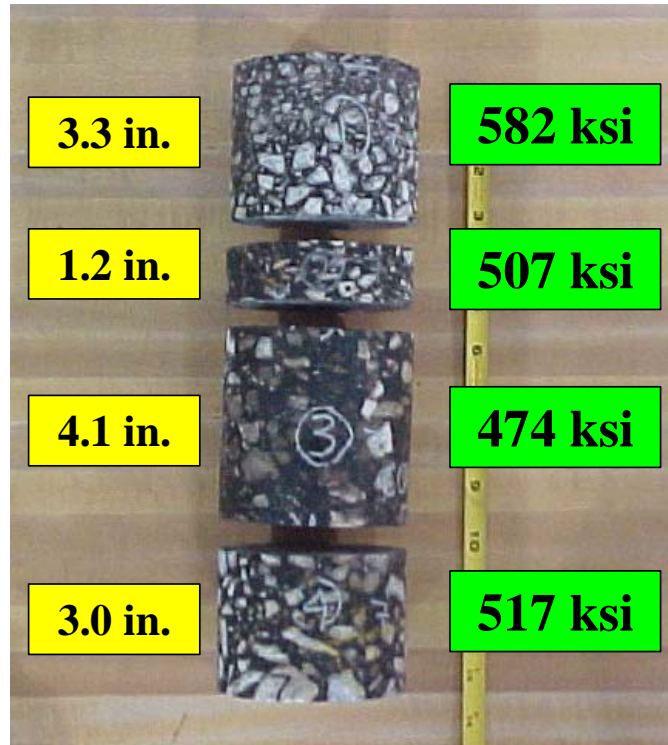


Figure 3-11. Variation in modulus of with depth for deteriorated I-20 core

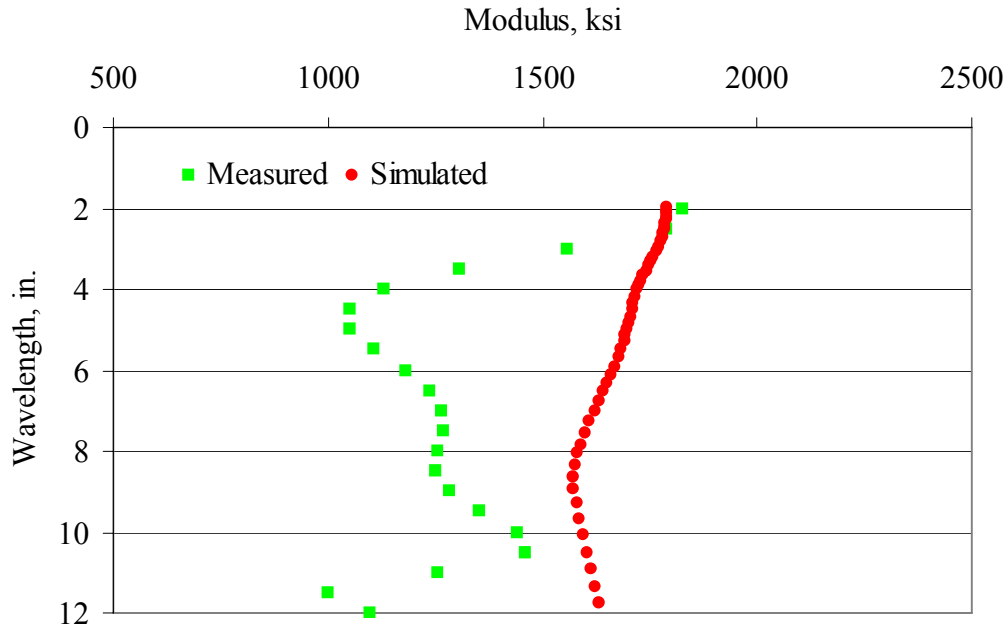


Figure 3-12. Experimental and theoretical dispersion curves from deteriorated I-20 core

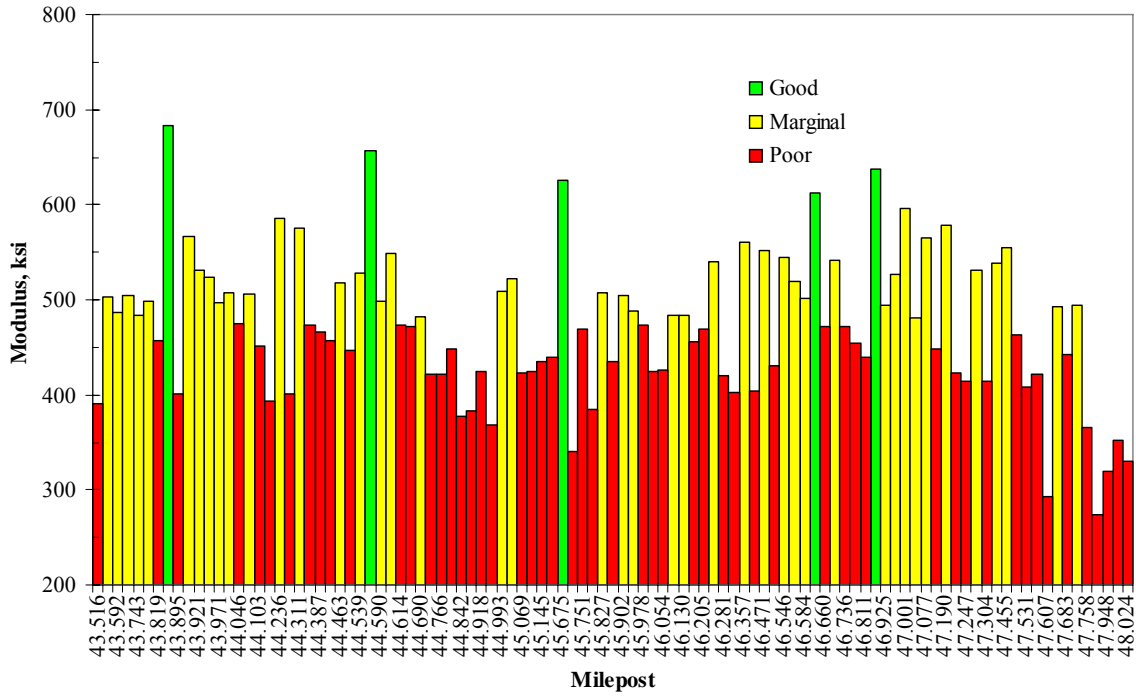


Figure 3-13. Variation in average modulus obtained with USW method along I-20 pilot project

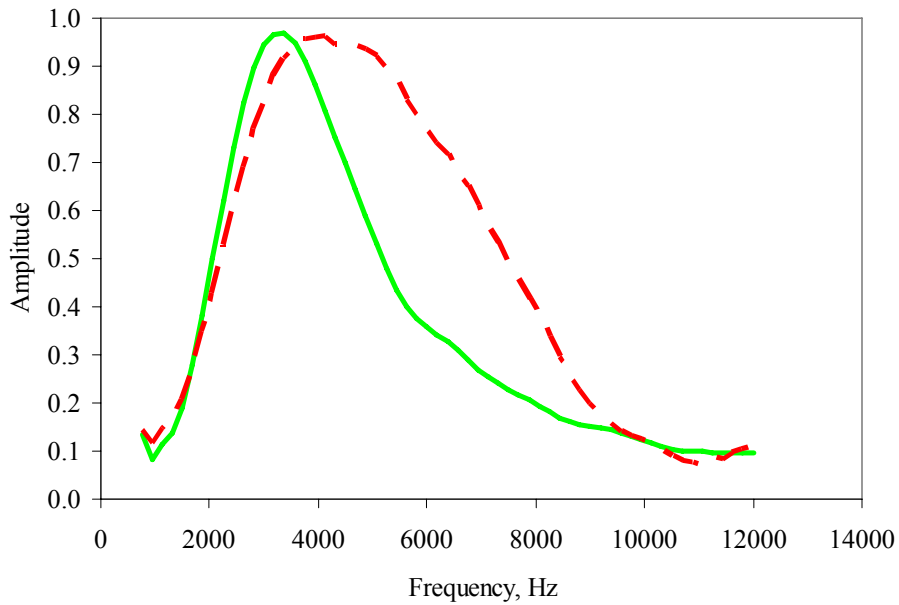


Figure 3-14. Impact echo amplitude spectra from intact and deteriorated locations

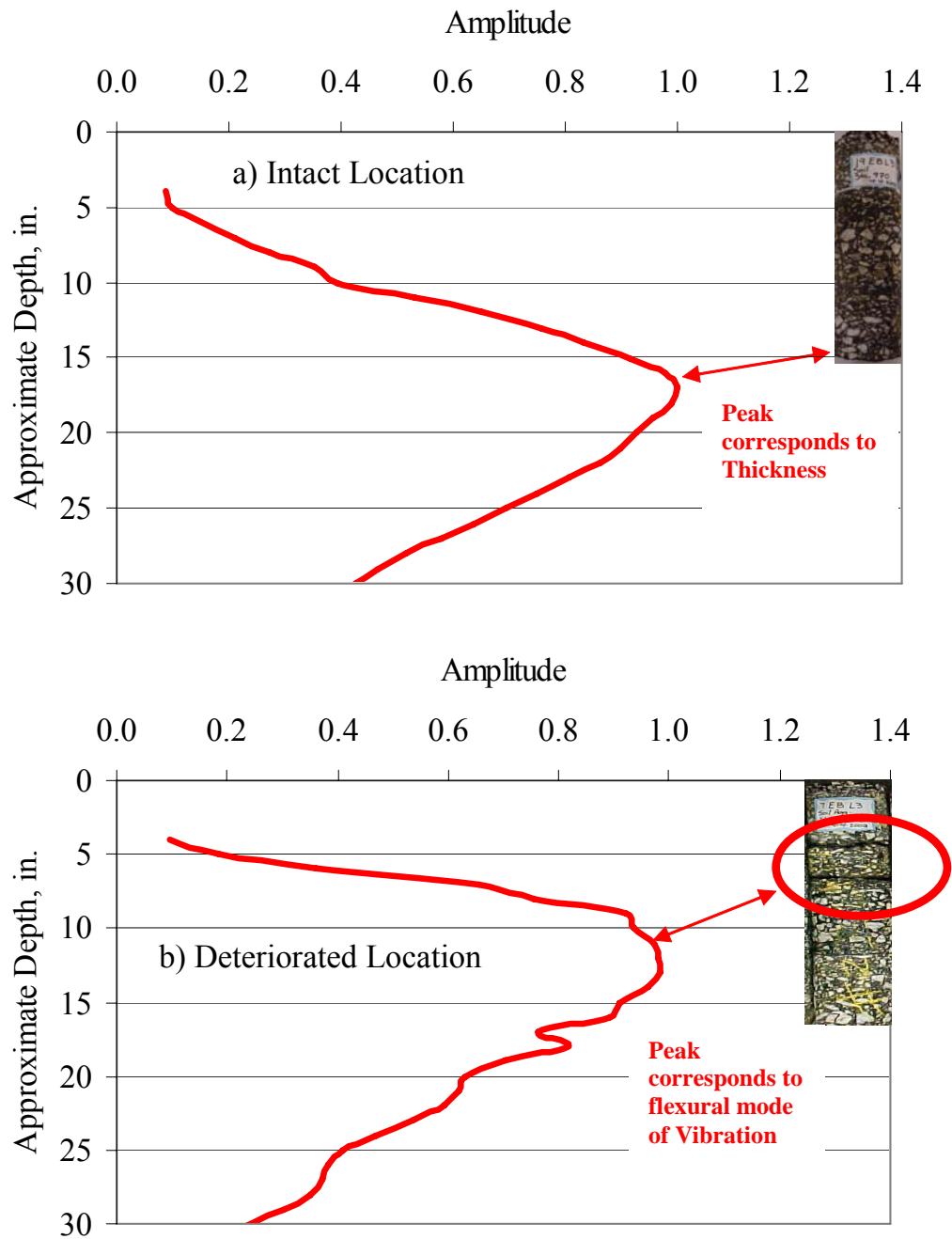


Figure 3-15. Impact echo amplitude spectra converted to thickness

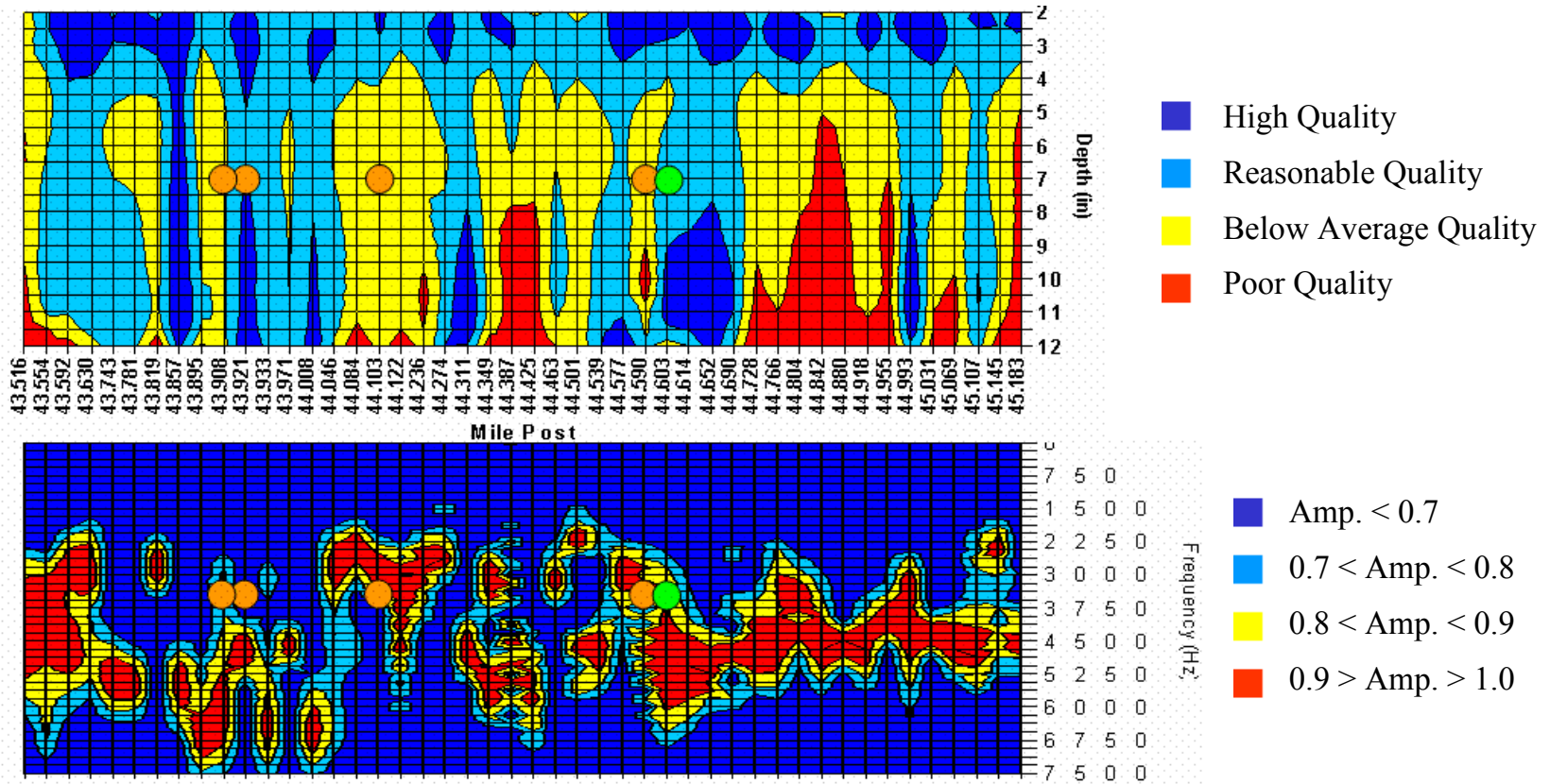


Figure 3-16. Variation in modulus and impact-echo amplitude from Day 1 of I-20 field tests

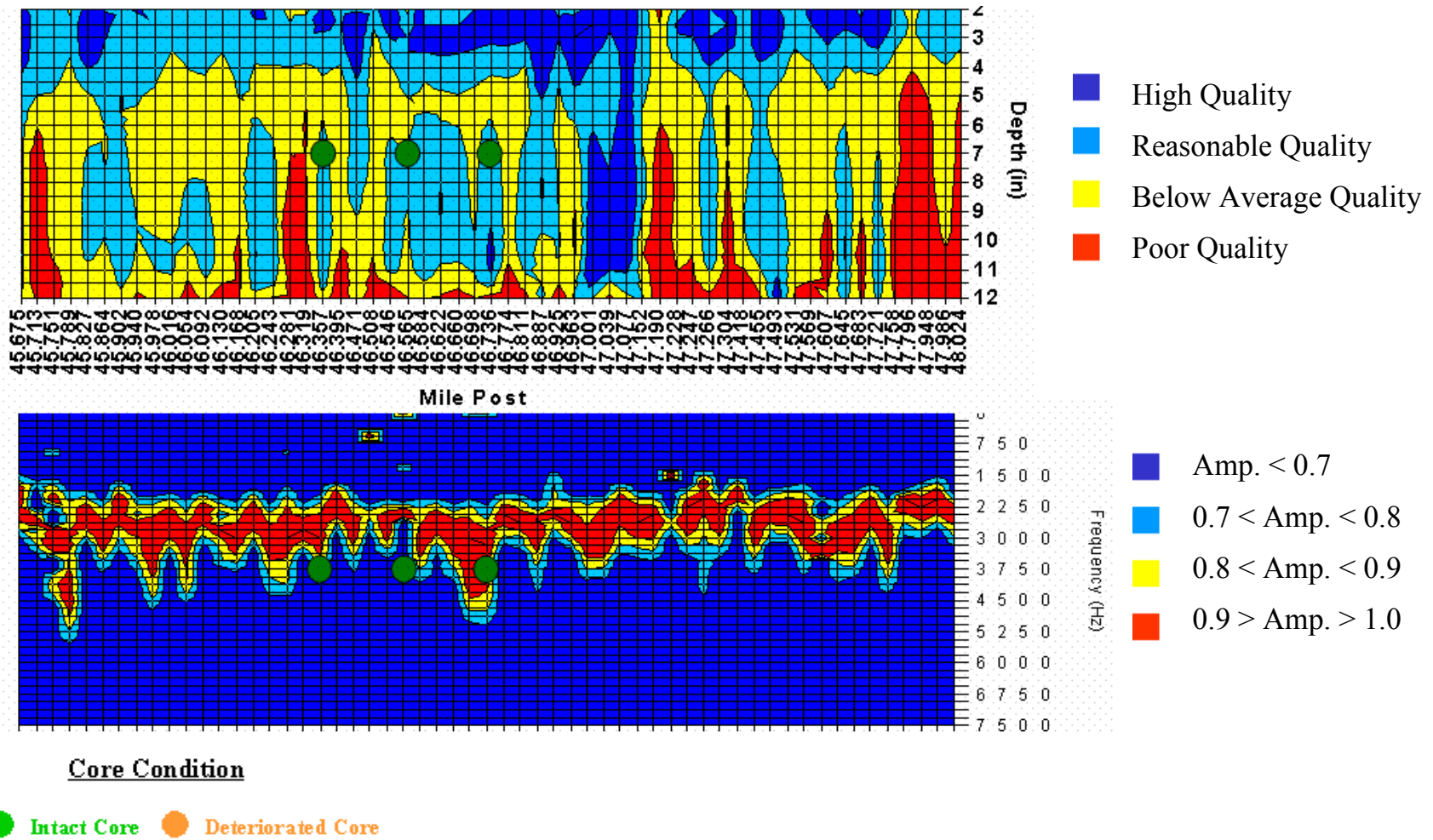


Figure 3-17. Variation in modulus and impact-echo amplitude from Day 2 of I-20 field tests

Eight cores were obtained at this site in April 2003. The location and condition of each core as reported by GDOT are also superimposed on Figures 3-16 and 3-17. In general, the conditions of the cores and the results from the USW and IE amplitude correlate reasonably well. All the intact cores are in the areas where their moduli are within the reasonable quality and higher except for the depths of 4 to 6 inches, where they are in the marginal condition. For the last intact core, which is located around MP 46.800, our analyses contradict the condition of the core as being intact.

For the first two deteriorated cores the moduli are reasonable, but the IE is erratic, indicating some debonding has occurred. The third and fourth deteriorated cores are located in areas that are more severely deteriorated, because the moduli are in the below average or poor quality condition. The IE amplitude is also erratic indicating debonding.

3.3.5 *Falling Weight Deflectometer*

FWD data were collected and analyzed using the methods described in Chapter 2. Because testing on both days was conducted under very similar conditions (Table 3-1) a single day apart, temperature corrections were not necessary. Most temperature correction algorithms are approximate and relate the asphalt modulus to the temperature of the asphalt at mid-depth. During the data collection, periodic surface temperature measurements were made indicating that the surface temperatures varied from a low of 86°F to a high of 101°F. Surface temperature is highly dependent upon daily cycles of insolation, while mid-depth temperature depends upon longer-term temperature trends.

Figure 3-18 summarizes the results from FWD testing conducted on Lane 3 of I-20 eastbound between Stations 820+00 (approximately MP 43.5) and 1058+00 (MP 48) on April 27 and 28, 2004. Test sequences were conducted at 200 foot interval starting at Station 820+00, with additional test sequences conducted in the vicinity of each identifiable core location. A total of five tests sequences were conducted in the immediate vicinity of each core locations: at the core hole and 25 and 50 feet on each side of the core hole. The data points in the plots represent individual test locations, while the smoothed curves are moving averages calculated using a smoothing window of approximately 1000 ft.

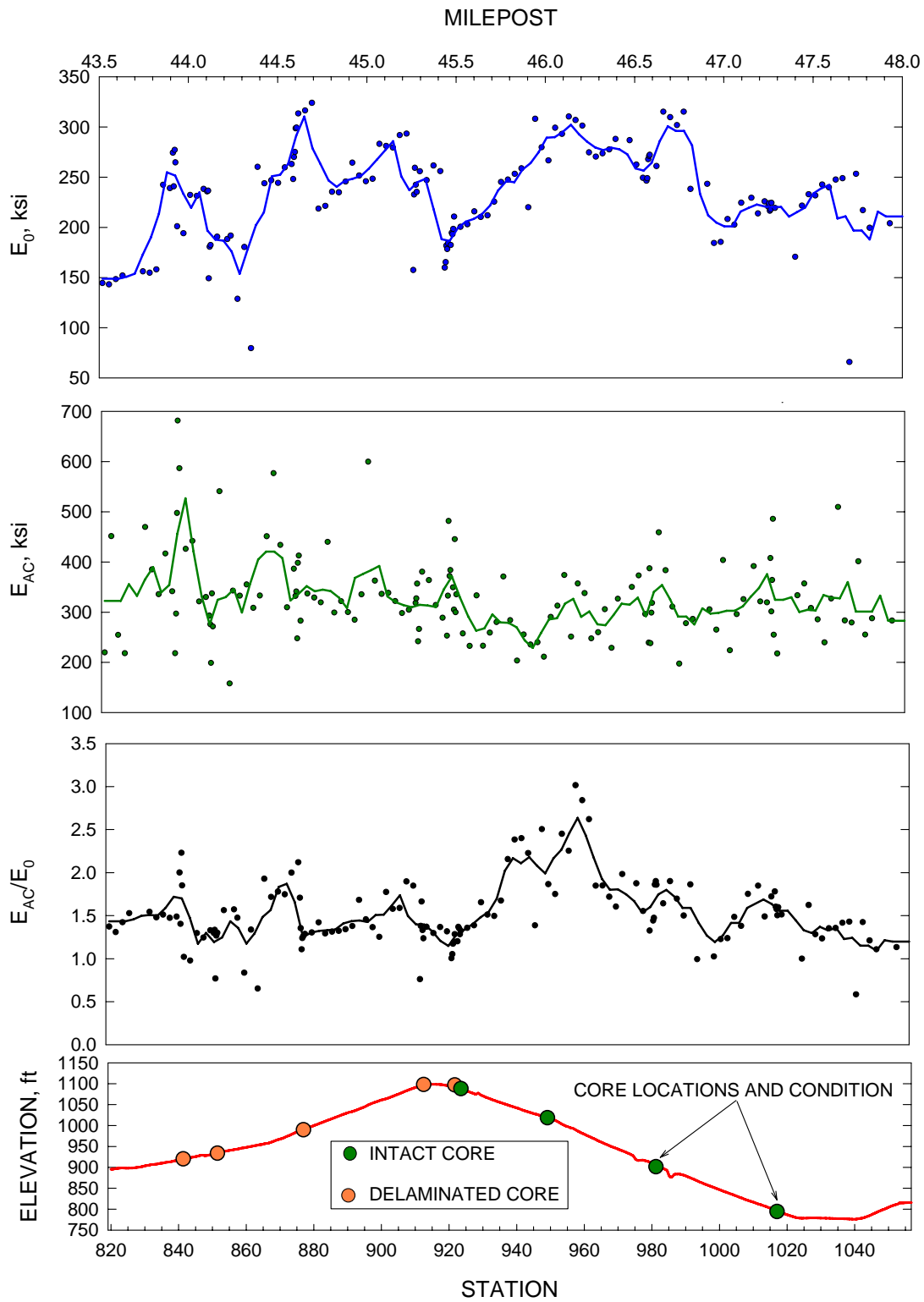


Figure 3-18. I-20 FWD results summary

The overall pavement stiffness (E_0) was estimated using forward calculation techniques from the pressure under the FWD load plate and the deflection at the center of the load plate (D0). These values are plotted in the uppermost plot in Figure 3-18.

The stiffness of the bound layer (E_{AC}) was estimated using the forward calculation techniques described in Chapter 3. For this analysis, a representative bound layer thickness of 16.5 inches was used. The second plot from the top of Figure 3-18 shows typical results of the FWD tests. All results in this figure are averages of all of the drops from the test sequence at the location. The average value of the asphalt stiffness over the entire pilot section is 328.5 ksi with a standard deviation of 113.1 ksi. The median value was 309.1 ksi.

In an effort to compare the stiffness of the bound layer to overall stiffness of the pavement structure, the ratio of E_{AC} to E_0 was calculated. This modular ratio is also plotted in Figure 3-18. The stiffness of the AC averages about 1.5 times the overall stiffness of the pavement structure.

A more detailed examination of the data from the vicinity of the core holes was performed. First, data from all tests conducted within 50 ft of the core-hole locations were analyzed. The thickness of the bound layer at the core hole as assigned to each core within 50 ft. At cores 5, 7, 8, 11, and 13, the cores were observed have experienced delamination, while cores 16, 20, and 22 were observed to be in “good condition” or intact. The average value of the forward-calculated asphalt stiffness for the delaminated cores was 333.6 ksi with a standard deviation of 117.5 ksi. These values are very similar to the statistics for the entirety of Lane 3. The mean and standard deviation for the intact cores was 352.9 ksi and 144.0 ksi, respectively. To test whether the difference between the mean values of the stripped and good cores were statistically significant, a Student’s t-test assuming unequal variances was performed at 5% significance level. This test revealed that possibility that the two means are from identical populations cannot be rejected, i.e., the observed difference in mean values are not statistically significant.

Next the data at the core holes was further evaluated. Table 3-4 presents a comparison of the FWD results at the core locations that indicated stripping (Cores 5, 7, 8, 11, and 13) with the results from locations where the cores were observed to be in good condition (Cores 16, 20, and 22).

Table 3-4. Forward calculated stiffness near I-20 core locations

Core	STA	MP	Thickness, inches	E_{AC} , ksi	E_0 , ksi	E_{AC}/E_0
Delaminated Cores						
5	841+41	43.9226	17.375	455.1	241.7	1.864
7	851+54	44.1144	16.75	194.7	191.2	1.016
8	877+00	44.5967	15.5	269.4	251.2	1.067
11	912+50	45.2690	16.75	348.4	265.8	1.304
13	921+81	45.4454	17.75	427.2	304.1	1.403
Mean			16.825	339.0	250.8	1.331
Standard Deviation			0.855	108.4	40.9	0.339
Intact Cores						
16	923+62	45.4796	18.75	362.3	290.0	1.217
20	981+50	46.5759	14.5	284.4	233.5	1.198
22	1017+25	47.2529	16.25	372.8	244.9	1.502
Mean			16.500	339.8	256.1	1.306
Standard Deviation			2.136	48.3	29.93	0.170

The bound layer stiffness data are shown graphically in Figure 3-19. The solid bars indicate the mean values, while the error bars indicated plus and minus one standard deviation. The overall means of the delaminated and intact cores are indicated by the dashed lines. Again, Student’s t-tests were performed at the 5% confidence level assuming unequal variances. The tests indicated that difference in the mean bound layer stiffness values (E_{AC}) between the stripped and good cores was not statistically significant. Similar results were obtained for the overall pavement stiffness (E_0) and the modular ratio (E_{AC}/E_0).

Figure 3-20 presents a direct comparison of bound layer stiffness values forward-calculated from the FWD with the stiffness values calculated from the seismic tests. Because the seismic data have been adjusted to a “design” value, the data were normalized by dividing each curve by the mean value over the entire pilot section. The data plotted in these curves are moving averages of five contiguous data points. As explained in section 4.5, a series of seismic data near the center of the pilot section was not collected because of equipment malfunction. Figure 4-18 reveals that the trends in the data are similar. An exception to this observation is noted in the last 3000 feet of the test section, where the seismic data indicates a significant decreasing trend in stiffness, while the FWD does not appear to pick up this trend until the last 500 feet of the section.

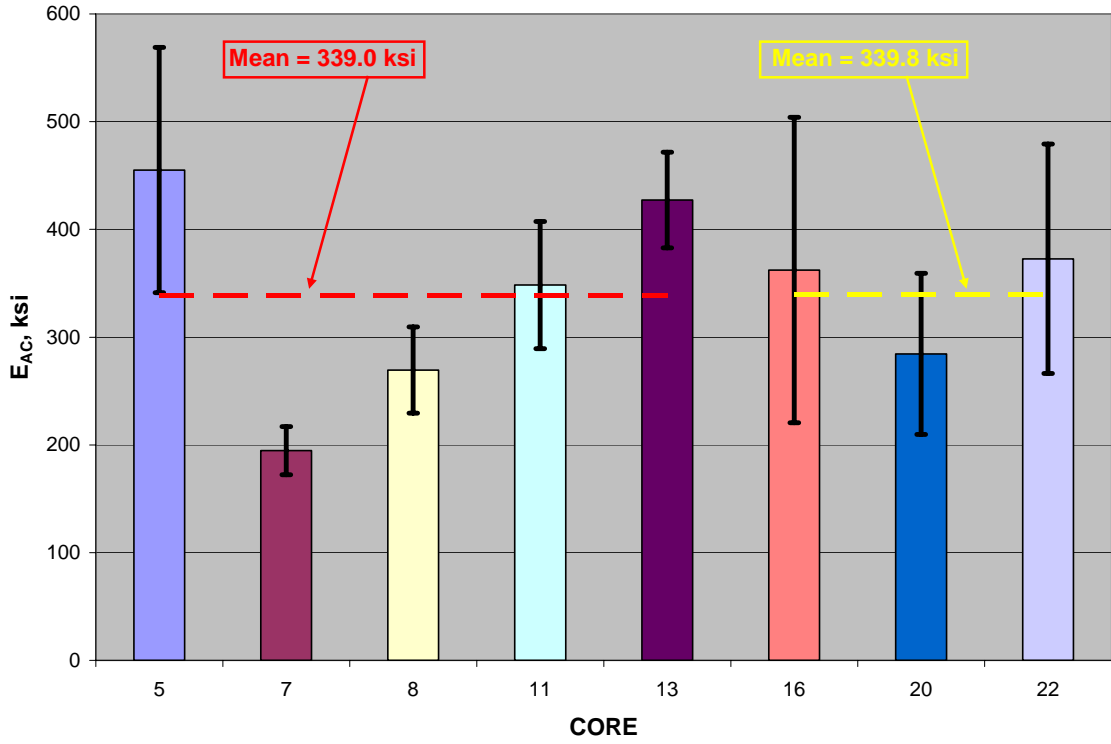


Figure 3-19. I-20 bound layer stiffness values from FWD

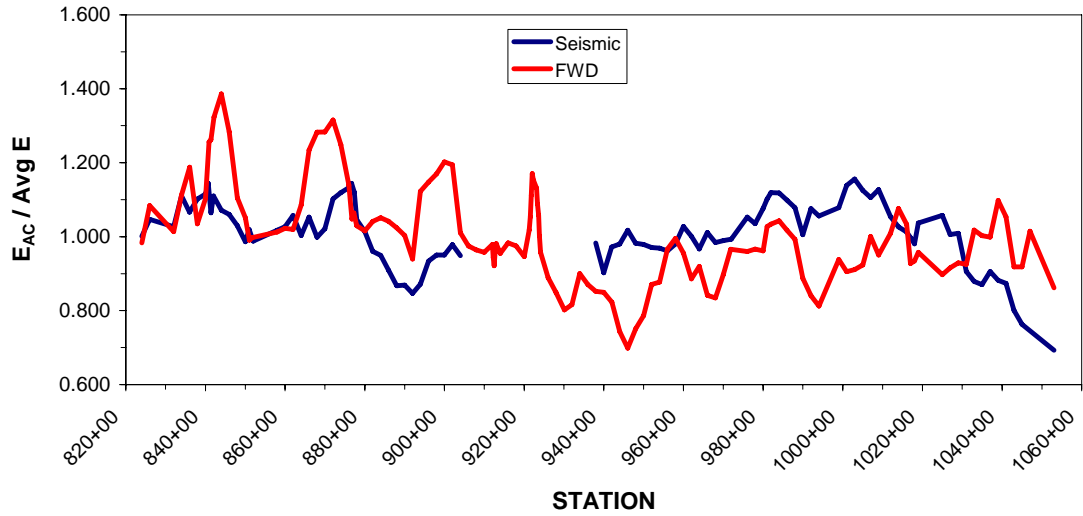


Figure 3-20. Comparison of I-20 normalized modulus values from seismic tests and FWD

3.3.6 Ground Penetrating Radar

The GPR data for I-20 for the full depth AC section shows three major layers within the AC structure, with the layer bottoms at approximately 3 inches, 5 to 6 inches, and 16 inches. Figure 3-21 shows an example of the raw GPR data showing these layer boundaries.

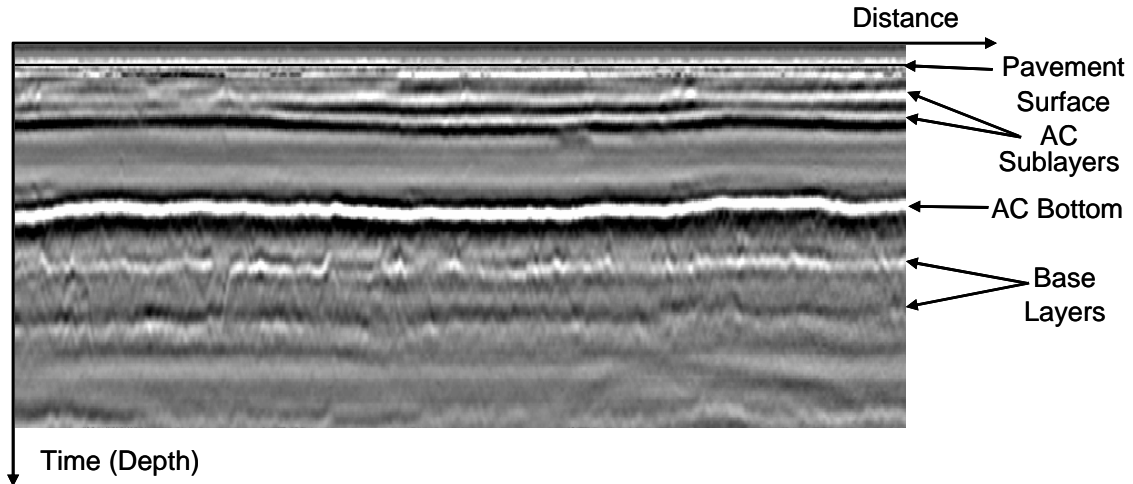


Figure 3-21. Sample GPR section data from I-20 Lane 3, centerline

The core data provided by GDOT for I-20 shows that stripping occurs at the boundaries of, and within the second of the three asphalt layers. Examples of cores showing this behavior are shown in Figure 3-22.



Figure 3-22. I-20 cores showing stripping from 4 to 6 inches from the surface

The above observation suggests that the occurrence of stripping is associated with strong reflections from the interfaces above and below the second layer. The GPR system produces a sequence of scans

(or waveforms), each scan representing 20 nanoseconds of round trip travel of the GPR wave. Let A_1 , A_2 , and A_3 be the reflection amplitudes from each of the three observed asphalt layers, respectively. Quantitatively, each 20 nanosecond scan is represented as 256, 16 bit data samples (12.8 samples/nanosecond). The possible numerical amplitude range of each sample is $\pm 32,768$. Thus, numerical amplitudes A_1 , A_2 , and A_3 are based on this quantitative scale. For example, a reflection amplitude of 18,000 is over half of full scale (a strong reflection).

The stripping is not likely when either:

- 1) A_1 or A_2 is zero
- 2) $A_2 < A_{2\text{threshold}}$
- 3) $A_3 > A_{3\text{threshold}}$

Equation 15

From the GPR data, $A_{2\text{threshold}} = 8,000$ and $A_{3\text{threshold}} = 18,000$. Otherwise stripping may occur.

Table 3-5 summarizes the correlation between the outcome of this rule and the reported observations for 30 cores taken from the full depth asphalt sections of I-20. The PCC overlaid section has not been included in this analysis. The GPR values were obtained from the data collected along the centerline of each lane. The results in the table show that the proposed rule correctly identifies the observed stripping in 23 of the 30 cores.

To obtain a graphical spatial picture of potential locations and distribution of stripping, the rule described above has been quantified in the form of a Stripping Index (SI), as follows:

$$SI = \frac{|A_2| - A_{2\text{threshold}} + A_{3\text{threshold}} - A_3}{5000}$$

Equation 16

$$SI = 0 \text{ if } A_1 \text{ or } A_2 = 0$$

The SI conveys, in numerical terms, the logic described in Equations 15. The denominator of 5000 in Equation 16 was selected to scale the numerator to a convenient range of 0 to 5.

The SI has been plotted for lanes 1, 2, and 3 versus a core condition rating, where 1 = good and 3 = stripped. For lane 3, the results have also been plotted against the results obtained from the PSPA testing. The PSPA index is based on the mean modulus obtained for an individual location as compared to the average of all of the local mean moduli. The index is calculated as

$$PSPA \text{ index} = \frac{\text{mean of all tests}}{\text{mean of local test}}$$

Equation 17

Locations where $PSPA \text{ index} < 1$ are where the local mean modulus is higher than average and the AC layers are in better relative condition. Where $PSPA \text{ index} > 1$, the local mean modulus is less than average and stripping is more likely.

Figures 3-23 through 3-29 show plots of the SI , core index, and PSPA index. The PSPA index axis is on the left with the SI axis. It appears that a good match between the SI and the core condition might be achieved by setting a stripping threshold of 0.5 for the SI .

Table 3-5. Correlation of SI with I-20 cores

Core No.	STA	Lane	GPR Layer Amplitudes			GADOT Core Condition Rating	GPR Core Condition Rating	Agreement
			L1	L2	L3			
1	822+34	1	15537	5283	15513	good	good	yes
2	821+06	2	8500	-9299	30564	good	good	yes
3	841+36	2	5899	-10109	20255	stripped	good	no
5	841+37	3	0	-8534	17513	stripped	good	no
6	851+60	2	9126	-10874	12825	stripped	stripped	yes
7	851+47	3	3405	-9774	17058	stripped	stripped	yes
8	876+92	3	9029	0	17467	stripped	good	no
10	897+66	1	8176	0	7572	good	good	yes
11	912+50	3	6722	-12114	20069	stripped	good	no
13	921+67	3	9154	-13828	18415	stripped	good	no
15	924+86	2	8387	-3553	11932	stripped	good	no
16	923+49	3	11191	-13267	17704	good	stripped	no
17	950+37	1	23361	0	13301	good	good	yes
18	970+86	2	4979	-7698	14828	good	good	yes
19	949+10	3	7020	-3763	17828	good	good	yes
20	981+22	3	10818	-12111	19572	good	good	yes
21	990+93	2	4734	-11371	22711	good	good	yes
23	1003+49	1	11392	0	11438	good	good	yes
24	1004+51	2	8613	-16281	23784	good	good	yes
25	1057+47	1	4708	0	9582	good	good	yes
26	1075+90	2	9345	-3349	17649	good	good	yes
28	1093+74	1	10976	0	19001	good	good	yes
29	1095+48	3	8521	-10594	17236	poor	stripped	yes
30	1098+82	2	3526	0	12458	good	good	yes
31	1098+75	3	8803	-19374	15733	poor	stripped	yes
32	1105+88	2	11043	0	15413	good	good	yes
33	1105+78	3	3046	-12662	21367	good	good	yes
34	1125+68	3	0	-14075	21198	good	good	yes
38	1204+37	1	8222	6667	6342	good	good	yes
43	1237+71	1	7354	-5135	5863	good	good	yes
30 = Total # of Cores						Percent Correct =		77%

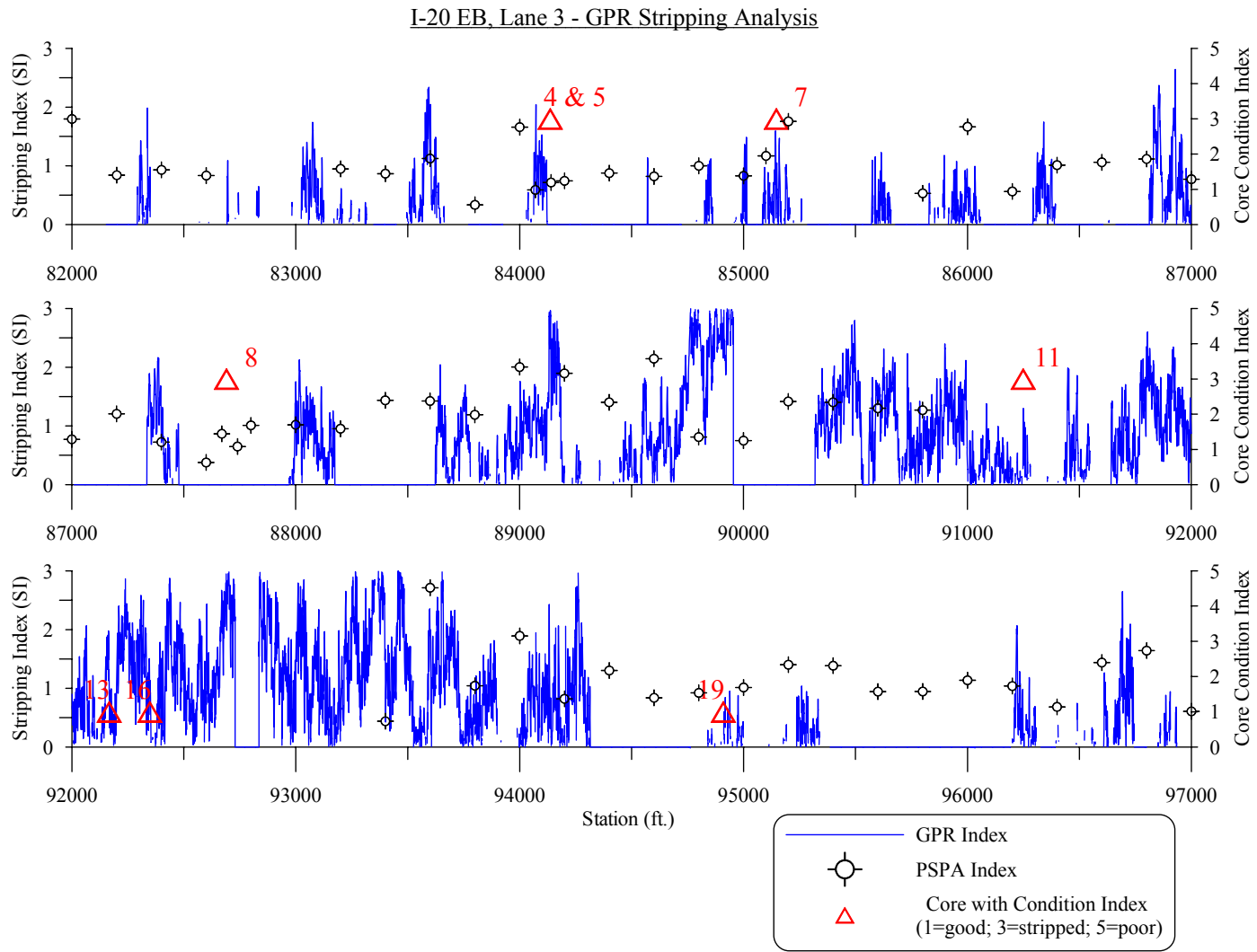


Figure 3-23. GPR stripping analysis, I-20 Lane 3, STA 820 to 970

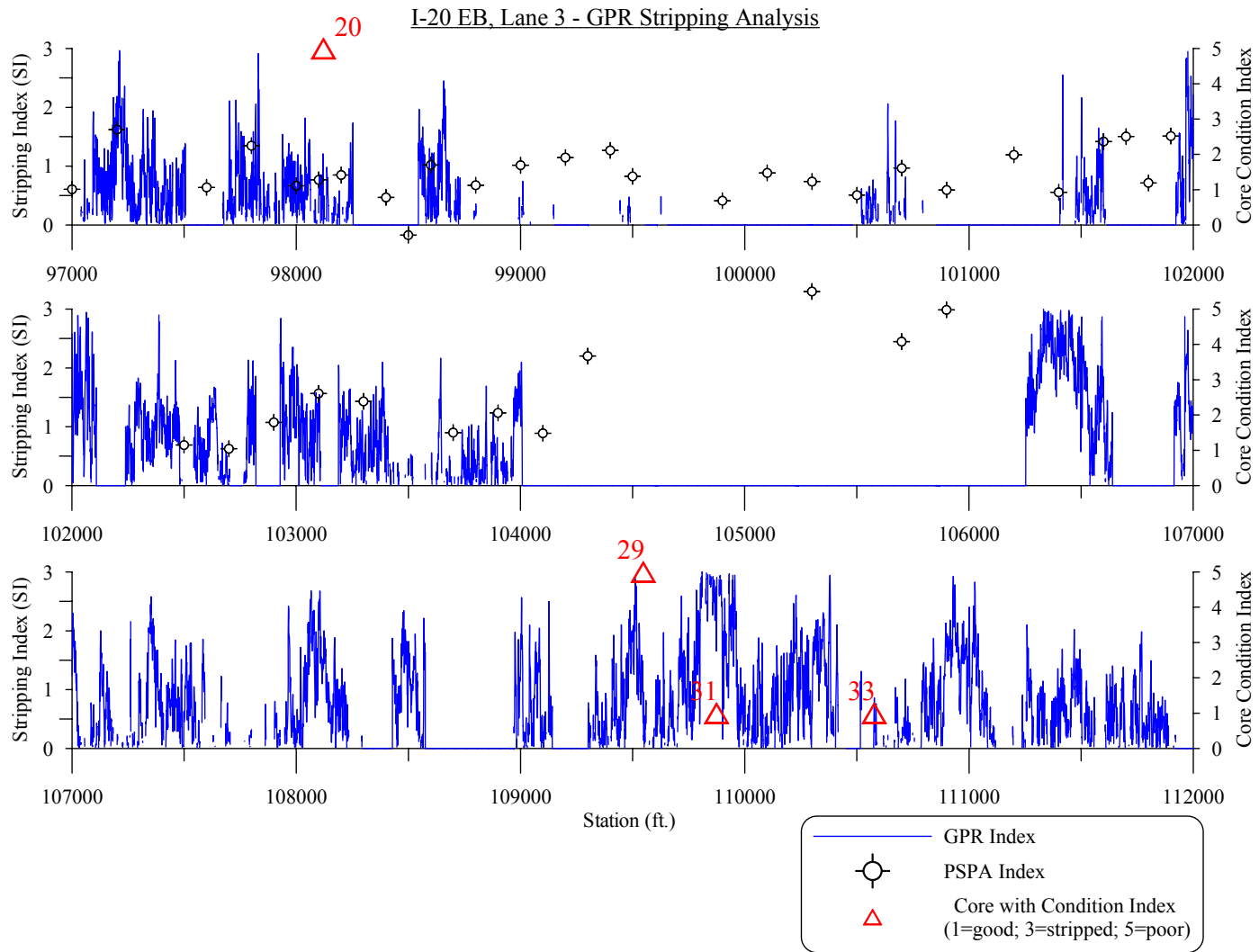


Figure 3-24. GPR stripping analysis, I-20 Lane 3, STA 970 to 1120

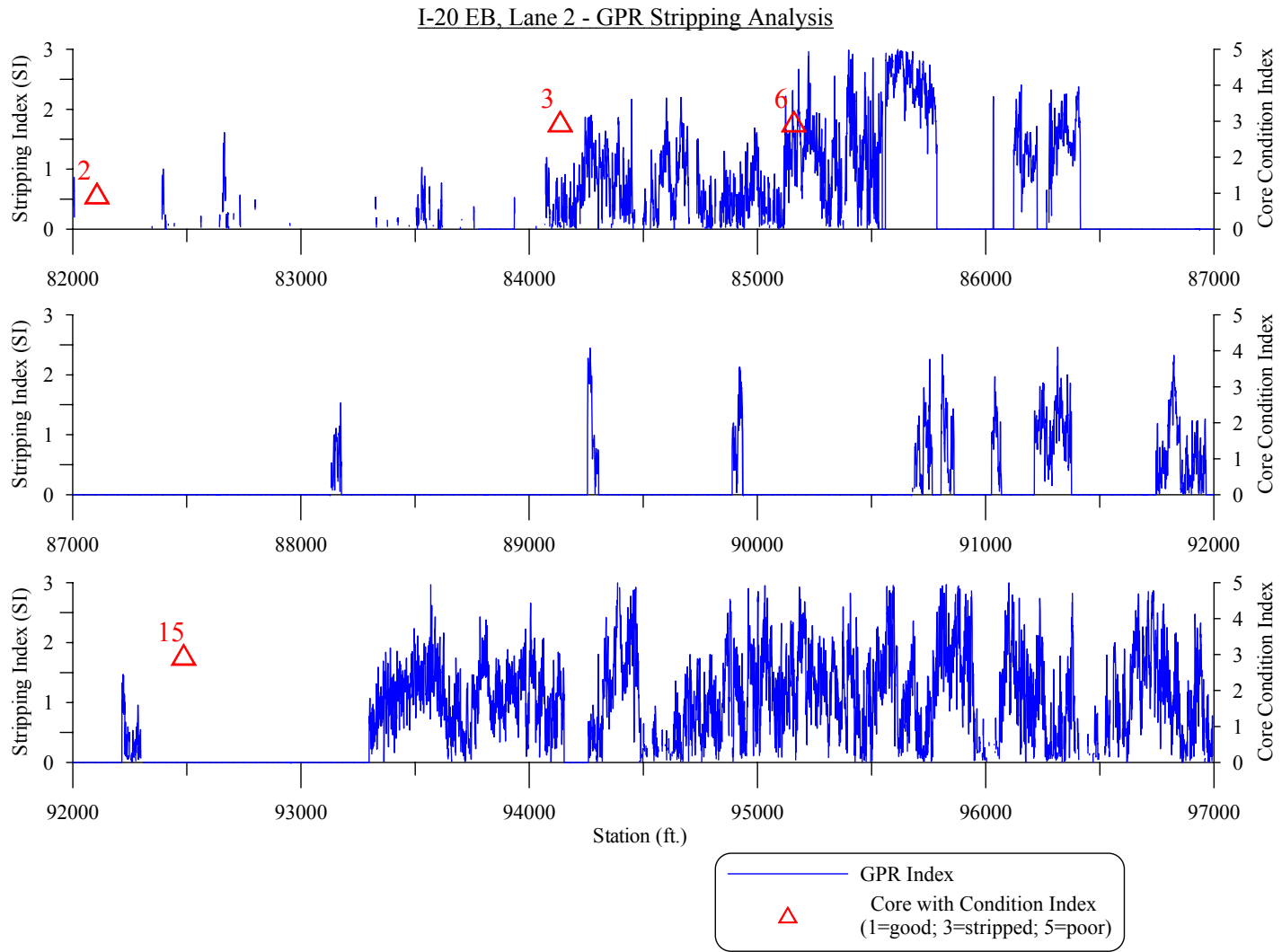


Figure 3-25. GPR stripping analysis, I-20 Lane 2, STA 820 to 970

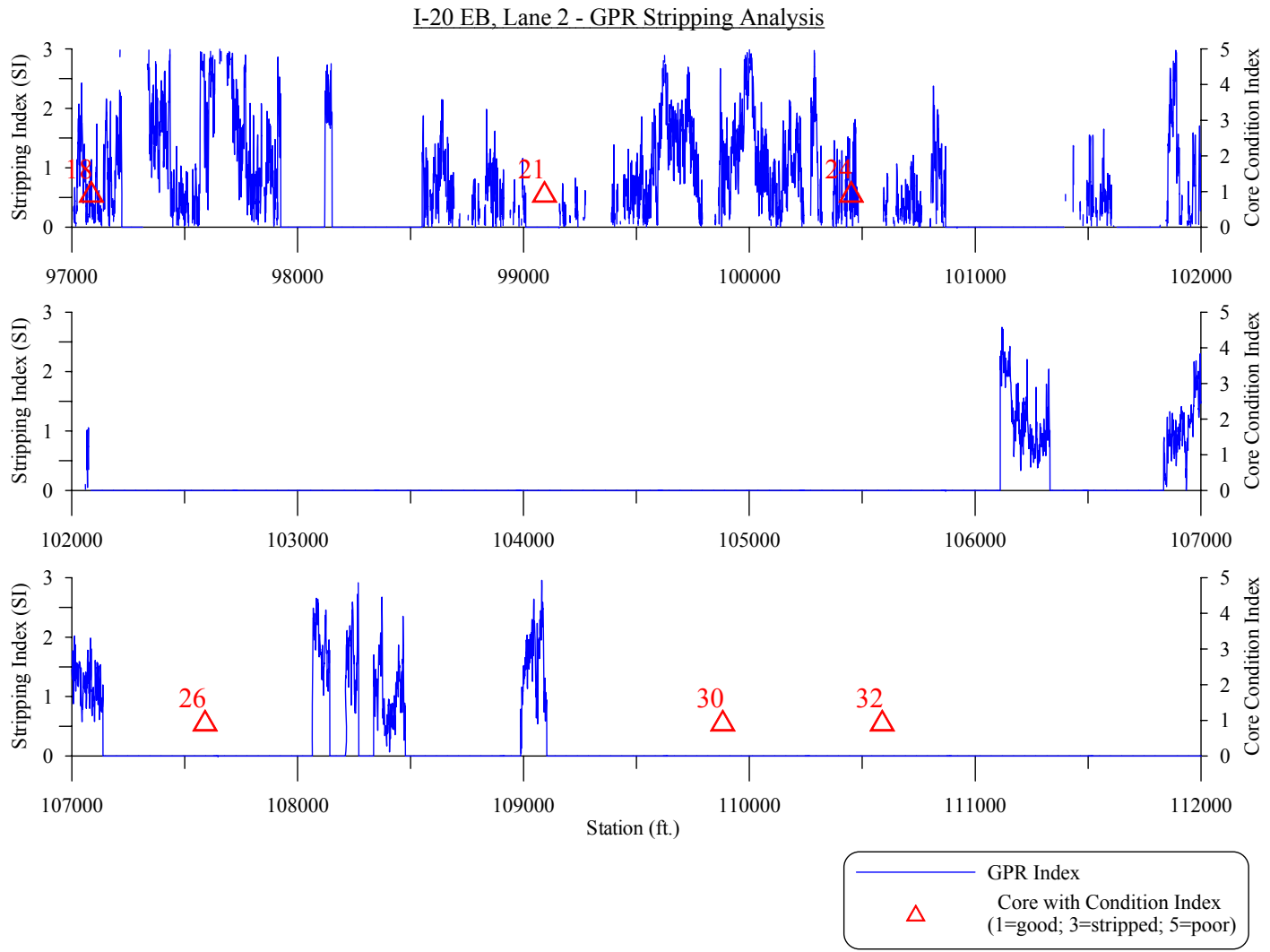


Figure 3-26. GPR stripping analysis, I-20 Lane 2, STA 970 to 1120

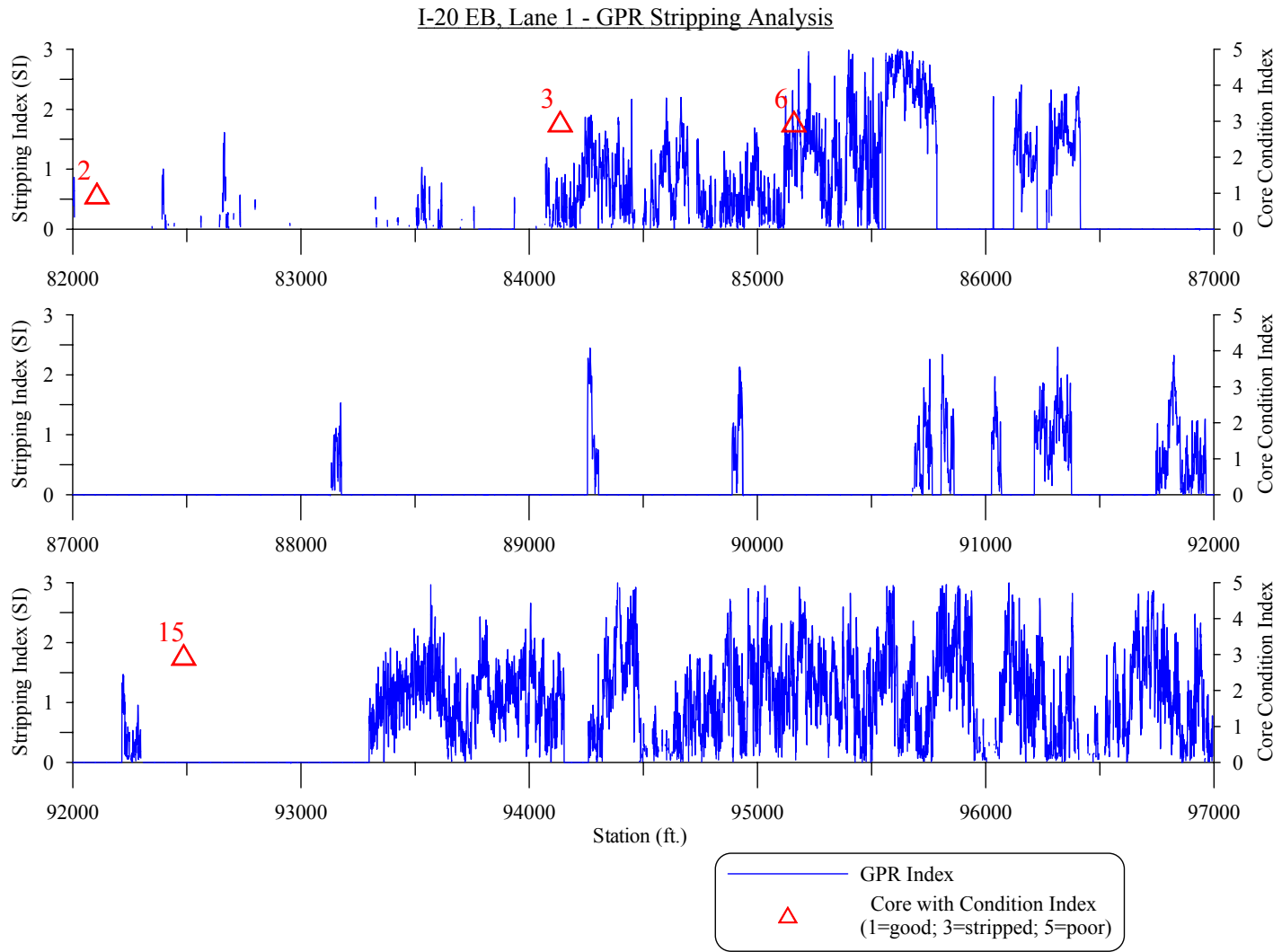


Figure 3-27. GPR stripping analysis, I-20 Lane 1, STA 820 to 970

I-20 EB, Lane 1 - GPR Stripping Analysis

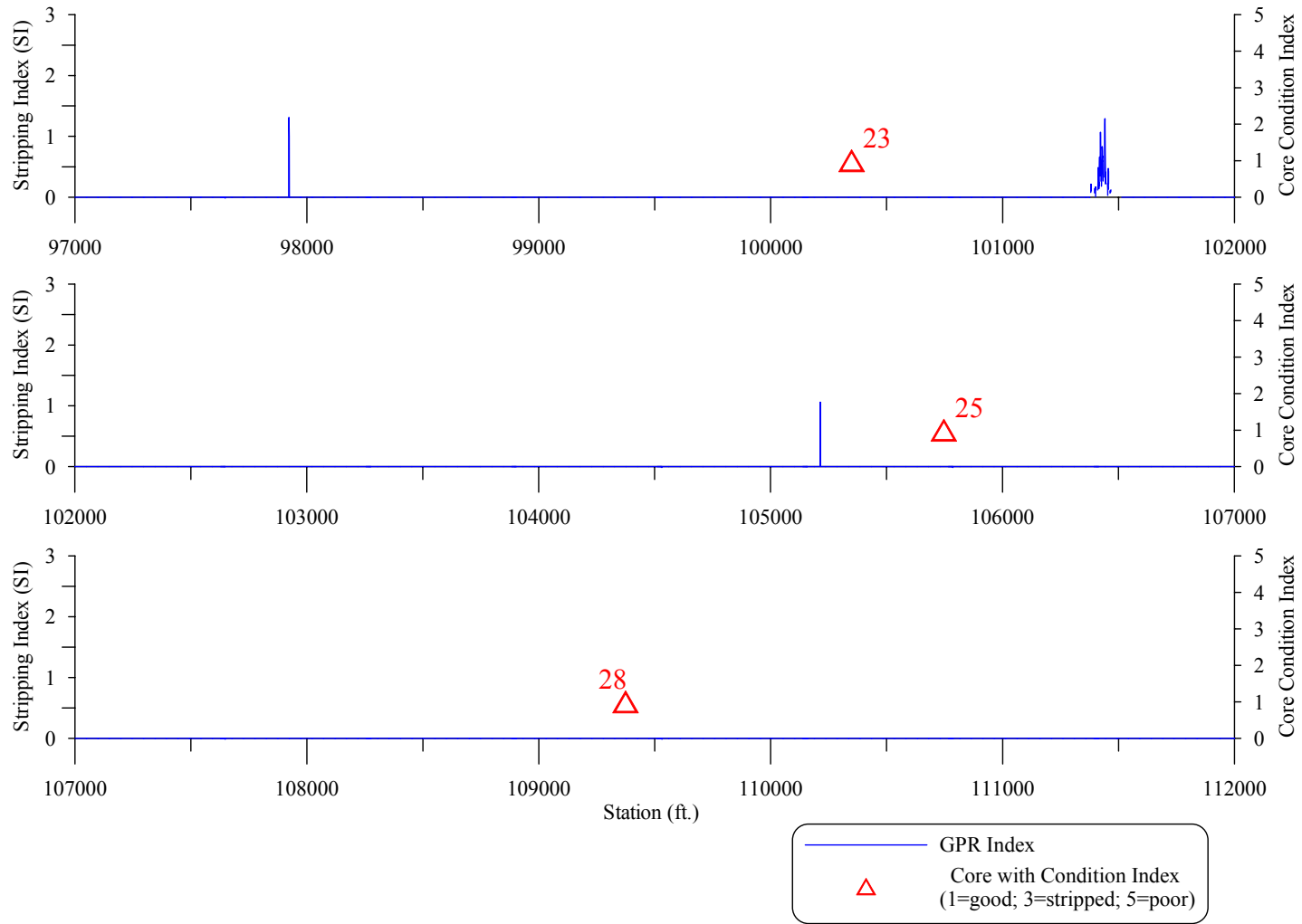


Figure 3-28. GPR stripping analysis, I-20 Lane 1, STA 970 to 1120

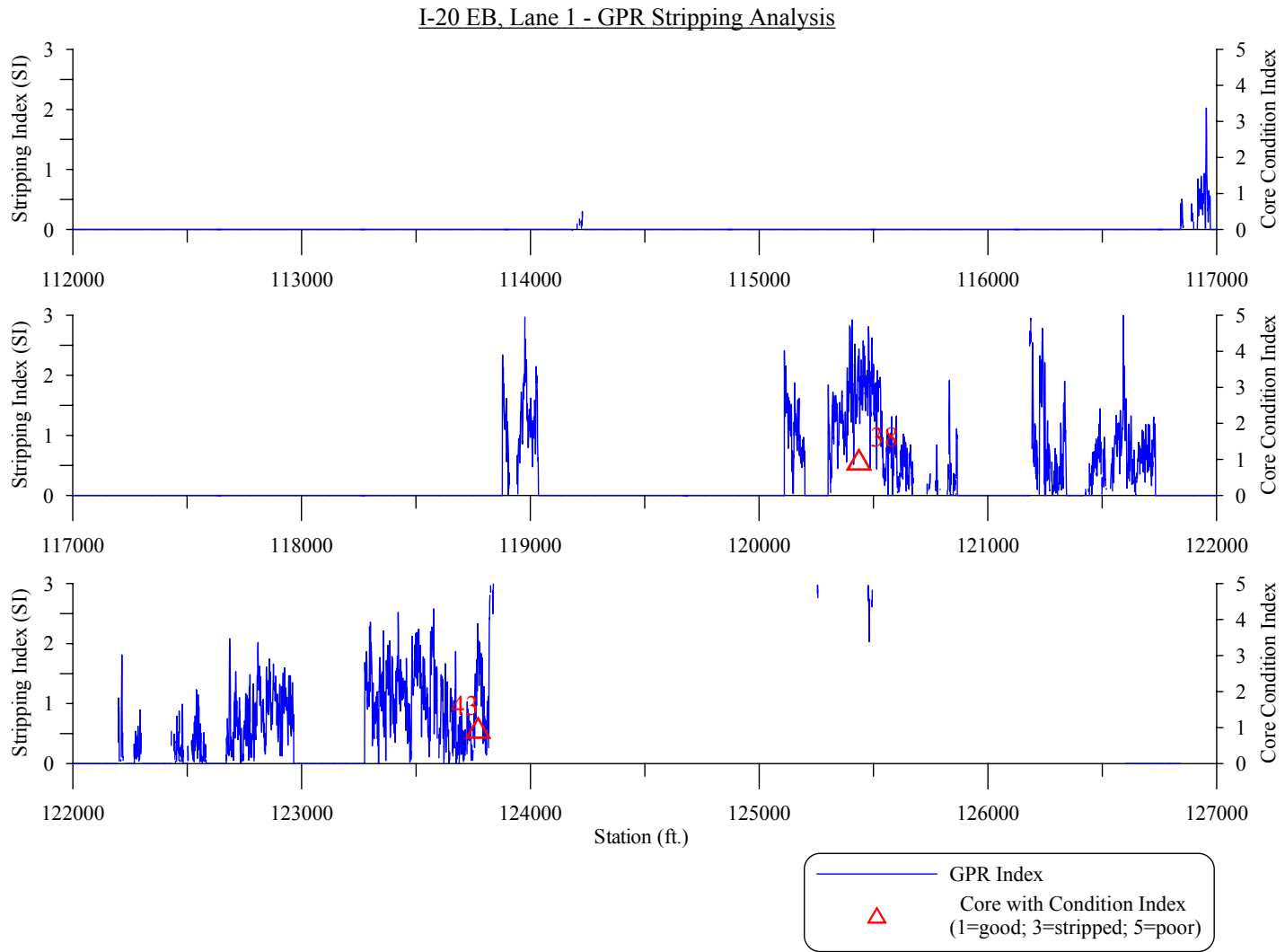


Figure 3-29. GPR stripping analysis, I-20 Lane 1, STA 1120 to 1270

3.4 Analysis of Results

3.4.1 Baseline HMA Layer Modulus – No Moisture Damage

To evaluate the hypothesis that deflection basin data and seismic test results can be used to measure the modulus of HMA, the baseline or target modulus of a good quality HMA mixture without any moisture damage must be known. The modulus versus temperature relationship for an HMA mixture without any moisture damage is referred to within this report as the baseline values for a specific mixture.

The a dynamic modulus regression equation commonly referred to as the Witczak equation (Andrei, Witczak, and Mirza 1999) was used to estimate the modulus at different temperatures and depths within the pavement structure:

$$\log E^* = -1.249937 + 0.02932\rho_{200} - 0.001767(\rho_{200})^2 - 0.002841\rho_4 - 0.058097V_a - 0.802208\left(\frac{V_{beff}}{V_{beff} + V_a}\right) + \frac{3.871977 - 0.0021\rho_4 + 0.003958\rho_{38} - 0.000017(\rho_{38})^2 + 0.005470\rho_{34}}{1 + e^{(-0.603313 - 0.313351 \log(f) - 0.393532 \log(\eta))}}$$

Equation 18

where:

E^*	=	dynamic modulus, 10^5 psi.
η	=	bitumen viscosity, 10^6 Poise.
f	=	loading frequency, Hz.
V_a	=	air void content, %.
V_{beff}	=	effective bitumen content, % by volume.
ρ_{34}	=	cumulative % retained on the $\frac{3}{4}$ in sieve.
ρ_{38}	=	cumulative % retained on the $\frac{3}{8}$ in sieve.
ρ_4	=	cumulative % retained on the No. 4 sieve.
ρ_{200}	=	% passing the No. 200 sieve.

In addition, repeated load tests completed on various HMA mixtures sampled during construction in the late 1980's for different Georgia mixtures (Von Quintus 1991) were also used to estimate the baseline modulus values.

Figures 3-30 and 3-31 illustrate the dynamic modulus of intact, good quality HMA for an average year in the Atlanta area. Table 3-7 summarizes the dynamic modulus for an intact, good quality HMA for the average temperatures that were used for evaluating the field tests along I-20. These baseline values were adjusted from modulus testing completed on HMA mixtures sampled from different Georgia projects for National Cooperative Highway Research Program (NCHRP) Project 9-6(1) in the late 1980's (Von Quintus 1991). Adjustments were made based on type of test (resilient versus dynamic), loading frequency and age.

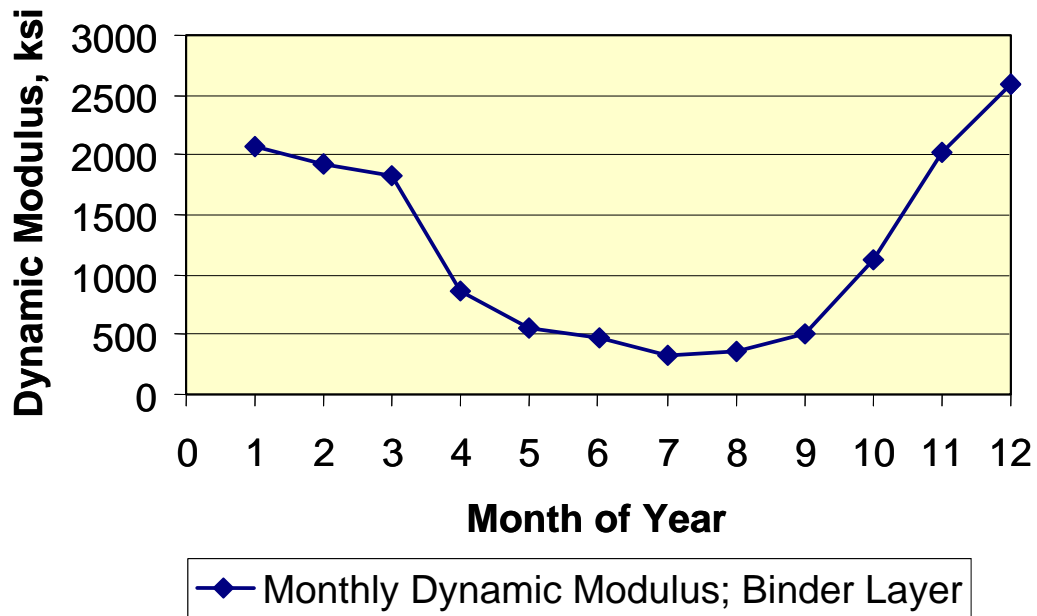


Figure 3-30. Dynamic modulus of an intact, good quality HMA binder mixture about 6 inches below the surface

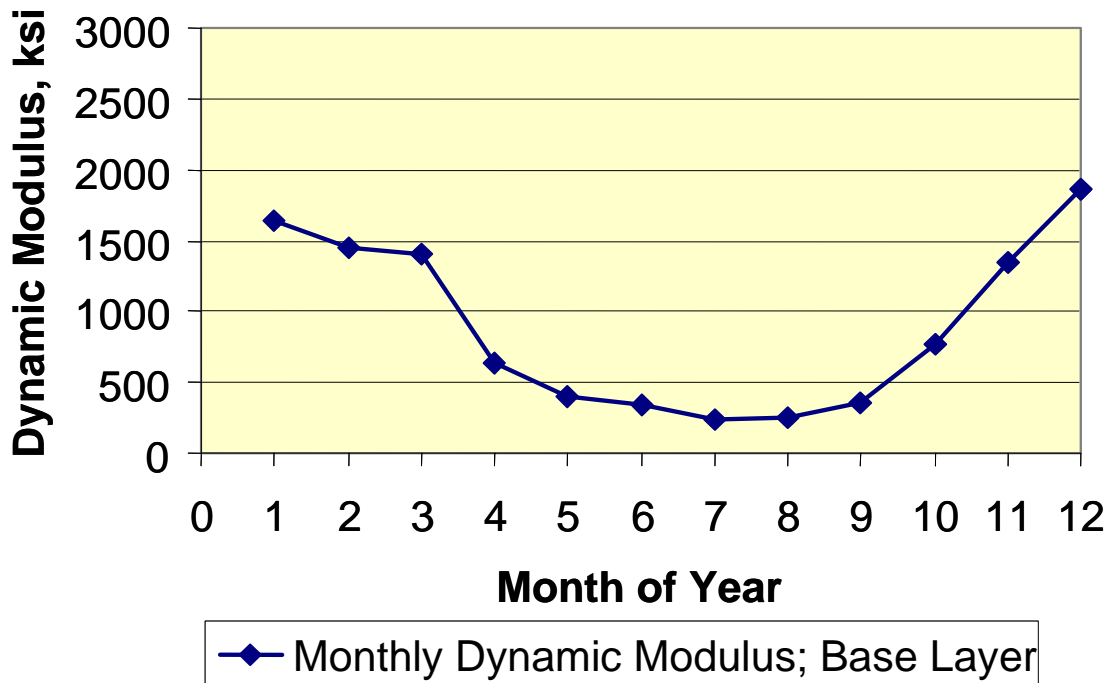


Figure 3-31. Dynamic modulus of an intact, good quality HMA base mixture about 10 inches below the surface

Table 3-6. Summary of expected modulus values for intact HMA without moisture damage

Temperature, °F	Expected Value	HMA Surface Mix Modulus, ksi	HMA Binder Mix Modulus, ksi	HMA Base Mix Modulus, ksi
77	Low	500	400	300
	Mean	750	650	400
	High	1,000	900	600
85	Low	300	275	250
	Mean	500	450	350
	High	650	600	500

Figure 3-32 shows the HMA resilient modulus as a function of temperature based on results from hundreds of repeated load tests as reported in NCHRP Report 338 (Von Quintus 1991). It was assumed that the HMA mixtures placed along this segment of I-20 consist of unmodified mixtures. The expected baseline modulus-temperature relationship for the binder mix along I-20 is also shown in Figure 3-32.

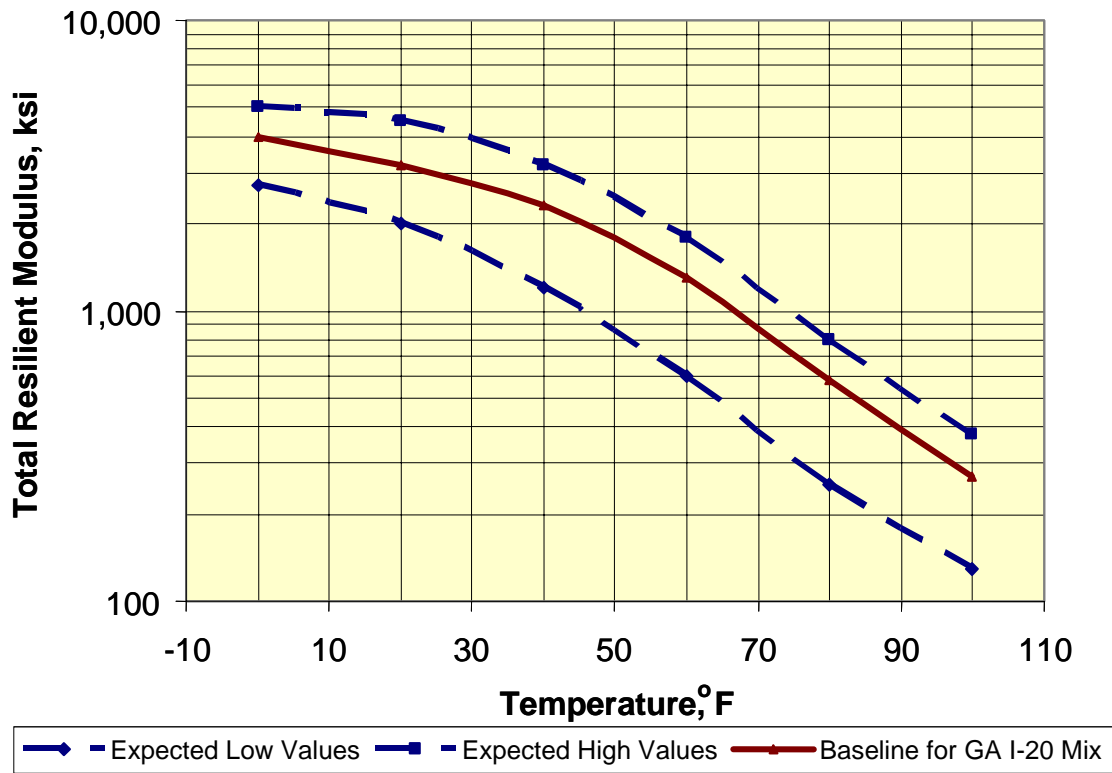


Figure 3-32. Expected high and low total resilient modulus values measured from indirect tensile repeated load testing of HMA mixtures sampled from around the U.S.

3.4.2 Modulus Values Estimated from NDT Technologies

Figure 3-33 shows the longitudinal profile of the seismic modulus that was adjusted to a loading frequency of 15 Hz and to a temperature of 77°F. The upper and lower limits and target value of the seismic modulus have been included on the graph as dashed lines. The target value for this mix was computed from typical volumetric properties using Equation 18.

As shown in Figure 3-33, most of the seismic modulus values are significantly less than the values that would be expected for an intact, good quality HMA at a depth of 4 to about 10 inches. Thus, the test results from the seismic testing indicate that the HMA has moisture damage or some other form of damage.

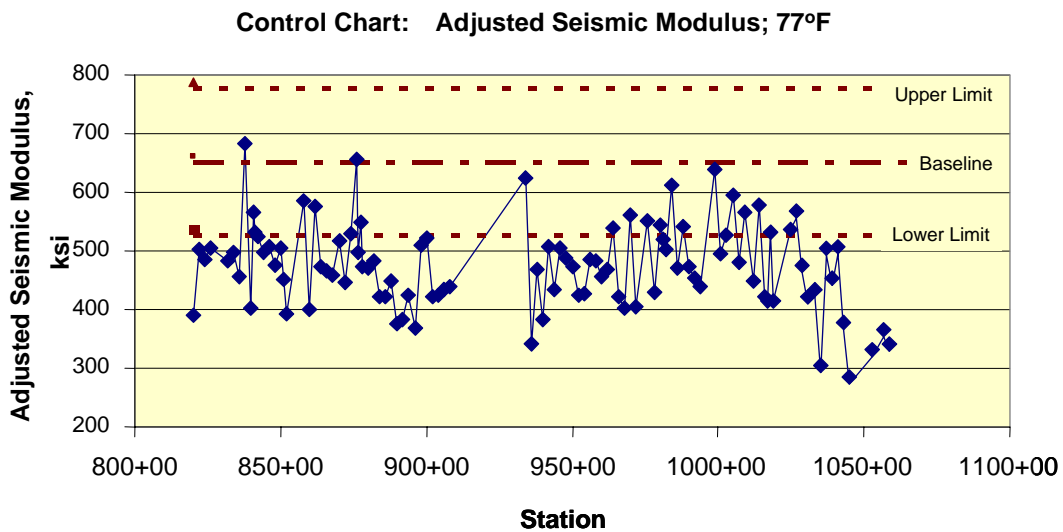


Figure 3-33. Adjusted I-20 HMA seismic modulus as compared to the range of expected modulus values

Figure 3-34 shows the longitudinal profile of the elastic modulus calculated from the FWD deflection basin data. Like the seismic modulus data, these data have been adjusted to a standard temperature of 77°F. As shown, most of the modulus values were found to be between the expected low and high baseline values for the HMA binder layer. These data suggest that moisture damage is not as extensive, as suggested by the seismic data. However, the variation in HMA layer thickness can significantly affect these values.

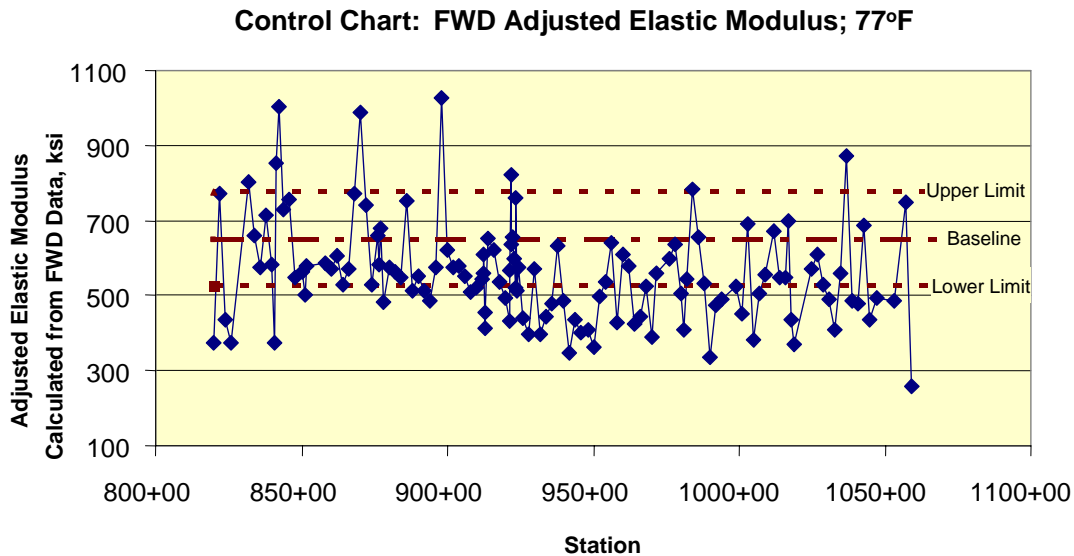


Figure 3-34. I-20 HMA elastic modulus calculated from FWD data as compared to the range of expected modulus values

Figure 3-35 shows a comparison was between the seismic and elastic modulus values estimated from the different NDT tests performed along I-20. The dashed lines in the figure show the modulus values that would be expected for an intact, good quality HMA mixture at the different test temperatures. As shown, most of the estimated or calculated values fall outside the typical values of an HMA mixture without stripping or moisture damage.

Figure 3-35 has been subdivided into nine regions based upon the expected modulus values for the seismic and FWD testing methods. The hypothesis is that the modulus can be used to identify areas along I-20 that have moisture damage. No data were measured within Regions III, VI, and IX. The severity of moisture damage can vary from a reduction in adhesion to total separation between the asphalt film and aggregate surface.

Region V in Figure 3-35 is the area where the modulus values produced by both the FWD and seismic testing would be representative of an HMA mixture that has no moisture damage or stripping. Region VII is an area where the modulus values from both test techniques would indicate an HMA mixture that has stripping or moisture damage. Most of the modulus data points fall within Region IV. The significant point to mention is that the seismic modulus values have a much greater variance from the expected average baseline modulus value based on laboratory testing of similar materials. These lower values suggest potential for stripping and moisture damage in the HMA layers.

More importantly, no definite relationship was found between the two data sets. Thus, the FWD and seismic test results would indicate different findings. The FWD results suggest that moisture damage may not be severe and confined to specific areas, while the seismic results suggest that moisture damage is more extensive and occurs in most of the areas tested. As such, the hypothesis that modulus values from the deflection basin and seismic data will result in similar values when adjustments for temperature and loading frequency are properly taken into account was not found to be supported by the field test results.

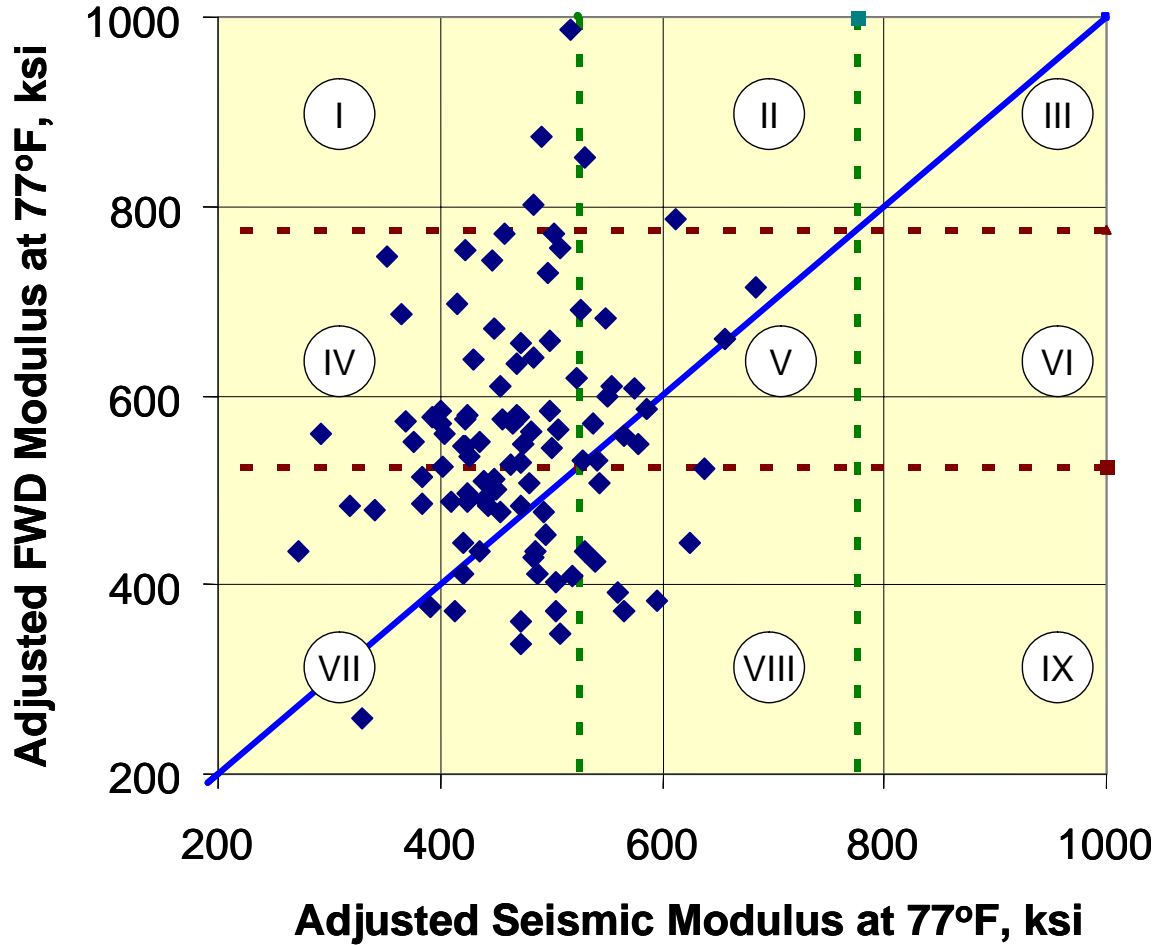


Figure 3-35. Comparison of the HMA modulus values estimated from the FWD and seismic testing

3.4.3 Stripping Predictions from GPR

Modulus by itself is not a reliable measure of moisture damage in terms of a reduction in adhesion. Cracking and other forms of damage will also cause a reduction in the intact modulus of an HMA layer. GPR tests were performed to identify areas with higher levels of moisture. The GPR data was reduced into stripping indices. Longitudinal profiles of the stripping indices were previously presented in the report and suggest more extensive stripping similar to the seismic data.

Figures 3-36 and 3-37 show the relationship between the GPR stripping indices determined from the GPR data and the adjusted seismic and elastic modulus values. As shown, there appears to be no relationship between the different data sets.

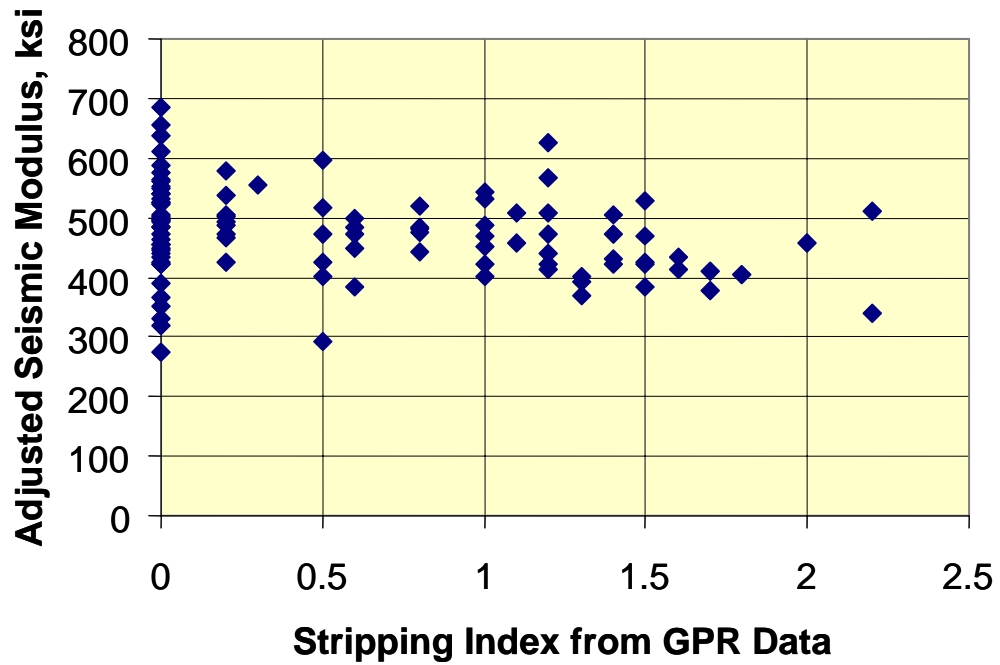


Figure 3-36. Comparison of GPR SI with adjusted seismic modulus for I-20 Lane 3

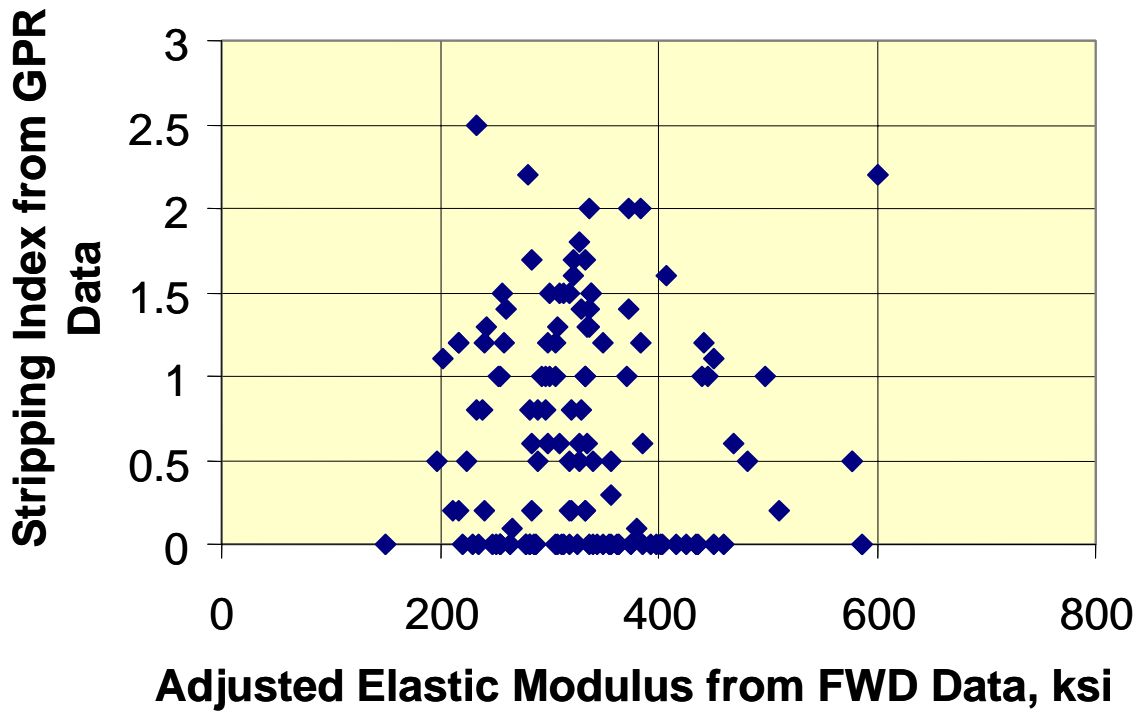


Figure 3-37. Comparison of GPR SI with FWD elastic modulus for I-20 Lane 3

3.4.4 Comparisons to Field Cores

A core index was assigned to each core based on the amount of stripping or disintegration that occurred during the coring operation. Table 3-8 summarizes the average values calculated for each core condition based on visual observations of the cores. There is limited data from the field testing to fill out the table, but the SI from the GPR tests seem to have a reasonable correspondence to the observed stripping and deterioration within the cores. Thus, $SI > 0.5$ is believed to indicate that moisture or stripping has occurred in the area represented by the core. There are too few areas with cores and FWD and seismic test results to determine the critical modulus values correlated to the core condition. The cores were taken in all three lanes, while the initial evaluation of the NDT test results was confined to Lane 3.

Table 3-7. Summary of GPR SI, average FWD and seismic modulus values, and I-20 core condition data

Lane	NDT Damage Index		Core Condition				
			Good	Fair	Poor	Deteriorated	Stripping
			0	1	2	3	4
3	SI from GPR	Mean	0.35		2.5	1.1	
		St. Dev.				0.613	
	Seismic, Modulus	Mean	469			466	
		St. Dev.	52.1			61.0	
	FWD, Modulus	Mean	498			638.5	
		St. Dev.	87.5			70.4	
All Lanes	SI from GPR	Mean	0.48		2.5	1.2	
		St. Dev.	0.718			0.659	
	Seismic, Modulus	Mean					
		St. Dev.					
	FWD, Modulus	Mean					
		St. Dev.					

3.4.5 Laboratory Tests on Field Cores

Laboratory testing was performed on selected cores in accordance with NCHRP Report 338--The AAMAS Procedure (Von Quintus 1991). Figure 3-38 compares the dynamic modulus measured on test specimens with and without moisture damage to the values that would be expected on undamaged mixtures without significant aging. As shown, the dynamic modulus values measured on the test specimens without moisture damage are within or greater than the expected range of a typical undamaged mix. One reason for the higher dynamic modulus values is that the test specimens have been aged, while the regression equation used to compute the expected range represents non-aged mixture. Thus, the laboratory test results confirm that the layer with the moisture damage is confined to the HMA binder or intermediate layer.

Table 3-9 summarizes the average values for each mix condition tested. As shown, the dynamic modulus and tensile strengths for the test specimens without any moisture damage based on visual observations are much higher than for those test specimens with moisture damage.

Figure 3-39 compares these average values to those measured on a typical mix that was used at the AASHTO Road Test. As shown, the HMA base and binder layers without any moisture damage have better fracture characteristics than the binder layer with moisture damage, as expected. The HMA binder layer that has had a significant loss of stiffness is more susceptible to fracture than the base layer.

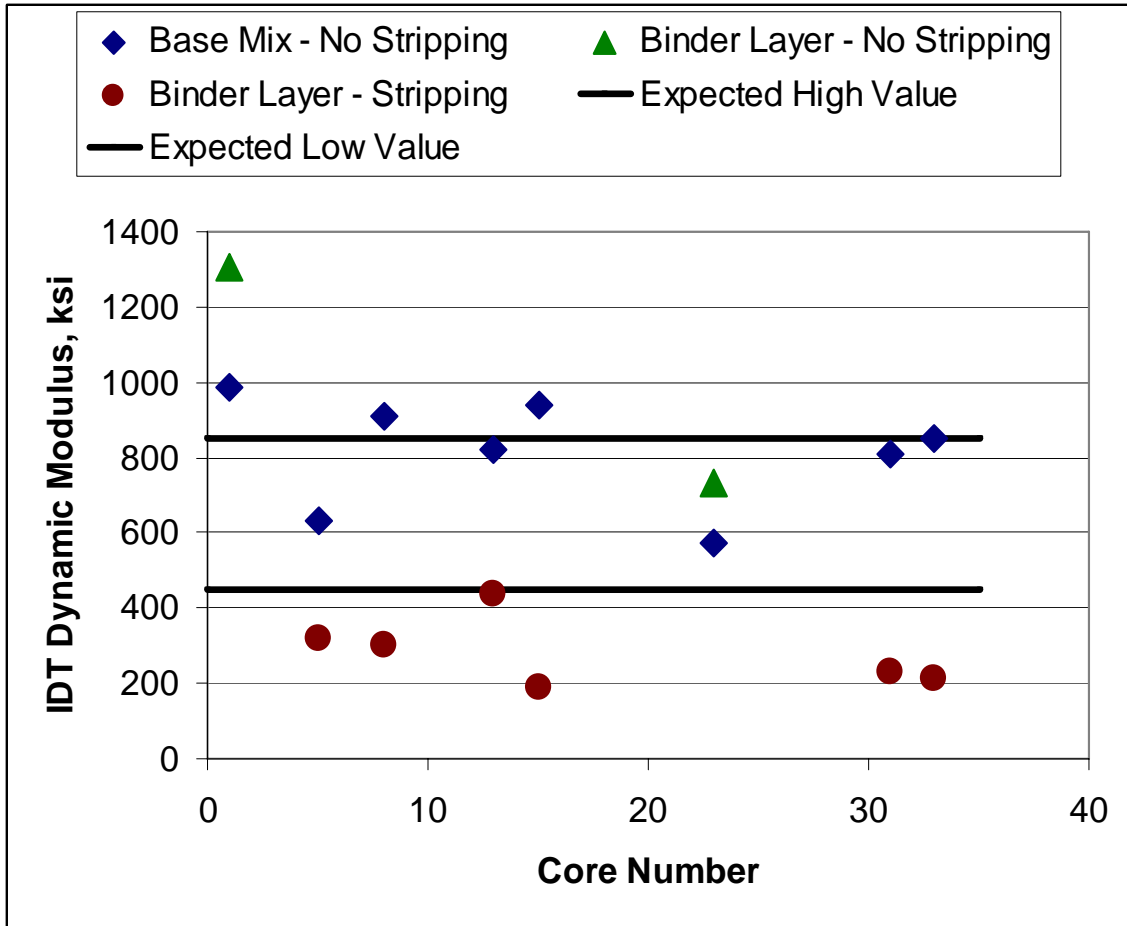


Figure 3-38. Comparison of the IDT dynamic modulus values from I-20 cores with expected values from non-aged cores

Figure 3-40 shows all of the laboratory test data on a single graph. In comparing the different mix conditions and layers, the averages should be used because of the higher variability in measuring the indirect tensile strain at failure and dynamic modulus (refer to Table 3-9).

Figure 3-41 provides a comparison of the dynamic modulus and indirect tensile strain at failure measured on the binder layer for the different levels of the GPR SI. As shown, there is correspondence between the results, with the exception of two cores. Core 13 was taken from an area with a high SI (1.8), but the laboratory test results indicate less stripping than some of the other cores. In addition, core 15 has an SI of 0, but the laboratory test results suggest significant moisture damage.

Table 3-8. Average IDT mix properties for each of the mixture conditions tested

HMA Mix Property	Layer & Condition	Mean Value	Standard Deviation	Coefficient of Variation, %
IDT Dynamic Modulus, ksi	Base Mix; No Stripping	814.4	143.9	17.7
	Binder Mix; No Stripping	1018.8	403.9	---
	Binder Mix; Some to Extensive Stripping	281.3	91.53	32.5
Tensile Strain @ Failure, in./in.	Base Mix; No Stripping	5.004	1.0002	19.8
	Binder Mix; No Stripping	4.540	2.1680	---
	Binder Mix; Some to Extensive Stripping	6.404	1.2500	19.5
Tensile Strength, psi	Base Mix; No Stripping	220.1	26.0	11.8
	Binder Mix; No Stripping	245.0	49.4	---
	Binder Mix; Some to Extensive Stripping	90.0	12.4	13.7
Poisson's Ratio	Base Mix; No Stripping	0.219	0.0331	15.1
	Binder Mix; No Stripping	0.195	0.0495	---
	Binder Mix; Some to Extensive Stripping	0.372	0.0293	7.9
Phase Angle	Base Mix; No Stripping	30.79	4.129	13.4
	Binder Mix; No Stripping	27.5	0.1414	---
	Binder Mix; Some to Extensive Stripping	35.2	1.769	5.0

It is difficult to compare the seismic modulus determined from the field tests to those dynamic modulus values measured in the laboratory using the indirect tensile test, since there were only two cores that were taken from the area with the seismic test results. Cores 5 and 8 were taken from the area where the seismic tests were conducted. The other cores were taken either from a different lane or in a different area. The seismic test results in the area represented by cores 5 and 8 suggest little to no moisture damage. The test results from the binder layer of core 8 plot above the standard line and suggest little moisture damage, while the test results from core 5 suggest significant moisture damage.

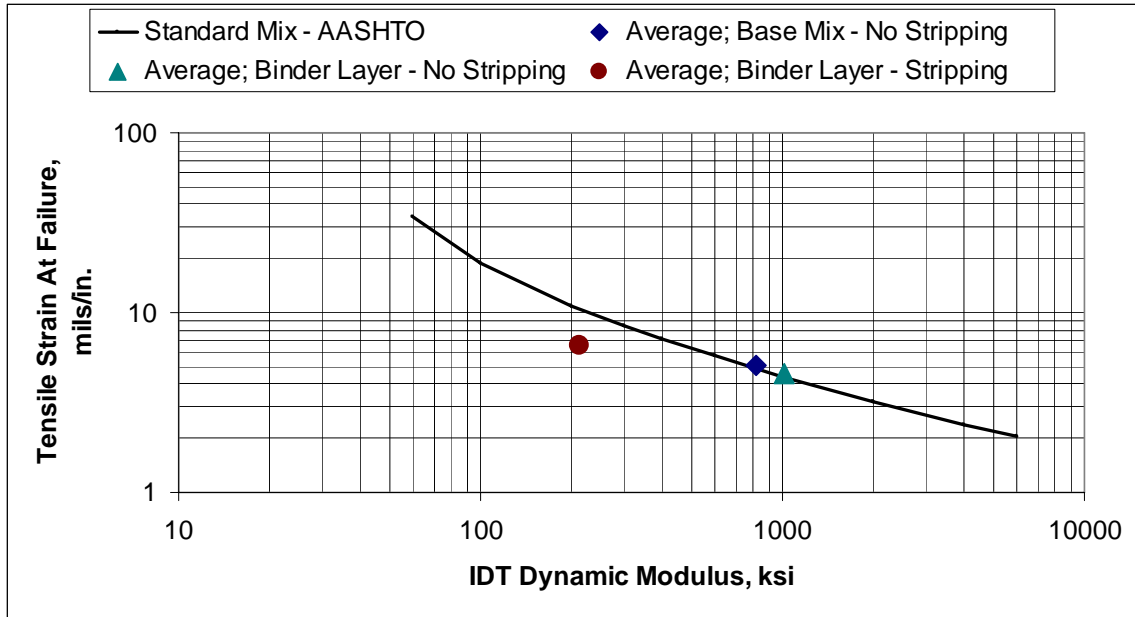


Figure 3-39. Comparison of the average IDT dynamic modulus and tensile strain at failure for the different layer conditions tested

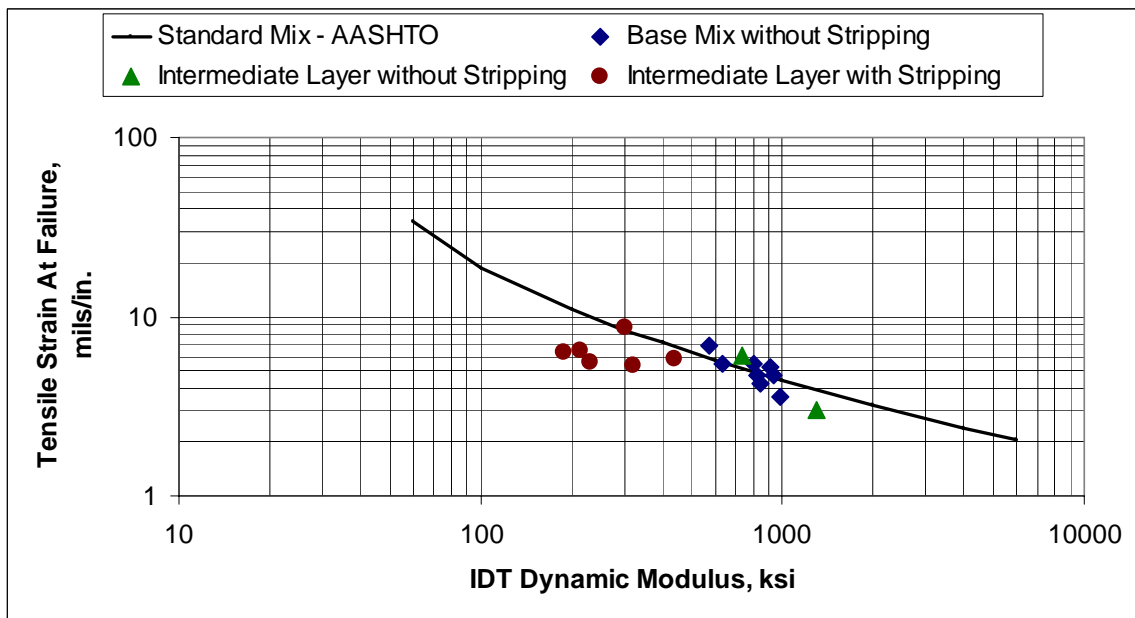


Figure 3-40. Comparison of the IDT dynamic modulus strain at failure to the typical values expected for a mix without moisture damage

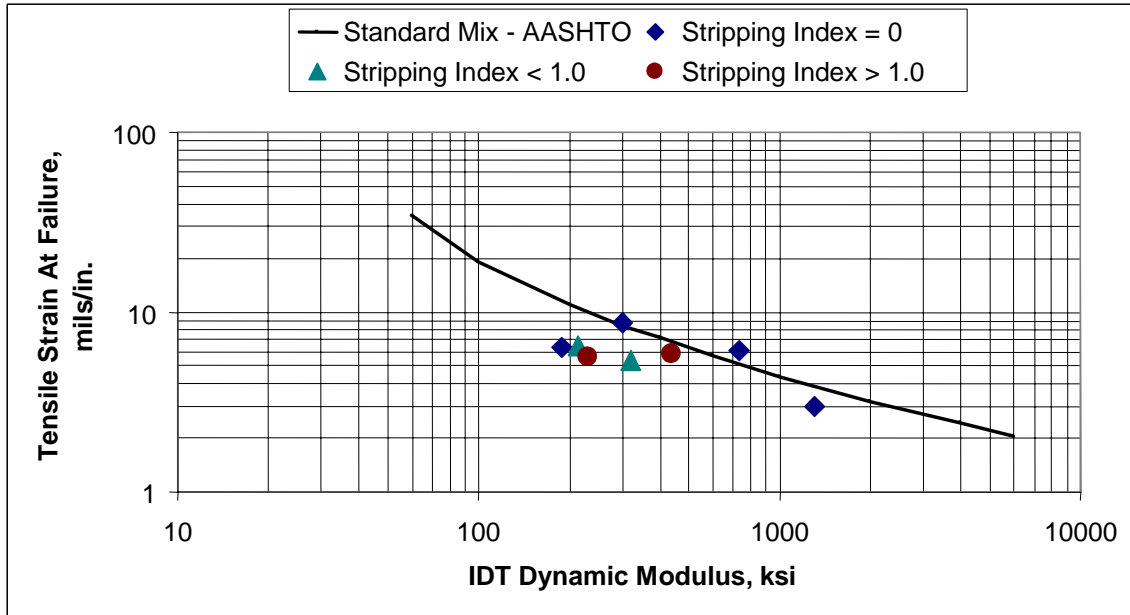


Figure 3-41. Comparison of the IDT dynamic modulus and strain at failure for test specimens prepared from the binder layer with various levels of the GPR SI

3.4.6 Discussion

Using a GPR SI of 0.5 as the critical value identifying areas with stripping, the average modulus values from the seismic and FWD data were calculated for areas with a GPR SI greater than and less than 0.5. These average modulus values are listed in Table 3-10 and compared in Figure 3-42. As shown, the average modulus estimated from the seismic tests has a reasonable correlation to the GPR results--the higher the SI, the lower the average seismic modulus. These modulus values for the ranges of expected stripping also compare reasonable well with the baseline modulus values included in Figure 3-33 and Table 3-7. Thus, the seismic and GPR testing compliment one another and should be used in further analyses, as a minimum. We expected that areas with SI > 0.5 and a modulus value less than 475 ksi at 77°F indicate some degree of moisture damage. The average modulus from the FWD tests showed no correlation with the GPR SI.

Most of the seismic test results suggest that the HMA binder layer from Lane 3 has moisture damage or some type of anomaly that would cause a significant lower modulus than expected for undamaged mix (refer to Figure 3-33). The average seismic modulus values for the moisture-damaged areas as predicted from the GPR test results would suggest that any seismic value less than 475 ksi, on the average, has some type of damage or anomaly that reduces the stiffness of the binder layer (refer to Figure 3-42). The laboratory test results suggest and confirm that the value of 475 ksi is a reasonable value, based on the results shown in Figure 3-38. To be conservative, a modulus of 500 ksi was selected as the critical value for rehabilitation design.

Table 3-9. Average HMA modulus values for the areas with different GPR stripping indices

GPR SI	Seismic Measured Modulus, ksi			FWD Calculated Modulus, ksi		
	Number of Tests	Mean	Standard Deviation	Number of Tests	Mean	Standard Deviation
0 to 0.4	51	491	82.4	55	563	81.0
0.5 to 1.0	16	462	67.0	23	559	82.3
1.1 to 1.4	23	465	62.2	31	553	75.5
>1.4	13	429	52.2	19	575	76.1

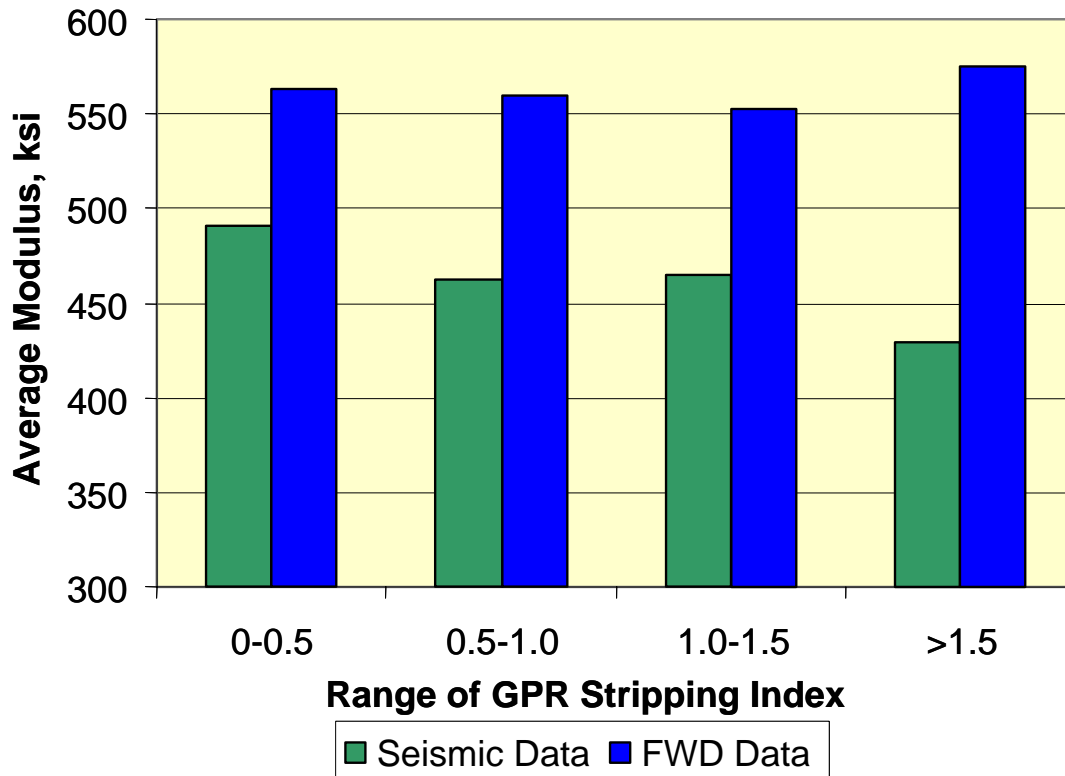


Figure 3-42. Comparison of the average estimated modulus values within ranges of GPR SI

3.5 Alternative to Stripping Index

As an alternative to the SI, we explored another GPR index as an indicator of moisture damage. Moisture damage is a deterioration process characterized by local changes in the asphalt physical properties associated with increased porosity and higher moisture content. These changes in the physical properties of the HMA are accompanied by corresponding changes in the electromagnetic properties. Increased reflections from affected layers produce localized reflection anomalies within otherwise homogeneous layers. The SI proposed in this report used the algebraic sum of these reflection amplitudes as an indicator of the intensity of reflection activity. However, it is clear from the results of the I-20 pilot project that SI alone is inadequate to identify moisture damage, and the name is undeserved.

Because these deterioration processes tend to occur non-uniformly in the pavement, a measure of the uniformity of the electromagnetic properties may be more useful in segmenting the roadway into features which can subsequently be used to plan seismic testing and coring. As a GPR indicator, we define the GPR Uniformity Index (UI) as the normalized average absolute amplitude of the GPR scan as follows:

$$UI(x) = \frac{\bar{A}(x)}{\bar{A}\left(x \pm \frac{L}{2}\right)}$$

Equation 19

where \bar{A} is the average reflection amplitude, x is the current station, and L is the normalization length. When compared to the values from neighboring locations, the index shows changes in reflection activity, which, if sufficient, may be related to moisture damage or stripping.

Normalization allows us to work with a number which varies around 1.0, and thus permits us to compare lane to lane and site to site without concern for the absolute values. For the initial site screening and segmentation, the normalization length can be selected as the entire project length. For detailed mapping of areas with potential moisture damage, a smaller normalization length may be appropriate to highlight local variability.

Another key parameter in the UI computation is the depth range over which this scan amplitude is calculated. The depth range should be selected to highlight the depth in which stripping is believed to be occurring. If this is not known, then a larger range can be used. Once cores are obtained and other data is available, this range can be reduced, and the index recalculated.

The UI definition used above is a simplification of the SI. However, because it is numerically different, we have revisited the I-20 data and carried out analyses of the data using the UI definition. The result and the comparison with the PSPA data are shown in Figure 3-43.

Note that the data for I-20 shows significant variability in both the seismic modulus and the UI. At a number of locations the seismic moduli are below the 425 ksi threshold, and the UI goes above 1.2 in many areas. The cores for I-20 indicated that there was extensive stripping, and the GPR and PSPA results confirmed this finding. To further test the utility of the UI, it was decided to employ this concept on the I-75 pilot project in lieu of the SI originally proposed for I-20.

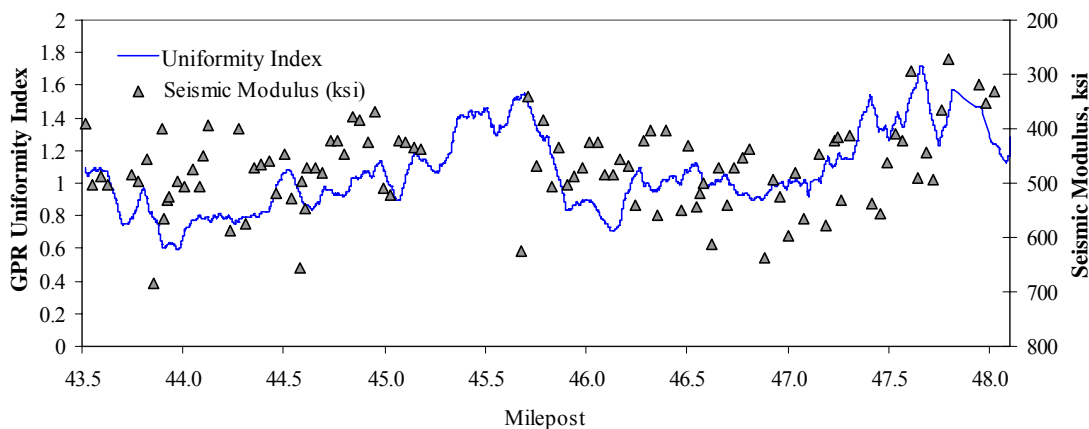


Figure 3-43. Comparison of seismic modulus to GPR UI for I-20 pilot section, approximate depth range: 3 to 11 inches

3.6 Rehabilitation Recommendation for I-20

The elastic layer theory program entitled EVERSTRS was used to calculate stresses and strains within the pavement structure to recommend the rehabilitation strategy and determine the milling depth for this segment of I-20. The layer modulus values used in the simulation were taken from the seismic test results, but adjusted to account for the appropriate temperature and loading frequency. The baseline values, no moisture damage, were taken from the dynamic modulus regression equation and adjusted for the values expected during construction or overlay placement.

The design criteria used in the rehabilitation design analyses were vertical strains in the HMA layers. The recommended depth of milling was determined based on limiting the vertical compressive strain in the HMA layer to values below those that would cause extensive damage or distortion during construction and with time under truck traffic. A zero milling depth obviously means that an HMA overlay was placed directly over the existing pavement structure, and a milling depth of 8 inches means that all of the HMA mixture with moisture damage and stripping was removed.

EVERSTRS is limited to five layers, so all layers beneath the HMA base mixture were combined for computing vertical strains in the various HMA layers. The rehabilitation design analyses were only completed based on distortions in the HMA layers. Fatigue cracking was not checked for this report.

The results from these design computations are listed in Table 3-11 and graphically shown in Figure 3-44. The loads used in the computations represent HMA delivery trucks. Figure 3-45 shows the distortion strain ratio expected for different milling depths. The distortion strain ratio is simply the ratio of the vertical compressive strain to the strain at failure and provides a quick check on the level of applied strain to the value that will result in excessive distortion. Although no testing was completed on the field cores, the failure strain used in this evaluation study was taken from NCHRP Report 338 (Von Quintus 1991).

Table 3-10. Summary of computations with EVERSTRS to determine an appropriate milling depth to minimize potential for distortion

Milling Depth, inches		Maximum Vertical Strain in Layer with Moisture Damage, Binder Layer, in./in.	Maximum Deflection, mils
0	Wearing surface left in place	-0.000692	17.4
2		-0.001215	19.9
4	Wearing surface completely removed	-0.001703	22.2
6		-0.001915	21.2
8	Wearing surface and moisture damaged layer removed	-0.000529	20.5

A distortion strain ratio criteria of 0.10 is shown on Figure 3-45 and represents a value during construction or placement of the HMA overlay. The milling depth is selected to keep the distortion strain ratio less than 0.10. As a result, any milling requires that the wearing and HMA layer with the moisture damage be removed. If the HMA layer with moisture damage and stripping remains in place, significant distortions would be expected under the HMA delivery trucks that would damage that layer and result in significant rutting after HMA overlay placement. However, the HMA overlay thickness can be designed to prevent this distortion with future truck traffic. The HMA overlay thickness to prevent significant rutting was not determined within this initial analysis.

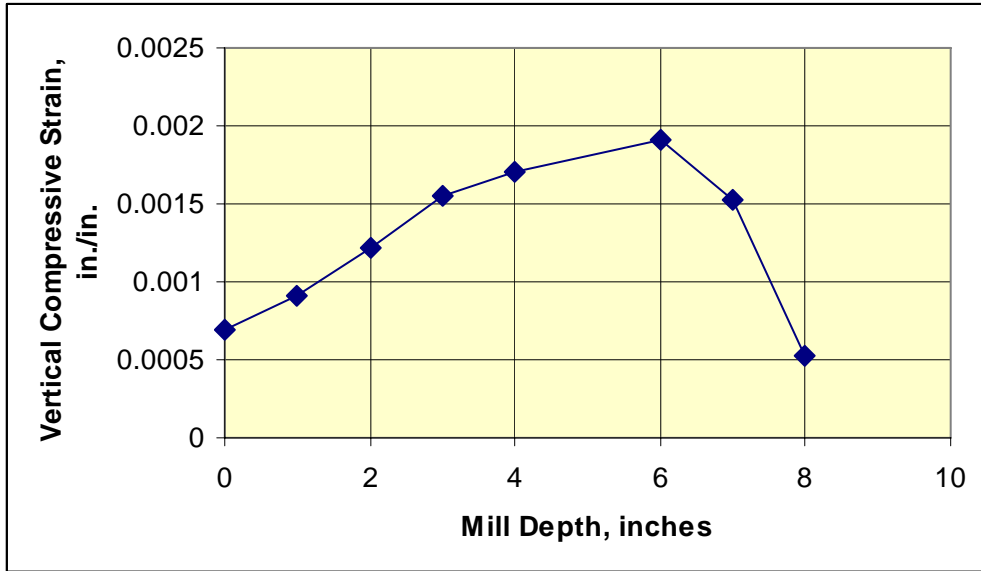


Figure 3-44. Maximum vertical compressive strain in the HMA layer for different milling depths

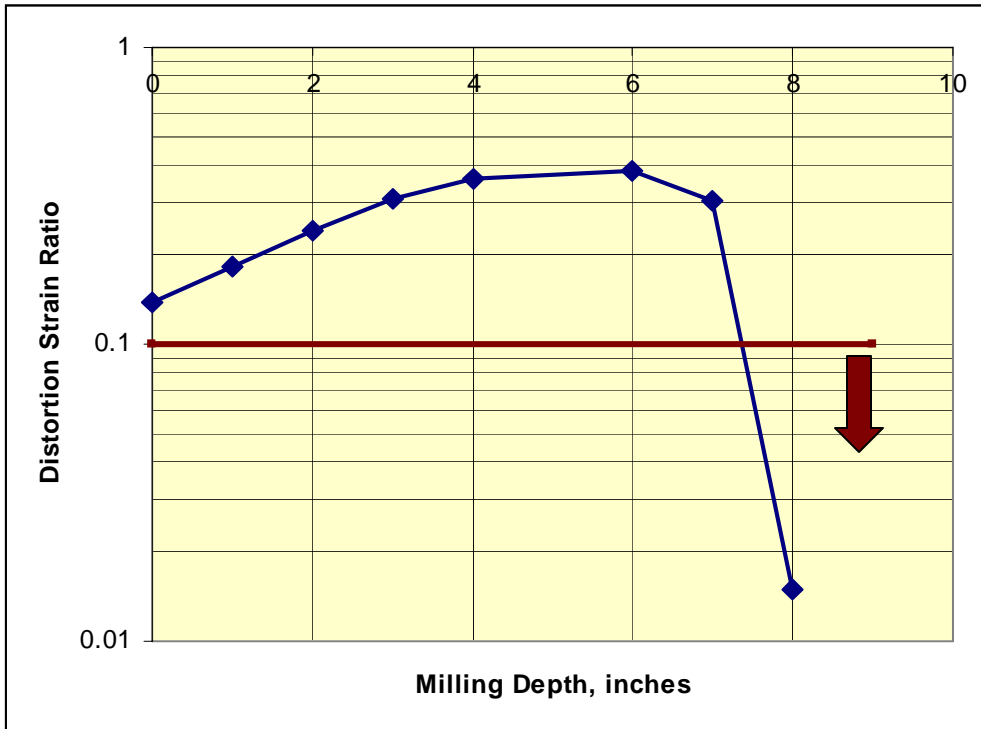


Figure 3-45. Distortion strain ratio for different milling depths

3.7 Additional Observation

One additional observation from an evaluation of the laboratory test results is that the reduction in stiffness of the HMA binder or intermediate layer may not have been caused solely by moisture. The test results show that the dynamic modulus and strength are significantly lower in the HMA binder or intermediate layer. The tensile strain at failure is also lower than but not as much as the other two parameters for some of the test specimens. Figure 3-40 illustrates that the HMA intermediate has inferior fracture characteristics, when compared to the HMA base mix. However, the test results are not as different as for other mixtures with significant moisture damage. This suggests more of a cohesion failure rather than an adhesion failure that would be typical for mixtures with moisture damage.

To determine the potential cause of a reduction in cohesion of the asphalt requires much more extensive testing. This additional testing, however, would not change the final results related to the rehabilitation recommendations that were provided for this segment of I-20. Thus, it is not recommended for this field pilot study.

One potential cause for a cohesion failure in the asphalt, in addition to a reduction in adhesion for some areas, is contamination of the asphalt with unburned fuel. The HMA intermediate layer was placed in the 1970's when drum mix plants were being operated around the country using "dirty fuels." If those dirty fuels were not properly preheated, then contamination of the asphalt is a possibility. Potential contamination of the asphalt would also help explain some of the discrepancies or differences between the seismic, GPR and laboratory test results.

3.8 Findings

The following are the findings from the data analyses conducted on the I-20 pilot section:

1. Visual observations of the cores are inconclusive. Laboratory tests on the cores are required to characterize the stripping and discriminate between areas of "good" and "bad" pavement.
2. Classical indicators of stripping as described by Kandhal and Rickards (2001) were not visible on the surface. There are, however, areas of increased fatigue cracking and rutting, primarily in lower-elevation areas.
3. Thermal anomalies are not good indicators of deterioration from stripping in full-depth asphalt pavements.
4. Average modulus values obtained from seismic tests indicate, in general, that the HMA quality is poor.
5. Significant areas of delamination are predicted by the seismic tests, particularly in the first mile of the pilot section.
6. Seismic tests indicate that the uppermost layer (3 to 4 inches) is in good condition.
7. Seismic tests indicate lower quality material between 4 and 6 inches below the surface.
8. Seismic tests indicate pockets of poorer quality material at depths below 6 inches. This could be caused by delamination.
9. GPR was able to locate the various layers within the pavement system.
10. Non-uniform electromagnetic properties may indicate non-uniform physical properties characteristic of moisture-damaged HMA.

11. The GPR SI was in agreement with core visual observations at a rate of 77% over the entire 24 lane miles of the pilot section.
12. Moisture damage is believed to be indicated by GPR SI > 0.5 and a seismic modulus less than expected for good-quality HMA.
13. The GPR UI is an indicator of the local uniformity of the electromagnetic properties of the HMA. Average modulus estimated from the seismic tests has a reasonable correlation with the GPR UI.
14. The average modulus from the FWD tests shows no correlation with the GPR SI.
15. The laboratory IDT results confirm that the moisture damage or anomalies are confined to the binder or intermediate layer along I-20.
16. The laboratory IDT results confirm that a seismic modulus value less than about 475 ksi, on the average, would indicate moisture damage in the HMA binder or intermediate layer along I-20.
17. Seismic and GPR technologies should be used in combination to improve on the reliability of identifying layers with moisture damage or other anomalies beneath the pavement surface.
18. Moisture damage may not be the only cause for the reduction in the dynamic modulus of the HMA intermediate layer that was placed in the 1970's. It is expected that this reduction in modulus is related to asphalt cohesion, as well as adhesion between the aggregate and asphalt film. If this mix was produced by a drum mix plant and a dirty fuel was used that was not properly preheated, then this could explain the lower IDT modulus and strength values, while the tensile strains at failure are not as low as expected for an adhesion problem. This cause would also help explain the difference in some of the test results between the seismic, GPR and laboratory testing.

4 PHASE II: I-75 PILOT PROJECT

4.1 Pilot Project Hypotheses

The hypotheses used for the I-75 pilot project are as follows:

1. The modulus, strength, and tensile strain at failure of an HMA mixture are significantly affected by the level of moisture damage. In other words, these properties of an HMA mixture with moisture damage are significantly less than those properties measured for the same HMA mixture without moisture damage. In addition, these properties will continue to decrease with increasing levels of moisture damage progressing from a loss of cohesion in the asphalt to advanced stripping.
2. Non-uniformity in electromagnetic properties, as indicated by the GPR UI, may indicate changes in the physical properties of the HMA.
3. Seismic tests can be used to determine the modulus of HMA mixtures. The adjusted seismic modulus is significantly affected by the level of moisture damage in the HMA mixture.

4.2 Pilot Project Description

4.2.1 Location

The I-75 pilot project was located on the northwest quadrant of the Atlanta metropolitan area in Cobb, Cherokee, and Bartow Counties. The approximate extent of the project is indicated by the box on the map in Figure 4-1. The project was limited to the northbound lanes from the MP 270 to MP 280. GPR, rutting, and roughness data were collected on all three northbound lanes between MP 270 and 280. Seismic and cracking data were only obtained in Northbound Lane 3 (outside lane) between MP 270 and 274. FWD testing and infrared thermography were not performed on the I-75 pilot, as these technologies were ineffective in locating areas of stripping on the I-20 pilot.

4.2.2 Construction History

This section of I-75 was constructed in two projects. The first project began just north of the Roberts Road interchange and continued to the Cherokee-Bartow county line. The second project began at the Cherokee-Bartow county line and continued to the Bethany Beach Road interchange.

Construction on the roadway was begun in May 1976 and completed in December 1977. Figure 4-2 shows a photograph of the northbound traffic lanes. The roadway consists of three 12-ft wide travel lanes in each direction with 10-ft wide inside and outside paved shoulders. The northbound and southbound travel lanes were separated by a variable-width median. Figure 4-3 shows the best available information on the pavement structure and the approximate dates of construction.

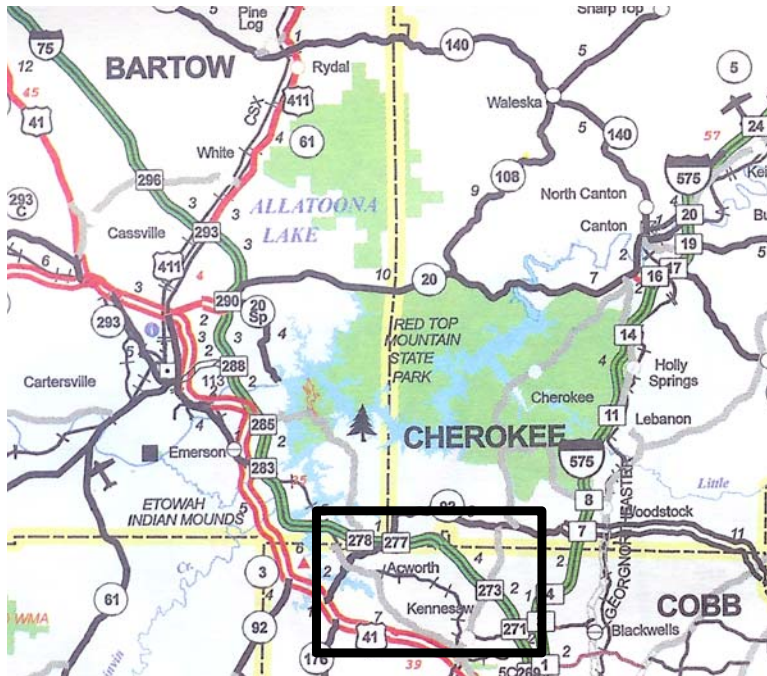


Figure 4-1. Approximate extent of I-75 pilot project



Figure 4-2. Photo of I-75 northbound lanes near MP 270.5

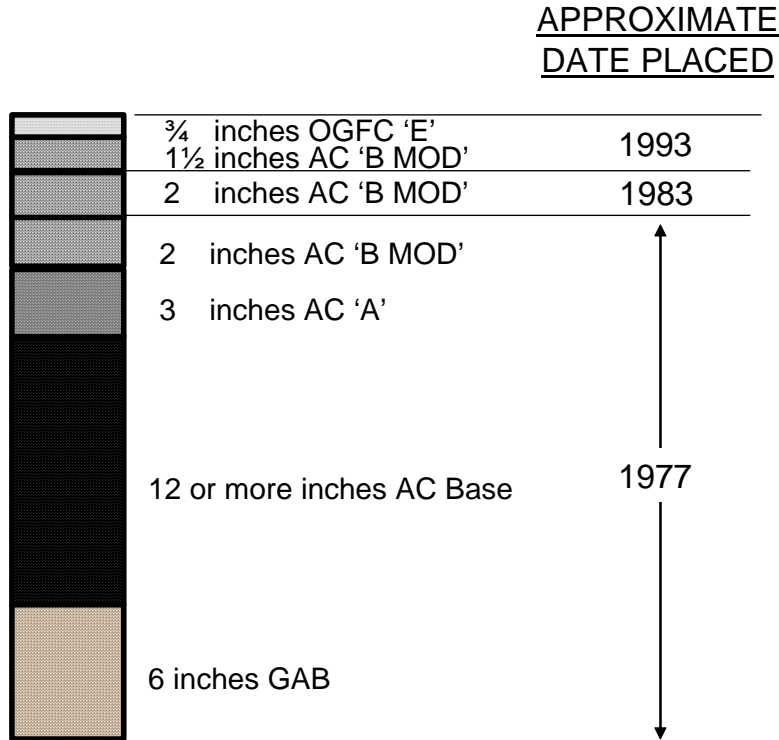


Figure 4-3. Pavement structure and approximate construction dates, I-75

4.2.3 Test Conditions

GPR data collection was conducted on the northbound lanes of I-75 on September 2, 2004. Surface condition data were collected on September 18, 2004. Neither of these data collection events required lane closures.

GDOT maintenance crews performed daytime lane closures on northbound Lane 3 between MP 270 and MP 274 on September 28 and 29, 2004 between the hours of approximately 9:30 AM to 2:00 PM. All seismic tests were performed during these lane closures. The weather conditions during the seismic data collection were partly cloudy with mild temperatures. Table 4-1 presents the weather data from Atlanta’s Hartsfield-Jackson International Airport (ATL) for the period of September 23 through April 29, 2004. The heavy rainfall reported on September 27th occurred as a result of the remnants of Hurricane Jeanne moving through the area.

Table 4-1. Weather conditions at ATL, September 2004

Date	High Temperature, °F	Low Temperature, °F	Mean Temperature, °F	Rainfall inches
September 29, 2004	78	62	70	0.00
September 28, 2004	78	65	72	0.00
September 27, 2004	72	67	70	4.89
September 26, 2004	79	63	71	0.00
September 25, 2004	81	64	73	0.00
September 24, 2004	82	66	74	0.00
September 23, 2004	85	62	74	0.00

4.3 Test Results

4.3.1 Cores

4.3.1.1 Core Locations

A total of 16 cores were extracted from northbound Lane 3 between MP 270 and 274 by GDOT on September 28 and 29, 2004. All cores were 4 inches in diameter. Table 4-2 presents the core locations and condition descriptions.

4.3.1.2 Observations from Cores

Photographs of each of the cores are presented in Appendix C. Moisture damage was observed in some of cores, but it had not progressed to advanced levels characteristic of stripping. Many of the cores broke at various depths during coring, mostly one or more interfaces between adjacent HMA layers. This observation suggests weak interlayer bonds. The HMA mixture generally stayed intact and did not disintegrate around the fracture; only a few cores exhibited mixture disintegration at the layer interface. This condition reinforces the opinion that moisture is basically confined to the layer interface. This moisture has reduced the bond between layers, but has not affected the integrity of the HMA mixture itself – at least near the surface. Most mix disintegration occurred near the lower portion of the base layer.

4.3.1.3 Laboratory Tests on Cores

Six HMA cores recovered along I-75 were selected for laboratory testing to cover the range of values measured with the seismic and GPR technologies. Specimens from these cores were tested using the IDT test to measure properties of the HMA mix that are affected by moisture damage.

Two to three test specimens were cut from each core. One test specimen was sawed from the HMA binder layer placed in 1983, and one to two specimens were sawed from the base layers placed in 1977 (refer to Figure 4-3). The existing surface layers (OGFC and B-MOD mixtures) were too thin to recover a test specimen from these layers. It is expected that these layers will be milled as part of the rehabilitation strategy and need not be tested.

The type of IDT test performed on these test specimens included the dynamic modulus and strength test. Stress-strain curves from the IDT tests are presented in Appendix D. Table 4-3 summarizes the results from the dynamic modulus tests for each loading frequency used in the test program, while Table 4-4 summarizes the results from the indirect tensile strength test in comparison to the dynamic modulus at a frequency of 10 Hz. Table 4-5 provides the average properties for each layer measured in the laboratory and shows that there is a significant difference in the properties measured for each layer. These results indicate that the HMA base placed in 1977 is the weaker or softer mixture.

Table 4-2. I-75 core descriptions

Core No.	Dist. North of MP 270, ft	MP	Thickness, inches	Field Notes	Condition of Core	Visual ID for Stripping
1	0	270.000	> 17½	Core broken off in asphalt base	Damage near surface, fractured at mid-depth	Low
2	500	270.095	> 17½	Core broken off in asphalt base	Fractured at interface in base layer	None to Low
3	1,080	270.205	22	Complete core to GAB	Disintegration near surface from coring	Likely in surface
4	1,500	270.284	26½	Complete core to GAB	Fractured at interface; damage in base layer	Low
5	2,000	270.379	> 17	Core broken off in asphalt base	Fractured and loss of material from coring in base layer	Likely in base
6	2,500	270.473	> 17	Core broken off in asphalt base	Intact	None
7	3,000	270.568	> 13	Core broken off in asphalt base	Fractured at interface in binder & base layers	Low
8	3,500	270.663	> 17	Core broken off in asphalt base	Fractured at interface in surface & base layers; damage in base mix	None to Low
9	9,635	271.825	25½	Complete core to GAB	Fractured at interface in base layers	None to Low
10	10,016	271.924	25	Complete core to GAB	Fractured at interface in base layers	None to Low
11	11,044	272.092	24	Complete core to GAB	Fractured at interface in binder & base layers	None
12	11,086	272.100	23	Complete core to GAB	Fractured at interfaces throughout core, loss of material in base mix	Likely in base
13	11,502	272.178	> 18	Core broken off in asphalt base	Fractured at interface in base mix	None
14	11,595	272.196	> 13½	Core broken off in asphalt base	Intact	None
15	9,063	271.716	> 21½	Core broken off in asphalt base	Fractured at interface near surface; loss of mix in lower base layer.	Likely in base
16	8,941	271.693	25½	Complete core to GAB	Fractured at interface throughout core	Low

Table 4-3. Dynamic modulus values measured at different frequencies for each test specimen

Core Number	Test Frequency, Hz	Test Specimen Depth Below Surface, inches		
		3 to 5	7 to 10	14 to 16
11	1	347.5	263.9	232.3
	5	597.2	400.5	335.2
	10	717.7	533.5	394.2
12	1	619.0	507.1	185.4
	5	853.9	696.5	273.7
	10	986.7	729.2	323.0
13	1	574.6	329.7	---
	5	818.5	492.6	---
	10	907.5	588.4	---
14	1	609.6	519.0	---
	5	857.7	697.8	---
	10	957.6	780.9	---
15	1	635.4	450.5	370.9
	5	846.1	674.0	554.1
	10	950.9	791.1	674.0
16	1	893.9	694.3	---
	5	1204.5	957.6	---
	10	1229.4	1157.1	---

Table 4-4. Summary of the laboratory test results on selected cores recovered from I-75

Core Number	Depth, inches	Dynamic Modulus @10 Hz, ksi	Phase Angle	Poisson's Ratio	Tensile Strength, psi	Tensile Strain at Failure, mils/in
11	3 to 5	717.7	31.5	.25	192.5	5.891
12		986.7	27.1	.19	213.3	4.636
13		907.5	32.0	.20	209.8	4.159
14		957.6	25.2	.19	247.8	3.141
15		950.9	24.7	.19	260.3	5.156
16		1229.4	26.6	.17	247.7	3.586
11	7 to 10	533.5	30.7	.29	116.5	5.339
12		729.2	29.4	.23	157.8	5.103
13		588.4	30.0	.27	125.8	4.894
14		780.9	32.9	.22	174.3	5.419
15		791.1	30.7	.22	191.4	4.293
16		1157.1	27.2	.17	179.2	3.452
11	14 to 16	394.2	38.0	.34	93.2	6.545
12		323.0	25.8	.36	79.1	5.810
15		674.0	33.6	.25	149.5	6.228

Table 4-5. Average IDT mix properties for each of the mixture conditions tested

HMA Mix Property	Layer	Mean Value	Standard Deviation	Coefficient of Variation, %
IDT Dynamic Modulus @10 Hz, ksi	Surface, 3 to 5 inches	958.3	164.2	17.1
	Binder, 7 to 10 inches	763.3	219.5	28.8
	Base, 14 to 16 inches	463.7	185.5	40.0
Tensile Strain @ Failure, in./in.	Surface, 3 to 5 inches	4.4282	1.0150	22.9
	Binder, 7 to 10 inches	4.750	.7528	15.8
	Base, 14 to 16 inches	6.194	.3687	6.0
Tensile Strength, psi	Surface, 3 to 5 inches	228.6	26.9	11.8
	Binder, 7 to 10 inches	157.5	30.3	19.2
	Base, 14 to 16 inches	107.3	37.3	34.7
Poisson's Ratio	Surface, 3 to 5 inches	0.20	0.03	13.7
	Binder, 7 to 10 inches	0.23	0.04	18.1
	Base, 14 to 16 inches	0.32	0.06	18.5
Phase Angle	Surface, 3 to 5 inches	27.9	3.2	11.3
	Binder, 7 to 10 inches	30.2	1.9	6.2
	Base, 14 to 16 inches	32.5	6.2	19.0

4.3.2 *Surface Distress*

Figure 4-4 summarizes the cracking observed in the Lane 3 of the pilot section. To simplify the interpretation of the data, the maximum observed level of severity of fatigue cracking has been plotted. The plot shows that at the time of the survey, the majority of Lane 3 did not exhibit fatigue cracking. Where fatigue cracking was observed, the majority was low in severity, with only a few locations having medium severity cracking and no areas having high severity cracking.

Transverse profile measurements were used to calculate the average rut depths within each 20-ft-long sample unit in Lane 3 between MP 270 and 280. The data points in Figure 4-5 shows the average rut depth. The smoothed curve is a moving average with a sampling window of approximately 1000 ft. The average rut depth was typically less than 0.1 inch. Unlike the surveyed section of I-20, the magnitude of the rut depth does not appear to correlate to changes in elevation.

Longitudinal profile measurements were used to calculate the IRI for 0.1-mi roadway segments in the LWP, RWP, and average of the LWP and RWP. These data are plotted in Figure 4-5. No discernable pattern emerges from these graphs with the possible exception of increased roughness near bridges.

I-75 NB

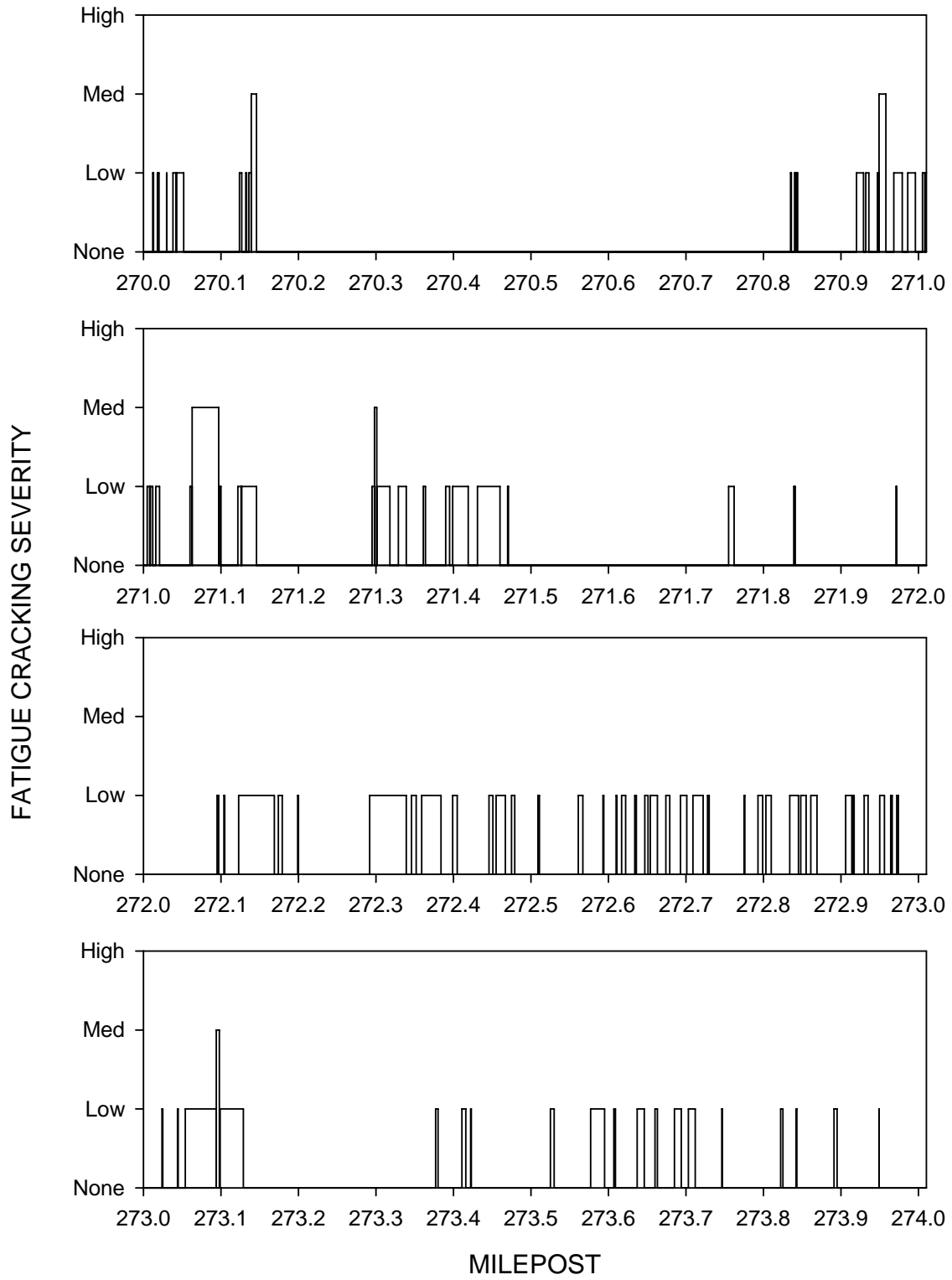


Figure 4-4. Fatigue cracking summary plot, I-75 Lane 3

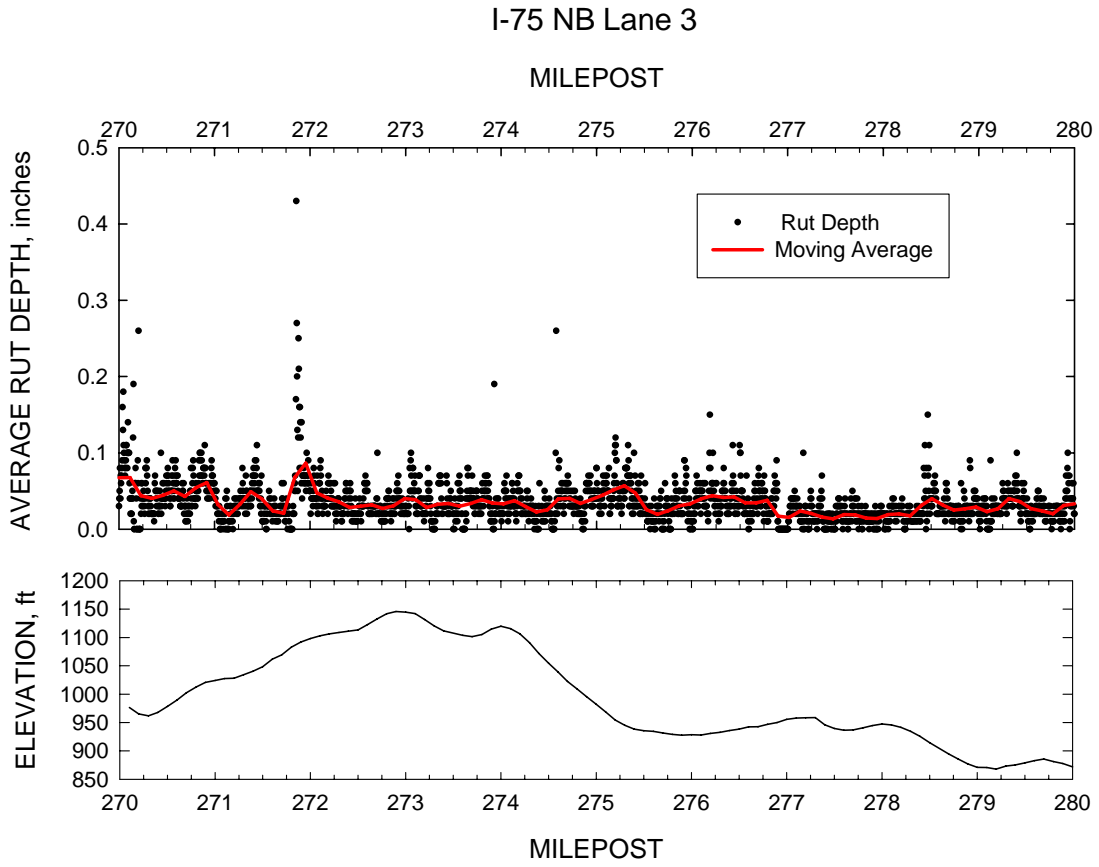


Figure 4-5. I-75 Lane 3 rutting summary plot

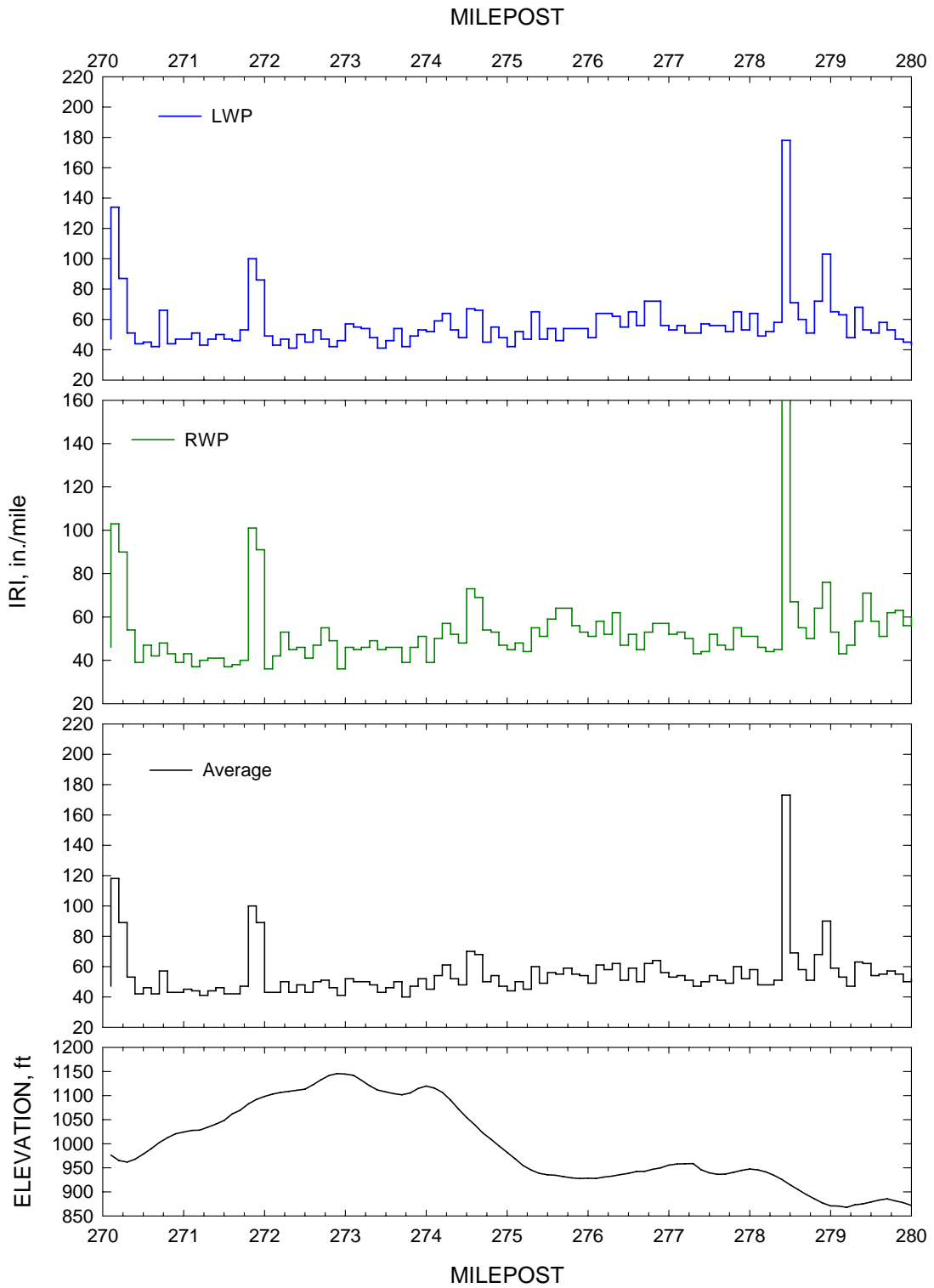


Figure 4-6. I-75 Lane 3 roughness summary plot

4.3.3 Seismic

Seismic tests were carried out on Lane 3 between MP 270 and 274 on September 28 and 29, 2004. Tests were conducted at 100 ft intervals in the center of the wheel paths of the lane. Tests along the two wheel paths were not conducted to avoid areas with alligator cracking and rutting.

4.3.3.1 Modulus Results

Appendix E contains dispersion curves from all the I-75 core locations. A typical dispersion curve obtained with the USW analysis from the location of an intact core is shown in Figure 4-7a. The variation in modulus from a depth (wavelength) of 2 inches down to 12 inches is demonstrated. The maximum and minimum depths are controlled by the sensor spacing of the PSPA used. In this case, a sensor spacing of 6 inches was used. Most moisture-damaged layers were deeper than 10 inches. With this sensor spacing, such defects may not be readily determined.

A straightforward but approximate manner of obtaining a representative modulus for the HMA layer at this location is to simply average the moduli presented in the figure. The solid line in the figure corresponds to this average value. To utilize this average value in the analysis, it was first adjusted to a temperature of 77°F, and then it was converted to a design modulus using the Aouad et al. (1993) procedure.

The shape of the dispersion curve is also important. As reflected in the picture of the core in Figure 4-7a, the top 12 inches of the material consists of at least four lifts. If the modulus of the lifts were nearly uniform, the dispersion curve would exhibit a constant modulus with depth. Observation of the dispersion curve reveals that the top layer is reasonably stiff. Between wavelengths of 4 inches to 8 inches the layer is of lower quality. Below 8 inches, once again, the material is of better quality. The intermediate low-quality material is evident in the core. It should be emphasized that the actual moduli from the second through fourth lift can only be obtained through a sophisticated backcalculation process.

Similarly, a typical dispersion curve from a deteriorated core location is shown in Figure 4-7b. The top layer seems to be stiffer than the one from the intact location. At depths between 4 inches and 6 inches, the HMA is of lower quality than the intact core. Below 6 inches, the modulus increases significantly, which is reflected in the dispersion curve as a rapid increase in modulus. The deteriorated material is not directly detected because it is sandwiched between two layers of extremely stiff HMA.

To further quantify the reasonableness of the results, the intact and damaged cores were cut into distinct layers and the seismic modulus of each layer was determined in the laboratory. The core pieces and their corresponding moduli are also shown in Figure 4-7. Considering experimental errors, fairly reasonable agreement between the dispersion curves and the quality of the materials is observed.

As indicated before, all points were tested using a PSPA sensor spacing of 6 inches. A number of points were also tested using 12-inch spacing so that the dispersion curve deeper within the HMA section can be obtained. The results from the deteriorated core are shown in Figure 4-8. In this case, the properties down to a depth of 24 inches can be sampled. However, the dispersion curve from depths less than 4 inches is not available. The dispersion curve below a depth of 10 inches tends toward lower moduli, even though the material below the damaged area is stiff. Again, this indicates that the less than 1-inch thick deteriorated layer at a depth of 10 inches cannot be detected. However, one should also consider that such a small region deteriorated at such a depth may not be considered a threat to the structural integrity of the pavement section.

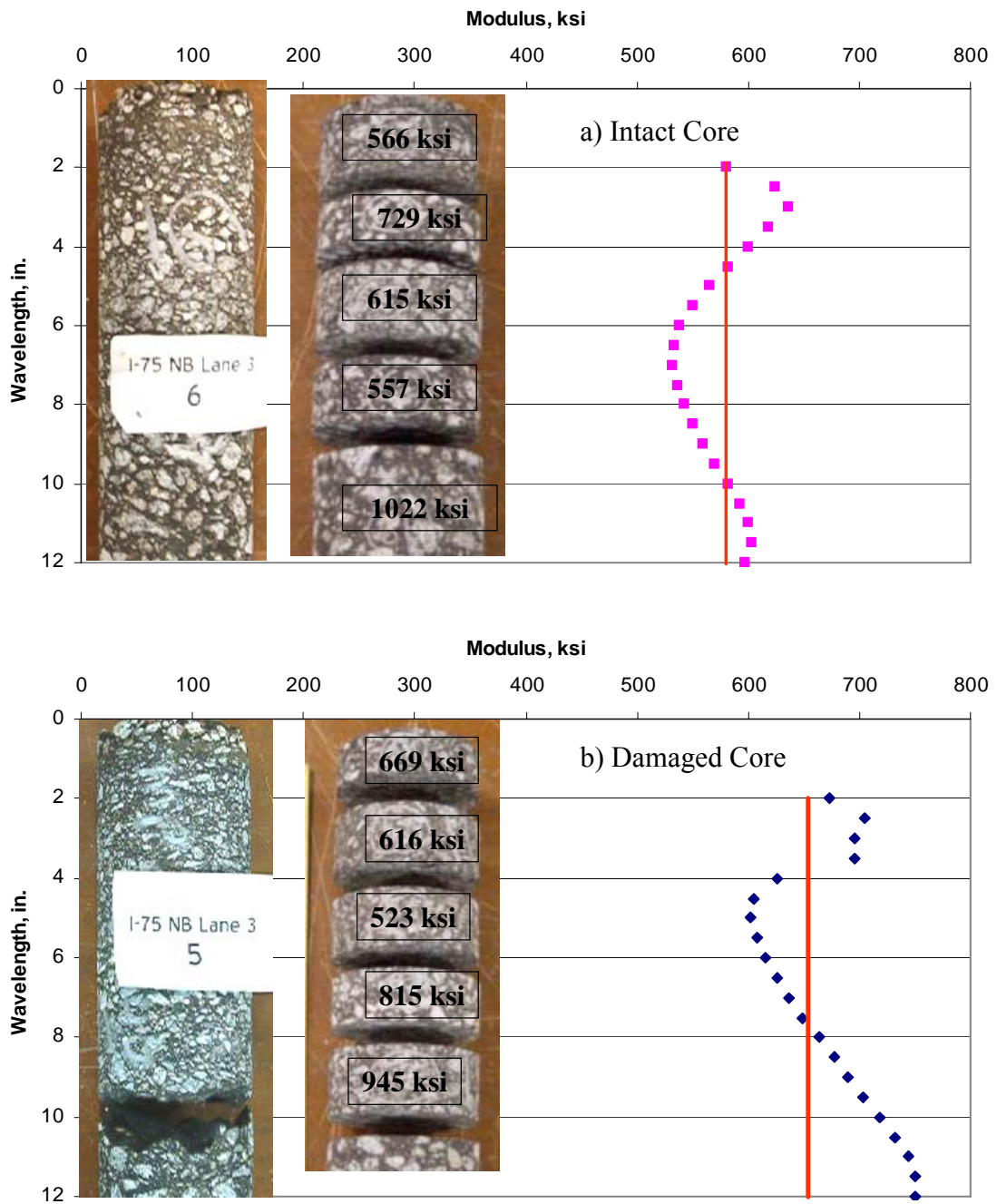


Figure 4-7. Typical dispersion curves from intact and deteriorated sections of I-75

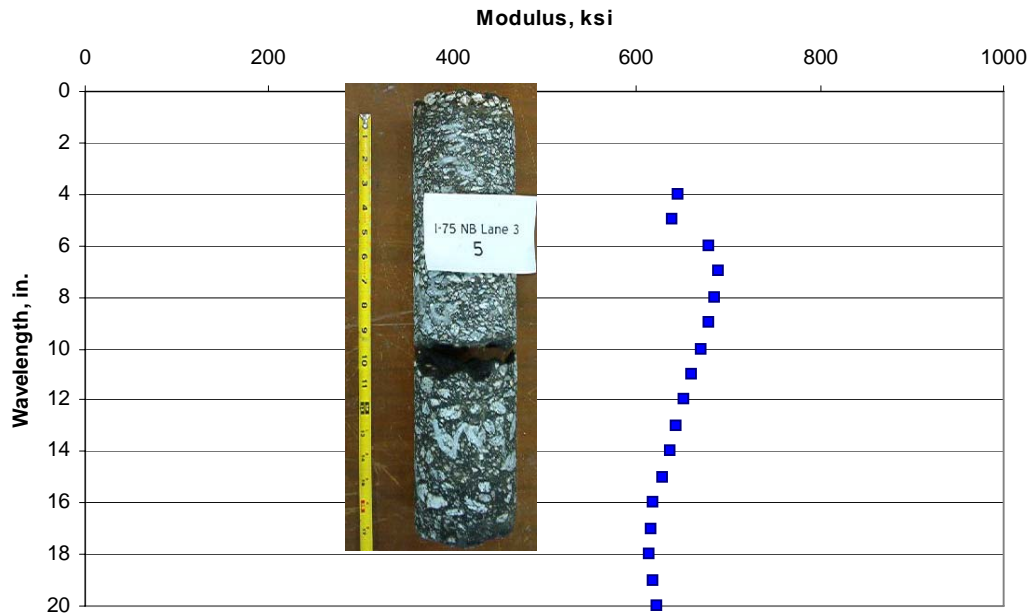


Figure 4-8. Typical dispersion curve from deteriorated section of I-75 using 12-inch PSPA sensor spacing

The variation in average modulus along the site is shown in Figure 4-9. The data are categorized into three groups: good, marginal and poor. Since the site was located on an interstate, we assigned a value of 600 ksi and above for a good-quality HMA layer. Majority of points between MP 270 and 272.2 place in this category. The marginal category was considered as a material with an average modulus between 475 ksi and 600 ksi. As reflected in the figure, most points north of MP 272.2 fall in this category. Finally a poor material is any material with a modulus less than 475 ksi. Several areas tested fall into this category.

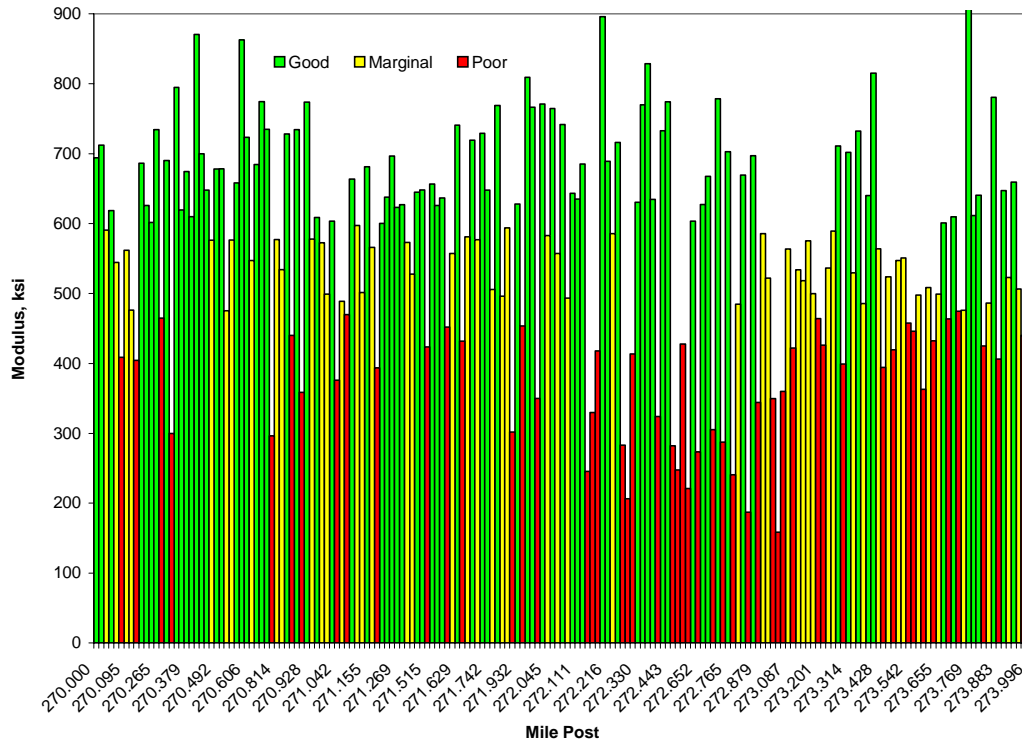


Figure 4-9. Variation in average modulus obtained with USW Method along the length of the I-75 pilot project

The modulus contour and the impact-echo contour maps along the site are shown in Figures 4-10 and 4-11 or the work performed on the first and second day, respectively. In the figures, the x-axes correspond to the mile post.

Figures 4-10a and 4-11a are three-dimensional representations of the dispersion curves obtained with the USW method. As such, the y-axes of these figures are wavelengths which are approximated as thickness. The color coding used to represent the modulus is as follows:

- Dark Blue: High Quality HMA (modulus of 650 ksi and above)
- Light Blue: Reasonable Quality HMA (modulus range of 525 ksi to 650 ksi)
- Yellow: Below Average Quality HMA (modulus range of 400 ksi to 525 ksi)
- Red: Poor Quality HMA (modulus of less than 400 ksi).

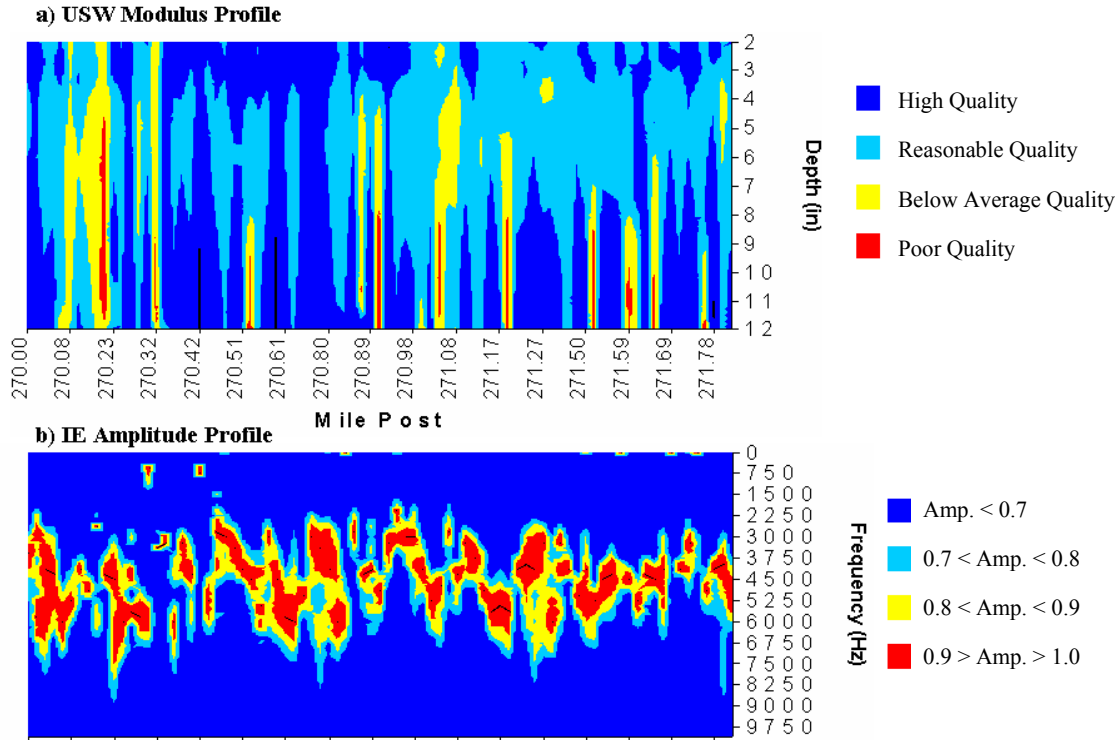


Figure 4-10. Variation in modulus and impact-echo amplitude from Day 1 of I-75 field tests

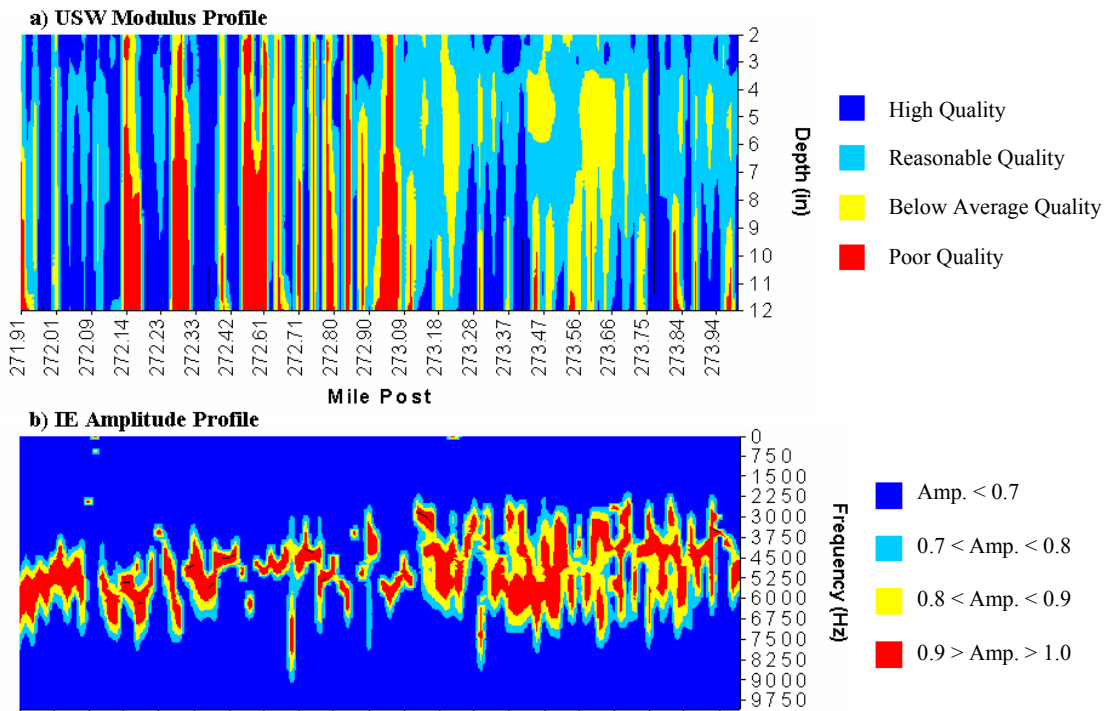


Figure 4-11. Variation in modulus and impact-echo amplitude from Day 2 of I-75 field tests

The red and yellow zones indicate of the areas of concern. It should be emphasized that the red and yellow contours may occur for several reasons. The most obvious reason is low quality materials that are either poorly constructed or have experienced moisture damage. The second reason can be the debonding of the HMA layers.

Figures 4-10b and 4-11b are the three-dimensional representations of the impact-echo amplitude. As such, the y-axes of these figures are frequency. The color coding, which used to represent the normalized amplitude is as follows:

- Dark Blue: Normalized Amplitude less than 0.7
- Light Blue: Normalized Amplitude between 0.7 and 0.8
- Yellow: Normalized Amplitude between 0.8 and 0.9
- Red: Normalized Amplitude between 0.9 and 1.0.

For tests conducted during the first day, as reflected in Figure 4-10a, the section between MP 270.0 and 270.3 are of concern. Past that point, the first 4 to 6 inches of the AC layer is typically of good quality. The quality of the material below a depth of 4 to 6 inches varies. The impact echo demonstrates signs of deterioration in some of the areas with good quality materials, especially between MP 271.500 and 271.900, and in the vicinity of MP 271.400.

The results from Day 2 of field work are shown in Figure 4-11. Once again, the top 3 to 4 inches of the material seems to be in good condition. Areas north of MP 272.3 are of concern. The materials north of MP 273.3 seem to be more reasonable, but the impact-echo graph indicates the possibility of delamination.

4.3.4 GPR

4.3.4.1 Data Collection

GPR data collection for the northbound lanes of Interstate 75 began on the PCC section and the ramp just south of MP 270 and continued to the bridge deck just north of MP 280. Four lines of data were collected in each of the 3 lanes – one in each wheel path, one in the centerline, and one along lane boundary line between lanes.

The GPR data for I-75 for the full-depth HMA section shows three major layers within the HMA structure, with the layer bottoms at approximately 4, 7, and 21 inches below the surface. Figure 4-12 shows an example of the raw GPR data showing these layer boundaries.

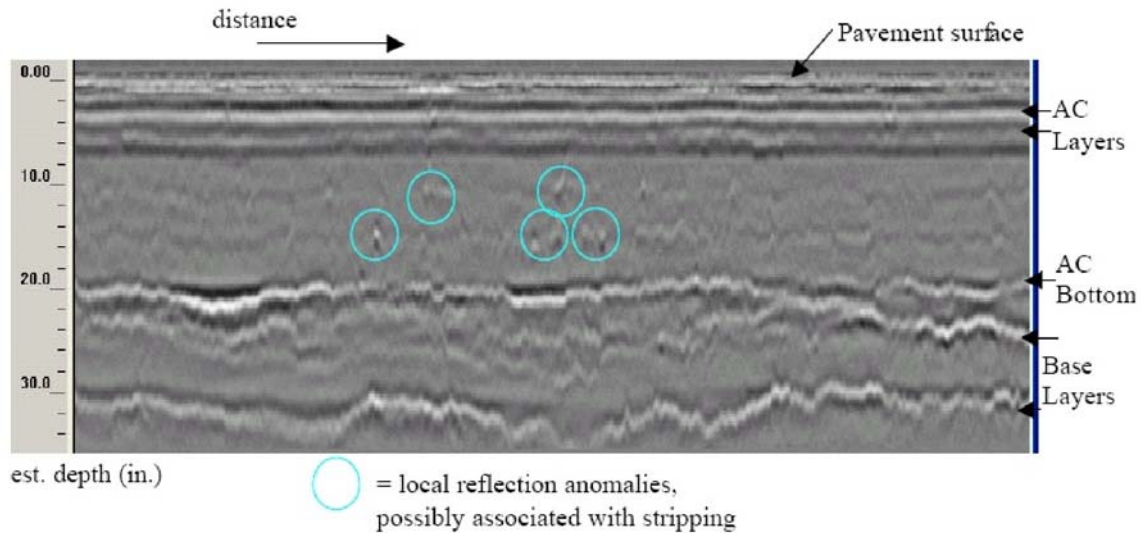


Figure 4-12. Sample GPR section data from centerline of Lane 3, I-75

4.3.4.2 Initial Analysis

The UI was calculated for the portion of the pavement between the upper AC layers (3 to 4 inches) and the upper part of the HMA base layer (~11 inches). This range coincides with the useful range of the PSPA data, and conditions below this depth are realistically not a major concern. The UI was correlated with the mean modulus values obtained from the PSPA testing, and the results of this comparison are shown in Figure 4-13. In Figure 4-13, the UI axis is on the left, and the PSPA modulus axis is on the right. Note that the PSPA modulus is plotted in descending order, since lower PSPA moduli should correspond with higher stripping indices. The values of the UI and the PSPA modulus compare reasonably well. Note that most of the UI values fall between 0.8 and 1.2, and most of the PSPA values are greater than 425 ksi.

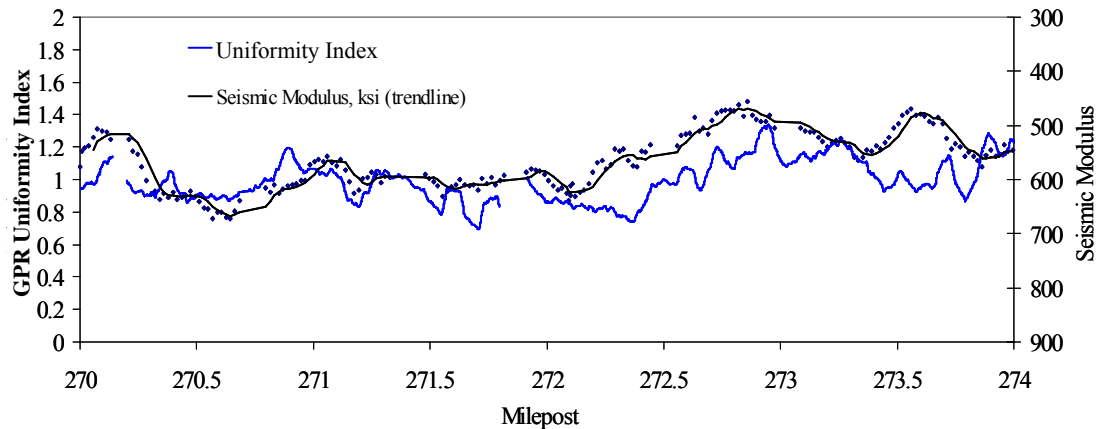


Figure 4-13. Comparison of seismic modulus to GPR UI for I-75 pilot section, approximate depth range: 3 to 11 inches

4.3.4.3 Detailed Correlations

Subsequent to this initial analysis of the I-75 GPR and PSPA data, additional data were generated using IDT testing. The IDT data identified a weak layer between depths of 7 to 16 inches, and little evidence of stripping in the upper layer. Based on this observation, the UI calculation was modified to focus on this deeper portion of the pavement cross section. Reflection anomalies occurring in this region, as depicted in Figure 4-12, could be indicators of stripping or other types of damage. In order to identify these local effects, the index was normalized by its running average over a 500 foot length. The normalization by the running average highlights local changes associated with damage, rather than the overall trends in pavement properties as indicated in Figures 4-13 and 4-14.

Based on this refined analysis, a more detailed correlation was carried out between the UI, core data, and seismic data. The core data obtained for I-75 is summarized in Table 4-2. All cores were taken in the centerline of the low speed lane. The data shows that most of the core breaks occur at depths of 7 inches and below.

A detailed analysis of the core conditions was carried out as part of this step. This detailed analysis concluded that weakness in the layers revealed by the PSPA data and the cores were not directly related to stripping. The damage detected in the cores and PSPA data could possibly be due to inconsistencies in the original construction process.

In order to calibrate a threshold for the GPR UI described above, the UI values were computed at the approximate core locations in the GPR data. The approximation is due to possible calibration differences between the GPR DMI and the distance measuring device used to locate the cores. These values are shown in Table 4-6.

Cores 1, 4, 6, and 14, all of which appear to be in good condition, have UI values all less than 1.05. Cores 3, 5, and 15, all either damaged or likely stripped, have a high UI values (at least one value > 1.34). Core 8, however, also obviously in poor condition based on PSPA data, has low UI values. Based on the UI values, we would expect poor conditions in Cores 9 and 13. There is no PSPA data for Core 9, but the observations show fractures at 9.5 inches and 13.5 inches. These fractures could be related to moisture damage. Core 13 PSPA data shows weakness from 2 to 4 inches, but it is not clear whether this is moisture damage.

Table 4-6. UI values at I-75 core locations

Core	UI		Core/PSPA Analysis
	3 to 7 inches	7 to 16 inches	
1	0.98	1.03	No damage below 2 inches
2	1.37	0.73	Weaker from 4 to 6 inches
3	1.07	1.72	Damaged at 3 inches and below 11 inches; low modulus and modulus ratio
4	1.05	0.72	No damage
5	0.82	1.10	Damage at 3 to 4 inches
6	1.05	0.66	No damage
7	1.07	0.88	Weaker from 3 to 5 inches
8	0.82	0.80	Damaged at 3 and 8 inches
9	1.16	1.96	Fracture at 9.5 inches and 13.5 inches
10	0.81	1.75	Fracture at 12.5 inches
11	0.82	0.89	Weaker from 2 to 4 inches, fracture at 14.5 inches
12	1.08	1.00	Weakness at 3 inches; fracture at 13.5
13	1.67	1.45	Weaker from 2 to 4 inches
14	0.88	1.07	No damage
15	1.60	1.80	Fracture at 6 inches; rubble from 12 to 14 inches
16	0.78	0.63	Broken at 6 and 15 inches; high modulus

4.3.4.4 Final Condition Maps

The locally normalized UI has been calculated for each pass of the survey, and the results have been contour plotted as shown in Appendix F. Two separate analyses have been carried out – one for the upper layers (approximately 3 to 11 inches) and one for the lower layers (approximately 7 to 22 inches). Based on the discussion above, threshold values of 1.20 and 1.40 have been selected for the upper and lower level mapping of the UI, respectively. The maps show all areas with UI exceeding these thresholds, and the map color is proportional to the UI value as shown in the color key below each map. The areas revealed by the maps are showing relatively high reflection activity in the GPR data. This activity could be related to moisture damage or to other types of conditions altering the density and moisture content of the material.

4.4 Analysis of Results

4.4.1 Baseline HMA Layer Modulus – No Moisture Damage

In order to evaluate whether seismic test can be used to determine the modulus of HMA mixtures (Hypothesis 3, see Section 4.1). The modulus versus temperature relationship for an HMA mixture without any moisture damage is referred to within this report as the baseline value for a specific mixture. As was the case for the I-20 pilot project, the Witzak dynamic modulus regression equation (Equation 18) was used to estimate the modulus of the HMA mixtures at different temperatures and

depths within the pavement structure. Figures 3-30 and 3-31 show the average dynamic modulus by month for a good quality HMA binder and base mixture for an average year in the Atlanta area, respectively.

Repeated load resilient modulus tests conducted on typical Georgia HMA mixtures were also used to estimate the baseline modulus values for this study. These tests were completed under National Cooperative Highway Research Program (NCHRP) Project 9-6(1) in the late 1980's (Von Quintus 1991) on various Georgia mixtures that were sampled during construction in the 1980's. Figure 5 shows the HMA resilient modulus as a function of temperature, which is based on the results from hundreds of repeated load tests from that NCHRP project. All mixtures used in that test program were unmodified mixtures. It was assumed that the HMA mixtures placed along this segment of I-75 consist of unmodified mixtures. The expected baseline modulus-temperature relationship for the binder mix along I-75 is also shown in Figure 4-15.

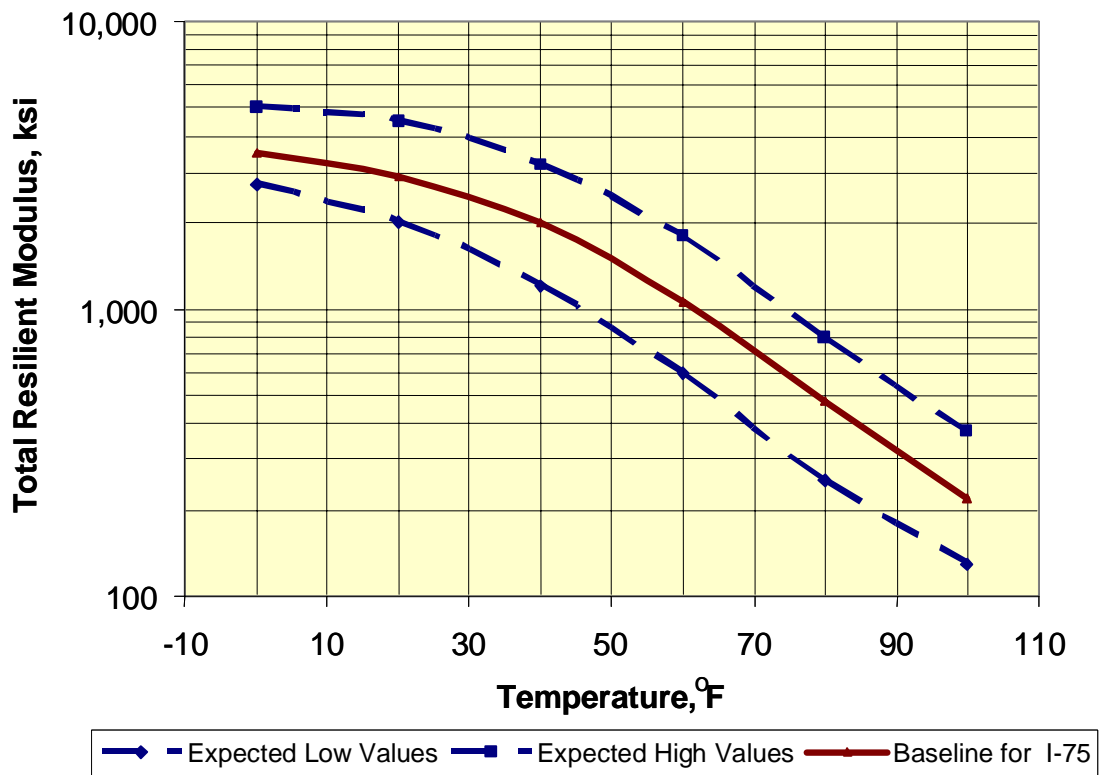


Figure 4-14. Expected high and low total resilient modulus values

Table 4-7 summarizes the dynamic modulus for an intact, good quality HMA mixture for the average temperatures that were used for evaluating the field tests along I-75. These baseline values were adjusted from modulus testing completed on similar HMA mixtures that were placed on Georgia roadways in the 1980's. Adjustments were made based on type of test (resilient versus dynamic), loading frequency, and age.

Table 4-7. Summary of the expected modulus values for HMA without moisture damage

Temperature, °F	Modulus, ksi				
	Expected Value	HMA Surface Mix	HMA Binder Mix	HMA Base Mix	Equivalent Value
77	Low	500	450	350	425
	Mean	700	650	500	600
	High	900	850	650	775
Notes:					
<ol style="list-style-type: none"> 1. The expected high and low values for the HMA binder and base layers were adjusted to account for different loading frequencies and mix volumetric properties. 2. The equivalent layer dynamic modulus values represent those similar to the methodology used during the seismic testing. 					

4.4.2 GPR Results

GPR tests were conducted to identify areas with higher levels of moisture or areas with significantly different responses. The testing and data interpretation procedures were previously presented in this report.

UI values were calculated for two depths: 3 to 7 inches and 7 to 16 inches. No significant differences could be observed between the two depths, with the exception that the higher indices were measured closer to the surface. Longitudinal profiles of the UI were previously presented in the report, and suggest fairly uniform conditions or responses along this segment of I-75.

4.4.3 Seismic Tests

Seismic tests were conducted to estimate the dynamic modulus of the HMA mixtures. The testing and data interpretation procedures were previously discussed in this report. The seismic data was reduced into seismic modulus values. The seismic modulus values were adjusted to a standard loading frequency of 15 Hz. and a temperature of 77 °F. Figure 4-16 shows the longitudinal profile of the adjusted seismic modulus values. Similar to the GPR findings, these results suggest fairly uniform conditions along I-75.

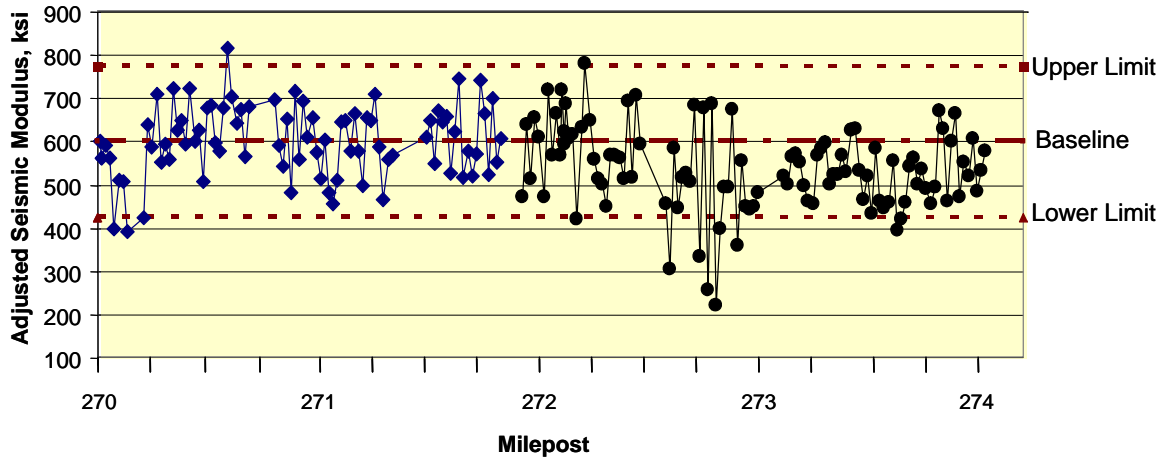


Figure 4-15. Longitudinal profile of the adjusted seismic modulus along I-75 compared to the expected range without moisture damage

The upper and lower limits and baseline value of the seismic modulus have been included on the longitudinal profile as dashed lines (refer to Figure 4-16 and Table 4-7). With the exception for a few areas, most of the seismic modulus values are within the range expected for an intact, good quality HMA mixture. Another observation from the profile is that the segment of I-75 from MP 270.150 to 270.557 (Station 135) has a higher modulus than the other segments.

There are two areas where the adjusted seismic modulus values were significantly less than the lower values expected for good quality HMA mixtures without moisture damage. One area is near the beginning of the project (milepost MP 270.07 to 270.25) and the other is towards the end of the project (MP 272.5 to 272.9). These two areas also have the higher GPR UI values. Although the GPR UI are generally higher for the lower seismic modulus values, the correlation between these two measurements is poor along this segment of I-75.

Table 4-8 shows that the adjusted seismic modulus measured at or near each core location is significantly higher than the lower-bound baseline modulus value of 425 ksi (see Figure 4-16 and Table 4-7). Moisture damage or stripping was visually observed in four of the cores. This observation suggests that the adjusted seismic modulus is not related to the condition of the cores. However, the depth of the HMA mixture showing signs of moisture damage is below the seismic test depth (generally 14 inches below the surface). More importantly, no cores were taken in the one area with the lowest adjusted seismic modulus (MP 272.5 to 272.9).

Based on the hypotheses, the degree of reduction in the modulus of the HMA layer from the baseline value should be significantly less than found for the HMA layers along I-20. The baseline modulus value is defined as the average modulus for an intact, good quality HMA mixture without any moisture damage. Thus, we conclude that most of the area tested does not have stripping and only minimal moisture damage. The moisture that was detected by the GPR tests is believed to be confined to interfaces between HMA layers and has not caused advanced levels of moisture damage.

Table 4-8. Core condition compared with adjusted seismic modulus

Core Number	Milepost	Condition of Core	Visual ID for Stripping	Seismic Adjusted Modulus, ksi
1	270.000	Damage near surface, fractured at mid-depth	Low	566
2	270.095	Fractured at interface in base layer	None to Low	510
3	270.208	Disintegration near surface from coring	Likely in surface	425
4	270.284	Fractured at interface; damage in base layer	Low	553
5	270.379	Fractured and loss of material from coring in base layer	Likely in base	650; damage below test depth
6	270.473	Intact	None	507
7	270.568	Fractured at interface in binder & base layers	Low	680
8	270.663	Fractured at interface in surface & base layers; damage in base mix	None to Low	566
9	271.818	Fractured at interface in base layers	None to Low	608
10	271.932	Fractured at interface in base layers	None to Low	641
11	272.092	Fractured at interface in binder & base layers	None	721
12	272.100	Fractured at interfaces throughout core, loss of material in base mix	Likely in base	594; damage below test depth
13	272.178	Fractured at interface in base mix	None	633
14	272.196	Intact	None	780
15	271.723	Fractured at interface near surface; loss of mix in lower base layer.	Likely in base	744; damage below test depth
16	271.705	Fractured at interface throughout core	Low	573

4.4.4 Laboratory Tests

Figure 4-17 compares the dynamic modulus measured on the test specimens recovered from the three layers to the values that would be expected on undamaged mixtures without significant aging. As shown, the dynamic modulus values measured on the test specimens sawed from the binder and upper base layers are within or greater than the expected range of a typical undamaged mix. One reason for the higher dynamic modulus values is that the test specimens have been aged, while the regression equation used to compute the expected range represents non-aged mixture.

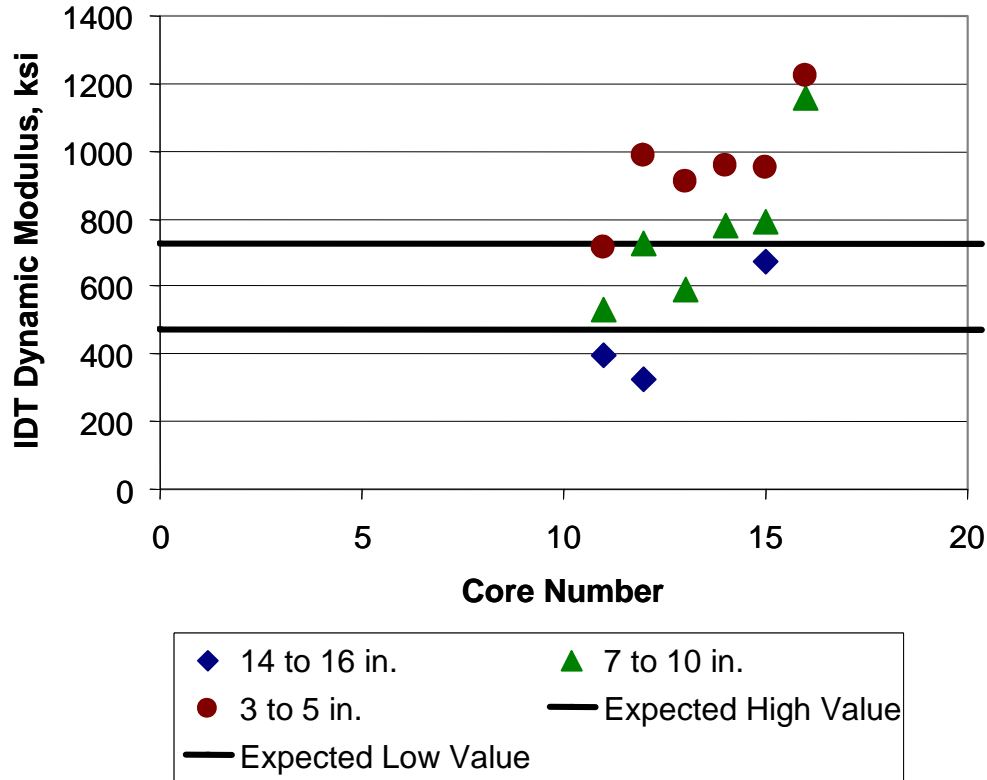


Figure 4-16. Comparison of measured IDT dynamic modulus from I-75 cores to expected values from non-aged mix

The dynamic modulus measured in two of the three test specimens taken from the lower base layer (placed in 1977) are below the lower baseline value. These lower modulus values could suggest moisture damage, but could be the result of higher air voids, lower asphalt contents, or micro-fatigue cracks near the bottom of the layer. If the lower modulus values for the lower base layer are a result of moisture damage, the relationship between strength and modulus for the moisture damaged layer should be different from those layers without moisture damage. Figure 4-18 shows the relationship between the indirect tensile strength and dynamic modulus for the different layers included in the test program. As shown, all three layers have consistent relationship between strength and modulus, suggesting that the lower modulus values may be related to differences in volumetric and asphalt properties, rather than related to moisture damage.

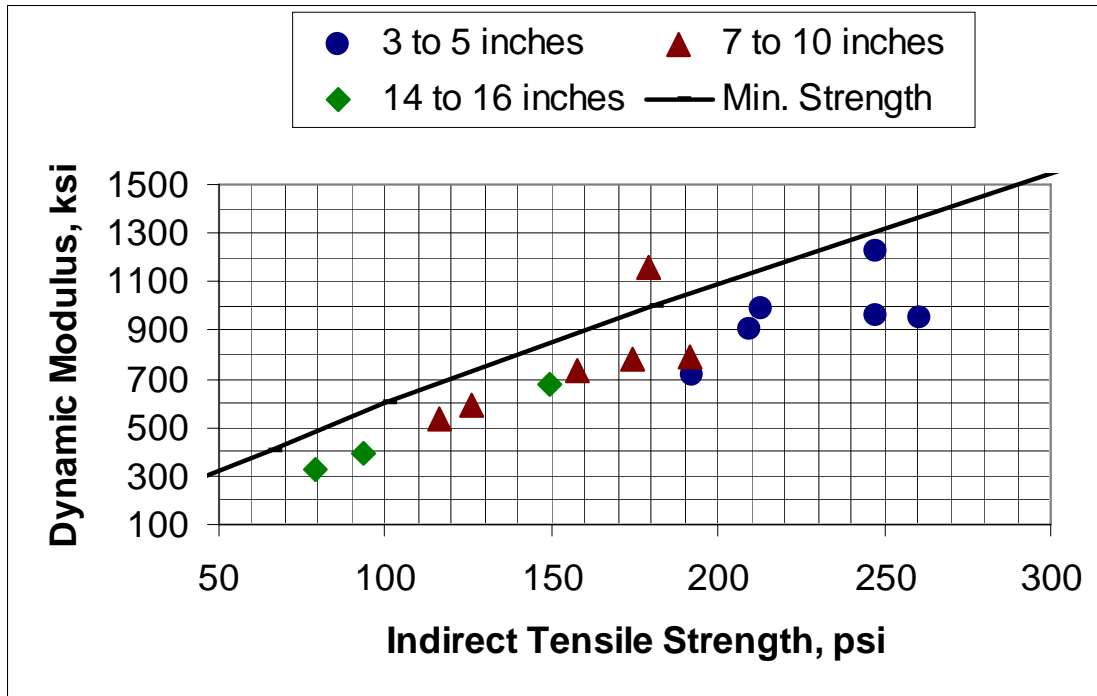


Figure 4-17. Relationship between IDT strength and dynamic modulus for each layer tested along I-75

Figure 4-18 compares dynamic modulus and tensile strain at failure on a standard mixture without moisture damage to test data from the I-75 and I-20. Values below the standard mixture curve exhibit low tensile strain at failure, and thus can be said to have inferior fatigue properties. Two general categories of materials with inferior fatigue properties are represented: *moisture damaged* and *brittle* materials. HMA mixtures with moisture damage have low modulus and low tensile strain at failure, while brittle HMA mixtures exhibit high modulus with low tensile strain at failure. From Figure 4-18, we see that the I-20 base mixture appears to be significantly affected by moisture damage, while the I-20 binder mixture is consistent with undamaged material. For the I-75 cores, one base course sample exhibits behavior consistent with moisture damage. The I-75 binder and surface course exhibit behavior typical of normal to brittle HMA materials.

4.4.5 Summary

The following provides a summary of the field and laboratory tests completed on the HMA mixtures placed at different times along I-75.

- Results from the GPR and seismic tests suggest reasonably uniform conditions and responses measured along this section of I-75.
- Results from the GPR tests suggest that moisture is present along the entire length of this section of I-75.
- Results from the seismic tests and field cores, however, suggest that moisture damage is present in only localized areas.

- Many of the cores were fractured at the interface during the coring operation, suggesting a weak bond between the layers. The moisture detected by the GPR tests is believed to be confined to the layer interface, which has weakened the bond between layers.
- Two areas were identified from the GPR and seismic tests that have potential moisture damage within the top 10 inches. These areas are listed below and should be considered separately for the rehabilitation design.
 - MP 270.05 to 270.15
 - MP 272.65 to 273.35
- Layers showing signs of actual stripping or disintegration are well below the surface and were below the detection depth of the seismic tests.

In summary, moisture damage does exist along I-75 but only in localized areas. The lower portion of the HMA base exhibits more advanced levels of moisture damage or stripping. However, the damaged layer is far enough below the surface so that it should not have a detrimental effect on the rehabilitation strategy for this segment of I-75. A rehabilitation strategy of milling the top two layers (2½ inches) and placing an HMA overlay is appropriate for this portion of I-75, with the exception of the area between milepost 272.5 and 272.9. For that area, the top 4½ inches should be milled. For the rehabilitation design, the strength and modulus of the lower portion of the HMA base layer should be reduced in determining the overlay thickness.

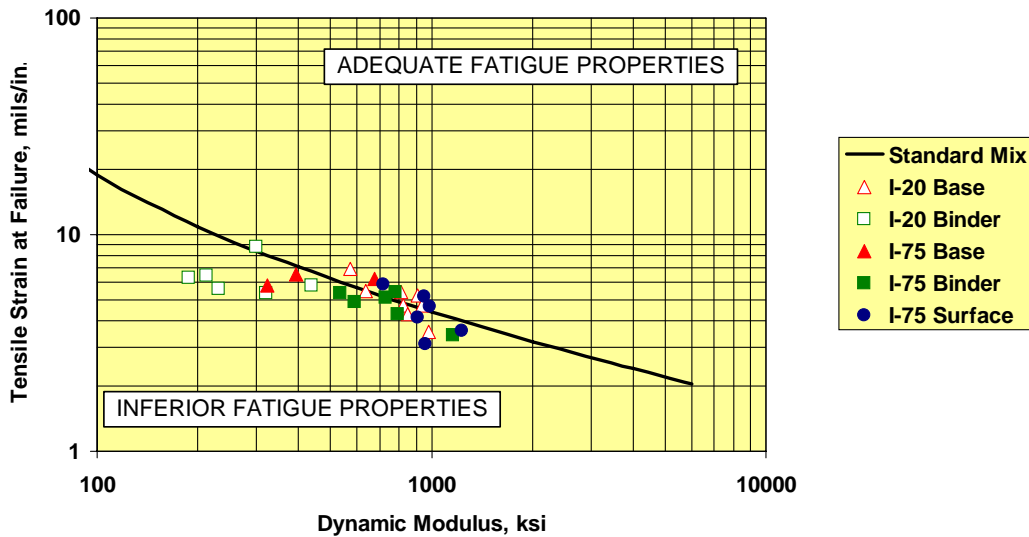


Figure 4-18. Comparison of the IDT dynamic modulus and strain at failure to typical values expected for a mix without moisture damage

5 RECOMMENDED PROCEDURE TO IDENTIFY AREAS WITH MOISTURE DAMAGE

5.1 Procedure to Identify Areas with Moisture Damage

The goal of the GDOT is to develop a rapid, comprehensive, and reliable procedure to survey potential mill and overlay projects for the presence of stripping. In current GDOT practice, coring and visual examination is the preferred method for detecting the presence of stripped asphalt. Coring is time-consuming and is a point sampling method. AASHTO T283 (Resistance of Compacted Bituminous Mixture to Moisture Induced Damage) is the laboratory method commonly used to determine moisture damage in HMA mixtures. However, the reliability of AASHTO T 283 is considered low at best.

The steps needed to identify areas with moisture damage for use in rehabilitation design are listed below. These steps are illustrated in flow chart form in Figures 5-1 and 5-2.

1. Review construction history of the roadway segment under evaluation to determine the pavement cross section and layer thickness. Review the construction files to determine the volumetric and physical properties of the different HMA layers that have been placed along the segment of roadway under evaluation.
2. If a distress survey is not available (for example, from pavement management system), perform one to identify the surface condition for use in developing the field sampling plan (refer to step 7), further analyses of the NDT data, rehabilitation design, and strategy selection.
3. Calculate the dynamic modulus as a function of temperature for each HMA layer, and estimate the lower baseline value. The lower baseline value is the modulus at the NDT test temperature that would represent an HMA mixture without any moisture damage. This baseline value should be tied to laboratory test results – combination of unconditioned and moisture conditioned samples.
4. Perform GPR on each lane included in the roadway segment under evaluation. From the GPR data, determine the UI along the project. The UI should be calculated as the GPR amplitude (at a specific location and depth range of interest) divided by the average GPR amplitude over a normalization range. This will yield an UI centered about the value of 1.0.
5. Segment the project by GPR uniformity indices. The following threshold values are recommended:

$$\begin{aligned} & \text{UI} < 0.50 \\ & 0.50 \leq \text{UI} < 0.85 \\ & 0.85 \leq \text{UI} < 1.15 \\ & 1.15 \leq \text{UI} < 1.50 \\ & \text{UI} > 1.50 \end{aligned}$$

6. Prepare a field test plan for the seismic testing. Conduct at least three seismic tests within each of these areas segmented from the UI. Determine the seismic modulus for each test point at a loading frequency of 15 Hz. Identify the areas where the seismic modulus is less than the lower baseline value determined from step 3.

7. Develop a field sampling plan to take cores in segments where the GPR UI is greater than 0.85 and in segments where the seismic modulus is less than the lower baseline value.
8. Correlate the GPR UI, seismic modulus, and core condition to confirm the initial criteria used. Make any adjustments for the specific HMA mixture, and rerun the correlation analysis using the revised criteria to identify areas with moisture damage, if necessary.
9. Prepare a laboratory test plan to measure the modulus and indirect tensile strain at failure for each area sampled. Perform the laboratory tests on cores recovered from areas with and without moisture damage, if possible. The laboratory tests should confirm the areas with moisture damage and the seismic modulus used in the evaluation.
10. Designate the areas with various levels of moisture damage for use in rehabilitation design.

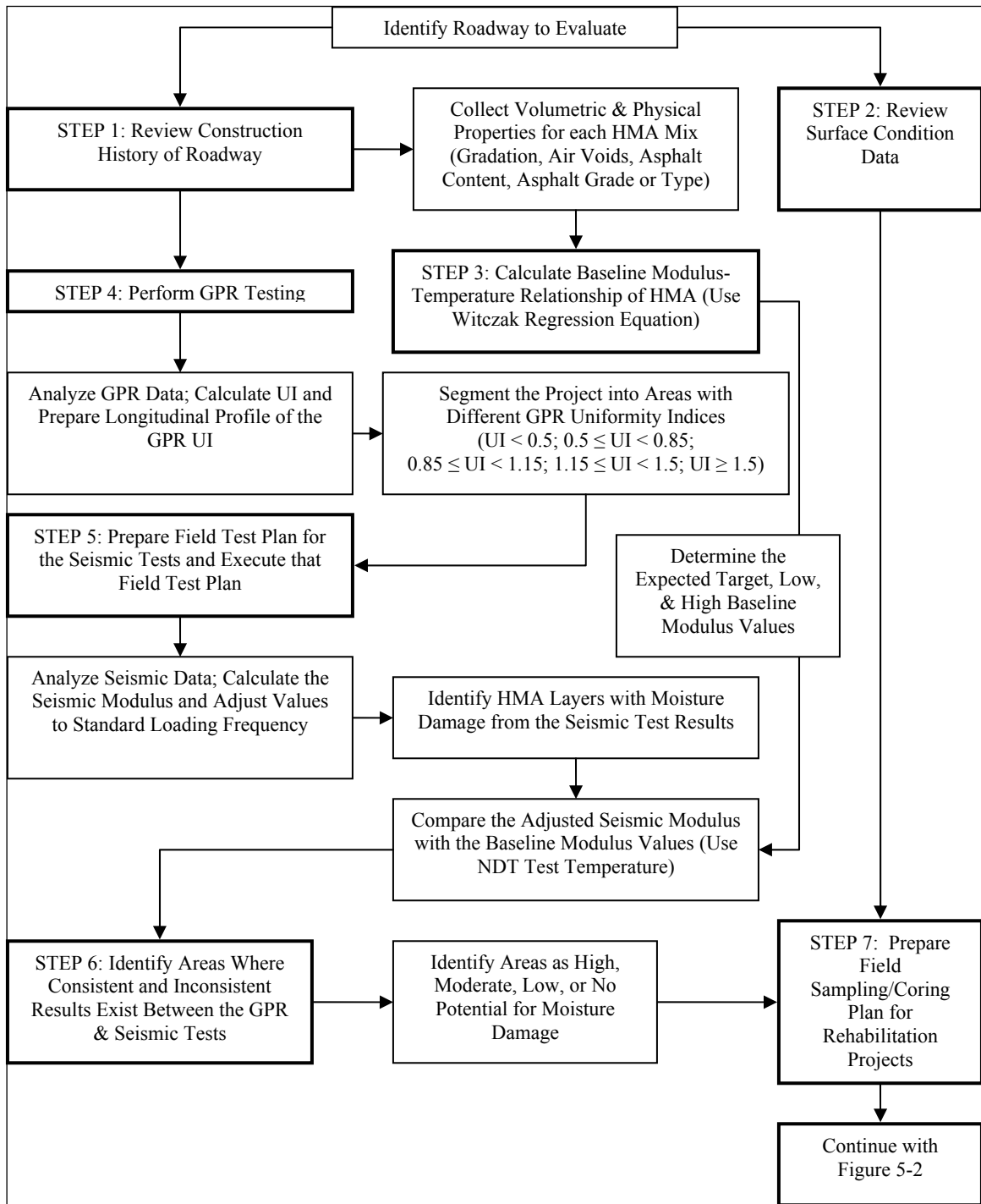


Figure 5-1. Rehabilitation flow chart, part 1

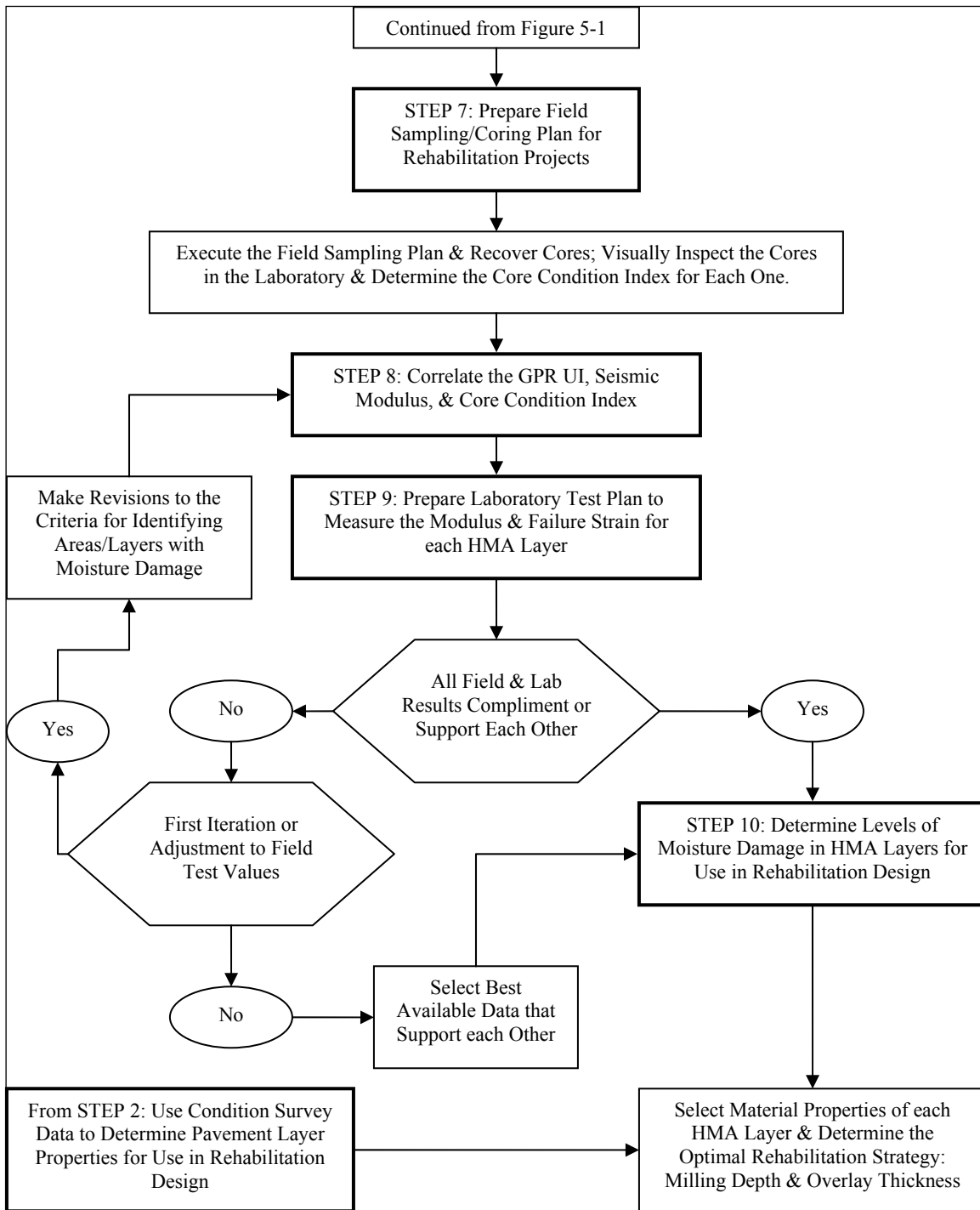


Figure 5-2. Rehabilitation flow chart, part 2

6 CONCLUSIONS AND RECOMMENDATIONS

6.1 Conclusions

From the research performed on the two pilot test sections in Georgia, the following conclusions can be drawn:

6.1.1 General

This research has developed a procedure to identify the areal extent and depth of moisture damage in HMA pavements. This procedure involves observation of surface distresses, a complete GPR survey, seismic testing of selected areas, limited coring, and laboratory testing of selected cores. By following the procedures identified by this research, areas with various levels of moisture damage can be discriminated so that effective rehabilitation strategies can be developed.

Visual observations of cores are inconclusive. Laboratory tests on the cores are required to characterize the stripping and discriminate between areas of “good” and “bad” pavement.

6.1.2 Moisture Damage

Moisture damage begins with a reduction of cohesion in the asphalt binder or a reduction of adhesion between the asphalt binder and aggregate surface. Moisture damage often occurs in HMA without actual stripping. When advanced stripping is present, cores recovered from the roadway will often disintegrate during the coring operation.

The dynamic modulus and tensile strength of an HMA mixture are significantly affected by the level of moisture damage. In addition, these properties will continue to decrease with increasing levels of moisture damage progressing from a loss of cohesion in the asphalt to advanced stripping.

When moisture damage has not yet progressed to stripping, visual observations of cores are inconclusive. Laboratory tests on the cores are required to characterize the degree of the moisture damage.

6.1.3 Non-Destructive Techniques

Forward-calculated HMA stiffness values from FWD deflection basins did not prove to be sensitive to moisture damage in relatively thin HMA layers, when those layers are located between thicker HMA layers without moisture damage. In fact, FWD modulus values differed significantly from seismic test modulus values even when appropriate adjustments were made for temperature and loading frequency.

Thermal anomalies were not found to be reliable indicators of moisture damage in HMA. Therefore, infrared thermography imaging did not prove useful in this study.

The seismic technique, when adjusted for temperature and loading frequency, appears to be effective in identifying areas where HMA stiffness is less than expected for intact, sound HMA. The adjusted seismic modulus is significantly affected by the level of moisture damage in the HMA mixture. However, moisture damage is not the only mechanism that can cause a reduction in stiffness. Other mechanisms, such as higher air voids, lower asphalt contents, or micro-fatigue cracks, can have a similar effect. Thus, a complementary method is required to isolate areas with reduced modulus and high moisture levels.

GPR technology is effective in detecting layer thicknesses and identifying areas where non-uniform electromagnetic properties may indicate changes in physical properties consistent with moisture damage.

Seismic and GPR technologies should be used in combination to improve on the reliability of identifying layers with moisture damage, stripping, or other anomalies beneath the pavement surface. Seismic tests can be used to determine the modulus of HMA mixtures. GPR can be used to detect the higher levels of moisture. Where the two conditions co-exist, some level of moisture damage can be expected.

6.1.4 Pilot Projects

6.1.4.1 I-20

The results of the GPR survey and seismic tests indicate that widespread moisture damage exists within the HMA intermediate (binder) layer along the I-20 project at a depth of 4 to 8 inches below the surface of the pavement. While little of this damage has progressed to full-blown stripping, the integrity of the material has been compromised to the extent that rehabilitation design strategies will be impacted. Significant reductions in dynamic modulus were observed from the seismic test data and laboratory tests on core extracted from the project.

6.1.4.2 I-75

The results from the seismic tests and field cores suggest that moisture damage is isolated to localized areas. The GPR survey suggests that moisture is present along the entire length of the pilot project; however, this moisture is believed to be primarily confined to the interfaces between layers. This moisture has reduced the bond between layers, but has not affected the integrity of the HMA mixture itself – at least near the surface. Most mix disintegration has occurred near the lower portion of the base layer. However, any damaged material is far enough below the surface so that it should not influence the rehabilitation strategy.

Laboratory tests on selected I-75 cores indicated a reduced dynamic modulus for the lower base layer (placed in 1977). However, all HMA layers from I-75 cores have a consistent relationship between strength and modulus, suggesting that the lower modulus values may be related to differences in volumetric and asphalt properties, rather than related to moisture damage.

6.2 Recommendations

6.2.1 Survey Strategy

The following ten step process is recommended to develop effective rehabilitation design strategies where HMA moisture damage is suspected:

1. Review the construction history of the roadway to determine the pavement cross section and volumetric and physical properties of the different HMA layers (if possible).
2. Review the surface condition as an aid in developing the field sampling plan and, later, the rehabilitation design strategy.
3. Estimate the lower baseline HMA dynamic modulus value. The lower baseline value is the modulus at the NDT test temperature that would represent an HMA mixture without any moisture damage.

4. Perform a complete GPR survey on the roadway. From the GPR data, determine the UI along the project.
5. Segment the roadway based on the UI values.
6. Conduct at least three seismic tests in each segmented area.
7. Develop a field sampling plan to take cores within each of the different segmented areas.
8. Correlate the GPR UI, seismic modulus, and core condition index to confirm the initial criteria used.
9. Validate by performing laboratory tests on a few cores recovered from areas.
10. Designate the areas with various levels of moisture damage for use in rehabilitation design.

6.2.2 Safety Considerations

Seismic surveys require lane closures. GPR surveys can be conducted without lane closures. However, it is recommended that an attenuator truck follow the GPR survey vehicle (particularly in heavy traffic) to provide protection from aggressive or non-attentive drivers.

6.2.3 Rehabilitation Strategy for I-20 Pilot Project

A milling depth of 8 inches is recommended to remove all moisture damaged material. This will provide a stable construction platform and competent structural support for subsequent HMA layers. Otherwise, distortions from heavily loaded asphalt delivery trucks may result in significant rutting after HMA overlay placement. For the rehabilitation design, the strength and modulus of the lower portion of the HMA base layer should be reduced in determining the overlay thickness.

6.2.4 Rehabilitation Strategy for I-75 Pilot Project

A rehabilitation strategy of milling the top two layers (2½ inches) and placing an HMA overlay is appropriate for this portion of I-75, with the exception of the area between milepost 272.5 and 272.9. For that area, the top 4½ inches should be milled. The actual HMA overlay thickness should be determined to ensure that the rehabilitation strategy will be adequate for the 20-year design traffic level.

7 REFERENCES

Andrei, D., M.W. Witzczak, and M.W. Mirza. 1999. "Development of a Revised Predictive Model for the Dynamic (Complex) Modulus of Asphalt Mixtures." NCHRP 1-37A Inter Team Report, University of Maryland.

Aouad, M. F., K. H. Stokoe and R. C. Briggs. 1993. "Stiffness of Asphalt Concrete Surface Layer from Stress Wave Measurements," Transportation Research Board, No. 1384, Washington, DC, pp. 29-35.

Kandhal, Prithvi S. and Ian J. Rickards. April 2001. *Premature Failure of Asphalt Overlays from Stripping: Case Studies*, NCAT Report No. 01-01, National Center for Asphalt Technology, Auburn, AL.

Federal Highway Administration. June 2003. *Distress Identification Manual for the Long-Term Pavement Performance Program*, FHWA-RD-03-031, McLean, Virginia

Federal Highway Administration. August 2000. *LTPP Manual for Falling Weight Deflectometer Measurements Operational Field Guidelines, Version 3.1*, McLean, Virginia

Ferry, J.D. 1970. *Viscoelastic Properties of Polymers*. 2nd edition, John Willy, New York.

Li, Y. and S. Nazarian, 1994. "Evaluation of Aging of Hot-Mix Asphalt Using Wave Propagation Techniques," *Engineering Properties of Asphalt Mixtures And the Relationship to Their Performance*, ASTM STP 1265, Philadelphia, Pa., pp.166-179.

Nazarian, S. and M.R. Desai. 1993. "Automated Surface Wave Method: Field Testing," *Journal of Geotechnical Engineering*, Volume: 119 Issue: 7, ASCE, New York, NY, pp 1094-11.

Nazarian, S., M. Baker, and K. Crain. 1997. "Assessing Quality of Concrete with Wave Propagation Techniques," *Materials Journal*, American Concrete Institute, Farmington Hills, MI, Vol. 94, No. 4, pp. 296-306

Nazarian, S., D. Yuan, V. Tandon, and M. Arellano. 2003. "Quality Management of Flexible Pavement Layers with Seismic Methods," Research Report 1735-3F, Center for Highway Materials Research, UTEP, El Paso, TX.

NCHRP (1996), "Nondestructive Testing to Determine Material Properties of Pavement Layers," Interim Report, NCHRP 10-44, Washington, DC.

Sansalone, M. and N. J Carino. 1986. "Impact-Echo: A Method for Flaw Detection in Concrete Using Transient Stress Waves," Report NBSIR 86-3452. National Bureau of Standards, Gaithersburg, MD.

Scullion, T. and E.H. Rmeili. October 1997. *Detecting Stripping in Asphalt Concrete Layers Using Ground-Penetrating Radar*, Research Report 2964-S. Texas Transportation Institute, College Station, TX.

Stubstad, Richard N. October 2002. *LTPP Data Analysis: Feasibility of Using FWD Deflection Data to Characterize Construction Quality*, NCHRP Web Document 52 (Project 20-50[9]), NCHRP, Transportation Research Board, Washington, DC.

Tandon, T., S. Nazarian and X. Bai. 2004. "Assessment of Relationship between Seismic and Dynamic Modulus of Hot Mix Asphalt Concrete," *International Journal of Road Materials and Pavement Design*.

Ullidtz, Per. 1987. *Pavement Analysis*, Elsevier.

Von Quintus, Harold. 1991. "Asphalt-Aggregate Mixture Analysis System (AAMAS)." NCHRP Report 338, Transportation Research Board, Washington, DC.

Yuan, Deren and Soheil Nazarian. 2000. "Feasibility of Detecting Flaws in Concrete Walls of Nuclear Power Plants," Center for Highway Materials Research, The University of Texas at El Paso, El Paso, TX.

APPENDIX A. PHOTOGRAPHS OF CORES FROM I-20 EASTBOUND



GDOT Core 1 (Lane 1)



GDOT Core 2 (Lane 3)



GDOT Core 5 (Lane 3)



GDOT Core 13 (Lane 3)



GDOT Core 15 (Lane 2)



GDOT Core 23 (Lane 1)



GDOT Core 31 (Lane 3)



GDOT Core 33 (Lane 3)



Sta 842 (Lane 3)



Sta 876 (Lane 3)



Sta 884 (Lane 3)



Sta 890 (Lane 3)



Sta 934 (Lane 3)



Sta 936 (Lane 3)

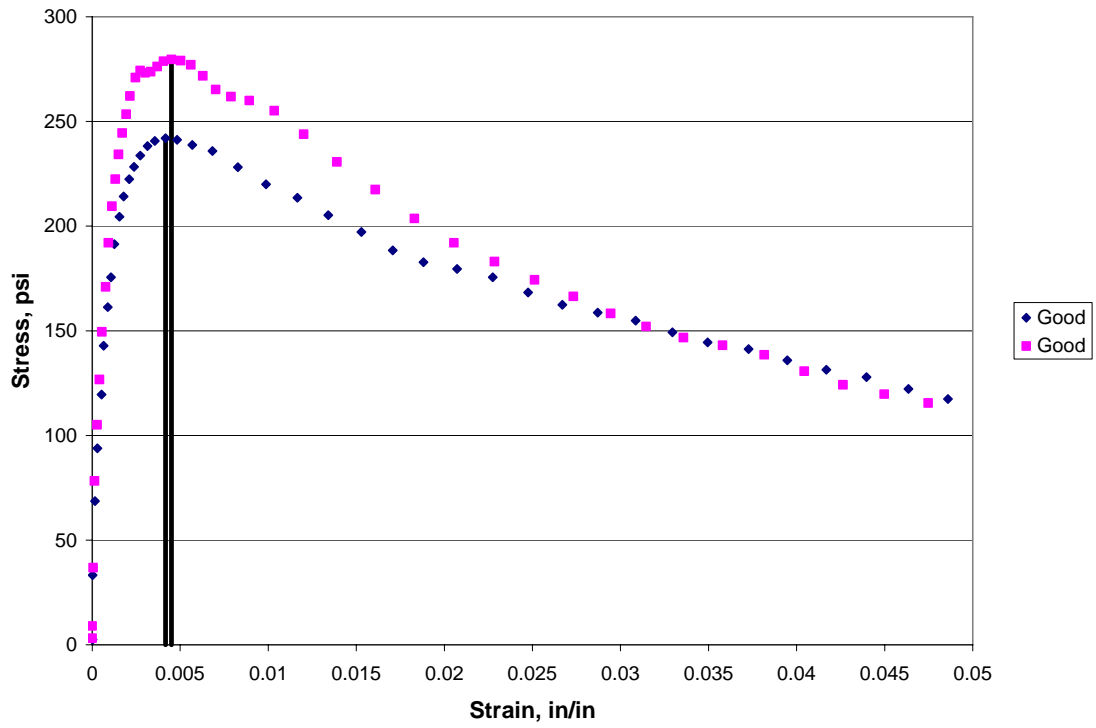


Sta 999 (Lane 3)

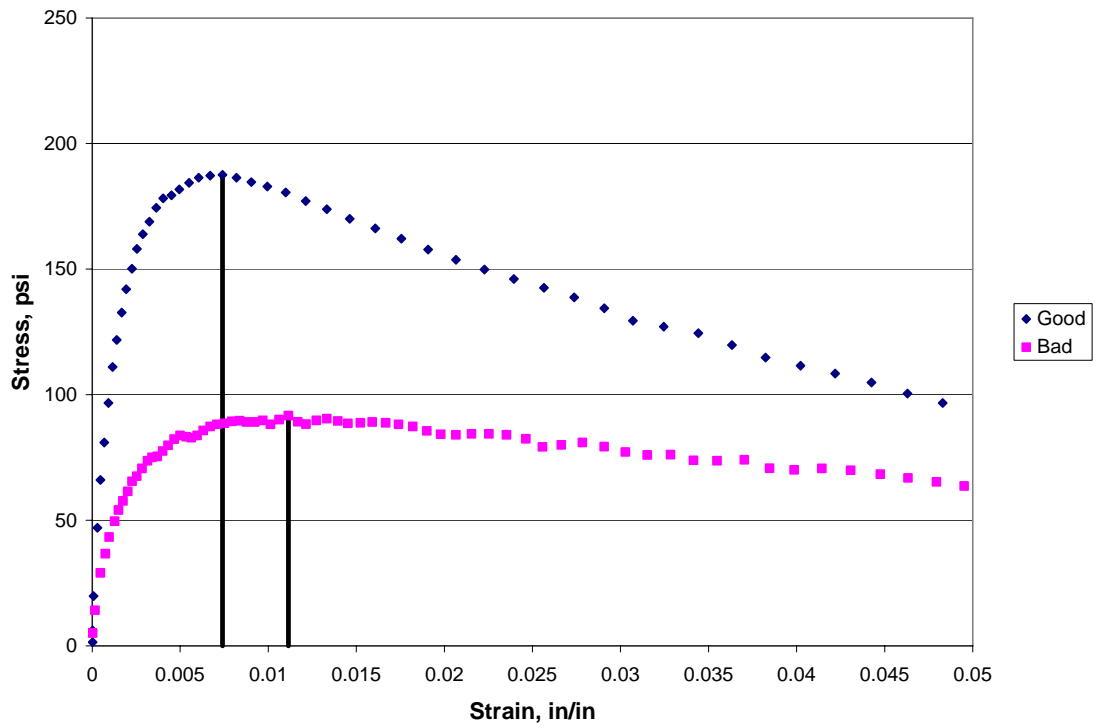


Sta 1045 (Lane 3)

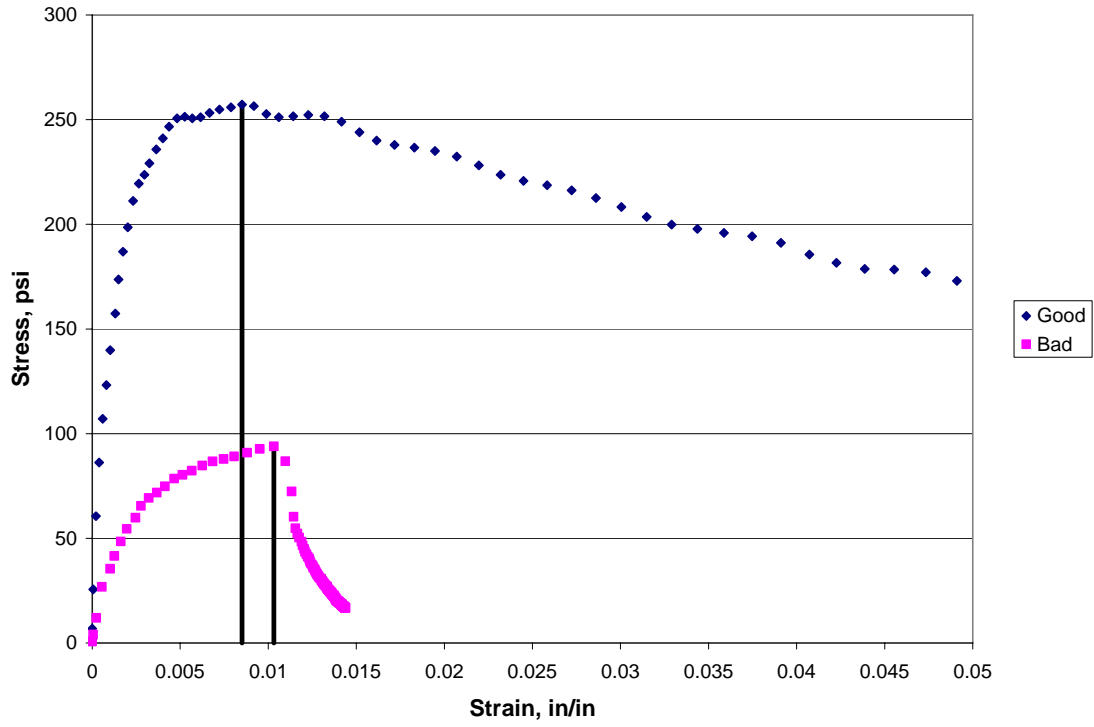
APPENDIX B. STRESS-STRAIN CURVES FROM IDT TESTS ON I-20 CORES



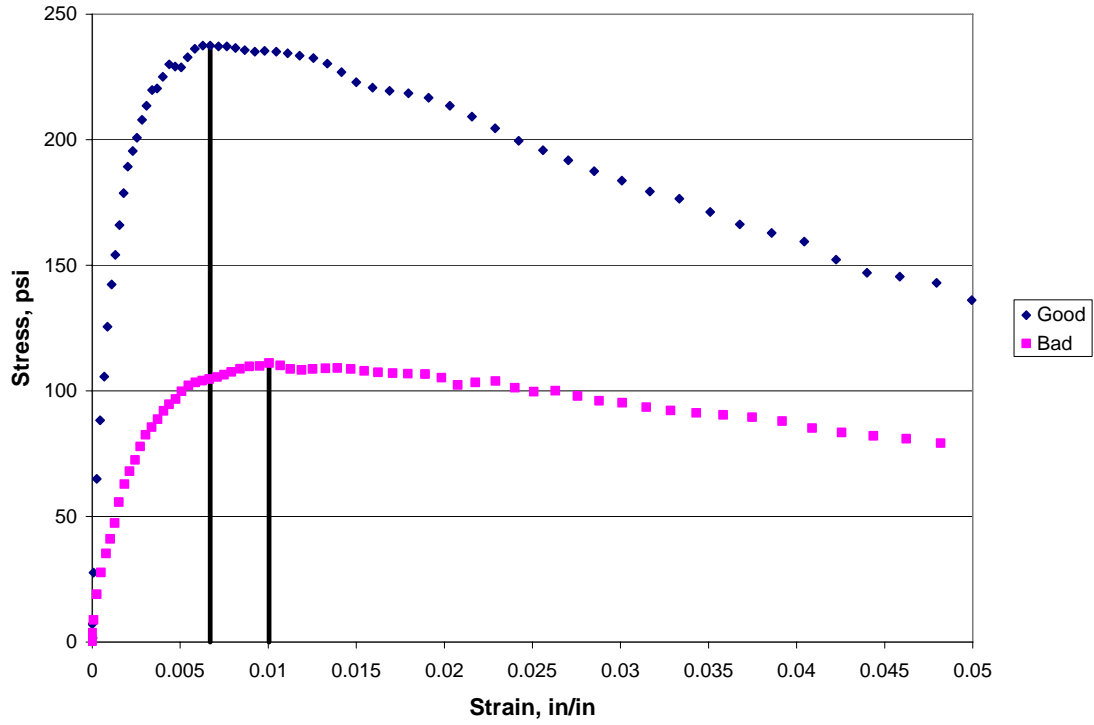
I-20 Core 1



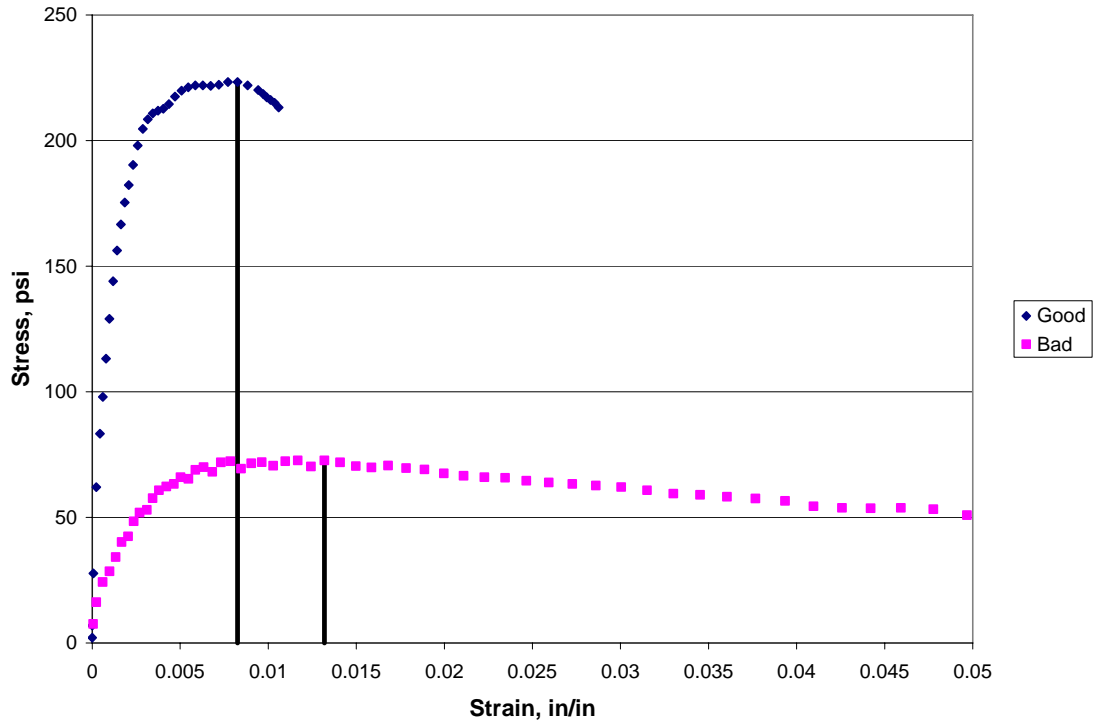
I-20 Core 5



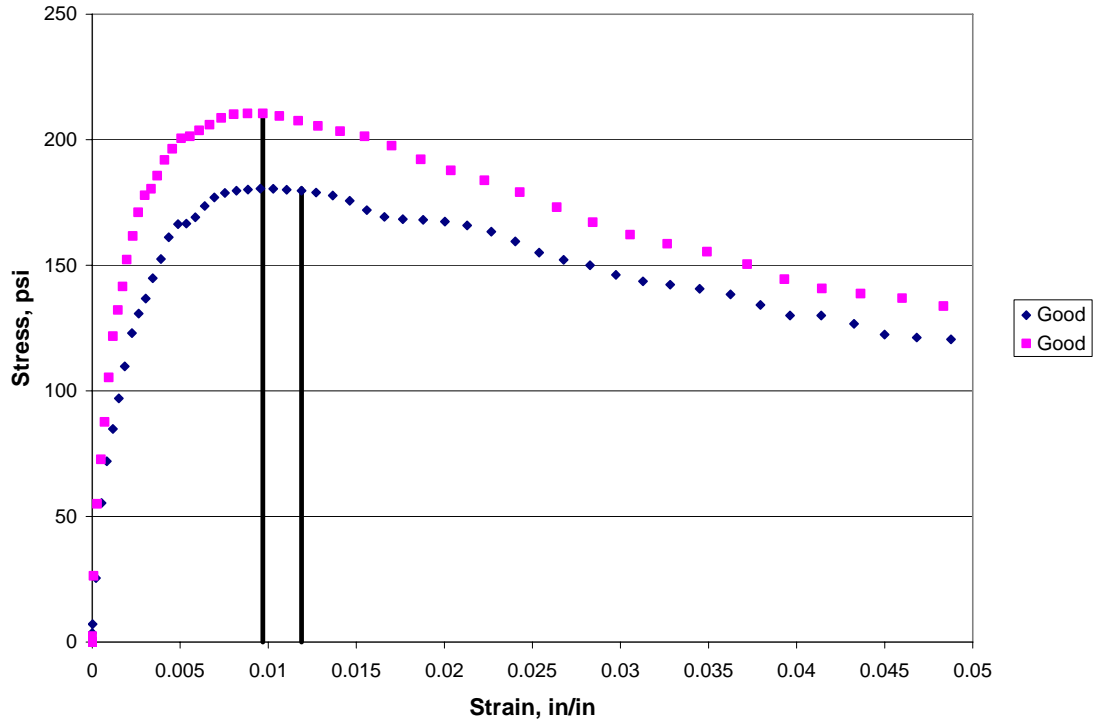
I-20 Core 8



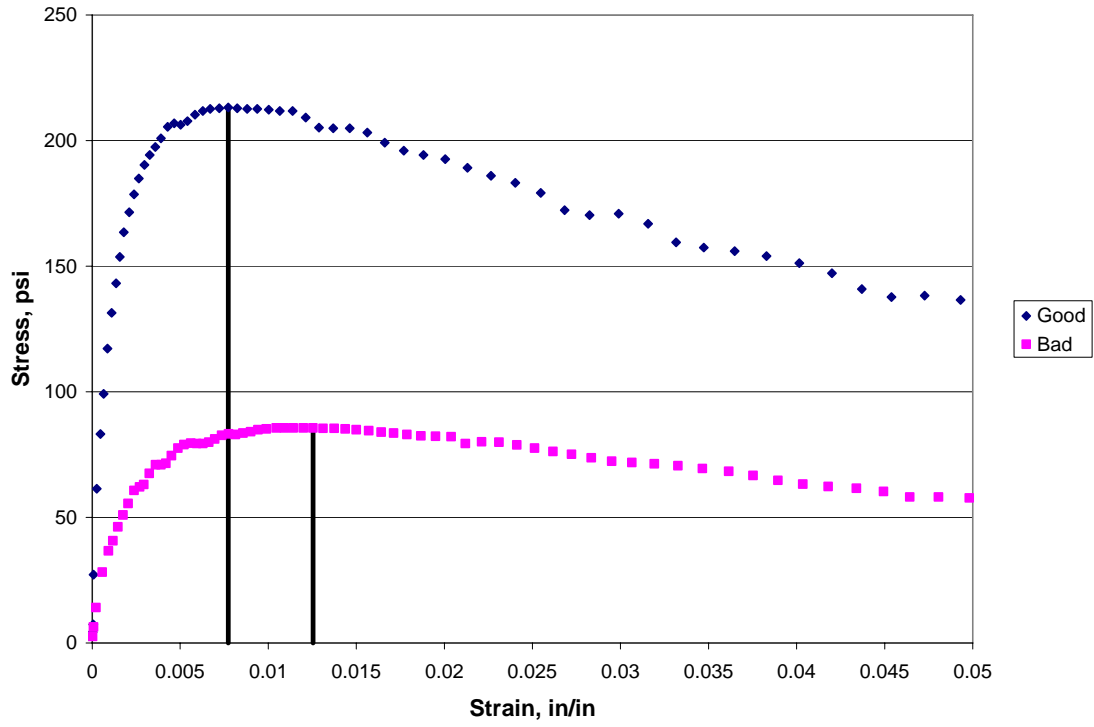
I-20 Core 13



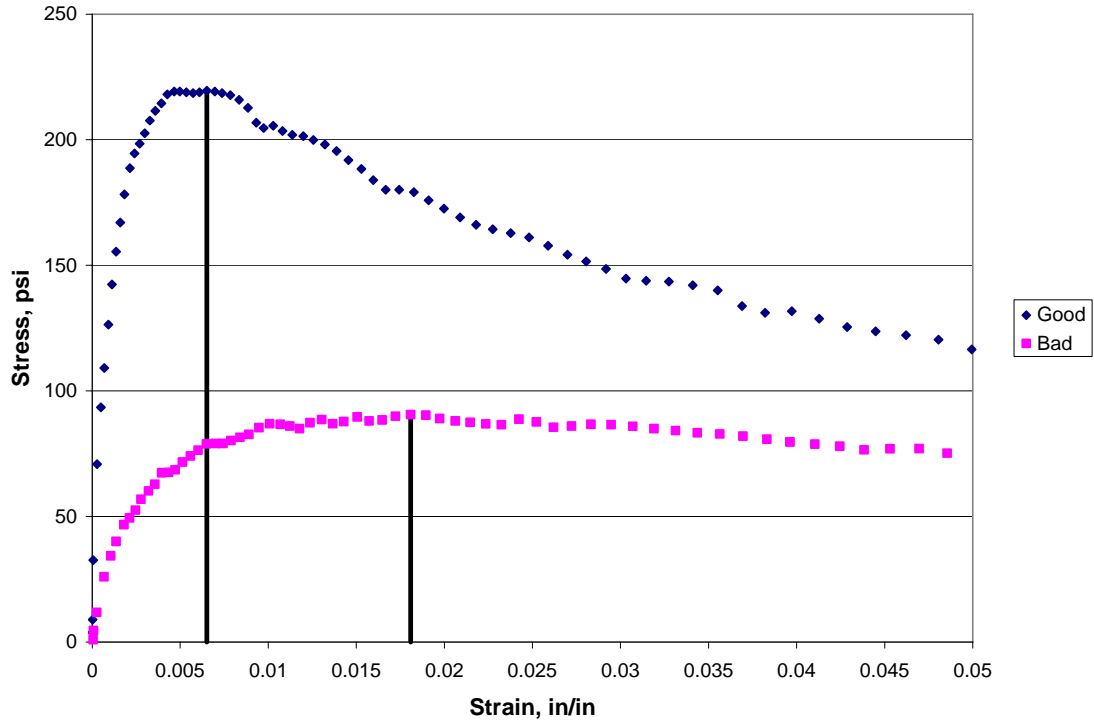
I-20 Core 15



I-20 Core 23



I-20 Core 31



I-20 Core 33

APPENDIX C. PHOTOGRAPHS OF CORES FROM I-75 NORTHBOUND



Core 1 (Lane 3)



Core 2 (Lane 3)



Core 3 (Lane 3)



Core 4 (Lane 3)



Core 5 (Lane 3)



Core 6 (Lane 3)



Core 7 (Lane 3)



Core 8 (Lane 3)



Core 9 (Lane 3)



Core 10 (Lane 3)



Core 11 (Lane 3)



Core 12 (Lane 3)



Core 13 (Lane 3)



Core 14 (Lane 3)

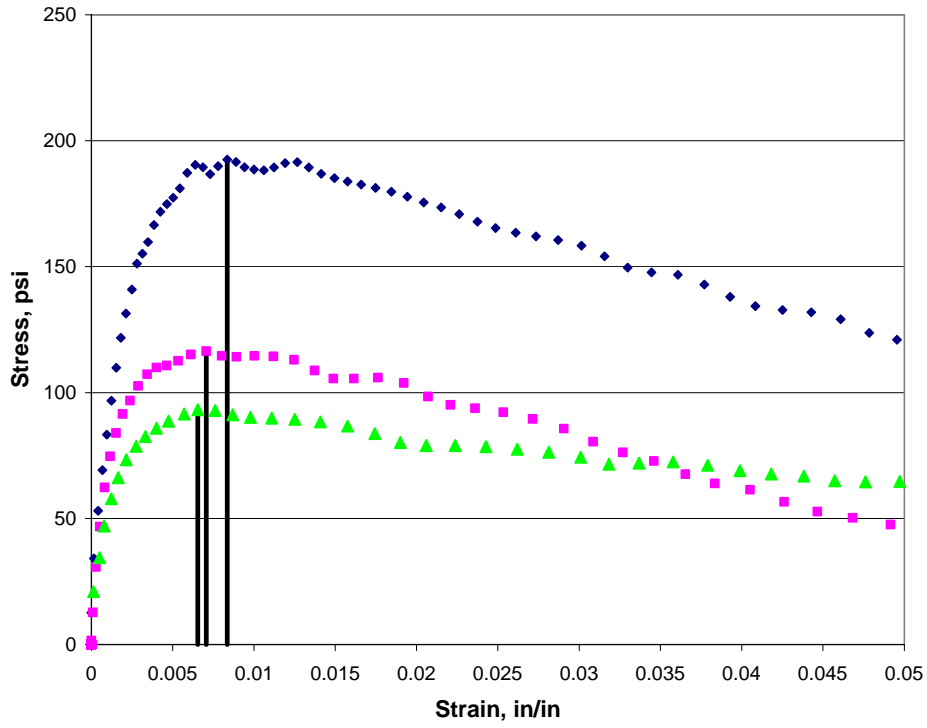


Core 15 (Lane 3)

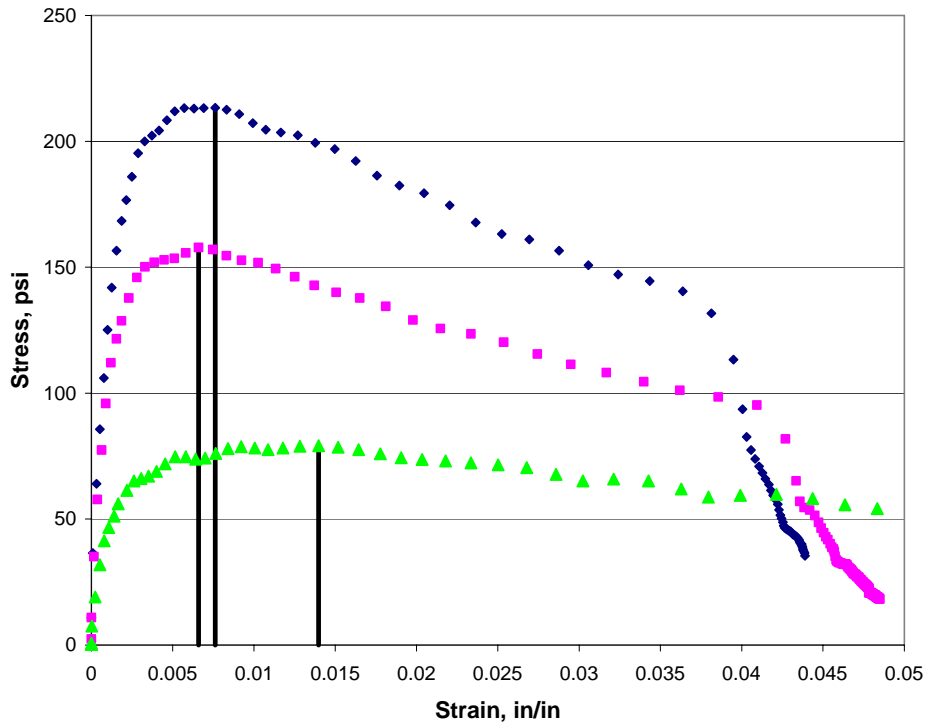


Core 16 (Lane 3)

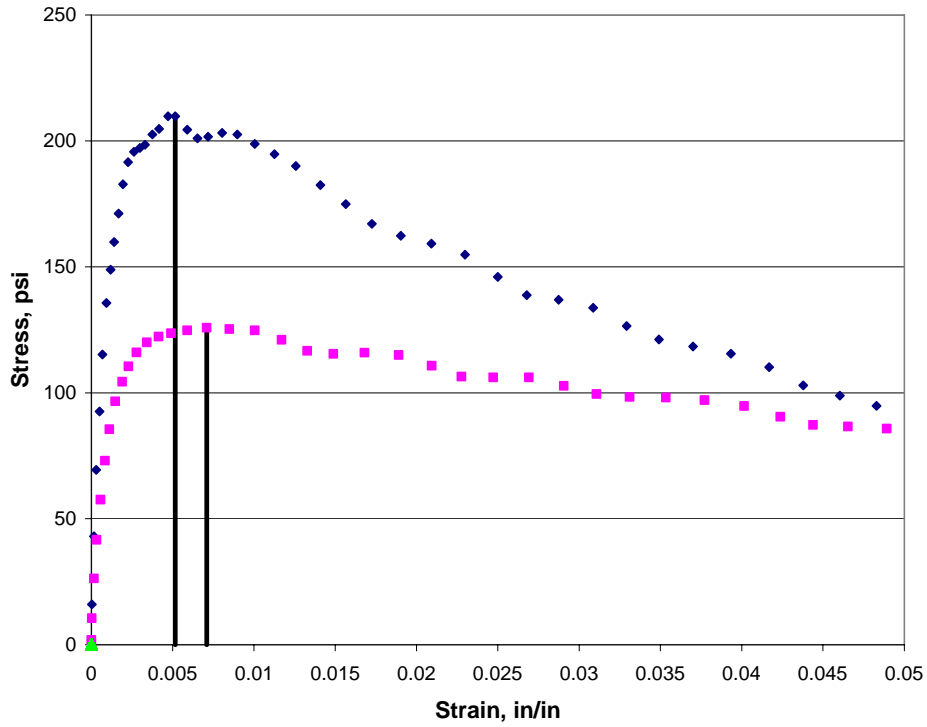
APPENDIX D. STRESS-STRAIN CURVES FROM IDT TESTS ON I-75 CORES



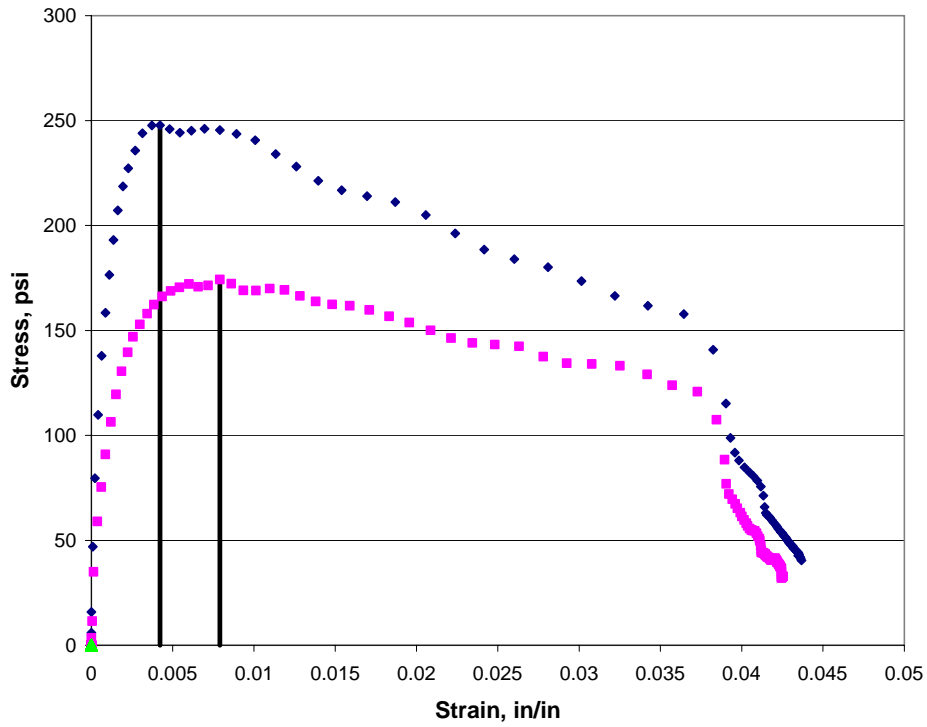
I-75 Core 11



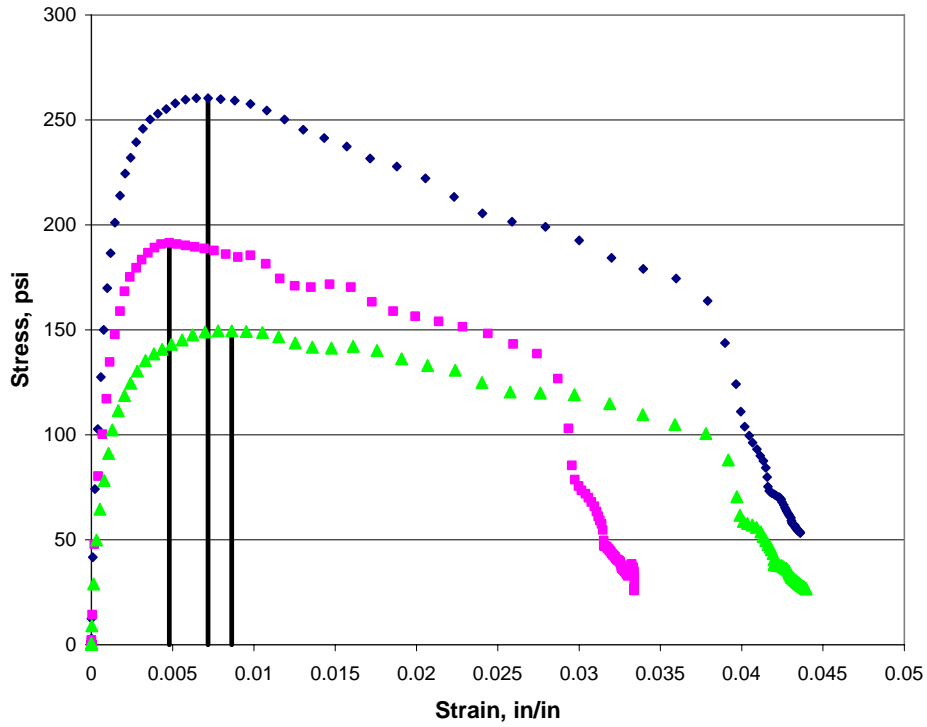
I-75 Core 12



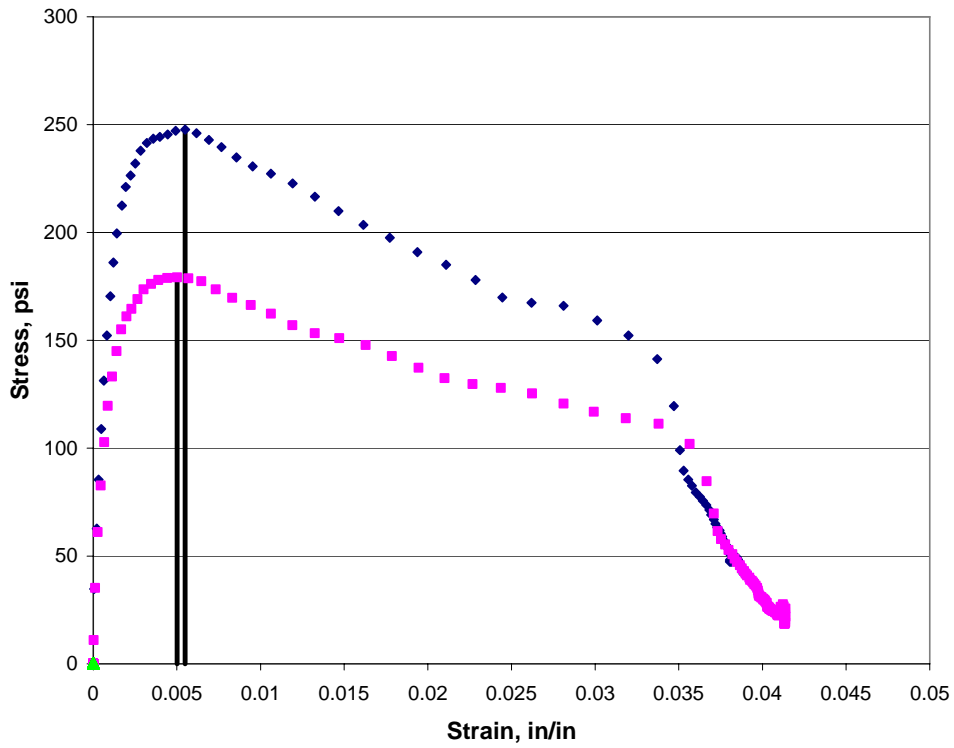
I-75 Core 13



I-75 Core 14



I-75 Core 15

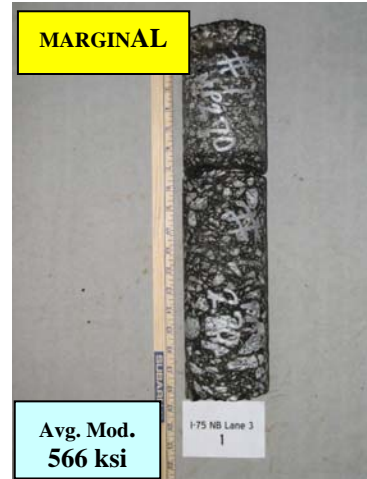
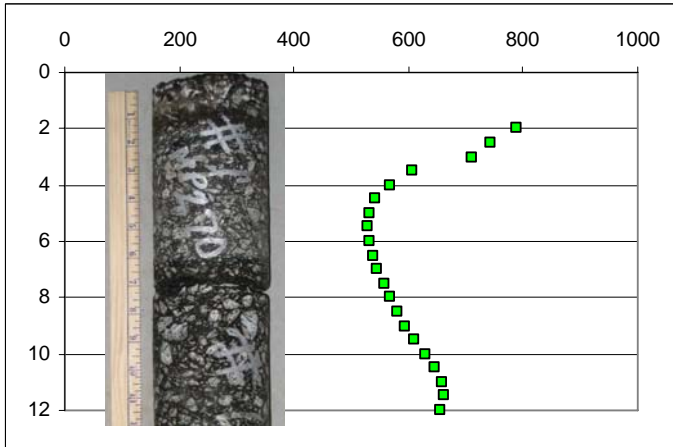


I-75 Core 16

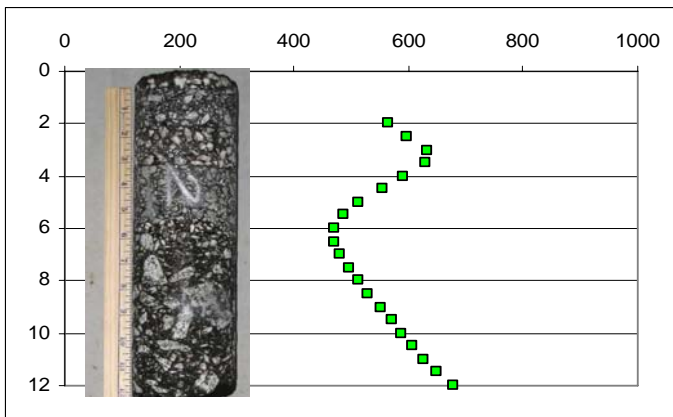
APPENDIX E. DISPERSION CURVES FOR I-75 CORES USING SHORT PSPA SPACING

Note: For all plots, Horizontal Axis = Dynamic Modulus, ksi
Vertical Axis = Depth, in.

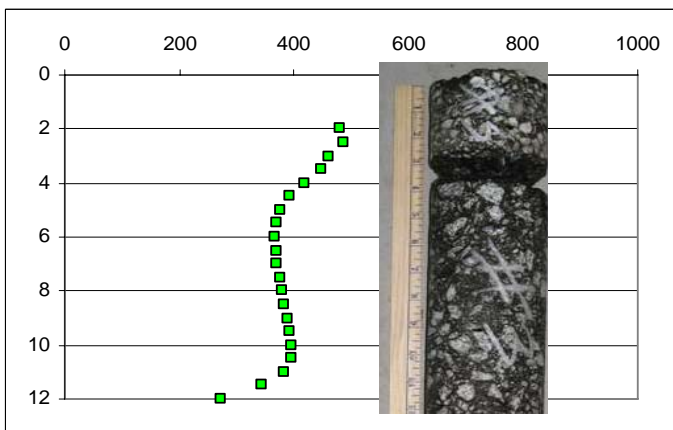
Core 1. MP 270.000



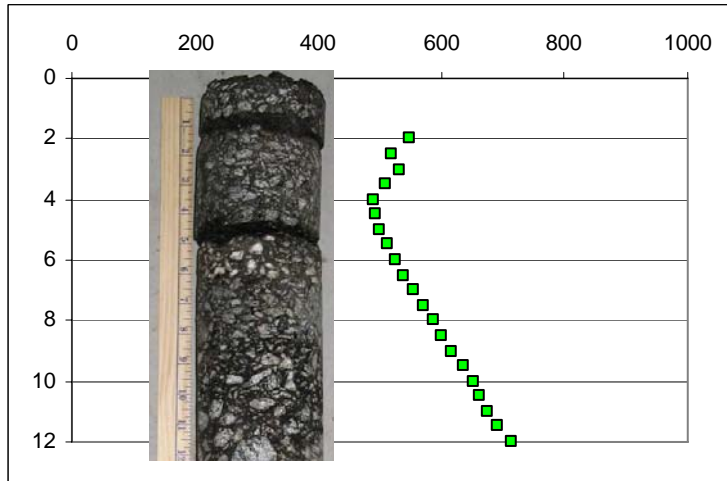
Core 2. MP 270.095



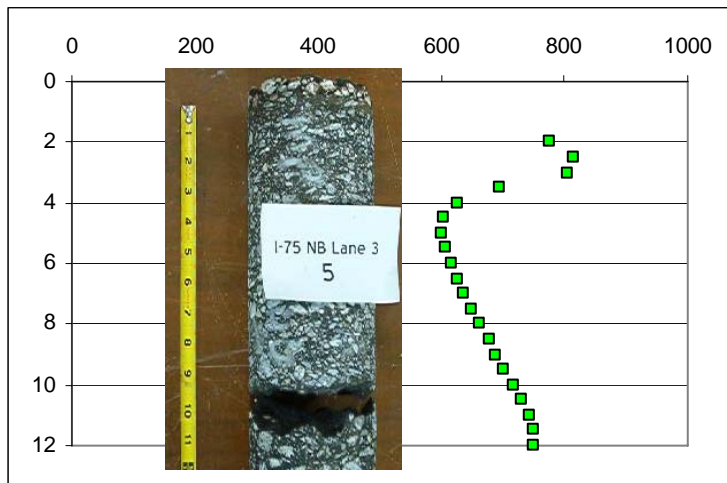
Core 3. MP 270.208



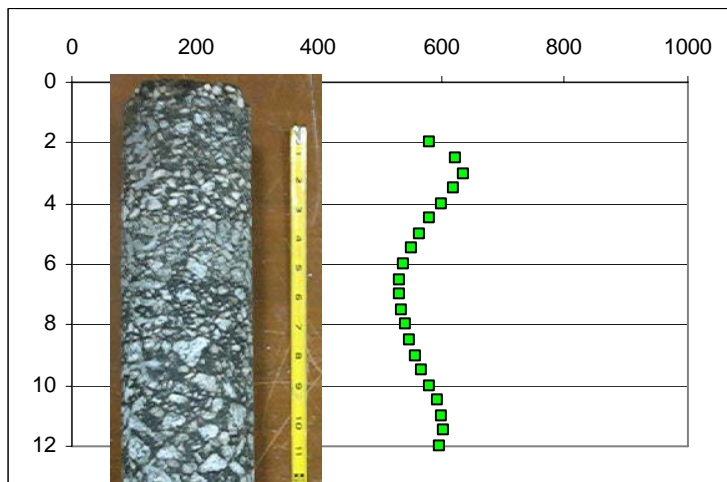
Core 4. MP 270.284



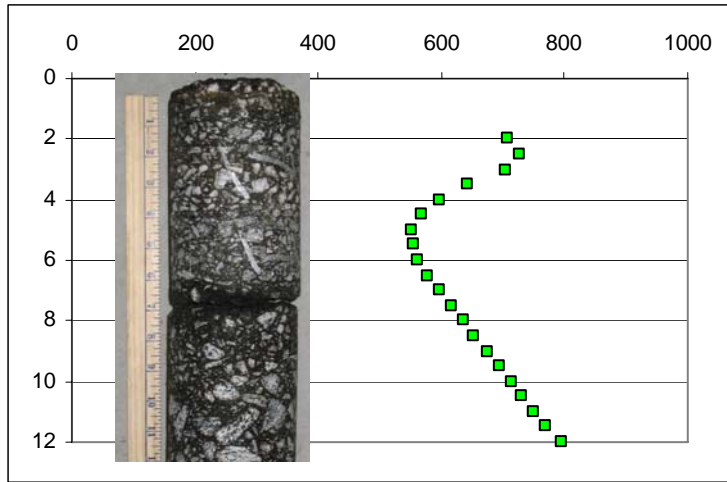
Core 5. MP 270.379



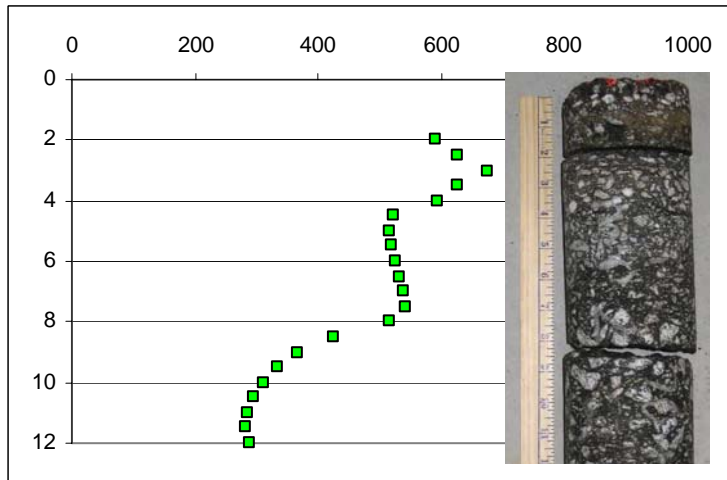
Core 6. MP 270.473



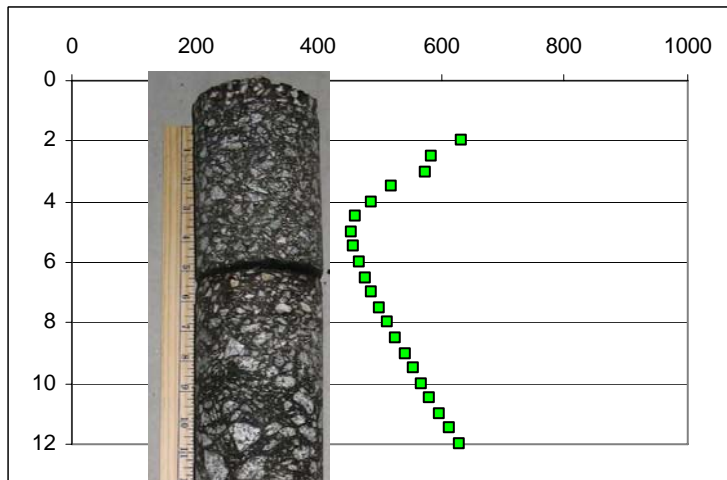
Core 7. MP 270.568



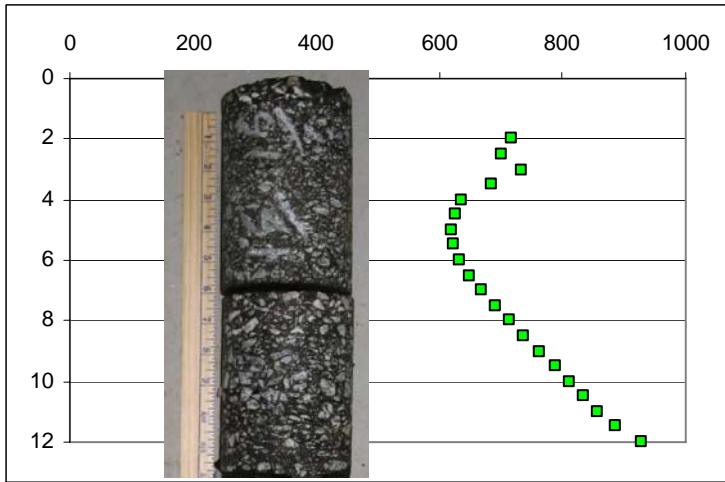
Core 8. MP 270.663



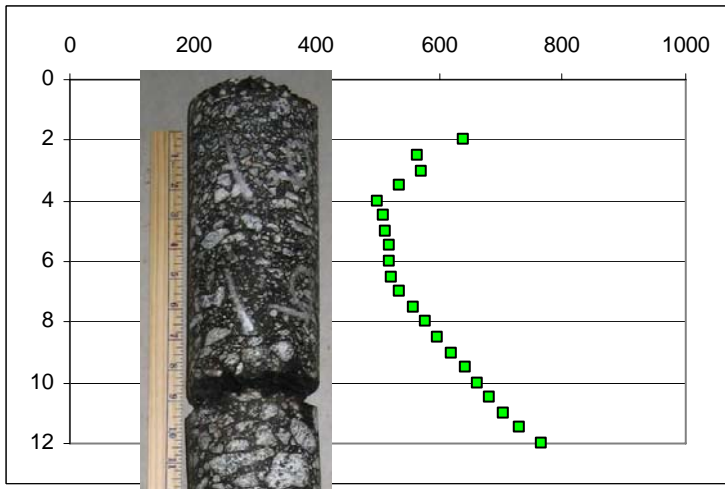
Core 16. MP 271.693 (PSPA at 271.686)



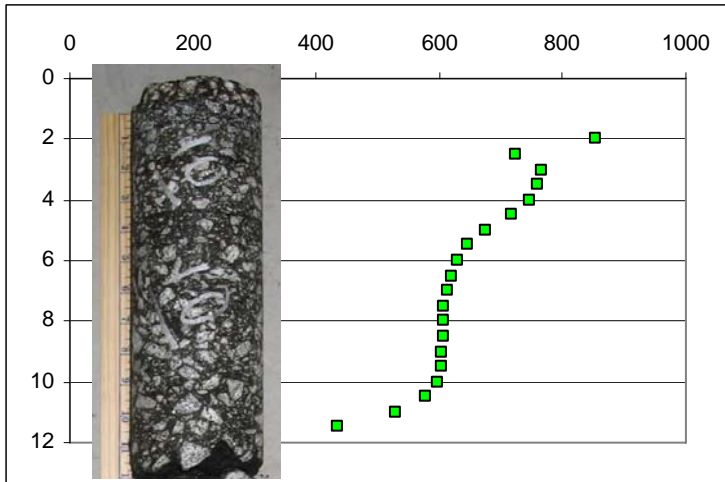
Core 15. MP 271.716 (PSPA at 271.723)



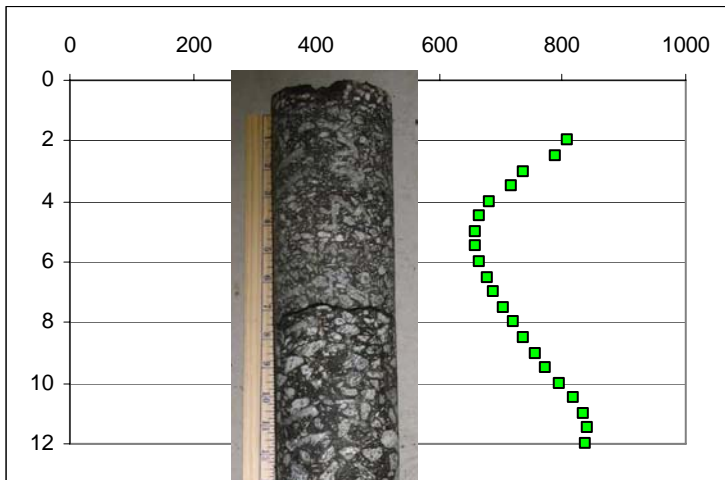
Core 9. MP 271.825 (PSPA at 271.818)



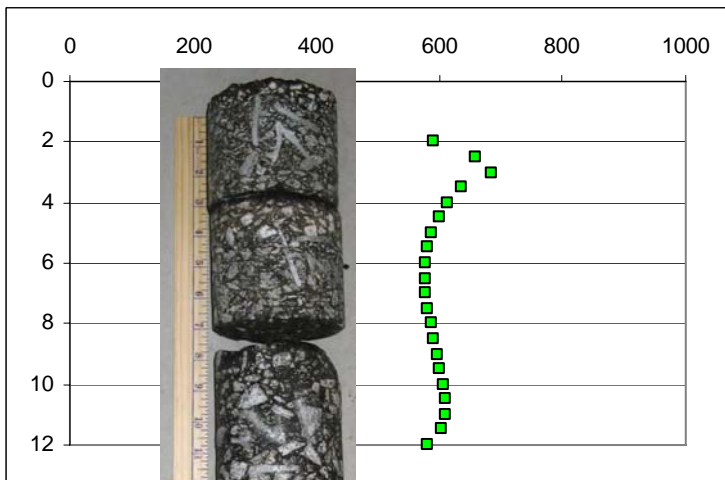
Core # 10. MP 271.924 (PSPA at 271.932)



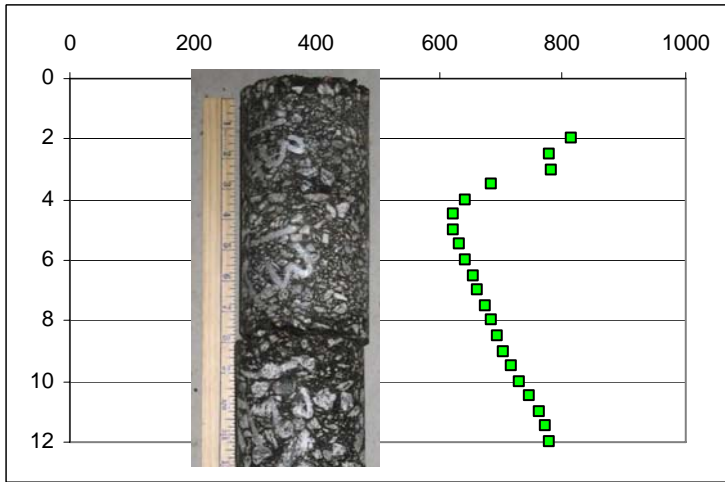
Core # 11. MP 272.092



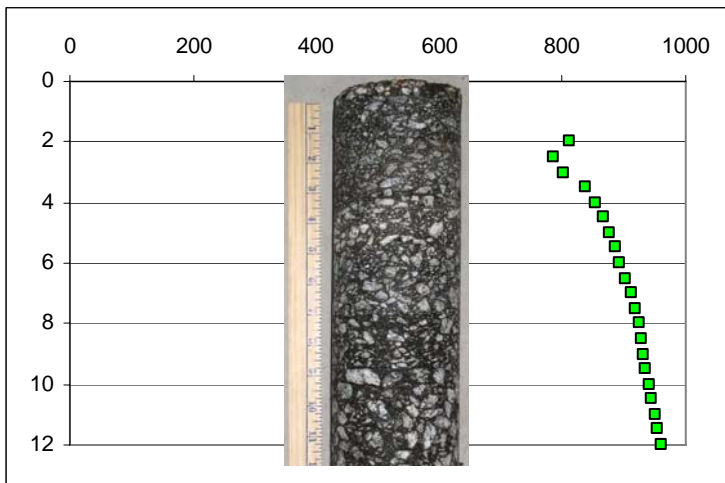
Core # 12. MP 272.100



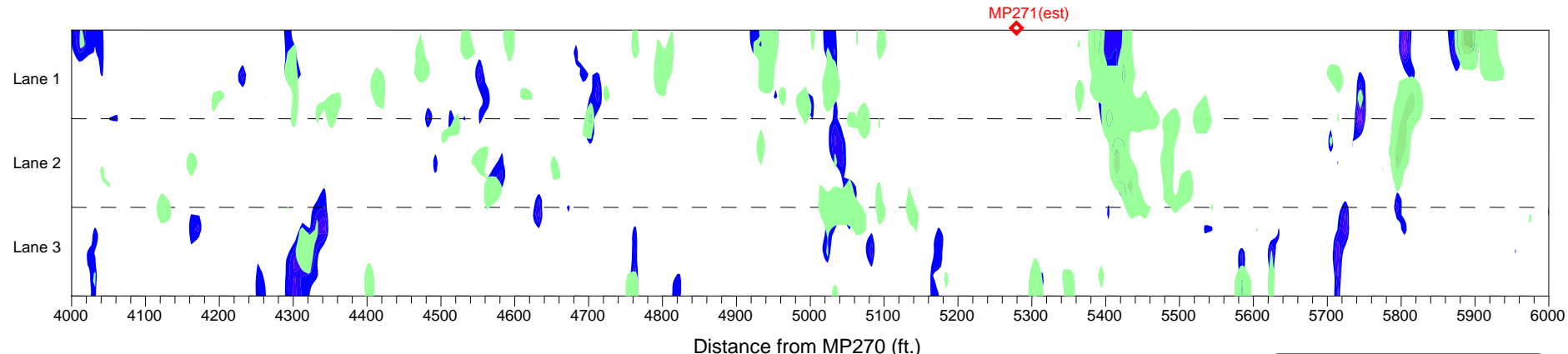
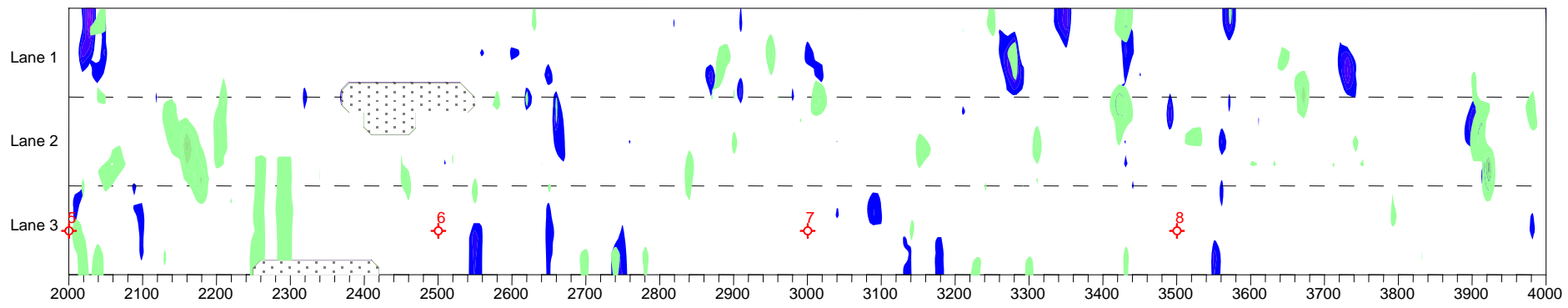
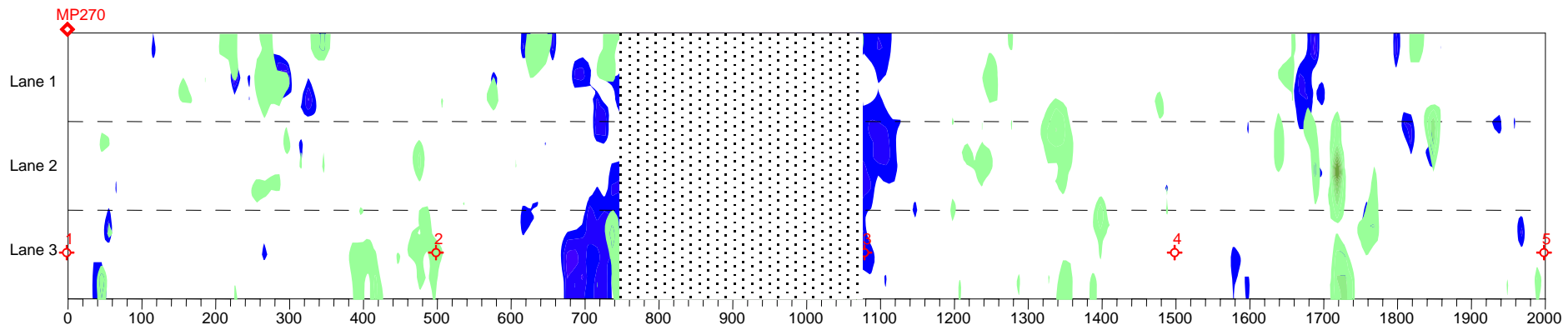
Core # 13. MP 272.178



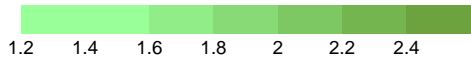
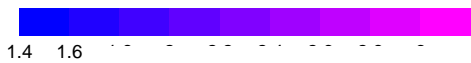
Core # 14. MP 272.196



APPENDIX F. I-75 GPR UNIFORMITY INDEX PLOTS

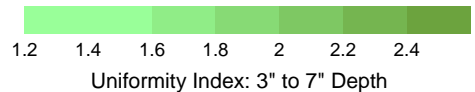
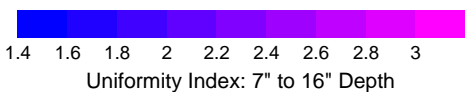
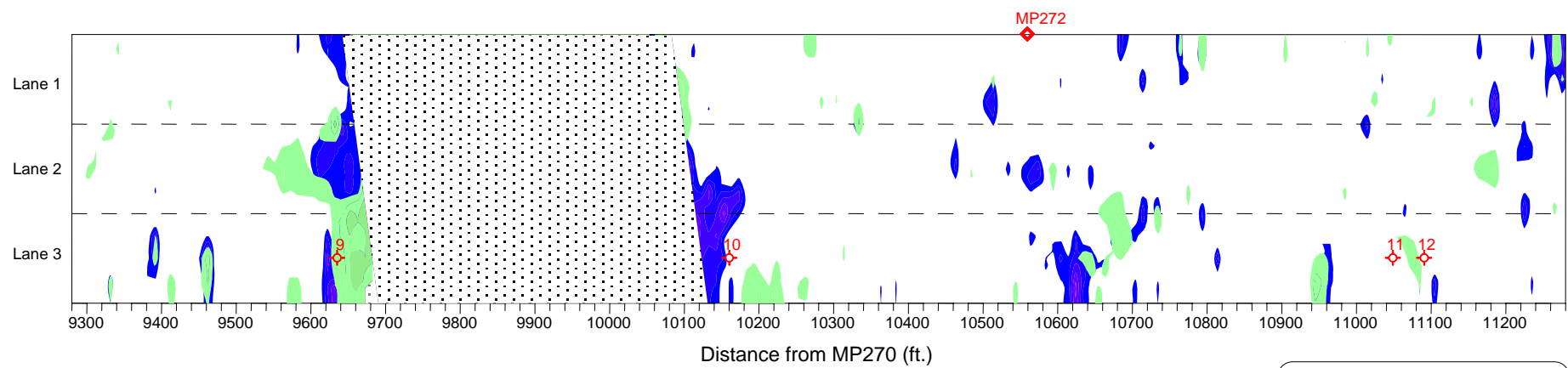
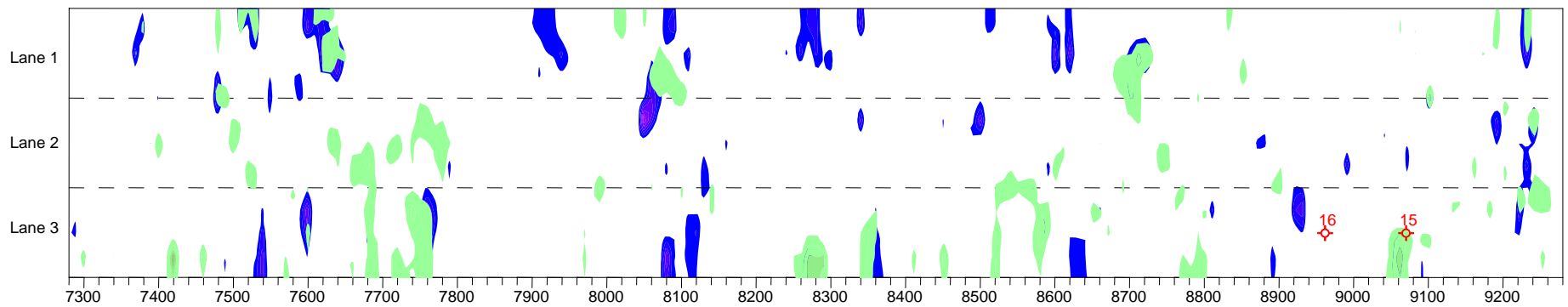
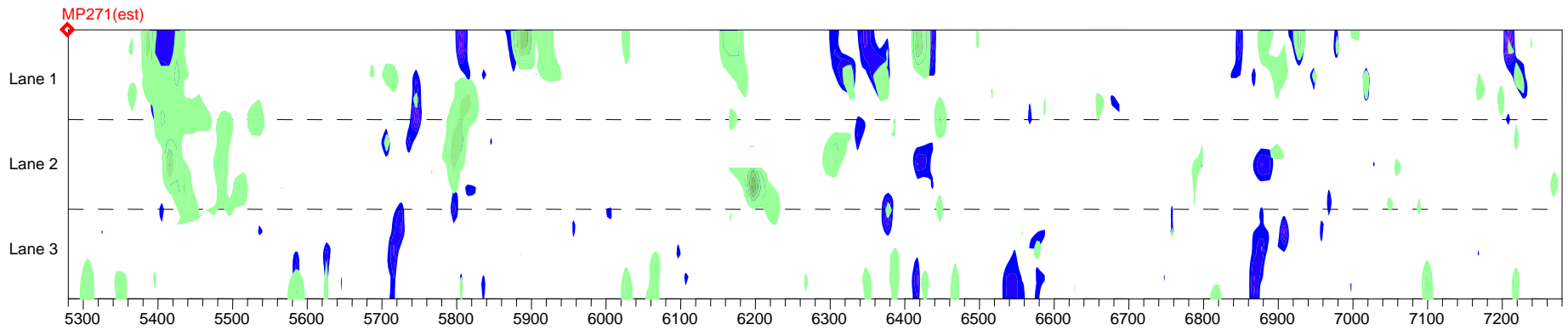


Distance from MP270 (ft.)

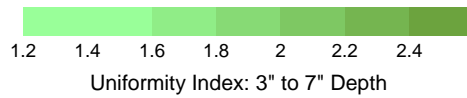
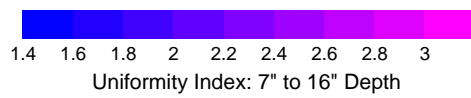
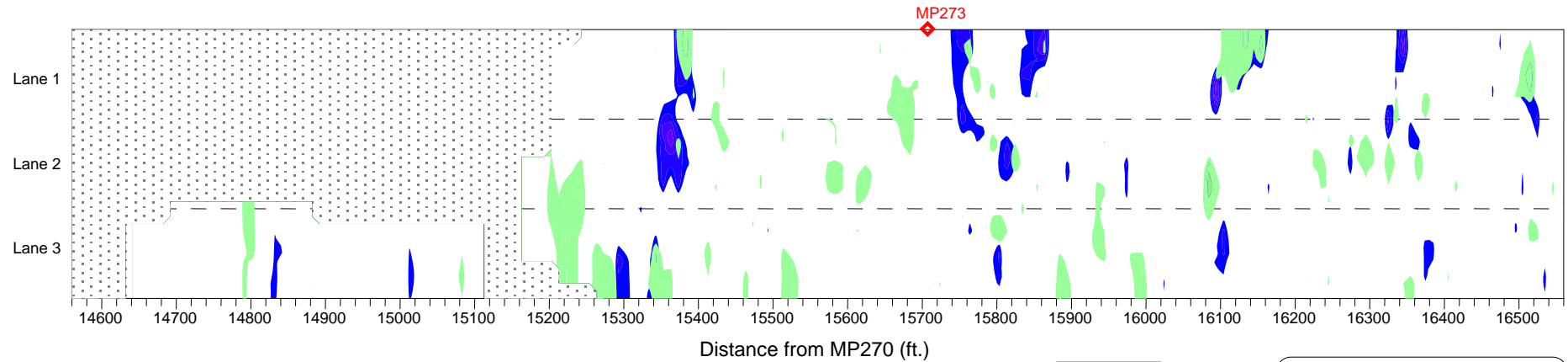
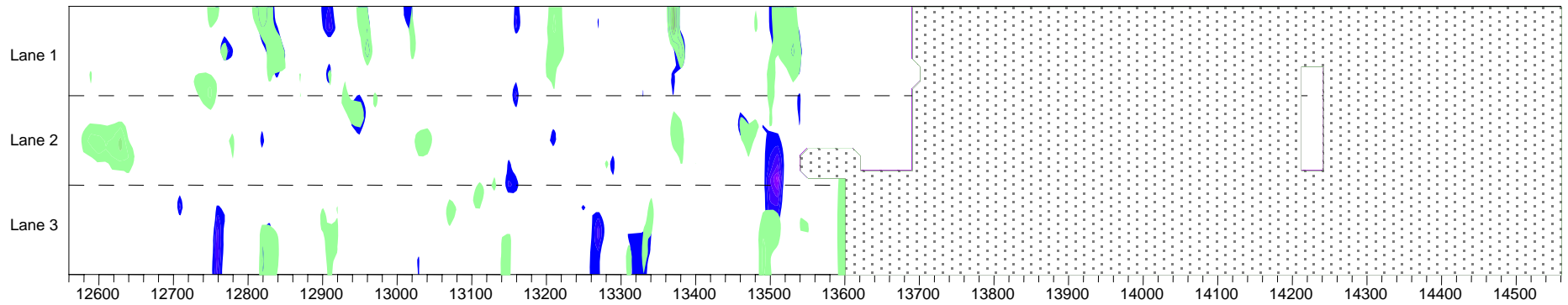
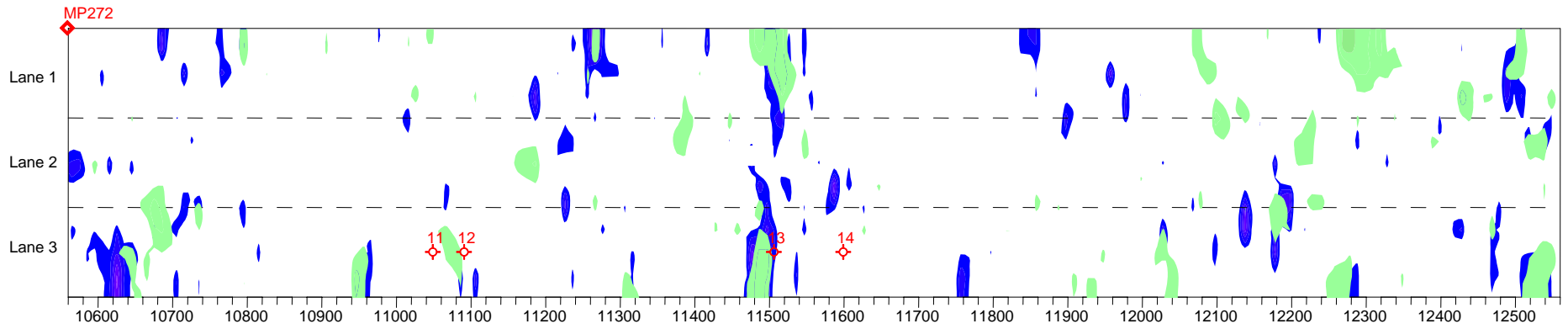



Uniformity Index: 3" to 7" Depth

I-75 Stripping Analysis
GPR Uniformity Index
 Analyzed by: LM Date: 01/17/05
 Checked by: KRM Date: 01/21/05
INFRASENSE, Inc.
 Arlington, MA 02476
 Sheet: 1 of 10

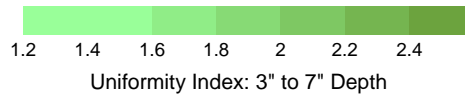
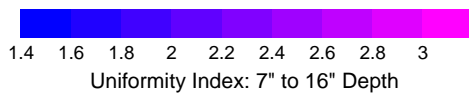
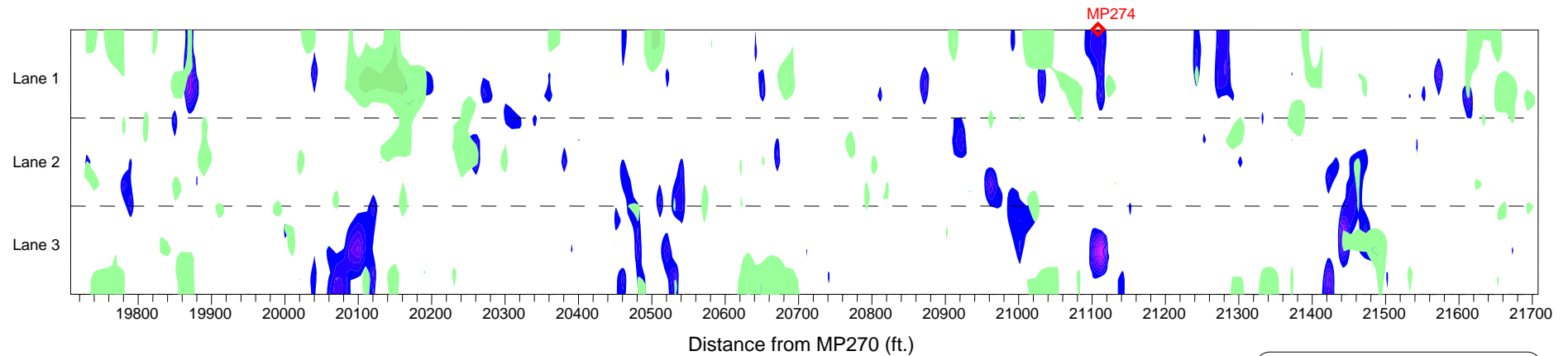
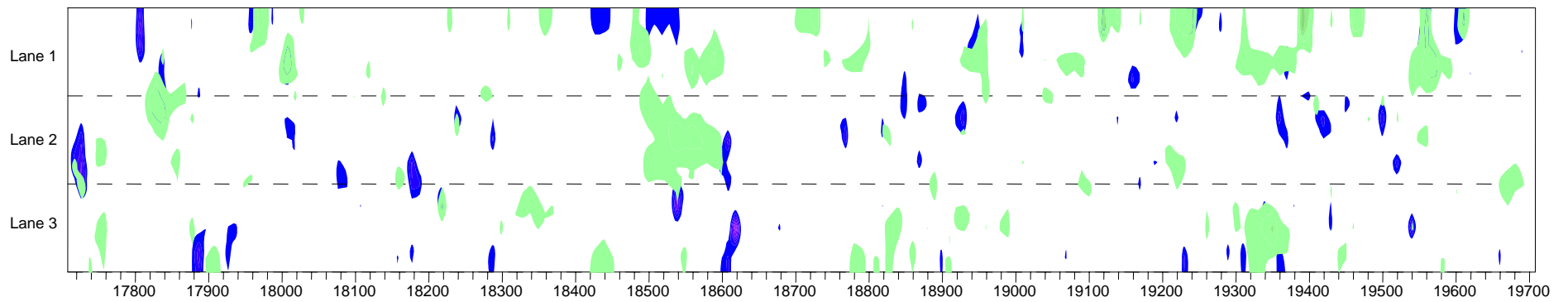
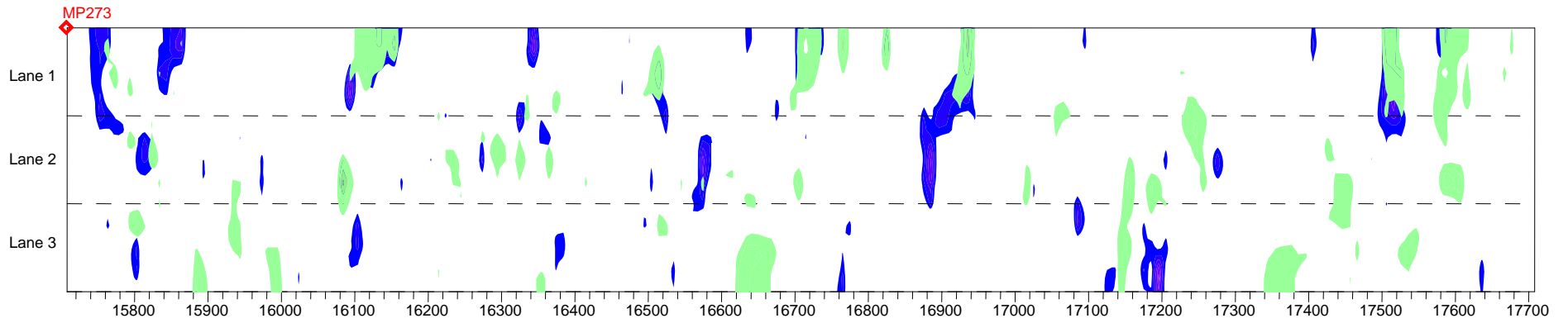


I-75 Stripping Analysis
GPR Uniformity Index
 Analyzed by: LM Date: 01/17/05
 Checked by: KRM Date: 01/21/05
INFRASENSE, Inc.
 Arlington, MA 02476
 Sheet: 2 of 10

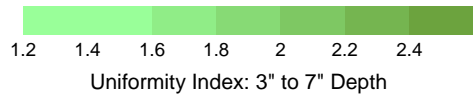
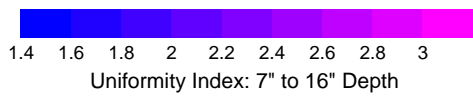
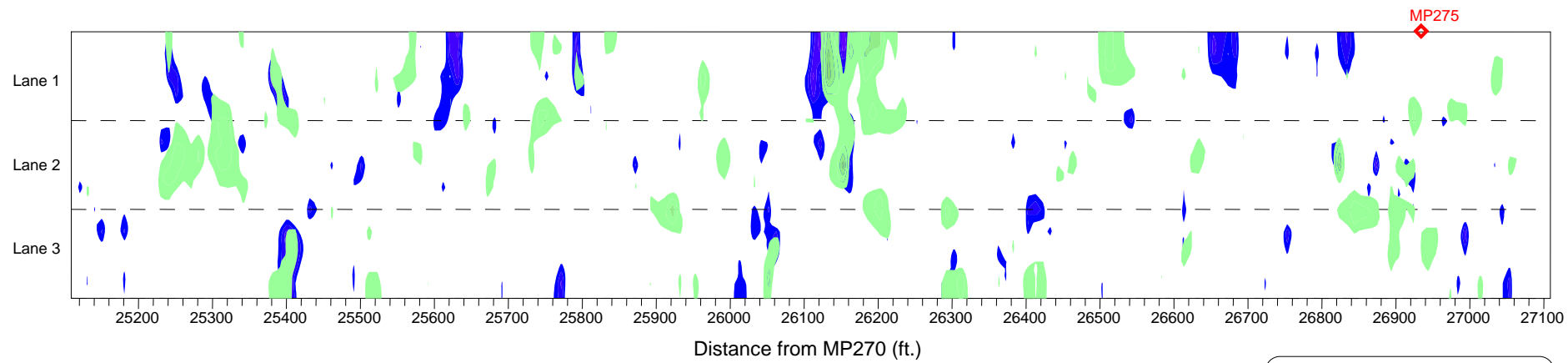
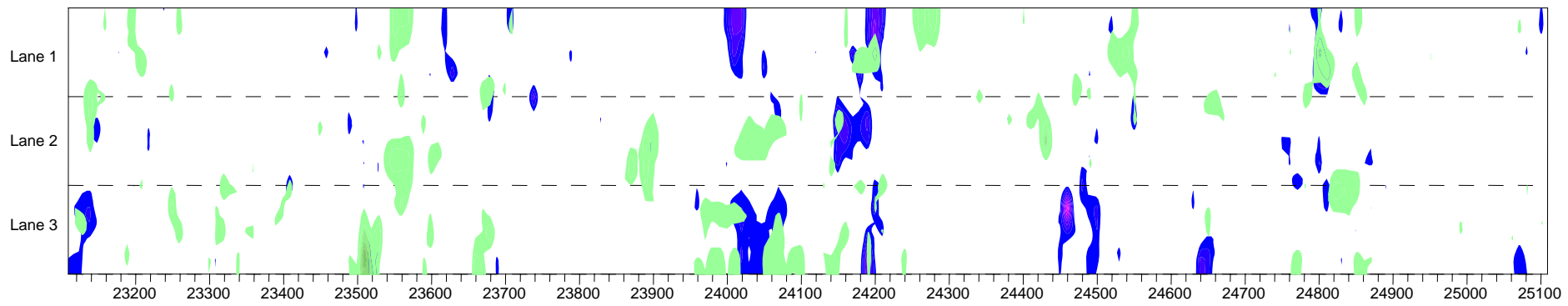
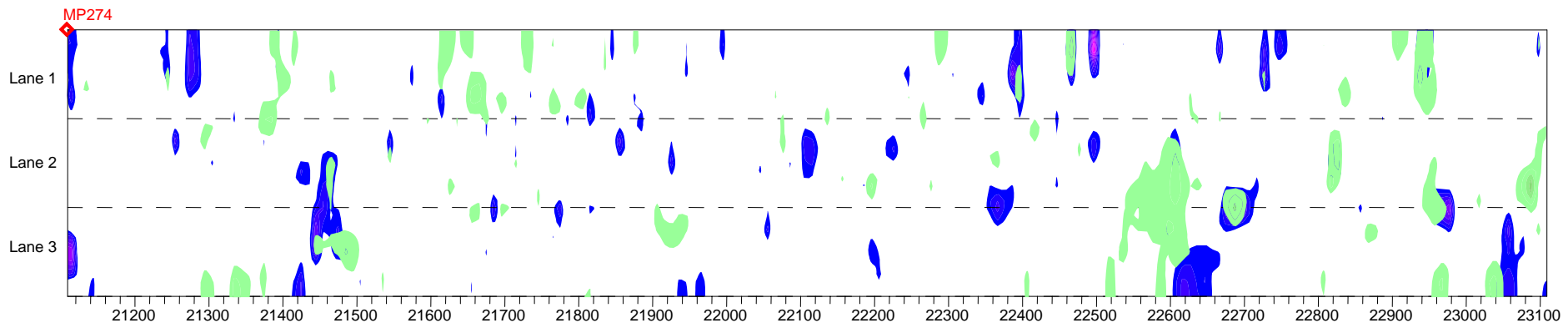


 = area not analyzed due to radio interference

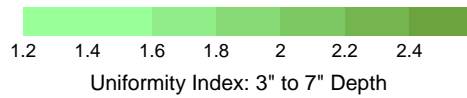
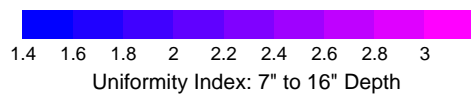
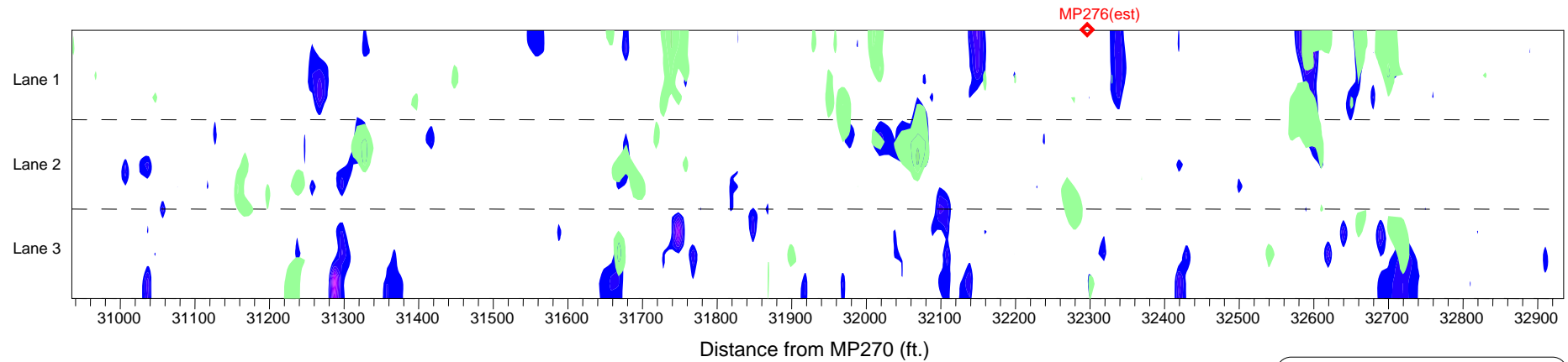
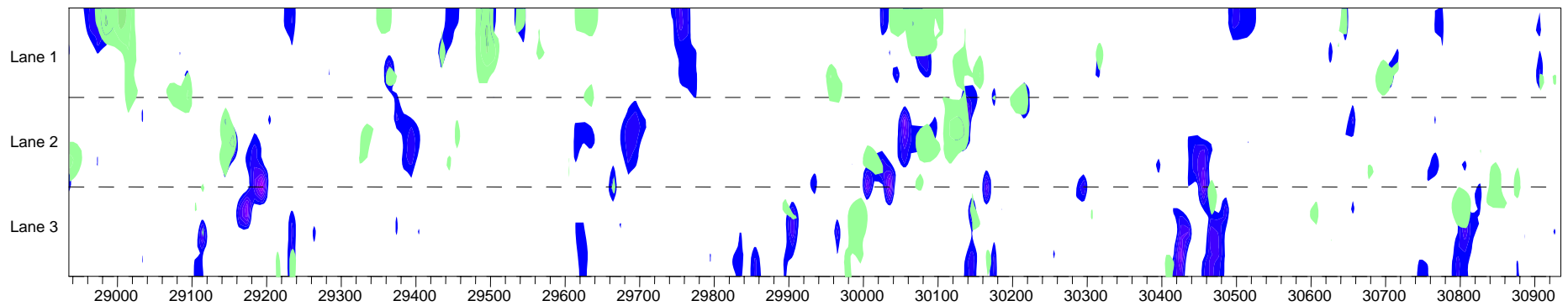
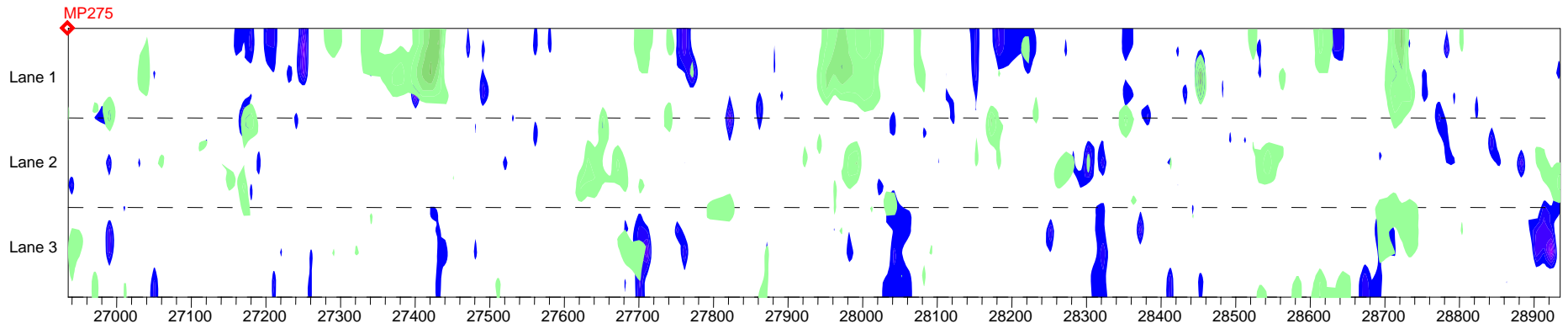
I-75 Stripping Analysis
GPR Uniformity Index
 Analyzed by: LM Date: 01/17/05
 Checked by: KRM Date: 01/21/05
INFRASENSE, Inc.
 Arlington, MA 02476
 Sheet: 3 of 10



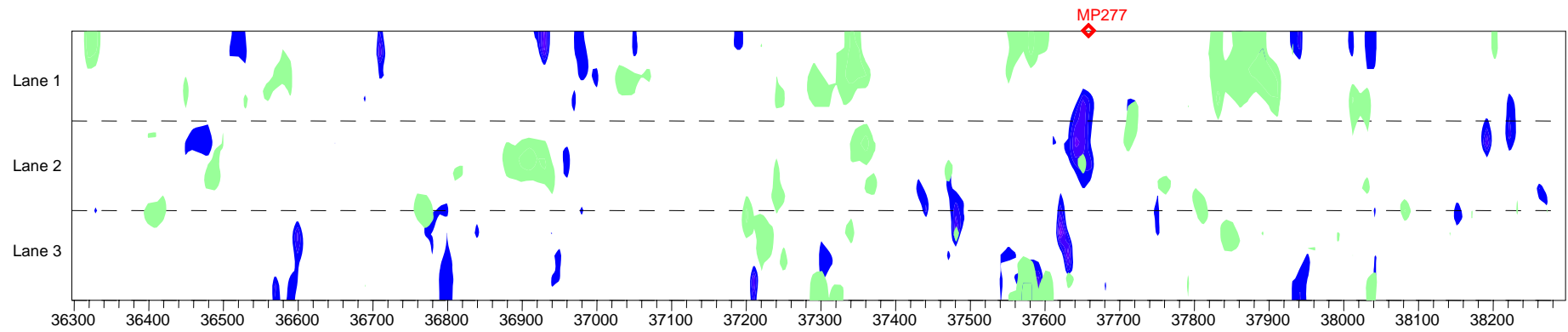
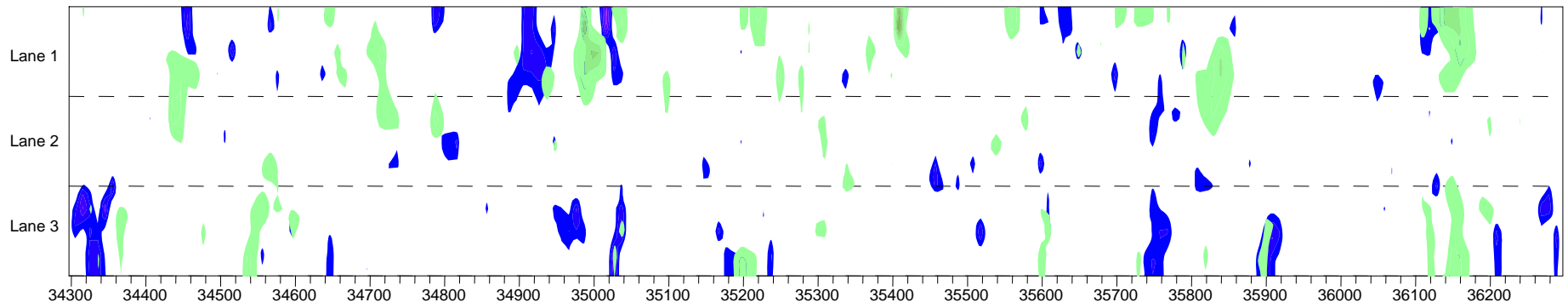
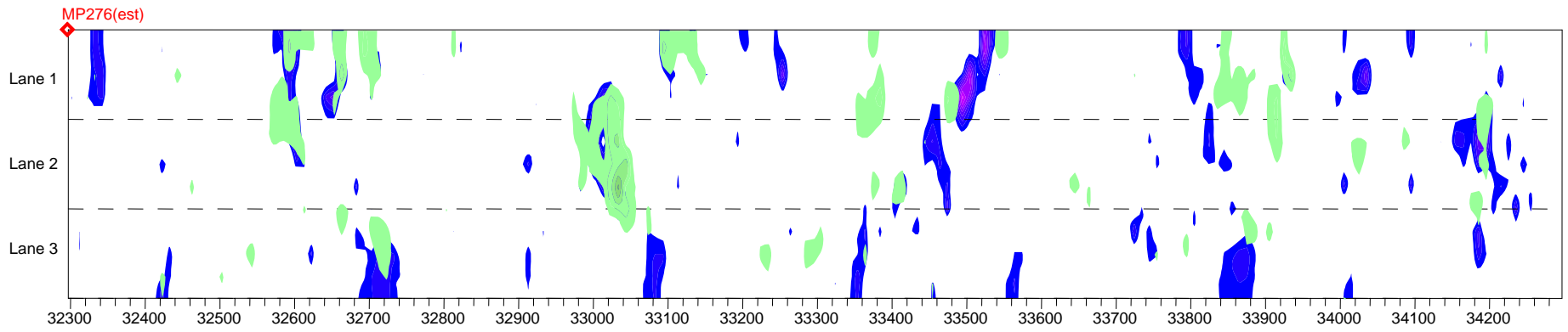
I-75 Stripping Analysis
GPR Uniformity Index
 Analyzed by: LM Date: 01/17/05
 Checked by: KRM Date: 01/21/05
INFRASENSE, Inc.
 Arlington, MA 02476
 Sheet: 4 of 10



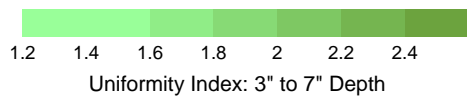
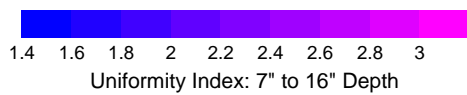
I-75 Stripping Analysis
GPR Uniformity Index
 Analyzed by: LM Date: 01/17/05
 Checked by: KRM Date: 01/21/05
INFRASENSE, Inc.
 Arlington, MA 02476
 Sheet: 5 of 10



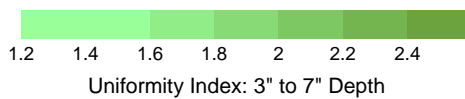
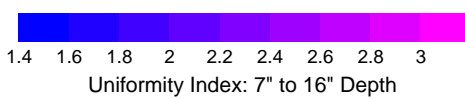
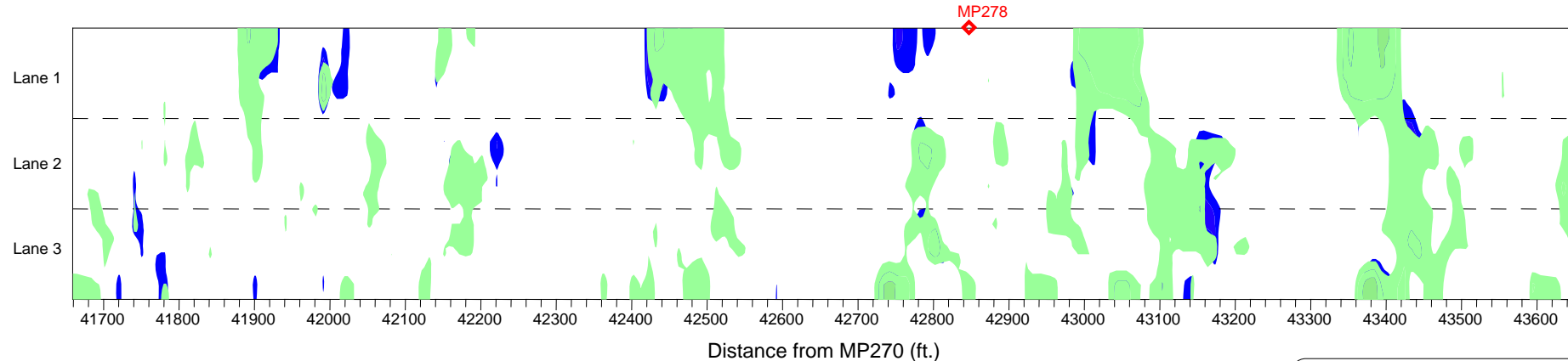
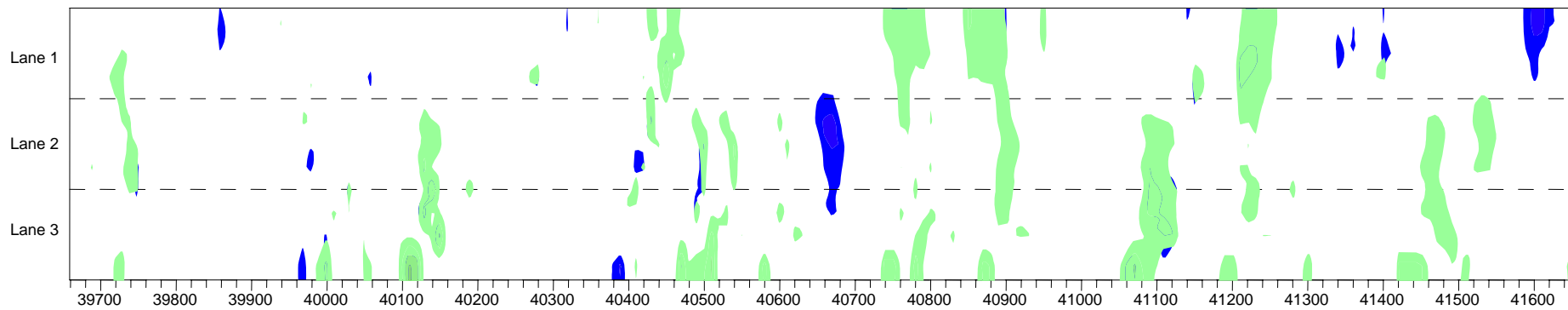
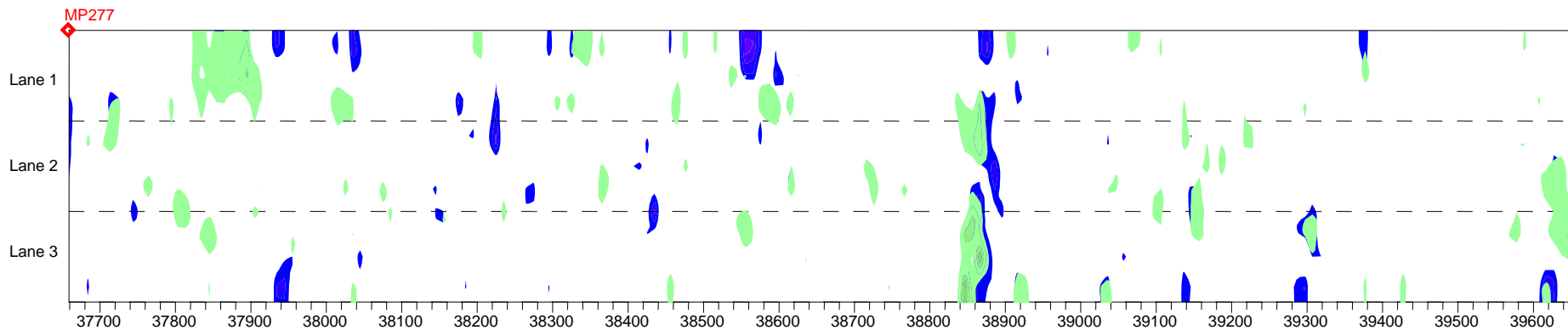
I-75 Stripping Analysis
GPR Uniformity Index
 Analyzed by: LM Date: 01/17/05
 Checked by: KRM Date: 01/21/05
INFRASENSE, Inc.
 Arlington, MA 02476
 Sheet: 6 of 10



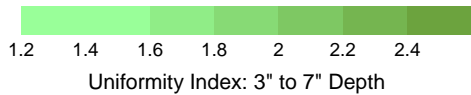
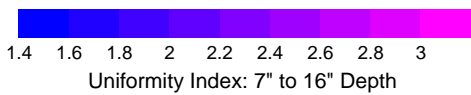
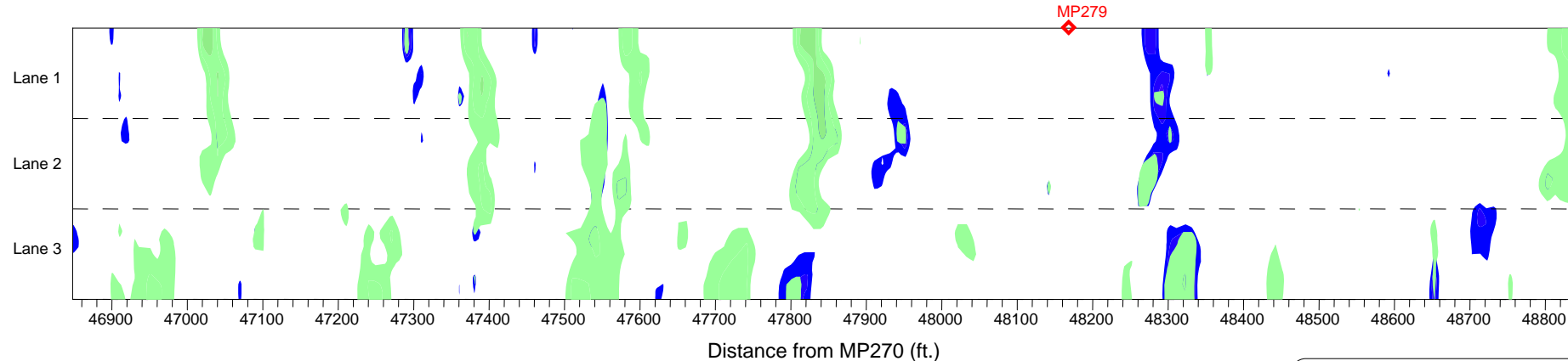
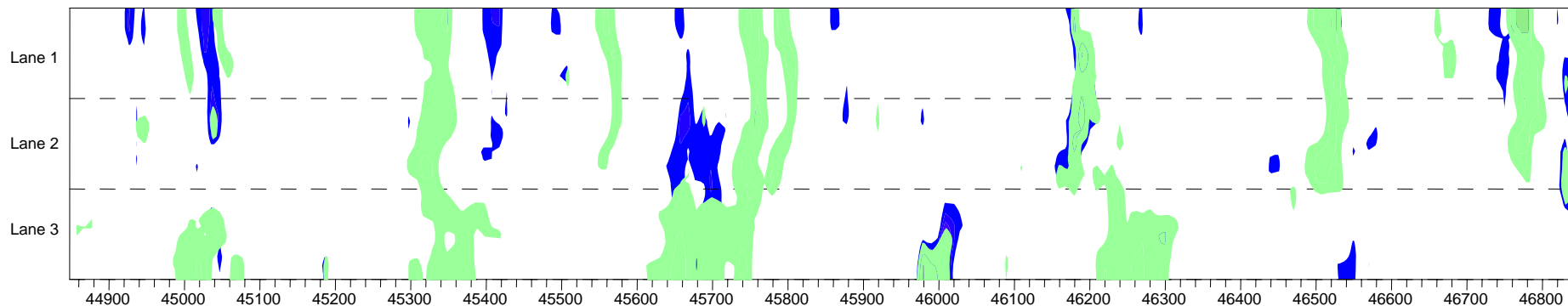
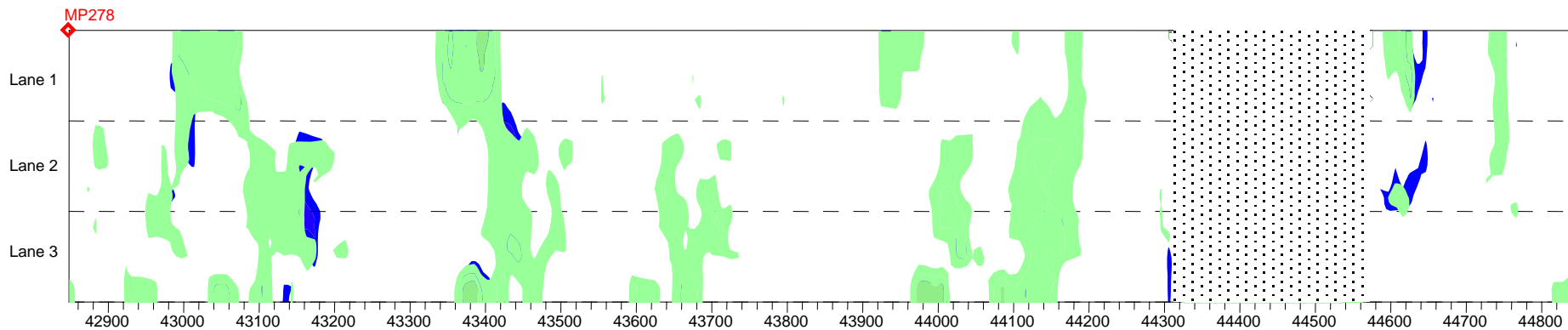
Distance from MP270 (ft.)



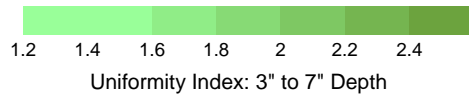
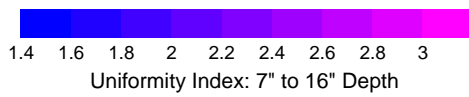
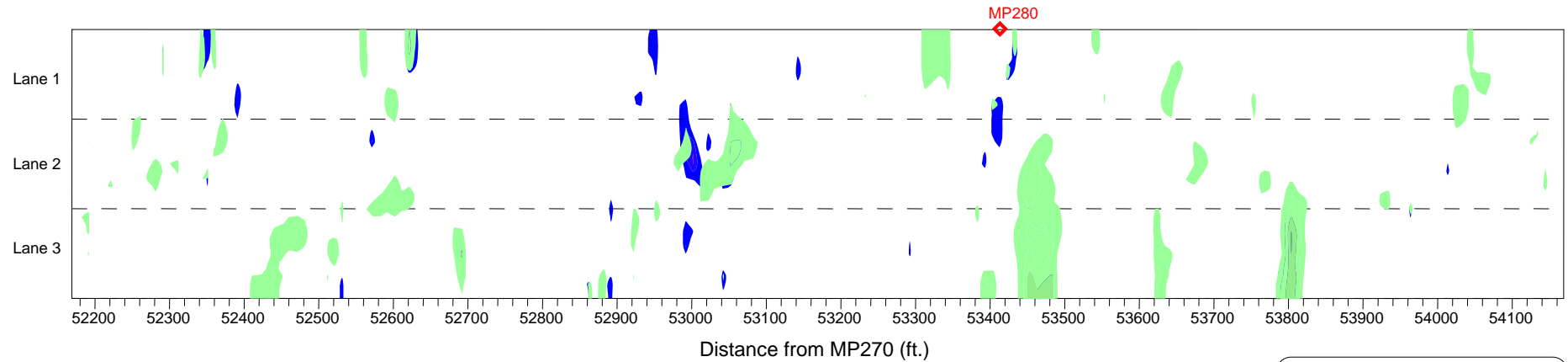
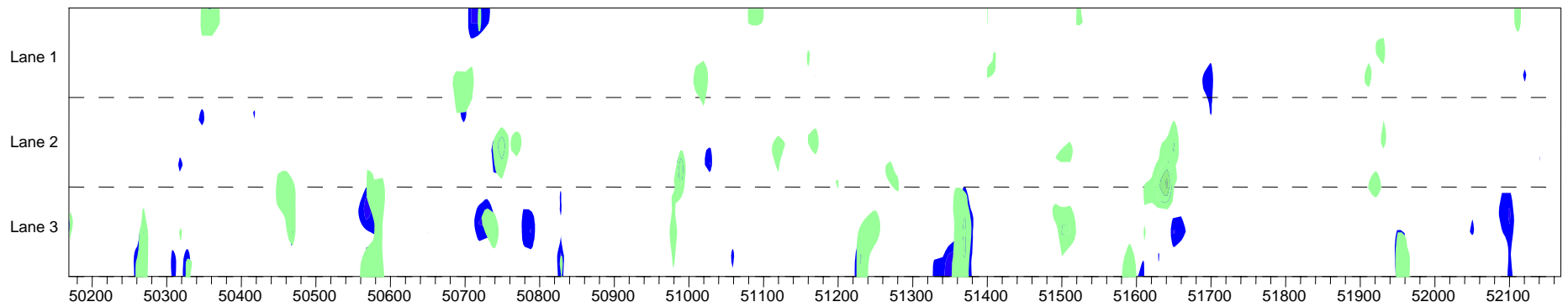
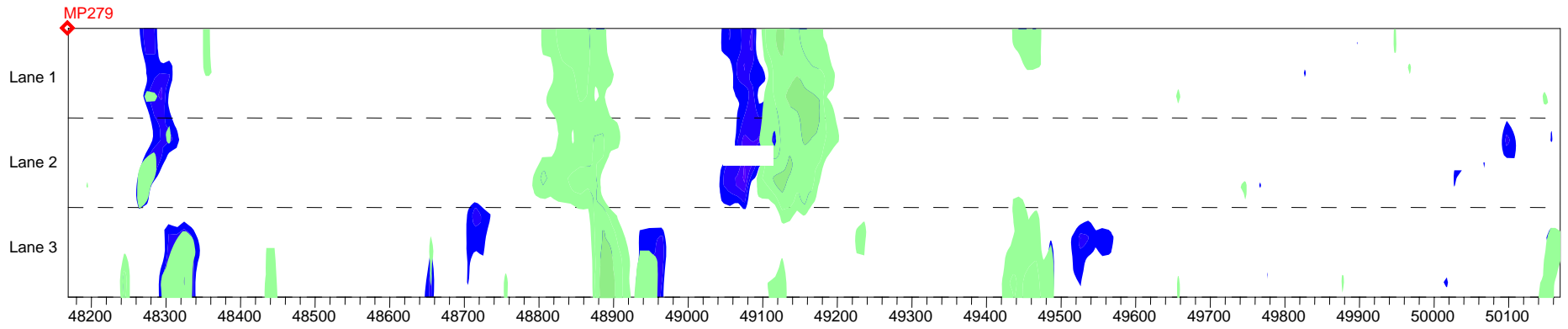
I-75 Stripping Analysis
GPR Uniformity Index
 Analyzed by: LM Date: 01/17/05
 Checked by: KRM Date: 01/21/05
INFRASENSE, Inc.
 Arlington, MA 02476
 Sheet: 7 of 10



I-75 Stripping Analysis
GPR Uniformity Index
 Analyzed by: LM Date: 01/17/05
 Checked by: KRM Date: 01/21/05
INFRASENSE, Inc.
 Arlington, MA 02476
 Sheet: 8 of 10



I-75 Stripping Analysis
GPR Uniformity Index
 Analyzed by: LM Date: 01/17/05
 Checked by: KRM Date: 01/21/05
INFRASENSE, Inc.
 Arlington, MA 02476
 Sheet: 9 of 10



I-75 Stripping Analysis
GPR Uniformity Index
 Analyzed by: LM Date: 01/17/05
 Checked by: KRM Date: 01/21/05
INFRASENSE, Inc.
 Arlington, MA 02476
 Sheet: 10 of 10